

**INFLUENCE OF Fe³⁺ AND Mn²⁺ IONS ON
STRUCTURAL, THERMAL, OPTICAL AND
MECHANICAL PROPERTIES OF MIXED ALKALI
ZINC BORATE GLASS SYSTEM**

Thesis

Submitted in partial fulfillment of the requirements for the degree of

DOCTOR OF PHILOSOPHY

IN

PHYSICS

by

SUBHASHINI

(Reg. No: 121194PH12F03)



DEPARTMENT OF PHYSICS

NATIONAL INSTITUTE OF TECHNOLOGY KARNATAKA,
SURATHKAL, MANGALORE – 575 025

December, 2019

DECLARATION

by the Ph.D Research Scholar

I hereby declare that the Research Synopsis entitled “**Influence of Fe³⁺ and Mn²⁺ ions on structural, thermal, optical and mechanical properties of mixed alkali zinc borate glass system**”, which is being submitted to the *National Institute of Technology Karnataka, Surathkal* in partial fulfillment of the requirements for the award of the Degree of *Doctor of Philosophy in Physics* is a *bonafide report of the research work carried out by me*. The material contained in this Research Thesis has not been submitted to any University or Institution for the award of any degree.

SUBHASHINI

(Register No.: 121194PH12F03)

Department of Physics

NITK, Surathkal – 575 025

Place: NITK, Surathkal

Date: 31/12/2019

CERTIFICATE

This is to *certify* that the Research Synopsis entitled “**Influence of Fe³⁺ and Mn²⁺ ions on structural, thermal, optical and mechanical properties of mixed alkali zinc borate glass system**”, submitted by **Subhashini (Register Number: 121194PH12F03)** as the record of the research work carried out by her, is *accepted* as the *Research thesis submission* in partial fulfillment of the requirements for the award of degree of *Doctor of Philosophy*.

Prof. H. D. Shashikala

Research Guide,
Department of Physics,
NITK Surathkal – 575025

Prof. N. K. Udayashankar

Additional Guide,
Department of Physics,
NITK Surathkal – 575025

Chairman - DRPC

(Signature with Date and Seal)

Dedicated to my beloved

Husband, Dr. Manjunatha S O and Daughter, Parnika

ACKNOWLEDGEMENT

It is an immense ecstasy for me to present this thesis and I take this opportunity to thank all the people who have enabled me to complete the work.

First and foremost, I am indebted to my research supervisor **Prof. H. D. Shashikala** and **Prof. N. K. Udayashankar** Department of Physics, NITK Surathkal, for their extensive guidance, patience, continuous encouragement and support at all the stages of my research work. I am always grateful for their valuable suggestions and support without which this thesis would have been impossible.

I am grateful to NITK, Surathkal for providing financial support to pursue Ph.D. under institution fellowship. I would also like to take this opportunity to thank the institution and department of Physics, specially then head of the department Prof. H.D. Shashikala, then Dean (Academics) Katta Venkataramana, Assistant Registrar Kamlabh Kumar Singh (Academics) for allowing me to pursue a part of my research work in Rutgers, The State University of New Jersey, USA. I express my sincere thanks to Dr. Ashuthosh Goel, Assistant Professor, department of Materials Science and Engineering, Rutgers-The State University of New Jersey for providing me an opportunity to work in his lab for the period of six months and explore practical knowledge.

I would like to take this opportunity to thank my RPAC members Dr. Arun M Isloor, department of Chemistry, NITK Surathkal and Dr. Ambha Shetty, department of Applied Mechanics, NITK Surathkal who spared their valuable time for constructive suggestions and comments during my research period.

I am grateful to all the teaching and non-teaching staff of department of Physics, NITK, Surathkal for their continuous support throughout my research work. I also express my deep sense of gratitude to Prof. Umesh, for his moral support during my stay at NITK. I thank all my lab colleagues for extending their continuous support and co-operation during my research work.

I owe my gratitude to Dr. H. N. Vasana, Principal Research Scientist, Solid State and Structural Chemistry Unit (SSCU), IISc, Bangalore for allowing me to utilize his lab for conducting experiments during my undergraduate and post graduate studies. I express my deep gratitude for seeding the research interest in me.

My special thanks to my school teachers Mr. Aravind Rangadol, Mr. Charls E Bangera, Mrs. Gayathri (Late), Mr. Chandrashekarayya, Mrs. Vishalakshi and my pre university lecturer Mr. Nagesh Kanoor for their consistent support and encouragement. I would like to thank my undergraduate lecturers Dr. Desai (Late), Mr. Pandurangan, Dr. M. N. Chandrashekar, Dr. Nagaraj, Dr. Shivanna Gowder, Ms. Prema and my post graduate Professors, Prof. Thukaram, and then HOD Prof. Ashok Rao for their moral support.

I am deeply indebted to my all-time moral supporters Prof. D. S. Somshekar, then Principal, Thunga Maha Vidyalaya, Thirthahalli, Mr. Rudre Gowda, Shanthala factories, Shimoga. Bhagyalakshmi madam, Shanthamma madam, Mr. Jagadeesh, Mr. Mohan Kumar. I extend my thanks to my friends Mrs. Hamsa and Ms. Bindu K. My special thanks goes to my moral supporters Mrs. Balakrishna Shenoy, Mrs. Sujatha, Mr. Prashanth K. M., Mr. Vidyashankar Bhagavath, Mr. R H Sharada Prasad and Mrs. Nalini Prasad.

I would like to express my gratitude to my parents Mr. Lakshmikantha and Mrs. Rathna Laksmikantha for their unconditional love and support. Words are not sufficient to explain my deep sense of indebtedness. My special thanks to my grandmother Mrs. Gowramma for her unconditional love, encouraging and incorporating moral values in me. I express my deep sense of gratitude to my uncle Mr. Lokesh and aunt Mrs. Manjula Annappa who showered immense love on me and nurtured me to become a sensible human being. I express my deep sense of gratitude to my family members, sisters, nephews, uncles, aunts and cousins for their love and supports. My special thanks to my in-laws Mr. Raja Sirigere and Pushpa Sirigere for their consistent support and encouragement.

I am deeply indebted to my beloved husband Dr. Manjunatha S O for his unwavering love, unconditional sacrifices and motivation, which helped me to move towards my goals and stand today as what I am. His whole hearted support has been invisible strength that held me together in every crisis of my research and daily life. I don't have words to explain about my little wonder, my daughter Parnika Manjunath who is source of my strength and happiness.

Finally, I am very much grateful to almighty, the supreme power and my all spiritual gurus who blessed me with such a beautiful life.

Subhashini

ABSTRACT

The thesis contains the systematic study on the synthesis and characterization of two and three alkali zinc borate glass systems prepared by melt-quenching method. The structural, optical, thermal and mechanical properties are studied in detail.

The non-linearity observed in the mechanical, thermal and structural properties of alkali zinc borate glasses with nominal composition $5\text{Li}_2\text{O}-(25-x)\text{K}_2\text{O}-x\text{Na}_2\text{O}-60\text{B}_2\text{O}_3-10\text{ZnO}$ ($x= 0, 5, 10, 15, 20$ and 25 mol %) strongly suggests that there exists a strong mixed alkali effect (MAE) in this systems. It is also observed that the MAE is much stronger in three alkali doped system compared to that of two alkali doped glass system. The TMO doped $5\text{Li}_2\text{O}-x\text{K}_2\text{O}-(25-x)\text{Na}_2\text{O}-60\text{B}_2\text{O}_3-(10-y)\text{ZnO}-y\text{TMO}$ ($x= 0$ and 5 mol% and $y= 0$ and 0.1 mol%, TMO= Cr_2CO_3 , MnO_2 , Fe_2O_3 , Co_3CO_4 , and Ni_2CO_3) glass system revealed the presence of transition metal ions in specific valence and coordination states in the glass matrix. This results in varied optical absorption and hence, is responsible for the colour of the prepared glasses. Chromium and cobalt in both two alkali and three alkali glass matrix favors high valence and coordination states and therefore exhibit the intense colour.

The detailed comparative studies of Fe^{3+} and Mn^{2+} ions doping on the properties of two alkali $5\text{Li}_2\text{O}-25\text{Na}_2\text{O}-60\text{B}_2\text{O}_3-(10-y)\text{ZnO}-y\text{TMO}$ ($y = 0, 0.1, 0.3, 0.5, 0.7$ and 0.9 mol%, TMO= Fe_2O_3 and MnO_2) glass system with that of the three alkali $5\text{Li}_2\text{O}-x\text{K}_2\text{O}-(25-x)\text{Na}_2\text{O}-60\text{B}_2\text{O}_3-(10-y)\text{ZnO}-y\text{TMO}$ ($x = 0$ and 5 mol%, $y= 0, 0.1, 0.3, 0.5, 0.7$ and 0.9 mol%, TMO= Fe_2O_3 and MnO_2) glass system is done. Fourier Transform Infrared (FTIR) and Raman spectroscopy studies reveal that both Fe_2O_3 and MnO_2 act as network modifiers. Both Fe_2O_3 and MnO_2 are observed to enhance the thermal stability of these system of glasses. These glass systems therefore are good host materials for optical fiber fabrication which yield a crystal-free fiber. Optical band gap energy, E_g , of the studied glass systems is found to reduce with increasing Fe_2O_3 and MnO_2 content. Mechanical strength and fracture toughness of the prepared glass samples determined using Vickers micro-indentation technique, exhibit better mechanical properties with the incorporation of Fe_2O_3 and MnO_2 content. The inclusion of Fe_2O_3 and MnO_2 has proved to be of great importance in

tailoring the properties of the glass systems to make them promising candidates for optical filters.

Keywords: Alkali borate glasses; optical basicity; thermal stability; fracture toughness; Vickers hardness; Brittleness.

Contents

List of Figure	i
List of Tables	vi
Nomenclature	ix
CHAPTER 1	1-25
Introduction	1
1.1 Glasses	1
1.2 Glass formation	3
1.3 Glass preparation methods	6
1.3.1 Melt quenching techniques	6
1.3.2 Sol-gel processing method	7
1.3.3 Chemical vapour deposition method	8
1.4 Classification of glass system	8
1.4.1 Chalcogenide glasses	8
1.4.2 Halide and Oxy-Halide glasses	9
1.4.3 Oxide glasses	9
1.4.3.1 Silicate glasses	10
1.4.3.2 Phosphate glasses	10
1.4.3.3 Germanate glasses	11
1.4.3.4 Telluride and vanadium glasses	11
1.4.3.5 Borate glasses	11
1.4.3.5.1 Structure of Borate Glass	12
1.4.3.5.2 Alkali Borate Glass	13
1.4.3.5.3 Boron oxide anomaly	18
1.4.3.5.4 Mixed alkali effect	18

1.4.3.5.5 Transition metal doped alkali borate glasses	20
1.5 Scope and objective of the present research work	22
1.5.1 Scope	22
1.5.2 Objective	23
1.6 Organization of the thesis	24
CHAPTER 2	26 – 47
Materials and Methods	26
2.1 Glass synthesis	26
2.1.1 Precursors and composition used	26
2.1.2 Experimental Procedure	29
2.1.3 Surface polishing of the sample	30
2.2 Sample characterization	30
2.2.1 X-ray diffraction (XRD)	31
2.2.2 Fourier Transform Infrared (FTIR) spectroscopy and Raman spectroscopy	31
2.2.2.1 Fourier Transform Infrared (FTIR) spectroscopy	31
2.2.2.2 Raman Spectroscopy	32
2.2.3 Scanning Electron Microscopy (SEM)	32
2.2.4 Density measurements	33
2.2.5 Thermal Analysis	34
2.2.6 Optical properties	35
2.2.6.1 Refractive index (RI) measurement	35
2.2.6.2 UV-Visible spectroscopy	36
2.2.6.3 Electronic polarizability	37
2.2.7 Mechanical Properties	39
2.2.7.1 Micro indentation studies	39
2.2.8 Error analysis	43
2.2.8.1 Standard deviation of the mean (SDOM)	43
2.2.8.2 Quadrature sum of uncertainty	45

CHAPTER 3	47-61
INVESTIGATION OF MIXED ALKALI EFFECT ON MECHANICAL, STRUCTURAL AND THERMAL PROPERTIES OF THREE-ALKALI BORATE GLASS SYSTEM	
3.1 Results and Discussion	47
3.1.1 X-ray diffraction studies	47
3.1.2 Fourier Transform Infrared Spectroscopy	48
3.1.3 Density, Molar volume and atomic packing density	53
3.1.4 Thermal Analysis	55
3.1.5 Mechanical Properties	57
3.2 Summary	61
CHAPTER 4	62-85
EFFECT OF TMO ADDITION ON THE PROPERTIES OF 5Li₂O-25Na₂O-60B₂O₃-9.9ZnO-0.1TMO AND 5Li₂O-5K₂O-20Na₂O-60B₂O₃-9.9ZnO-0.1TMO GLASS SYSTEMS: A COMPARATIVE STUDY OF LN-TM AND LNK-TM ZINC BORATE GLASS SYSTEM.	
4.1 Results and Discussion	62
4.1.1 X-ray diffraction studies	62
4.1.2 Structural Studies	64
4.1.2.1 Fourier Transform Infrared Spectroscopy studies	64
4.1.2.2 Raman Spectroscopy studies	69
4.1.3 Optical studies	73
4.1.4 Mechanical properties	80
4.2 SUMMARY	84

CHAPTER 5

86-118

EFFECT OF Fe³⁺ ADDITION ON THE PROPERTIES OF 5Li₂O-25Na₂O-60B₂O₃-(10-x)ZnO-xFe₂O₃ AND 5Li₂O-xK₂O-(25-x)Na₂O-60B₂O₃-(10-y)ZnO-yFe₂O₃ GLASS SYSTEMS: A COMPARATIVE STUDY OF LN-Fe AND LNK-Fe ZINC BORATE GLASS SYSTEM.

5.1 Results and Discussion	87
5.1.1 X-ray diffraction studies	87
5.1.2 Structural Studies	88
5.1.2.1 Fourier Transform Infrared Spectroscopy studies	88
5.1.2.2 Raman Spectroscopy studies	93
5.1.3 Density (ρ), Molar volume (V_m) and atomic packing density (OPD)	98
5.1.4 Thermal studies	99
5.1.5 Optical studies	103
5.1.5.1 Electronic polarizability	110
5.1.5.2 Optical basicity	111
5.1.5.3 Metallization criterion	111
5.1.6 Mechanical properties	112
5.2 SUMMARY	117

CHAPTER 6

119-149

EFFECT OF Mn²⁺ Addition On The Properties Of 5Li₂O-25Na₂O-60B₂O₃-(10-x) ZnO-xMnO₂ AND 5Li₂O-xK₂O-(25-x)Na₂O-60B₂O₃-(10-y)ZnO-yMnO₂ GLASS SYSTEMS: A COMPARATIVE STUDY OF LN-Fe AND LNK-Fe GLASS SYSTEM.

6.1 Results and Discussion	119
----------------------------	-----

6.1.1 X-ray diffraction studies	119
6.1.2 Structural Studies	121
6.1.2.1 Fourier Transform Infrared Spectroscopy studies	121
6.1.2.2 Raman Spectroscopy studies	125
6.1.3 Density (ρ), Molar volume (V_m) and atomic packing density (OPD)	130
6.1.4 Thermal studies	131
6.1.5 Optical studies	135
6.1.5.1 Electronic polarizability	142
6.1.5.2 Optical basicity	143
6.1.5.3 Metallization criterion	143
6.1.6 Mechanical properties	144
6.2 SUMMARY	148
CHAPTER 7	149-151
7.1 SUMMARY AND CONCLUSIONS	149
7.2 SCOPE FOR THE FUTURE WORK	151
Bibliography	152
List of publications	161
Curriculum Vitae	166

List of Figures

1.1	Volume (enthalpy) versus temperature diagram for glass forming liquids	2
1.2	SiO ₂ glass structure modification with incorporation of alkali metal oxides	5
1.3	Raman band corresponding to boroxol ring structure in vitreous B ₂ O ₃	12
1.4	(a) Two-dimensional Zachariasen's random network diagram and (b) two-dimensional representation of vitreous Na ₂ O-B ₂ O ₃ structure (Note for colour representation: blue: tetrahedral boron atom, cyan: trigonal boron atom, red: bridging oxygen atom and black: Na ⁺ cation)	14
1.5	Schematic representation of (a) BO ₃ unit, (b) BO ₄ unit, and (c) boroxol group in borate glass matrix	15
1.6	Schematic representation of modifier alkali concentration dependent intermediate structures (dashed lines represents theoretical variations and solid lines represents experimental results)	16
1.7	Borate superstructural units (a) boroxol group, (b) pentaborate group, (c) triborate group, (d) di-pentaborate group, (e) diborate group, and (f) di-triborate group	17
2.1	The process flow of preparation and characterization of alkali zinc-borate glass systems	29
2.2	Schematic diagram of Vickers indentation on surface of sample.	40
2.3	Schematic diagram of cracks propagating from four corners of Vickers indentation	41
3.1	X-ray diffractogram of 5Li ₂ O-(25-x)K ₂ O-xNa ₂ O-60B ₂ O ₃ -10ZnO glass system	48
3.2	FTIR spectra of 5Li ₂ O-(25-x)K ₂ O-xNa ₂ O-60B ₂ O ₃ -10ZnO glass system	49

3.3	Peak positions variations of B-O-B bending and stretching as a function of compositional parameter R_{Na}	51
3.4	Peak position variations as a function of compositional parameter R_{Na} of (a) O-B-O bond bending and $[BO_4]$ tetrahedral vibration, (b) B-O stretching vibration of BO_4 tetrahedra and $[BO_3]^{3-}$ unit and (c) antisymmetric stretching vibrations of O-B-O group and OH bond bending modes, with compositional parameter R_{Na}	52
3.5	Variation of density and molar volume as a function of compositional parameter R_{Na}	54
3.6	Variation of Glass transition temperature (T_g) and glass crystallization temperature (T_c) as a function of compositional parameter R_{Na}	56
3.7	Variation of thermodynamic fragility and glass transition width as a function of compositional parameter R_{Na}	57
3.8	Variation of micro hardness and brittleness as a function of compositional parameter R_{Na}	58
3.9	Scanning electron micrograph of Vickers impression with radial cracks of glass sample A5	59
3.10	Variation of crack length and fracture toughness as a function of compositional parameter R_{Na}	60
4.1 (a)	X-ray Diffraction patterns of TMO doped LN-TM glass system.	63
4.1 (b)	X-ray Diffraction patterns of TMO doped LNK-TM glass system.	63
4.2 (a)	FTIR spectra of TMO doped LN-TM glass system.	65
4.2 (b)	FTIR spectra of TMO doped LNK-TM glass system.	65
4.3 (a)	Deconvoluted FTIR peaks of TM doped LN-TM glass system.	66
4.3 (b)	Deconvoluted FTIR peaks of TM doped LNK-TM glass system.	67
4.4 (a)	Raman spectra of TMO doped LN-TM glass systems.	70
4.4 (b)	Raman spectra of TMO doped LNK-TM glass systems.	70
4.5 (a)	Deconvoluted Raman spectra of TMO doped LN-TM glass system.	71

4.5 (b)	Deconvoluted Raman spectra of TMO doped LNK-TM glass system.	72
4.6 (a)	UV-visible absorption spectra for the TMO doped LN-TM glass system.	74
4.6 (b)	UV-visible absorption spectra for the TMO doped LN-TM glass system.	75
4.7 (a)	Variation of $(\alpha h\nu)^{1/2}$ as a function of photon energy ($h\nu$) for the TMO doped LN-TM glass system.	77
4.7 (b)	Variation of $(\alpha h\nu)^{1/2}$ as a function of photon energy ($h\nu$) for the TMO doped LNK-TM glass system.	77
4.8 (a)	Variation of $\ln(\alpha)$ as a function of photon energy ($h\nu$) for the TMO doped LN-TM glass system.	79
4.8 (b)	Variation of $\ln(\alpha)$ as a function of photon energy ($h\nu$) for the TMO doped LNK-TM glass system	80
4.9 (a)	SEM micrograph of Vickers indentation of TMO doped LN-TM glass system	82
4.9 (b)	SEM micrograph of Vickers indentation of TMO doped LNK-TM glass system	83
5.1 (a)	X-ray Diffraction patterns of Fe_2O_3 doped two alkali glass system.	87
5.1 (b)	X-ray Diffraction patterns of Fe_2O_3 doped three alkali glass system.	88
5.2 (a)	FTIR spectra of Fe_2O_3 doped two alkali glass system.	89
5.2 (b)	FTIR spectra of Fe_2O_3 doped three alkali glass system.	89
5.3 (a)	Deconvoluted FTIR spectra of Fe_2O_3 doped two alkali glass system.	90
5.3 (b)	Deconvoluted FTIR spectra of Fe_2O_3 doped three alkali glass system.	91
5.4 (a)	Raman spectra of Fe_2O_3 doped two alkali glass systems.	93
5.4 (b)	Raman spectra of Fe_2O_3 doped two alkali glass systems.	94
5.5 (a)	Deconvoluted Raman spectra of Fe_2O_3 doped two alkali glass system.	95

5.5 (b)	Deconvoluted Raman spectra of Fe ₂ O ₃ doped three alkali glass system.	96
5.6 (a)	DSC thermographs of Fe ₂ O ₃ doped two alkali glass system.	100
5.6 (b)	DSC thermographs of Fe ₂ O ₃ doped three alkali glass system.	100
5.7 (a)	UV-visible absorption spectra for the Fe ₂ O ₃ doped two alkali glass system.	104
5.7 (b)	UV-visible absorption spectra for the Fe ₂ O ₃ doped three alkali glass system.	104
5.8 (a)	Variation of $(\alpha h\nu)^{1/2}$ as a function of photon energy ($h\nu$) for the Fe ₂ O ₃ doped two alkali glass system.	106
5.8 (b)	Variation of $(\alpha h\nu)^{1/2}$ as a function of photon energy ($h\nu$) for the Fe ₂ O ₃ doped three alkali glass system.	106
5.9 (a)	Variation of $\ln(\alpha)$ as a function of photon energy ($h\nu$) for the Fe ₂ O ₃ doped two alkali glass system.	109
5.9 (b)	Variation of $\ln(\alpha)$ as a function of photon energy ($h\nu$) for the Fe ₂ O ₃ doped three alkali glass system.	109
5.10 (a)	SEM micrograph of Vickers indentation of two alkali A6 and F9 glass samples.	114
5.10 (b)	SEM micrograph of Vickers indentation of three alkali A5 and KF9 glass samples.	115
6.1 (a)	X-ray Diffraction patterns for the MnO ₂ doped two alkali glass system.	120
6.1 (b)	X-ray Diffraction patterns for the MnO ₂ doped three alkali glass system.	120
6.2 (a)	FTIR spectra of MnO ₂ doped two alkali glass system.	122
6.2 (b)	FTIR spectra of MnO ₂ doped three alkali glass system.	122
6.3 (a)	Deconvoluted FTIR spectra of MnO ₂ doped two alkali glass systems.	123
6.3 (b)	Deconvoluted FTIR spectra of MnO ₂ doped three alkali glass systems.	124
6.4 (a)	Raman spectra of MnO ₂ doped two alkali glass systems.	126

6.4 (b)	Raman spectra of MnO ₂ doped three alkali glass systems.	126
6.5 (a)	Deconvoluted Raman spectra of MnO ₂ doped two alkali glass systems.	127
6.5 (b)	Deconvoluted Raman spectra of MnO ₂ doped three alkali glass systems.	128
6.6 (a)	DSC thermographs of MnO ₂ doped two alkali glass system.	132
6.6 (b)	DSC thermographs of MnO ₂ doped three alkali glass system.	132
6.7 (a)	UV-visible absorption spectra for the MnO ₂ doped two alkali glass system.	137
6.7 (b)	UV-visible absorption spectra for the MnO ₂ doped three alkali glass system.	137
6.8 (a)	Variation of $(\alpha h\nu)^{1/2}$ as a function of photon energy ($h\nu$) for the MnO ₂ doped two alkali glass system.	139
6.8 (b)	Variation of $(\alpha h\nu)^{1/2}$ as a function of photon energy ($h\nu$) for the MnO ₂ doped three alkali glass system.	139
6.9 (a)	Variation of $\ln(\alpha)$ as a function of photon energy ($h\nu$) for the MnO ₂ doped two alkali glass system.	141
6.9 (b)	Variation of $\ln(\alpha)$ as a function of photon energy ($h\nu$) for the MnO ₂ doped three alkali glass system.	141
6.10	Representative SEM micrograph of Vickers indentation of two alkali A6 & M9 and three alkali A5 & KM9 glass samples.	146

List of Tables

1.1	Different quenching techniques and their rates of cooling.	7
2.1	Batch composition of three-alkali zinc borate glass system.	27
2.2	Batch composition of TMO doped two and three-alkali zinc borate glass system.	27
2.3	Batch composition of Fe ₂ O ₃ doped two alkali and three alkali glass system.	28
2.4	Batch composition of MnO ₂ doped two alkali and three alkali glass system.	28
3.1	Band assignments for IR spectra of 5Li ₂ O-(25-x)K ₂ O-xNa ₂ O-60B ₂ O ₃ -10ZnO glass system	50
3.2	Density (ρ), and molar volume (V_m) of 5Li ₂ O-(25-x)K ₂ O-xNa ₂ O-60B ₂ O ₃ -10ZnO glass system	53
3.3	Thermal parameters of 5Li ₂ O-(25-x)K ₂ O-xNa ₂ O-60B ₂ O ₃ -10ZnO glass system	56
4.1	Assignment of absorption bands present in FTIR spectra of TMO doped LN-TM and LNK-TM glass system	68
4.2	Assignment of absorption bands present in Raman spectra of TMO doped LN-TM and LNK-TM glass system	73
4.3	Optical band gap energy (E_g) and Urbach energy (E_u) of TMO doped LN-TM and LNK-TM glass systems	78
4.4	Vickers hardness (H_v), half crack length (C), fracture toughness (K_{IC}) and Brittleness (B) of TMO doped LN-TM and LNK-TM glass system	81
4.5	Young's modulus (E), bulk modulus (K), shear modulus (S), and atomic packing density (V_i) of TMO doped LN-TM and LNK-TM glass system	84
5.1	Assignment of absorption bands present in IR spectra of Fe ₂ O ₃ doped two alkali glass system and three alkali glass system.	92
5.2	Assignment of absorption bands present in Raman spectra of Fe ₂ O ₃ doped two alkali glass system and three alkali glass system.	97

5.3	The density (ρ), molar volume (V_m) and oxygen packing density (OPD) of Fe ₂ O ₃ doped two alkali glass system and three alkali glass system.	98
5.4	Glass transition temperature (T_g), onset crystallization temperature (T_x), crystallization temperature (T_c), melting temperature (T_m), glass forming ability (T_{rg}), glass stability (ΔT) and Hurby's parameter (H_R) of Fe ₂ O ₃ doped two alkali glass system and three alkali glass system.	101
5.5	Optical band gap energy (E_g), Urbach energy (E_u), refractive index (n), molar refractivity (R_m), refractive index based oxide ion polarizability ($\alpha_{o^{2-}}^{(n)}$), band gap energy based electronic polarizability ($\alpha_{o^{2-}}^{(E)}$), optical basicity (Λ) and metallization criteria (M) of Fe ₂ O ₃ doped two alkali glass system and three alkali glass system.	108
5.6	Vickers hardness (H_v), half crack length (C), fracture toughness (K_{IC}) and Brittleness (B) of Fe ₂ O ₃ doped two alkali glass system and three alkali glass system.	113
5.7	Young's modulus (E), bulk modulus (K), shear modulus (S), and atomic packing density (V_t) of Fe ₂ O ₃ doped two alkali glass system and three alkali glass system.	117
6.1	Assignment of absorption bands present in IR spectra of MnO ₂ doped two alkali glass system and three alkali glass system.	125
6.2	Assignment of absorption bands present in Raman spectra of MnO ₂ doped two alkali glass system and three alkali glass system.	129
6.3	Density (ρ) and molar volume (V_m) and oxygen packing density (OPD) of two alkali and three alkali glass system.	131
6.4	Glass transition temperature (T_g), onset crystallization temperature (T_{cx}), crystallization temperature (T_c), melting temperature (T_m), glass stability (ΔT), varies glass forming ability and thermal stability parameters (K_1 , K_2 , K_3 , K_W , K_{LL} and K_{gl}) and Hruby's parameter (H_R) of two alkali and three alkali glass system.	134
6.5	Optical band gap energy (E_g) and Urbach energy (E_u) of two alkali and three alkali glass systems.	140

- 6.6 Vickers hardness (H_v), half crack length (C), fracture toughness (K_{IC}) and Brittleness (B) of MnO_2 doped two alkali glass system and three alkali glass system. 144
- 6.7 Young's modulus (E), bulk modulus (K), shear modulus (S), and atomic packing density (V_t) of MnO_2 doped two alkali glass system and three alkali glass system. 149

Nomenclature

Symbol	Definition	Unit
T_m	Melting temperature	°C
T_f	Fictive temperature	°C
SiO_2	Silicon dioxide	
B_2O_3	Boron trioxide	
V_2O_5	Vanadium(V) oxide	
P_2O_5	Phosphorus pentoxide	
GeO_2	Germanium dioxide	
As_2O_3	Arsenic trioxide	
Sb_2O_3	Antimony trioxide	
TeO_2	Tellurium dioxide	
SeO_2	Selenium Dioxide	
Ga_2O_3	Gallium Oxide	
Al_2O_3	Aluminium oxide	
WO_3	Tungsten trioxide	
MoO_3	Molybdenum trioxide	
TiO_2	Titanium dioxide	

Bi_2O_3	Bismuth(III) oxide	
T_g	Glass transition temperature	$^{\circ}\text{C}$
ΔT_g	Glass transition width	
S	Thermodynamic stability	
As	Arsenic	
Sb	Antimony	
Ge	Germanium	
Si	Silicon	
BeF_2	Beryllium Fluoride	
ZnCl_2	Zinc Dichlorine	
RI	Refractive index	
Be	Beryllium	
Zn	Zinc	
FTIR	Fourier Transform Infrared	
TM	Transition Metal	
UV	Ultraviolet	
α	Thermal expansion coefficient	
Na_2O	Sodium Oxide	

NMR	Nuclear Magnetic Resonance	
MAE	Mixed Alkali Effect	
TMI	Transition Metals Ions	
EPR	Electron Paramagnetic Resonance	
E_{opt}	Optical band gap energy	eV
B ₃ O ₆	Boroxol	
NBO	Non Bridging Oxygen	
XRD	X-ray diffraction	
SEM	Scanning Electron Microscopy	
DTA	Differential Thermal Analysis	
DSC	Differential Scanning Calorimeter	
Li ₂ CO ₃	Lithium carbonate	
Na ₂ CO ₃	Sodium carbonate	
K ₂ CO ₃	Potassium carbonate	
H ₃ BO ₃	Boric acid	
Cr ₂ CO ₃	Chromium carbonate	
Mn ₂ O ₃	Manganese oxide	
Fe ₂ O ₃	Iron Oxide	

Co_3CO_4	Cobalt carbonate	
Ni_2CO_3	Nickel carbonate	
ρ_l	Density of O-Xylene	g/cm^3
ρ	Density	g/cm^3
w_a	Weight of sample in air	gm
w_l	Weight of sample in liquid	gm
V_m	Molar Density	
M	Molecular weight	gm
OPD	Oxygen packing density	
M_T	Total molecular weight	gm
T_x	Crystallization temperature	$^{\circ}\text{C}$
ΔT	Thermal stability	
H_R	Hruby parameter	
K_W	Weinberg parameter	
K_1 and K_2	Glass stability parameters	
I_0	Intensity of incident radiation	
I	Intensity of transmitted radiation	
α	Absorption coefficient	

$h\nu$	Photon energy	eV
E_U	Urbach energy	eV
R_m	Molar refraction	
α_m	Molar polarizability	
α_i	Molar cation polarizability	
A	Optical basicity	
H_V	Vickers Hardness	GPa
K_{IC}	Fracture toughness	MPa(m) ^{1/2}
E	Young's modulus	GPa
G_i	Dissociation energy density	KJcm ⁻³
X_i	Mole fraction	
V_t	Atomic packing fraction	
N_A	Avogadro's number	
B	Brittleness	μm ^{-1/2}
σ	Poisson's ratio	
S	Shear modulus	GPa
K	Bulk modulus	GPa
F	Fragility	

V_m	Molar Volume	cm^3/mol
T_{cx}	Onset of glass crystallization temperature	$^{\circ}\text{C}$
GFA	Glass Forming Ability	

Chapter 1

INTRODUCTION

Solid materials are broadly classified as crystalline and amorphous materials. Crystalline materials possess long range periodicity and symmetry in the arrangement of the constituent atoms or molecules, which is lacking in the non-crystalline solids. Both crystalline and non-crystalline solid materials find a large number of scientific and technological applications. In particular, non-crystalline solid materials have emerged as promising materials during the last few decades owing to their significant industrial applications. Hence, they have gathered much consideration in the branch of condensed matter physics, chemistry and materials science. Among non-crystalline materials, glass and glassy materials have acquired tremendous scope due to their significant technological applications (Le Bourhis 2008) particularly in the field of telecommunication as optical fibers. Further, they are extensively used in optical and electrical switching, in solar cells, in nuclear waste devitrification, etc.

Glass is known to mankind from ancient times, archaeological proofs confirmed that few glaze materials found to be dated back to 12, 000 B.C and purest form of glass materials were found during 700 B.C in Egypt (Doremus 1973). The word ‘glass’ is derived from Latin term ‘glaesum’ used to denote the transparent materials. One more word is often used to refer glassy materials is ‘vitreous’ which is originated from Latin word “vitrum”. In olden days, glass was used mainly for decorative purposes. In today’s date glass has considered to be most essential material without which it is difficult to imagine day to day life. As it is mentioned in the “Glass Source Book” by Jo Marshall (1990) quoted by K.J. Rao (2002) “It is only when one tries to imagine a world without glass that one realizes in how many ways it is used and extent of our unthinking acceptance of it”.

1.1 Glasses

X-ray diffraction studies reveal that glasses do not exhibit sharp peaks corresponding to long-range periodic arrangement of atoms. Instead, they show a broad

hump characteristic of amorphous materials. Therefore, glasses are called amorphous or non-crystalline solids. Glasses can be well defined as amorphous solids which do not show long-range periodicity in its atomic structure, and exhibit glass transition temperature (Shelby 2005). In general, all the amorphous solids may not be glasses. If an amorphous solid exhibits glass transformation behaviour then only it can be called as glass. In order to understand the concept of glass it is vital to know its glass transformation behaviour, which can be well understood by enthalpy versus temperature plot as represented in figure 1.1.

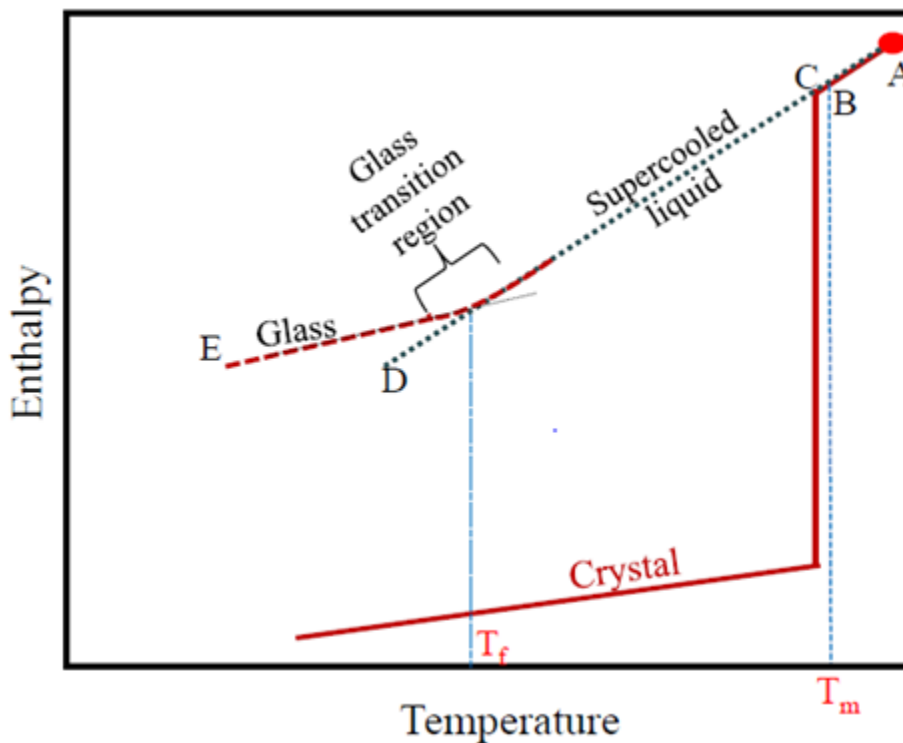


Figure 1.1: Enthalpy versus temperature diagram for glass forming liquids.

As shown in the figure 1.1, a small volume of liquid is considered at a temperature (point A) well above the melting temperature (T_m) of that particular substance, and that liquid is subjected to cooling to the T_m represented by point B, at T_m vapour pressure or Gibb's free energy is same for both solid and liquid. At this particular temperature there exists extremely insignificant quantity of crystals which are in thermodynamic equilibrium with the liquid. However, in order to get a noticeable level of crystallization further cooling is required just below the T_m (at point C).

Crystallization take place if and only if the following conditions are satisfied, (i) existence of sufficient number of nuclei and (ii) tendency for greater crystal growth rate. As represented in the figure 1.1, enthalpy will be largely effected by the crystallization process corresponding to the crystal, if cooling is further continued, enthalpy of the crystal will further decrease. If the cooling rate is high, crystallization does not occur instead the liquid reaches a state called supercooled liquid state through the straight line ABCD, which is the extrapolation of the line ABC. In this case unlike crystallization, there will be no sudden decrease in enthalpy since there is no continuous structural rearrangement. If liquid is further cooled down, the viscosity of the liquid will increase and eventually becomes so high that there will be no scope for atoms to rearrange to the equilibrium liquid structure. In this situation the enthalpy curve starts to deviate from the ABCD line and forms ABCE. This kind of change in equilibrium happens in a very narrow transformation range where the rate of change of enthalpy decreases suddenly with respect to temperature to a particular value which is equivalent to that of crystalline solid. The low temperature portion of ABCE curve acts fundamentally as a solid, this particular state can be called as 'glassy state'. The smooth curve region of the plot can be denoted as glass transition region, the upper region possess viscosity about 10^9 poise or lesser, the viscosity of glassy state needs to exceed nearly 10^{16} poise or more in order to become a solid glass. This state is not occurring at a sharp temperature value. The point where both glass line and the supercooled liquid lines interpolation intercept is called as fictive temperature (T_f), which can be defined as the temperature at which the supercooled liquid is rapidly frozen into glass.

1.2 Glass formation

In principle, glass can be formed by oxides, tellurides, halides and some polymeric organic compounds, etc. Among all, metal oxides are the most important class since they are used for commercial and technological applications. The oxides like SiO_2 , B_2O_3 , P_2O_5 , and GeO_2 which readily form glass on their own by forming three-dimensional random network when it is subjected to cooling from its liquid state are called as 'Glass formers' or 'network formers'. Oxides like As_2O_3 and Sb_2O_3 are also recognized as glass formers since they form glass subjected to rapid cooling from

their liquid state. On the other hand, there exist certain oxides like TeO_2 , SeO_2 , Ga_2O_3 , Al_2O_3 , WO_3 , MoO_3 , Bi_2O_3 and V_2O_5 which may not produce glass on their own but when mixed with suitable glass formers yield glasses. They are called as 'conditional glass formers' or 'intermediates'. The alkali and alkaline earth metal oxides form another important class of oxides in the glass synthesis. Even though they do not participate in the glass network formation, they however, contribute substantial structural modification when added with network formers and hence they are named as 'network modifiers'.

In the year 1932, Zachariasen made classification of oxides as glass forming oxides and non-glass forming oxides. Vitreous network is the crucial feature for glass formation, hence Zachariasen considered this aspect and categorized the oxides which yields such a network. Initially he suggested four fundamental rules known as 'Random Network Theory' which must be satisfied by an oxide to form a glass.

1. An oxygen atom may be linked to not more than two cations.
2. The number of oxygen atoms surrounding cations must be small (3 or 4).
3. The oxygen polyhedral share corners with each other, not edges or faces.
4. At least three corners in each oxygen polyhedron must be shared if the network is to be three dimensional.

The initially proposed rules satisfy the glass formation of simple oxide glasses but failed to define the formation of complex oxide glasses. Hence Zachariasen modified the initially proposed postulates and redefined them as given below, which contains complex oxide glasses as well as non-glass forming oxides.

1. The material should contain a high percentage of cations, which are bounded by either oxygen triangles or oxygen tetrahedral.
2. Polyhedra are associated only through their corners.
3. Some oxygen atoms are connected to only two such cations and do not form additional bonds with other cations.

The modified postulates pointed out the necessity of adequate cations presence in order to form continuous structure. Hence network is basically an open structure which requires enough bonds connecting to the Polyhedra in order to get continuity in network structure. The required cations can be isomorphically substituted in the glass network. Incorporation of such cations which are not glass formers are commonly termed as network modifiers since they participate in network modification by disrupting the continuous random network structure and produce non-bridging oxygen. For example, alkaline and alkaline earth metals substituted with the glass forming oxides enter the glass structure by breaking the glass network and create non-bridging oxygens. Figure 1.2 illustrates the formation of non-bridging oxygen in case of SiO_2 glass network consisting of SiO_4 units.

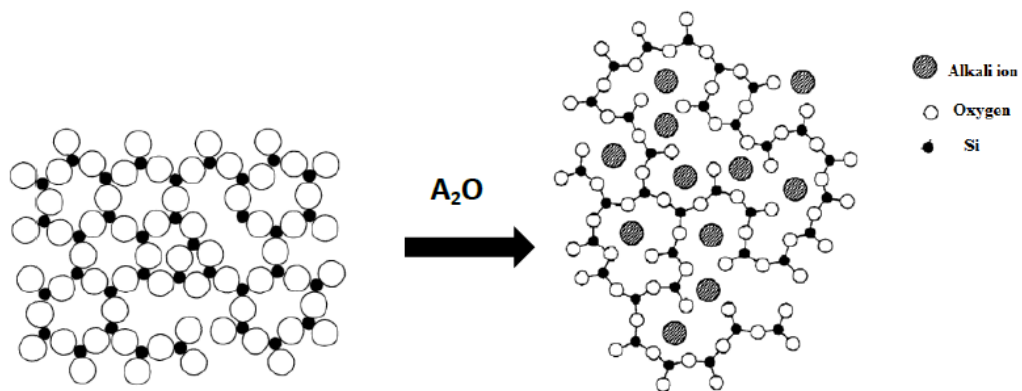


Figure 1.2: SiO_2 glass structure modification with incorporation of alkali metal oxides. (Shelby 2005)

The incorporated alkali metal ions firstly breakdown the continuity in the glass network and occupy the interstitial positions. These alkali ions bind to the negatively charged broken oxygen bonds in order to achieve charge balance. Alkali ions yield one non-bridging oxygen per cation whereas alkaline earth ions yield two non-bridging oxygens per cation. So, addition of alkaline earth ions produces more non bridging oxygens. This results in lowering the glass transition temperature and due to the reduction in cross-linking of the network, viscosity of the glass melt is lowered. The glasses which have absolutely no oxygen ions like chalcogenide glasses and heavy metal fluoride glasses do not fall under the Zachariasen ‘Random Network Theory’.

These type of non-oxide glass formation can be well described based on the ‘Kinetic Theory of Glass Formation’, since formation of these kind of glasses are subjected to the processing methodology where the kinetics of formation play a crucial role.

1.3 Glass preparation methods

Glasses can be prepared in different ways, but there are three important methods present in order to obtain glasses for practical applications. They are as follows

1. Melt quenching technique.
2. Sol-gel processing method.
3. Chemical vapour deposition method.

1.3.1 Melt quenching technique

It is one of the oldest methods used for preparation of glasses. It is a practice used to produce amorphous solid by rapid cooling (quenching) of the melt (viscous liquid) obtained by fusion of one or more precursors. Rapid cooling is used to bypass crystal nucleation and growth in order to retain the disordered state of the liquid in the solid state. In the process of melt quenching, stoichiometric proportion of fine powdered precursors are systematically mixed in an agate mortar to get glasses with desired property. The mixture is placed in a porcelain, silica or platinum crucible and melted in a furnace for a defined time period. The melt will be stirred regularly to acquire homogeneous liquid. The melt is then rapidly cooled to room temperature by squeezing the melt between two steel or bronze plates which has high thermal conductivity. A cooling rate of the order of 10 Ks^{-1} can be attained by this particular technique and is adequate for making most of the glasses. The synthesized glass samples were then annealed near the glass transition temperature (T_g) to eliminate thermal stresses developed in the process of glass formation owing to low thermal conductivity of glass. The cooling rate plays a crucial part in the process of glass formation. For some glass formers like B_2O_3 very slow cooling rate (1 Ks^{-1}) is enough and some metallic glasses need very high cooling rate of nearly 10^5 Ks^{-1} . Some of the different quenching technique and their rates of cooling are given in table 1.1

Table 1.1 Different quenching techniques and their rates of cooling.

Technique	Cooling rate (Ks ⁻¹)
Air quenching	1-10
Liquid quenching	10 ² -10 ³
Chill block splat cooling	10 ⁵
Melt spinning or melt extraction	10 ⁶ -10 ⁸

The advantages of the melt quenching technique compared to the other two methods are,

- i. The high flexibility of the geometry of a glass which is advantageous in obtaining material of large size required for the preparation of glasses with special properties.
- ii. The large flexibility of composition in preparation of glasses with a wide variety of compositions, consisting of several constituents at various ratios. It is possible because quenching of melt does not need stoichiometry among constituents. The addition of ions such as rare-earth or transition metal in comparatively lesser quantity is possible. This plays a major role in production of glasses with different properties.

The melt-quenching method has some disadvantages like it is difficult to prepare glasses of ultra-high purity and difficult to synthesize glasses having a greater quantity of refractory material such as SiO₂, TiO₂, etc., as they require extremely high temperature for melting.

1.3.2 Sol-gel processing method

Sol-gel method is one of the low temperature glass preparation techniques. Gel is an elastic solid matter formed suddenly from a sticky liquid through continuous polymerization. The gel obtained will be heat treated to eliminate the residual volatile components. The process is followed by the densification by sintering at suitable temperature to produce glass solid (Yamane and Asahara 2000). The sol-gel process is very beneficial in preparing glasses containing large quantity of refractory materials. In

this process, thermally unstable compounds can also be incorporated into glass due to the low processing temperature (especially well below the melting point) utilized. This is advantageous in preparing the glasses with unusual properties like high optical nonlinearity. The major disadvantage of this route is the formation of fracture initiated during the large shrinkage of wet gel during the heat treatment.

1.3.3 Chemical vapour deposition method

This method is used to prepare amorphous solids of polycrystalline materials. In this method, chemical decomposition of a vapour occurs promoting the deposition of a solid film on a substrate placed in plasma (Yamane and Asahara 2000). The formation of solid includes viscous sintering of the film deposited. The major benefit of this technique is the preparation of ultrahigh pure glasses. However, glasses incorporated with alkali, alkaline or rare-earth elements cannot be prepared using this method.

1.4 Classification of glass systems

Glass is one of the major oldest artificial materials in the history of mankind. There are wide variety of glass systems available depending on the network former used. Among all, the most exploited class of glasses are the oxide based glasses. They can be classified into categories called borates, phosphates, silicates, borosilicates, aluminium silicates, chalcogenide glasses etc. In addition, chalcogenide glasses, halide glasses, heavy metal fluoride glasses, metallic glasses and organic glasses are some of the other types of glasses which are of immense interest. Some of the important class of glasses are mentioned in the following section.

1.4.1 Chalcogenide glasses

These are the glass systems containing chalcogene elements viz., sulphur, selenium and tellurium of Group VI of the periodic table. In combination with other elements from III, IV or V group viz., As, Sb, Ge, Si etc, a wide variety of chalcogene glasses with outstanding properties can be prepared by melting these elements in an oxygen-free ambiance. Chalcogenide glasses exhibit band gap of the order 1-3 eV and

therefore behave as semiconductors with conductivity in the range of 10^{-3} to 10^{-13} ohm⁻¹ cm⁻¹. The atoms in these glasses are connected through covalent bonds in their structure whereas the oxide and halide glasses contain ionic bonds. In addition, the melts of these glasses contain rings and chains of sulphur, selenium and tellurium atoms. These glass systems are promising candidates for applications like fiber optics and X-ray imaging plates, IR transmission, host materials for IR lasers, switching devices for computer memories, xerography etc. (Fairman and Ushkov 2004).

1.4.2 Halide and Oxy-Halide glasses

Halide glasses are formed by rapidly cooling the melt of halides viz., BeF₂ and ZnCl₂ (K.J. Rao 2002). These glasses are widely in use owing to the least refractive index (RI) and highest Abbe number. The halides are tetrahedrally coordinated Be and Zn, with halogens forming bridges between the tetrahedra. The chemical bond in these systems are ionic in nature, and therefore they show certain desirable properties like good transparency to the IR radiation, low glass transition temperature, low phonon energies and acts as hosts for active rare earth ions (Adam 2001). The low linear and non-linear RI of BeF₂ enable these glasses to be used for high-power laser applications when doped with TM ions like Nd³⁺. The drawback of halide based glasses limiting their usage in practical applications is their toxicity and extreme hygroscopic behaviour. But, the halide glasses in combination with the oxide glasses, oxy-halide glasses in particular, are very interesting in terms of practical applications (Nazabal et al. 2012). The oxy-halide fluorophosphate glasses are used as host material for high power laser systems as they exhibit low dispersion and a low non-linear RI. The oxy-halide PbF₂-SnF₂-P₂O₅ glass system shows very low glass transition temperature and possesses excellent chemical durability.

1.4.3 Oxide glasses

Oxide glasses are mainly classified as

1. Silicate glasses

2. Phosphate glasses
3. Germanate glasses
4. Telluride and Vanadium glasses
5. Borate glasses

1.4.3.1 Silicate glasses

Silicate glasses are the most extensively investigated glasses, due to their commercial importance as they possess good chemical and weathering stability. In silicate glasses SiO_2 tetrahedron acts as glass former and appropriate modifiers are added to reduce the melting point of the silica. Modifiers are used to yield non-bridging oxygen and thereby reduce the melt viscosity. Silica glasses show a superior refractory nature, thermal shock resistance, optical transparency in both the UV and visible regions, and great chemical durability (Yamane and Asahara 2000). These glasses are mainly used in the semiconductor industry, photolithography and in opto-electronic (OE) devices.

1.4.3.2 Phosphate glasses

The network former in phosphate glass is P_2O_5 . Phosphate glasses consist of P-O-P chains of four-fold coordinated phosphorous. They consist of polymeric arrangement of PO_4 tetrahedral units. These glasses have the ability to accommodate high concentrations of transition metal ions and still remain amorphous (Shelby, 2005). Phosphate glass has proved to be very suitable, optically transparent dielectric material medium for growing small noble metal nanoparticles without any atmospheric oxidation and contamination (Uchida et al. 1994). These glasses can be easily synthesised due to their low glass transition temperature (T_g) and low melting temperature (T_m). They are used in various applications viz., solid state lasers (Shah et al. 2006, Arbuzov 2013), fast ion conductors (Martin 1991, Sdiri et al. 2015), non linear optical devices (Nazabal et al. 2012), nuclear waste vitrification (Krishnaiah et al. 2014) and biomedical industry (Hench 2006) because of their high thermal expansion coefficient (α) and biocompatibility (Pavie et al. 2014). They are also used as achromatic optical materials owing to the low dispersion and high RI compared to that

of silicate based optical glasses. On the other hand, poor thermal stability against crystallization, low chemical durability, volatile and hygroscopic nature of phosphate glasses limit their extensive practical applications (Sastry and Rao 2014, Harada et al. 2004).

1.4.3.3 Germanate glasses

Germanate glasses are prepared using GeO_2 as glass forming oxide. They consist of random 3D network of Ge-O-Ge bonds. These systems are studied in view of their academic interest as they have limited practical applications due to expensive raw materials and high melting point. They are used only for special applications like infrared transmitting glass. they possess higher infrared transmission properties compared to other silica glasses which make them potential material for ultra-low-loss optical fiber.

1.4.3.4 Telluride and Vanadium glasses

TeO_2 and V_2O_5 are also used for the preparation of glasses with special properties. Because of high refractive index, telluride glass is used as a nonlinear optical glass with ultra-fast response. V_2O_5 combined with P_2O_5 is used to prepare electronic conducting semiconductor glasses.

1.4.3.5 Borate glasses

Boric oxide (B_2O_3) is the network former of borate glass system. B_2O_3 is considered as one of the best network former attributing to its higher bond strength, lower cation size and smaller heat of fusion. Borate glasses are always treated as unique and special as they do not act as expected compared to other major glass forming oxides like silicates and phosphates. For example, (a) even though the bond between B-O is slightly stronger compared to the bond between Si-O, at 1200°C , the viscosity of liquid B_2O_3 is almost eleven order of magnitude lower than that of super-cooled liquid SiO_2 , (b) the glass transition temperature of vitreous B_2O_3 is 280°C which is considerably lesser compared to vitreous SiO_2 which is 1190°C (c) incorporation of network modifiers into silicate glass matrix results in variation of glass properties monotonically

with the variation of modifiers concentration, whereas in case of borates instead of monotonical variation, they exhibit an extrema at particular modifier concentration. This kind of borate behaviour which is exceptional is often referred as ‘borate anomaly’, and (d) at ambient pressure, pure anhydrous borates do not get crystallize, because in the case of B_2O_3 , crystallization is inhibited by the very high activation energy required to break up the boroxol groups, leading to zero nucleation and growth rates.

1.4.3.5.1 Structure of Borate Glass

Pure anhydrous B_2O_3 is made up of planar BO_3 units which are arbitrarily positioned by sharing the oxygen atoms with neighbouring BO_3 units in a three-dimensional network.

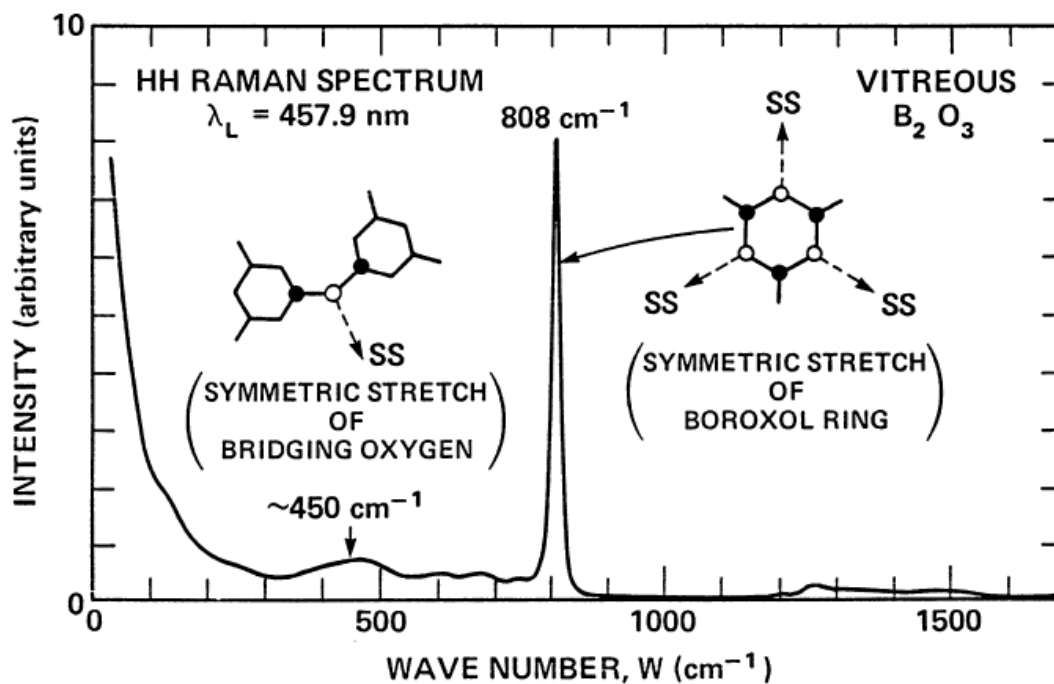


Figure 1.3: Raman band corresponding to boroxol ring structure in vitreous B_2O_3 (Galeener and Geissberger 1982).

The planar BO_3 unit apparently involved in SP^2 hybridization, while the third orbital will be unfilled and prolonging in the direction which will be perpendicular to the BO_3 plane. In order to have partial double bond, this unfilled orbital readily accepts

unpaired electrons from the oxygen atoms. It is believed that these BO_3 triangular units will join together and formulate a well-defined ring structure, known as ‘boroxol ring’ or ‘boroxol group’ which will be present in vitreous B_2O_3 in a large concentration. Existence of these boroxol rings was further supported by the presence of sharp band at 808 cm^{-1} in Raman spectrum. The Boroxol ring structure and the supporting Raman spectral observation are represented in figure 1.3.

1.4.3.5.2 Alkali Borate Glass

Borate glass gathered the significant attention of scientific community starting from 1936 till today due to its structural diversity which is not found in other oxide glasses. Introduction of modifier into borate matrix may results in (a) breaking up of B-O-B bonds by oxygen anions in order to create non-bridging oxygen, (b) the overlapping oxygen anions filled orbital with vacant p-orbital of boron atom leads to change in hybridization of boron atom to sp^3 tetrahedra. This results in the conversion of BO_3 triangular unit to BO_4 tetrahedral unit, and (c) an oxygen atom could perhaps donate a pair of electrons to the two BO_3 units which may result in conversion of sp^2 to sp^3 hybridization leading to change in the coordination of boron atom without creating any non-bridging oxygen.

Warren et al, in 1936, for the first time carried out a detailed structural study on the alkali borate glasses. They confirmed that the BO_3 units are linked together by sharing the oxygen atoms in a three dimensional random network as proposed by Zachariasen. The Zachariasen two dimensional representation of borate glass network is shown in figure 1.4 (a) which is recently redrawn in colour by Wright (2015). Later in the year 1938, Biscoe and Warren reported that the addition of alkali metal (Na_2O) modifier oxide to borate glasses converts the triangular BO_3 unit into tetrahedral BO_4 unit. Figure 1.4 (b) represents the two-dimensional glass network of Na_2O incorporated boron glass matrix, where the network modifying Na^+ cation occupied the interstices position in the borate glass network adjacent to the BO_4 tetrahedra. This change in coordination of boron atom led the authors to propose structural explanation for the ‘boron anomaly’. Finally, in 1960 the most important two features of borate structure were reported and made borate glasses stand unique among other oxide glasses. These

are (i) the incorporation of network modifier cation to the borate network at first involves the conversion of triangular BO_3 unit to tetrahedral BO_4 units rather than creating the non-bridging oxygen atoms. The creation of non-bridging atoms takes place only at higher concentration of network modifier cations, and (ii) As the concentration of network modifier increases up to the certain level which exhibits diborate composition, the structure of borates are mainly dominated by the superstructure units.

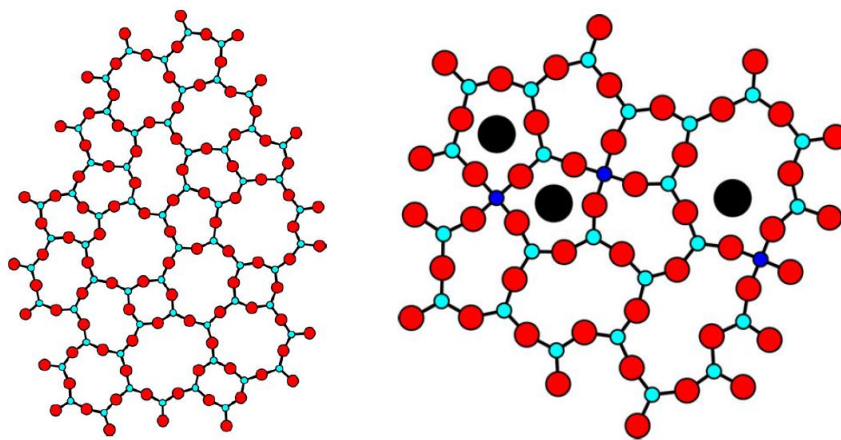


Figure 1.4: (a) Two-dimensional Zachariasen's random network diagram and (b) two-dimensional representation of vitreous $\text{Na}_2\text{O}-\text{B}_2\text{O}_3$ structure (Note for colour representation: blue: tetrahedral boron atom, cyan: trigonal boron atom, red: bridging oxygen atom and black: Na^+ cation). (Wright 2015)

These two characteristics of the borate glasses are mainly responsible for the unusual behaviour in the properties of borate glasses, which is called as boron anomaly. In the year 1958, Silver and Bray (Silver and Bray 1958) confirmed the change in boron coordination number using ^{11}B NMR spectroscopy technique for the first time, followed by this in the year 1963 by another important article (Bray and O'keefe 1963) which gave a clear insight into the basic structure of borate glasses depending on the modifier concentration. Hence the conversion of coordination number from 3- to 4-fold of boron atom was justified and it gave a clarity that creation of non-bridging oxygens takes place only at higher concentration of alkali cations.

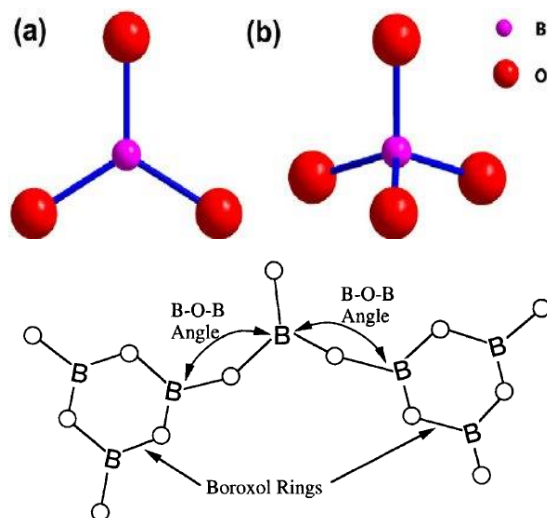


Figure 1.5: Schematic representation of (a) BO_3 unit, (b) BO_4 unit, and (c) boroxol group in borate glass matrix. (Wright 2015)

Thus incorporation of modifier alkali oxides to the borate glass network glasses mainly consist of triangular BO_3 units, tetrahedral BO_4 units and boroxol rings which are represented in figure 1.5. Further increase in the concentration of alkali content, eventually results in disappearance of boroxol rings. This is validated by the Raman spectra where the high intense band at 808 cm^{-1} (corresponds to boroxol rings) gradually decreases and disappears. On the other hand the tertaborates groups start converting into diborate groups which consist of two-tetrahedra per three membered ring. Finally, incorporation of alkali content about 25 mol% begins to create the non-bridging oxygens, all these composition dependent structural modifications were represented in figure 1.6. Superstructural units are some features which make borate glasses unique when compared to other oxide glasses. Superstructural units are basically rigid and combination of the fundamental structural units of borate glass which do not have any kind of internal degree of freedom in the form of variable bond or bond torsion angle. These are mainly based on three-membered rings of fundamental structural units. In the year 1960, Krogh-Moe (Moe 1960) published an article, which later turned out as a milestone in the history of borate structures. This explained the vital role of superstructural unit in the borate network., particularly in the case of lithium and sodium diborate glasses. In case of these $\text{Li}_2\text{O}-2\text{B}_2\text{O}_3$ and $\text{Na}_2\text{O}-2\text{B}_2\text{O}_3$ glass compositions Krogh-Moe (1958) proposed a structure which is completely

created on the basis of diborate groups (Krogh-Moe 1958, 1960, 1962, 1965). The distribution of superstructural units in the sodium borate glasses was explained up to the diborate composition.

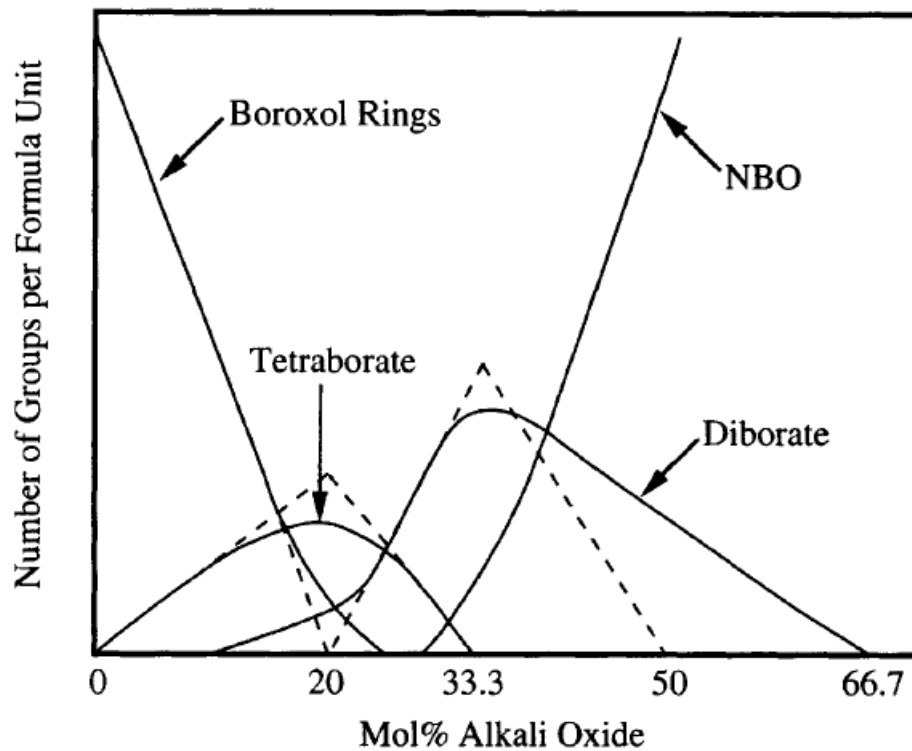


Figure 1.6: Schematic representation of modifier alkali concentration dependent intermediate structures (dashed lines represents theoretical variations and solid lines represents experimental results). (Shelby 2005)

This suggestion of Krogh-Moe was well captured by Griscom et. al. (1978) and they articulated the model for superstructural unit which led them to propose a complete structural model for borate glasses. This proposed model clearly convinced the fact that superstructural units connect together in order to form a random network in borate glasses rather than basic structural units. The schematic representation of superstructural units of borate glass network is represented in figure 1.7. The network modifying cations play a vital role in determining the structure and properties of borate glasses. It is crucial to understand that all the property changes of borate network are mainly influenced by the concentration of the modifier content. Another significant aspect of modifying cations are that they simply do not enter and occupy the space

formed by the surrounding vitreous glass network, rather they effectively modify their surrounding in order to fulfil their own specific requirements. In this regard the size (radius) of the network modifying cation plays an important role since it determines the space in which it enters to modify and reside in the network.

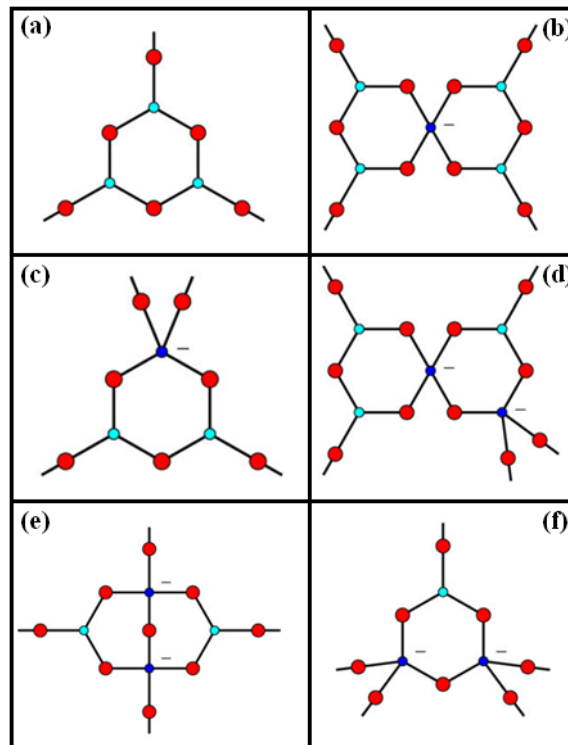


Figure 1.7: Borate superstructural units (Wright 2015) (a) boroxol group, (b) pentaborate group, (c) triborate group, (d) di-pentaborate group, (e) diborate group, and (f) di-triborate group

On the other hand, their nominal charge also should get compensated by the appropriate number of negative charges which is usually compensated by negatively charged tetrahedral BO_4 unit or by the non-bridging oxygen atom. Hence alkaline and alkaline earth modifiers bonding to non-bridging oxygen atoms show substantial covalent nature. Hence these glasses cannot be considered as purely ionic.

1.4.3.5.3 Boron oxide anomaly

Boron oxide anomaly or boron anomaly is the one of the unique properties of borate glasses. This is not seen in any other oxide glasses like silicate or phosphate glasses. As discussed in the introduction part of the borate structures, in other oxide glass systems when the modifier cation concentration increases the corresponding property of the glass system varies monotonically but in the case of borate glass system with a particular concentration of modifier cations, properties of the borate glasses show extreme behaviour which is not a usual trend in other oxide glass systems. For example, in case of sodium-borate glass system viscosity of the melt increases gradually with increasing mol % of sodium oxide content and suddenly attains a maximum value of viscosity at 16 mol% of sodium oxide content. In the same way thermal expansion coefficient exhibits a noticeable minimum at about 16 mol % of sodium oxide. According to Biscoe and warrens (1938) the incorporation of each alkali ion to boron oxide results in converting the triangular BO_3 unit into tetrahedral BO_4 unit without creating any non-bridging oxygen up to certain level of alkali concentration. Hence the connectivity increases which results in lowering the thermal expansion coefficient. The conversion of coordination number of boron atom stops at around 16 mol % of incorporated alkali content, thereafter, further addition of alkali oxides leads to the creation of non-bridging oxygens. This causes increase in expansion coefficient and decrease in viscosity. This kind of extreme behavior exhibited by borate glass system is often termed as 'boron anomaly' or 'boron oxide anomaly'.

1.4.3.5.4 Mixed alkali effect

If one alkali cation is progressively substituted by another alkali cation without disturbing the total alkali cation content, a few properties which are related to the movement and presence of alkali ions exhibit a maxima or minima variation with respect to alkali content. This behaviour is generally referred to as Mixed Alkali Effect (MAE). There are certain properties like ion diffusion, chemical durability, electrical conductivity, electrical loss and viscosity which are directly associated with the alkali ion movements with large deviation from linearity. On the other hand, the properties like density, refractive index and micro-hardness exhibit relatively less deviation (Day

1976, Isard 1969, Ahmed and Abbas 1986). In alkali borate glass system, each alkali oxide is associated with a proportional quantity of B_2O_3 so that the number of structural units depends on the nature and total concentration of the incorporated modifiers (Shelby 2005, Varshneya 1994.). Mixed alkali effect is useful in controlling the properties according to desired technological applications by selecting suitable modifiers (Day 1976). Therefore, understanding the mixed alkali effect is essential in order to gain the knowledge of physics and chemistry behind it. In fact, many theoretical models have been proposed for MAE (Maass 1999, Bunde et al. 1991, Van Ass and Stevels 1974a, 1974b). However, there is no generalized model present till date which can be applied to all possible oxide glass systems. Hence there remains a scope for experimental investigation in this regard. In recent years there has been extensive studies published on different types of alkali borate glass system.

Doweidar et al. (2008) extensively studied the density of mixed alkali borate glasses and noted that the ratio of alkali oxide/boron in any case would be that of the total alkali oxide/total boron oxide. In spite of the great change with composition of the volume of structural units in alkali borate glasses, the volumes of the borate structural units in mixed alkali glasses are the same as found in the corresponding binary alkali borate glasses. This conclusion would be useful for calculating the density and molar volume of multiple alkali borate glasses.

Focus has been also given to understand the mixed alkali effect in Vickers hardness measurements (Mohajerani and Zwanziger 2012). It has been concluded that the increase in the hardness of mixed alkali glasses is mainly due to their decreased plastic deformation, rather than any marked variation in their densification. The mixed alkali effect was also found less strongly in the length of measured radial cracks which may be due to the mixed contributions of Young's modulus on residual stresses and fracture toughness. The authors concluded that mixed alkali glasses showed modestly shorter cracks than single alkali glasses. This knowledge is certainly required to design the glasses for practical applications where hardness of the glass plays vital role.

1.4.3.5.5 Transition metal doped alkali borate glasses

One of the significant properties of glasses is their unique ability to accommodate various types of dopants, such as rare earth ions, transition metal ions, metal nanoparticles, etc. (Yamane and Asahara 2000). Any foreign atom can easily find a place to occupy inside the glass matrix because of its random network structure. The flexibility of chemical composition of glass facilitates the synthesis of glasses with special properties through doping of active elements. Transition metal (TM) doped oxide glasses possess both scientific and technological interest owing to their wide range optical properties. This is due to the presence of TM ions with varying valencies or co-ordinations with their respective colors (Ehrt et al. 2000) They also find potential applications in solid state lasers, optical filters, and optical fibers for communication devices (Sanghera et al. 2002).

In the recent developments, novel compositions (Flower et al. 2007) with superior physical and chemical properties such as high thermal expansion coefficients, low melting and softening temperatures and high ultra-violet and far infrared transmission (Liu et al.1997), make alkali borate glasses potential candidates for many technological applications, such as sealing materials, medical uses (Li et al. 2008), and solid state electrolytes (Brown et al. 2001). Among all, the transition metals ions (TMI), like Cr, Fe, Mn, Ni and Co doped borate glasses find enormous applications in microelectronics, optical glasses and solid state lasers (Wu et al.1999, Bogomolova et al. 1980). The TM ions doped alkali borate glasses exhibit non-linear behaviour which has applications in solid state devices, electro-optic modulators & switches, and non-linear optical parametric converters (Nazabal et al. 2001, Moustafa et al. 2013). The formation and the nature of the color centers in different types of glasses have received a considerable attention (Nazabal et al.2001). Doping of TM ions having multiple valences may enhance or reduce the coloration by changing the valence state or by trapping the released electrons, respectively. TM ions possess more than one valence state, broad radial distribution of outer d-orbital electron functions and are very sensitive to the change in the surrounding cations. This has considerable influence on the optical, electrical and magnetic properties of glasses (Naresh and Buddhudu 2012).

Zinc oxide possesses large band gap and therefore it is a potential candidate for applications in OE devices like laser diodes and laser emission covering a wide visible region (Ding 2008). Zinc oxide added borate glasses are potential candidates for applications in plasma display panels for high quality and performances (Gaafar et al. 2009, Raju et al. 2006). They are also used for large area, hang-on-wall TVs and computer monitors. Krishna et al. (2012) have reported that the divalent Zn acts both as network former and modifier in the glass network.

In the recent past Bhogi et al. (2018) investigated 15BaO-25Li₂O-(60-x) B₂O₃: xFe₂O₃ where x = 0, 0.2, 0.4, 0.6, 0.8 and 1 mol% glass system using RPR and UV Visible spectroscopy. They observed EPR spectra of Fe³⁺ ion to have resonances at g = 2.0032, 4.282 and 8.033. They noticed optical absorption spectra exhibiting a band at around 452 nm which was assigned to ⁶A_{1g}(S) → ⁴E_g(G) of Fe³⁺ ions with distorted octahedral symmetry. They found decrease in optical band gap energy (E_{opt}) with increase in iron ion concentration. This showed that the glasses become more semiconducting in nature and the Urbach energy values affirm the increase in defects with the increase of iron ion concentration in these glasses.

Moustafa et al. (2013) have studied the effect of gamma radiation on ultraviolet, visible and infrared optical studies of NiO, Cr₂O₃ and Fe₂O₃-doped alkali borate glasses. They observed that the borate glasses with basic composition xR₂O(100 - x)B₂O₃ where R = Na, K, were colored by adding one of or the mixture of TM ions like Ni, Cr, Fe. They observed a shift in the positions of the absorption bands according to the alteration of the composition of the base glass. The corresponding changes in the optical absorption of these glasses containing mixed NiO, Cr₂O₃ and Fe₂O₃ dopants are associated to the coordination or valence states of the TM ions.

Gaafar et al. (2009) have investigated the longitudinal and shear ultrasonic wave velocities in binary Li₂O-2B₂O₃ glasses doped with different TM ions like V₂O₅, Fe₂O₃, Cr₂O₃, NiO, TiO₂, MnO₂ and CuO using pulse echo technique. They have reported that both longitudinal and shear ultrasonic velocities and the Debye temperature values are increased with addition of small amounts of different TM ions. They attributed this to the increase in connectivity of the network structure. Elastic moduli and Poisson's ratio

increased, calculated values of thermal expansion coefficient decreased and number of bonds per unit volume increased, indicating the increase in rigidity of the network structure.

1.5 Scope and objective of the present research work

1.5.1 Scope

Designing glasses with unique functional properties is a topic of active research in view of providing solution to long standing problems in modern glass science and technology. Applications like photonics switching and information processing depend critically on the development of improved glass materials. This can be achieved by preparing glass materials with various dopants available such as rare earth ions, transition metal ions, chalcogenides, halides etc., as glasses possess inimitable capability to contain various dopants. Glasses are the best hosts for embedding active elements for the development of special properties like colour, high nonlinear susceptibility, emission of fluorescent light, etc. It is known that the chemical composition of glassy materials controls most of the properties of them. Doping of alkali ions into borate glass introduces interesting structural variations by creating BO_3 and BO_4 structural units and forming Non Bridging Oxygens (NBOs). These structural variations, pertaining to the mixed alkali effect (MAE), greatly controls the physical parameters of borate glasses. MAE enables the researchers to produce glasses according to industrial needs. In the present work, relatively less quantity of transition metal (less than 1mol%) ions are added which can considerably modify the optical properties of glasses with improved thermal and mechanical properties. These kind of glasses can be used as optical filters and in electro optical devices etc.

In the literature one can find a large number of studies on two-alkali borate glasses and mixed alkali effect but no serious systematic attempts have been made to understand the effect of adding third alkali ion into the two-alkali borate glass system. Hence, the present work is taken up to prepare, characterize and study the effect of incorporation of third alkali ion into two-alkali borate glass system in order to give clear insight into MAE in three-alkali borate system. In a similar way, transition metal ions

are added into both two and three alkali zinc borate glass system in order to develop glass materials with improved optical, thermal and mechanical properties.

1.5.2 Objectives

The main objective of this research is the synthesis and characterization of the two and three alkali zinc-borate glass system to explore the mixed alkali effect and to study the effect of addition of transition metal ions. This research focuses on

- Optimization of the influencing parameter like melting and calcination temperature, soaking time to obtain homogeneous alkali zinc borate glasses.
- Synthesis of alkali zinc-borate glasses of different compositions of $5\text{Li}_2\text{O}-(25-x)\text{K}_2\text{O}-x\text{Na}_2\text{O}-60\text{B}_2\text{O}_3-10\text{ZnO}$ ($x= 0, 5, 10, 15, 20$ and 25 mol%).
- Synthesis of transition metal doped alkali zinc-borate glasses of two and three alkali system of composition $5\text{Li}_2\text{O}-x\text{K}_2\text{O}-(25-x)\text{Na}_2\text{O}-60\text{B}_2\text{O}_3-(10-y)\text{ZnO}-y\text{TMO}$ ($x= 0$ and 5 mol%, $y= 0$ and 0.1 mol % and TMO= oxides of Cr, Mn, Fe, Co, Cr and Ni)
- Synthesis of transition metal doped alkali zinc-borate glasses of different compositions of $5\text{Li}_2\text{O}-(25-x)\text{K}_2\text{O}-x\text{Na}_2\text{O}-60\text{B}_2\text{O}_3-(10-y)\text{ZnO}-y\text{TMO}$ ($x= 0$ and 5 mol%, $y= 0, 0.1, 0.3, 0.5, 0.7$ and 0.9 mol% and TMO= Fe_2O_3 and MnO_2).
- Structural investigation of synthesized glasses using X-ray diffraction (XRD), Fourier transform infrared (FTIR) spectroscopy, Scanning electron microscopy (SEM).
- Study of optical properties like optical band gap energy, Urbach energy and refractive index of the prepared samples.
- Study of the thermal properties like glass transition temperature, crystalline temperature and melting temperature of the synthesized glass samples using Differential thermal analysis (DTA).
- Study of the mechanical properties like micro hardness, fracture toughness and brittleness by indentation technique.

1.6 Organization of the thesis

The thesis is organized as follows

- Chapter 1 includes a brief general overview to various glasses and their properties. In particular, it includes thorough introduction of oxide glasses, specially, the borate glasses. A brief overview of theory of glass formation, glass preparation techniques and methodology is discussed in this chapter. This chapter includes brief literature review on the properties and applications of borate glasses. It also includes the scope and objective of the present research work.
- Chapter 2 includes detailed description of materials and synthesis techniques used for the preparations of glasses proposed under the present research work. Various structural and morphological characterization techniques used such as XRD, FTIR, Raman and SEM are discussed briefly in this chapter. Also the method used for investigating physical, optical and mechanical properties of glasses are discussed in detail.
- Chapter 3 presents the results on structural, physical, optical, thermal and mechanical properties of glass system with composition $5\text{Li}_2\text{O}-(25-x)\text{K}_2\text{O}-x\text{Na}_2\text{O}-60\text{B}_2\text{O}_3-10\text{ZnO}$ ($x=5, 10, 15, 20$ and 25 mol%) prepared using melt-quenching technique. The chapter also includes a brief summary of the investigation carried out on this system of glasses.
- Chapter 4 presents the results on structural, physical, optical and mechanical properties of glass system with composition $5\text{Li}_2\text{O}-x\text{K}_2\text{O}-(25-x)\text{Na}_2\text{O}-60\text{B}_2\text{O}_3-(10-y)\text{ZnO}-y\text{TMO}$ ($x=0$ and 5 mol%, $y=0.1$ and TMO= oxides of Cr, Fe, Mn, Co and Ni). This chapter presents the effect of TMO on two alkali and three alkali system.
- Chapter 5 presents the results on structural, physical, optical, thermal and mechanical properties of glass system with composition $5\text{Li}_2\text{O}-x\text{K}_2\text{O}-(25-x)\text{Na}_2\text{O}-60\text{B}_2\text{O}_3-(10-y)\text{ZnO}-y\text{TMO}$ ($x=0$ and 5 mol%, $y=0, 0.1, 0.3, 0.5, 0.7$ and 0.9 mol% and TMO= Fe_2O_3). This chapter discusses the effect of Fe_2O_3 on properties of the synthesized glasses and gives a detailed

comparison between the effect of Fe_2O_3 on two alkali and three alkali glass system.

- Chapter 6 presents the results on structural, physical, optical, thermal and mechanical properties of glass system with composition $5\text{Li}_2\text{O}-x\text{K}_2\text{O}-(25-x)\text{Na}_2\text{O}-60\text{B}_2\text{O}_3-(10-y)\text{ZnO}-y\text{TMO}$ ($x= 0$ and 5 mol%, $y= 0, 0.1, 0.3, 0.5, 0.7$ and 0.9 mol % and $\text{TMO}=\text{MnO}_2$). This chapter discusses the effect of MnO_2 on properties of the synthesized glasses and gives a detailed comparison between the effect of MnO_2 on two alkali and three alkali glass system
- Chapter 7 summarizes the important findings of the present research work along with conclusions. This chapter also comprises of scope for further research work in the area of borate glass system.

Chapter 2

MATERIALS AND METHODS

2.1 Glass Synthesis

In the present investigation alkali zinc-borate glasses of different compositions have been prepared. Glass systems with two and three alkali elements were prepared to investigate in detail the mixed alkali effect (MAE) in these systems. The glass system with composition $5\text{Li}_2\text{O}-(25-x)\text{K}_2\text{O}-x\text{Na}_2\text{O}-60\text{B}_2\text{O}_3-10\text{ZnO}$ ($x=0, 5, 10, 15, 20$ and 25 mol%) was synthesized using melt-quenching technique. Also, transition metal doped alkali zinc-borate glasses of different compositions were synthesized and the effect of transition metals in two and three-alkali borate glass system was studied. Number of preliminary experiments were carried out to optimize multiple synthesis parameters to get homogeneous glasses.

2.1.1 Precursors and compositions used

Alkali zinc-borate and transition metal doped alkali zinc-borate glasses of various compositions were prepared through melt-quenching technique using high purity (99.9% - Analytical Grade chemicals supplied by Sigma Aldrich) precursors viz., Lithium carbonate (Li_2CO_3 with 99.9% purity), Sodium carbonate (Na_2CO_3 with 99.8% purity), Potassium carbonate (K_2CO_3 with 99.9% purity), Boric acid (H_3BO_3 with 99% purity), Zinc oxide (ZnO with 98% purity), Chromium carbonate (Cr_2CO_3 with 99% purity), Manganese oxide (MnO_2 with 99% purity), Iron Oxide (Fe_2O_3 with 99% purity), Cobalt carbonate (Co_3CO_4 with 99% purity) and Nickel carbonate (Ni_2CO_3 with 99% purity). The compositions of the glasses prepared in the present investigation and their nomenclature are given in table 2.1, table 2.2, table 2.3, and table 2.4.

Table 2.1 : Batch composition of three-alkali zinc borate glass system and their nomenclature.

Glass system	Glass code	Li ₂ O (mol%)	Na ₂ O (mol%)	K ₂ O (mol%)	B ₂ O ₃ (mol%)	ZnO (mol%)
LNK	A1	5	-	25	60	10
	A2	5	05	20	60	10
	A3	5	10	15	60	10
	A4	5	15	10	60	10
	A5	5	20	05	60	10
	A6	5	25	-	60	10

Table 2.2 : Batch composition of TMO doped two and three-alkali zinc borate glass system and their nomenclature.

Glass system	Glass code	Li ₂ O (mol%)	K ₂ O (mol%)	Na ₂ O (mol%)	B ₂ O ₃ (mol%)	ZnO (mol%)	TMO
LN-TM	A6	5	-	25	60	10	-
	Cr1	5	-	25	60	9.9	0.1 Cr
	M1	5	-	25	60	9.9	0.1 Mn
	F1	5	-	25	60	9.9	0.1 Fe
	Co1	5	-	25	60	9.9	0.1 Co
	N1	5	-	25	60	9.9	0.1 Ni
LNK-TM	A5	5	5	20	60	10	-
	KCr1	5	5	20	60	9.9	0.1 Cr
	KM1	5	5	20	60	9.9	0.1 Mn
	KF1	5	5	20	60	9.9	0.1 Fe
	KCo1	5	5	20	60	9.9	0.1 Co
	KN1	5	5	20	60	9.9	0.1 Ni

Table 2.3: Batch composition of Fe₂O₃ doped two alkali and three alkali glass system.

Glass system	Glass code	Li ₂ O (mol%)	K ₂ O (mol%)	Na ₂ O (mol%)	B ₂ O ₃ (mol%)	ZnO (mol%)	Fe ₂ O ₃ (mol%)
LN-Fe	A6	5	-	25	60	10	-
	F1	5	-	25	60	9.9	0.1
	F3	5	-	25	60	9.7	0.3
	F5	5	-	25	60	9.5	0.5
	F7	5	-	25	60	9.3	0.7
	F9	5	-	25	60	9.1	0.9
LNK-Fe	A5	5	5	20	60	10	-
	KF1	5	5	20	60	9.9	0.1
	KF3	5	5	20	60	9.7	0.3
	KF5	5	5	20	60	9.5	0.5
	KF7	5	5	20	60	9.3	0.7
	KF9	5	5	20	60	9.1	0.9

Table 2.4: Batch composition of MnO₂ doped two alkali and three alkali glass system.

Glass system	Glass code	Li ₂ O (mol%)	K ₂ O (mol%)	Na ₂ O (mol%)	B ₂ O ₃ (mol%)	ZnO (mol%)	MnO ₂ (mol%)
LN-Mn	A6	5	-	25	60	10	-
	M1	5	-	25	60	9.9	0.1
	M3	5	-	25	60	9.7	0.3
	M5	5	-	25	60	9.5	0.5
	M7	5	-	25	60	9.3	0.7
	M9	5	-	25	60	9.1	0.9
LNK-Mn	A5	5	5	20	60	10	-
	KM1	5	5	20	60	9.9	0.1
	KM3	5	5	20	60	9.7	0.3
	KM5	5	5	20	60	9.5	0.5
	KM7	5	5	20	60	9.3	0.7
	KM9	5	5	20	60	9.1	0.9

2.1.2 Experimental Procedure

Melt quenching method has been employed to prepare the glass samples of proposed composition.

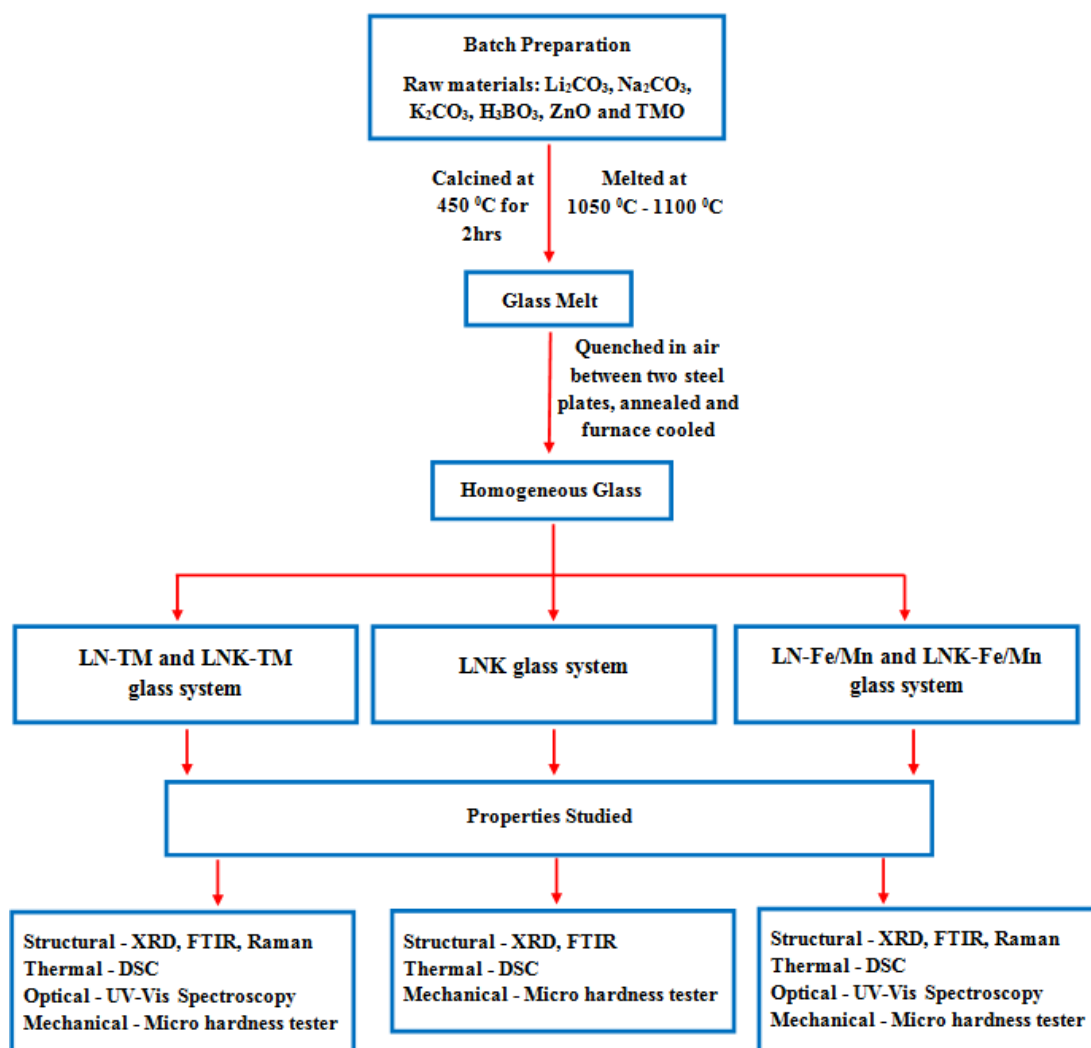


Figure 2.1. The process flow of preparation and characterization of alkali zinc-borate glass systems.

The precursors corresponding to batch composition were weighed using sensitive analytical balance with a precision of 0.1mg and then mixed in an agate mortar thoroughly for about 30 to 45 min. The homogeneous mixture was then transferred to an alumina crucible and calcined at $450\text{ }^\circ\text{C}$ for 2 hr in an electric furnace. After calcination the content of crucible was again transferred to agate mortar, ground

thoroughly and then melted at 1050-1100 °C about an hour in muffle furnace. The glass melt was swirled frequently in order to avoid bubble formation. Further, the melt was rapidly quenched between the well-polished steel plates maintained at 100 °C to get bubble free disc shaped glass samples. The as prepared glass samples were quickly transferred to an electric furnace and annealed at 400 °C for 2 hours in order to remove the residual internal stresses evolved during quenching process. The process flow of preparation and characterization of proposed glass systems is given in figure 2.1.

2.1.3 Surface polishing of the sample

The synthesized glass samples were fine polished on both sides to obtain flat surfaces with fine optical quality and suitable for investigating mechanical properties. Grinding and polishing of glasses were performed on motorised polishing machine (Chennai Metco, Grinder-Polishing machine). Silicon carbide abrasive sheets with various grit size from 120 to 2000 were used to achieve optically smooth surface. Then, final polishing was carried out using silk cloth to remove possible scratches created by abrasive sheets to obtain smooth optical quality surfaces. The samples were then subjected to ultrasonic cleaning to eliminate the residues of polishing agents. These fine polished samples were then used for the optical, electrical and mechanical characterization.

2.2 Sample characterization

The synthesized glass samples were subjected to various studies viz., structural, morphological, thermal, mechanical and optical to investigate their various properties. Structural and morphological properties of the prepared glass samples were examined using X-ray diffraction (XRD), Fourier transform infrared (FTIR) spectroscopy, Raman spectroscopy and Scanning electron microscopy (SEM). Density of the samples was measured using the Archimedes principle. The optical properties of the samples were studied using the UV-Visible spectroscopy and refractive index measurements. Thermal properties were studied using Differential scanning calorimeter (DSC). The mechanical properties of the samples were studied using Vickers micro indentation measurement.

2.2.1 X-ray diffraction (XRD)

It is one of the most powerful non-destructive structural characterization methods used to analyze the crystal structure, geometry, identification of unknown materials and defects etc. In the present investigation, to confirm the amorphous nature and identify presence of phases, all the prepared samples were characterized using X-ray diffraction (XRD) using a Bragg-Brentano diffractometer (PANalytical – X'Pert Pro MPD) with $\text{CuK}\alpha_1$ radiation in the diffraction angle (2θ) range of 10° to 80° with the scan rate of $2^\circ/\text{min}$.

2.2.2 Fourier Transform Infrared (FTIR) spectroscopy and Raman spectroscopy

Owing to the lack of availability of a particular method to study the structure of an amorphous materials, the determination of structure in glasses is a complex task (Meyer 1997). FTIR and Raman are two essential tools, which demonstrate dependence of local structure on composition and help to comprehend the effect of composition on glass properties (Velli et al. 2005). It is observed that, certain transitions that are allowed in Raman are forbidden in IR spectroscopy. So these techniques are often used in complementary way to determine the structure of materials. These complimentary techniques proved to be extremely important in differentiating the trigonal and tetrahedral borate units and to determine the concentration of NBOs per unit. In addition, they are also helpful in identifying the local building units constituting the glass network and the anionic sites hosting the modifying metal cations and super structural units, such as rings and chains, or the combination of rings. Hence both these techniques are used to study short and intermediate range ordering in a glass.

2.2.2.1 Fourier Transform Infrared (FTIR) spectroscopy

It is one of the vibrational spectroscopic techniques used to reveal the existence of various structural groups in the glasses. Various chemical bonds in a molecule or molecular structure of materials can be identified by analysing the infrared absorption or transmission spectrum with peaks corresponding to the frequencies of vibration

between the atomic bonds making up the material. Absolute intensity and the frequency of lines corresponding to IR active transitions give information about the molecular structure. In the present investigation, FTIR spectra of samples were recorded in the range of 400-4000 cm^{-1} at an average resolution of 32 scans per cm using Shimadzu FTIR 8400S spectrophotometer using KBr pellet method.

2.2.2.2 Raman Spectroscopy

It is one of the vibrational spectroscopic techniques to study the structure of the glasses. Glasses constitute the network of molecular units with random orientation in three dimension. The Raman spectroscopic technique records the modes of vibration that are Raman active. For a mode to be Raman active change in the polarizability of the molecule must be involved during the interaction of light with the molecule. In its simplest form it can be thought of as a process where a photon of light (usually from a laser) interacts with a sample to produce scattered radiation of different wavelengths (inelastic scattering).

In the present investigation, Raman spectroscopy is used to identify the subtle changes in the glass structure by varying glass composition. The spectra of fine powder glass samples were collected in the wavenumber range 400–2000 cm^{-1} using a Laser Confocal Raman microscope (inVia, Renishaw, UK) equipped with an argon ion laser source of 100 mW power and 514 nm wavelength.

2.2.3 Scanning Electron Microscopy (SEM)

It is the most unique and versatile electron microscopic technique that provides image of a sample providing information about the surface of the specimen at much higher magnification, higher resolution and large depth of focus compared to optical microscopy. This is due to very low wavelength of accelerated electrons. This examination can yield information about the topography (surface features of an object) and morphology (shape and size of the particles making up the object) of the samples.

In the present investigation, surface morphology of the samples and indentations with median-radial cracks formed by the Vickers indentation on the

samples surface were examined using SEM (SEM, ZEISS Sigma FE-SEM). The length of the generated crack was estimated by images obtained.

2.2.4 Density measurements

Archimedes principle is employed to determine to density of glasses in order to get an insight into the modifications in the structure of glasses as it is related to molar volume and atomic packing density. It is also crucial in obtaining information about short range structure of oxide glasses. Density of the samples is highly sensitive to physical properties such as compactness, softening, cross link density, modifications of geometrical configuration, coordination number and dimension of interstitial spaces of the glass.

In the present investigation, Archimedes principle was adopted at room temperature using O-Xylene as the immersion liquid. The choice of the immersion liquid is based on the chemical durability of the sample (Shelby 2000). A highly sensitive balance, with 0.1mg accuracy, was used to measure the weight of glass samples. The samples were weighed both in air and when suspended in O-Xylene of density $\rho_l = 0.86$ g/cc (at room temperature). The difference in weights gives the weight of the displaced liquid. The density of the glass is calculated using the formula

$$\rho = \frac{w_a}{w_a - w_l} \rho_l \quad (2.1)$$

where ρ is the density of the sample, ρ_l is the density of the immersion fluid, w_a and w_l respectively are the weight of sample in air and liquid, respectively. The average density of three specimens of each composition is considered for further analysis.

The molar density for the samples is calculated using the formula given by,

$$V_m = \frac{M}{\rho} \quad (2.2)$$

where M is the calculated molecular weight of the glass samples based on their respective compositions.

Oxygen packing density OPD can be defined as the number of oxygen atoms per formula unit and can be determined by the relation,

$$\text{Oxygen packing density} = \frac{\rho \times O}{M_T} \quad (2.3)$$

Where M_T represents the total molecular weight and O represents the total number of oxygen atoms.

2.2.5 Thermal Analysis

In the present investigation, the thermal analysis for the samples was done to determine three main thermal parameters such as glass transition temperature (T_g), onset crystallization temperature (T_x) and melting temperature (T_m). The measurements for the samples were carried out using a simultaneous thermal analyser (Perkin Elmer STA 8000). The differential scanning calorimetry (DSC) data in the temperature range of 30 °C to 1100 °C at a heating rate of 10 °C cm⁻¹ under a constant flow of nitrogen gas was recorded. The DSC data was recorded on fine crushed glass granules of size of the range 0.85 to 1mm.

Thermal stability of glasses against crystallization was evaluated by taking difference between their T_x and T_g values

$$\Delta T = T_x - T_g \quad (2.4)$$

Glasses with higher ΔT value would show better thermal stability against crystallization (Donald et al. 2006). Glass forming ability of samples was obtained by calculating Hruby's parameter (H_R), which is given as

$$H_R = \frac{T_x - T_g}{T_m - T_x} \quad (2.5)$$

Thermal stability and glass forming ability play a crucial role in preparing large scale glasses for practical applications and academic studies. The other thermal parameters which are proposed for the oxide glass system (Nascimento et al. 2005 and Saffarini et al. 2000) are also evaluated using the following formulae.

Weinberg parameter (Nascimento et al. 2005), $K_W = \frac{T_x - T_g}{T_m}$

$$(2.6)$$

Parameter proposed by Lu and Liu (Lu et al. 2003), $K_{LL} = \frac{T_x}{T_g + T_m}$

$$(2.7)$$

Glass stability parameters K_1 , and K_2 (Saffarini et al. 2000)

$$K_1 = T_m - T_g \quad (2.8)$$

$$K_2 = \frac{T_x}{T_m} \quad (2.9)$$

2.2.6 Optical properties

2.2.6.1 Refractive index (RI) measurement

The refractive index of any material is defined as the ratio of the velocity of light in vacuum and the velocity of light in that material. Magnitude of refractive index is always needed to interpret different types of spectroscopic data. The RI coefficients are significant factor in the design of a solid state laser. RI of glasses largely depend on electron density and polarizability of the ions coordinated with anion, field strength of the ions, number of NBO atoms etc. Increase in either electron density or polarizability of ions present in the glass matrix increases the refractive index of glass samples (Shelby 2005).

In the present work, refractive indices of fine polished samples were measured at room temperature using an Abbe (MAR-33) refractometer with an accuracy of ± 0.001 . Mono-bromo naphthalene was used as the contact layer between the glass and refractometer prism. Measurements were carried out for two specimens of each composition and the average value of refractive index was obtained.

2.2.6.2 UV-Visible spectroscopy

Ultraviolet and visible (UV-Vis) absorption spectroscopy is the measurement of the attenuation of a beam of light with a wavelength in the range after it passes through a sample or after reflection from a sample surface. Difference between the intensity of incident radiation (I_0) to the transmitted radiation (I) gives the amount of light absorbed by a sample. The amount of light absorbed is expressed as either transmittance or absorbance. A plot of intensity of absorption against the wavelength or frequency of the electromagnetic radiation is called the absorption spectrum. The prominent optical properties of glasses like refractive index, dispersion, and transmission mainly depend on their chemical composition among other factors.

In case of glasses since they obey dipole selection rule, possibility of transitions may be direct or indirect. The absorption coefficient (α) can be related by the following equation,

$$I = I_0 \exp(-\alpha t) \quad (2.10)$$

where I_0 denotes the incident light intensity, t is the thickness of the glass sample. By means of the equation (2.10) together with the Davis and Mott relation (Fu et al. 2012), magnitude of the absorption coefficient (α) can be linked to the optical band gap energy E_g as,

$$\alpha = \frac{B}{hv} (hv - E_g)^n \quad (2.11)$$

where B is a constant, hv signifies the incident photon energy, n denotes transition type viz., $n=1/2, 2, 3/2$ and 3 for direct, indirect, direct forbidden and indirect forbidden transitions, respectively.

Since indirect allowed transition takes place in glasses, considering the value of n as 2 , equation (2.11) can be simplified and written as,

$$(\alpha hv)^{1/2} = B^{1/2} (hv - E_g) \quad (2.12)$$

The band tails are characterized by Urbach energy, E_U (Narayanan et al. 2015) which is given by the relation,

$$\alpha = \alpha_o \exp\left(\frac{hv}{E_U}\right) \quad (2.13)$$

where α_o is a constant which is well known as the tailing parameter. Taking natural log on both sides of the equation (2.13), it can be simplified and written as,

$$\ln \alpha = \left(\frac{1}{E_U}\right) hv + \ln \alpha_o \quad (2.14)$$

In the present investigation, the optical absorption spectra of very well polished glass sample of 1.5 mm thickness (measured by employing a micrometre with 0.001 cm of precision) were recorded in the wavelength range of 200–850 nm using fiber optic spectrometer USB4000 (Ocean Optics Inc., USA).

2.2.6.3 Electronic polarizability

The cationic and anionic polarizability are consistent when they are combined to corresponding stoichiometric batch composition (Dimitrov et al. 1996). Consequently, the estimation of oxide ion polarizability for glasses is decisive as it plays a vital role in optoelectronic materials. For crystals, liquids, and glasses the molar refraction (R_m) based on n and V_m is determined using the Lorentz-Lorenz equation (Zhao et al. 2007), given by

$$R_m = \left(\frac{n^2-1}{n^2+2}\right) V_m \quad (2.15)$$

The molar polarizability, α_m can be determined using the relation (Azlan et al. 2016) given by,

$$\alpha_m = \frac{3}{4\pi} \left(\frac{R_m}{N_A}\right) = \frac{R_m}{2.52} \quad (2.16)$$

The oxide ion polarizability based on refractive index ($\alpha_{O^{2-}}^{(n)}$) and optical band gap ($\alpha_{O^{2-}}^E$) energy (Zhao et al. 2007, Mallur et al. 2015) can be determined by the equation given by,

$$\alpha_{O^{2-}}^{(n)} = \left[\frac{R_m}{2.52} - \sum \alpha_i \right] (N_{O^{2-}})^{-1} \quad (2.17)$$

$$\alpha_{O^{2-}}^E = \left[\frac{V_m}{2.52} \left(1 - \sqrt{\frac{E_g}{20}} \right) - \sum \alpha_i \right] (N_{O^{2-}})^{-1} \quad (2.18)$$

Where $\sum \alpha_i$ is the molar cation polarizability, $N_{O^{2-}}$ is the total number of oxygen ions in the chemical formula. Owing to the chemical reaction among constituent oxides in the glass systems, oxygen ions, O^{2-} always possess a tendency to transfer its negative charge to the cations. This ability of oxide ions to donate electrons to the surrounding cations is termed as optical basicity. The optical basicity of the both the series of glass systems is calculated using the equation, proposed by Duffy (Duffy 1996), given by

$$A = 1.67 \left(1 - \frac{1}{\alpha_o^{2-}} \right) \quad (2.19)$$

where α_o^{2-} is the refractive index based oxide ion polarizability.

The quantity $\frac{R_m}{V_m}$ provides the polarizability density of the glass systems. According to Hertzfeld metallization theory (Duffy 1996), if a material is densified to have the ratio $\frac{R_m}{V_m} = 1$ then the quantity $n^2 - 1$ will become equal to $n^2 + 2$, this can materialize only when $n = \infty$. According to this discussion, the electrons in the valance state which are quasi-elastically connected to the atoms are now liberated by means of polarization in the condensed state and this process is referred to as ‘polarization catastrophe’ (Chandrashekaraiyah et. al. 2018) The solid materials having the ratio $\frac{R_m}{V_m} \geq 1$ behave as metallic conductors whereas the materials having the ratio $\frac{R_m}{V_m} < 1$ behave as insulators. Dimitrov et. al. (1996) have evaluated the metallization criterion, M using the equation

$$M = 1 - \frac{R_m}{V_m} \quad (2.20)$$

They found that the modifier oxides with borate and silicate glasses have greater M , which lie in the range of 0.5-0.7. It is established that the materials with least value of metallization criterion usually exhibit narrow E_g .

2.2.7 Mechanical Properties

Glasses with outstanding mechanical and elastic behaviour are desired for practical applications viz., glass components for television tubes, architectural use, optical fibers for data transmission, temporary implants for bone repair and reconstruction etc. (Sehgal et al. 1995, Kurkjian 2000, Rao and Shashikala 2014a). Therefore, it is crucial to carryout systematic study of mechanical and elastic properties to decide the type of glasses suitable for technological and biomedical applications.

2.2.7.1 Micro indentation studies

Mechanical properties of glasses such as Young's modulus, hardness, fracture toughness and brittleness are usually investigated using simple indentation method. This method involves applying a known load to hard diamond tip and measuring the area, depth or length of the crack generated on the specimen surface. Different types of indenters like spherical, canonical and pyramidal are employed to measure the resistance to penetration by material's surface. Four sided diamond pyramid indenter known as Vickers indenter is usually used for micro indentation experiments.

In micro indentation experiments, a known load is applied to the indenter to indent on a sample surface for prescribed dwell time (10 s). Then area of residual impression formed on the surface of sample due to indentation is measured using optical microscope. Vickers hardness (H_V) of sample is obtained by dividing indentation load by measured area of the impression after unloading and is given by the relation

$$H_V = \frac{1.852P}{d^2} \quad (2.21)$$

where H_v is Vickers hardness in GPa, P is indentation load in N and d is half of the average length of two indentation diagonals in μm .

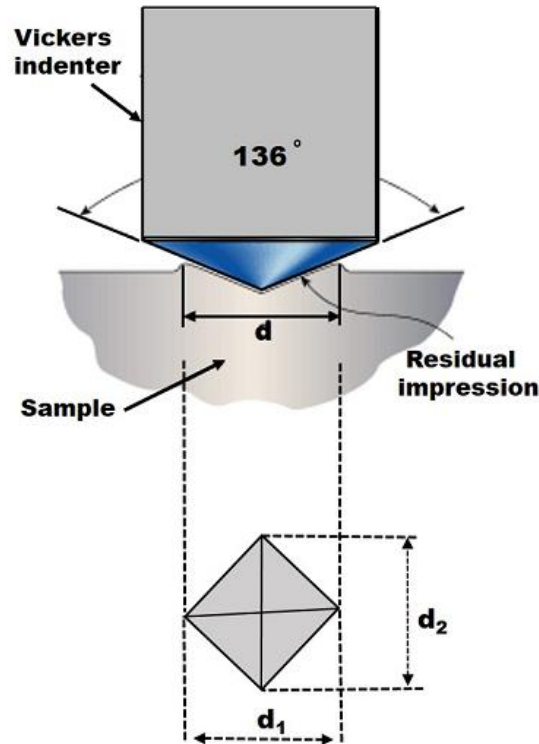


Figure 2.2: Schematic diagram of Vickers indentation on surface of sample.

So, Vickers hardness measures the resistance of sample to the permanent deformation caused by a sharp diamond indenter (compression load). Vickers hardness of a material depends on their bond strength, presence of defects, packing density of ions, surface features etc. Schematic diagram of residual impression formed on a surface of sample by Vickers indentation is shown in figure 2.2

Strength of glasses mainly depends upon two factors, crack initiation and crack propagation. Mechanical failure which results from crack initiation and subsequent propagation at the surface limit the practical applications of glasses (Sehgal and Ito 1999). Crack propagation can be evaluated by measuring fracture toughness (K_{IC}), which defines the ease with which a crack can propagate in a material. When Vickers indenter indents on a sample surface, median-radial cracks originate from four corners of the indentation outside the plastic zone as shown in figure 2.3.

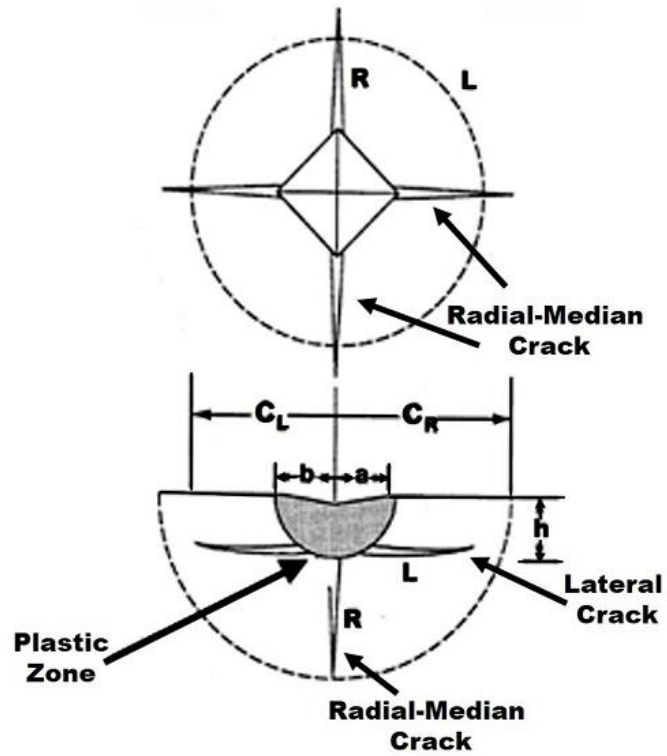


Figure 2.3: Schematic diagram of cracks propagating from four corners of Vickers indentation (Marshall 1983)

These median-radial cracks are used to determine fracture toughness (K_{IC}) of normal glasses. Fracture toughness of the glasses is usually calculated using an equation developed by Anstis et al. (1981), which involves the direct crack measurement method. This can be formulated as

$$K_{IC} = 0.016 \left(\frac{E}{H} \right)^{1/2} \left(\frac{P}{C^{3/2}} \right) \quad (2.22)$$

where K_{IC} is the fracture toughness in $\text{MPa (m)}^{1/2}$, E , H , P and C are Young's modulus (GPa), measured Vickers hardness (GPa), peak load applied (4.9 N) and measured half crack length (μm) respectively. The Young's modulus, E (GPa) is calculated using the equation

$$E = 83.6 V_t \sum_i G_i X_i \quad (2.23)$$

where G_i is the dissociation energy density of oxide constituents (G_i of $B_2O_3=82.8$ kJ/cm³, $ZnO=49.9$ kJ/cm³, $Li_2O=77.9$ kJ/cm³, $Na_2O=31.9$ kJ/cm³, $K_2O=19.2$ kJ/cm³, and $MnO_2=74.7$ kJ/cm³) (Chandrashekaraiiah et al. 2018 and Taha et al. 2018) and X_i represents the mole fraction corresponding to the i^{th} component and V_i is the atomic packing fraction (Fu et al. 2012), which is represented as,

$$V_t = \rho \frac{\sum_i V_i X_i}{\sum_i M_i X_i} \quad (2.24)$$

where M_i represents the molar weight of the i^{th} component. The volume occupied by the ions of i^{th} component is represented by V_i for a compound $M_p N_q$, given by

$$V_i = \frac{4}{3} \pi (pR_M^3 + qR_N^3) N_A \quad (2.25)$$

Where M_p and N_q are metal oxides. R is the radii of corresponding M and N ions. Avogadro's number is represented as N_A .

Crack initiation in glasses mainly depends on their brittleness (Sehgal and Ito 1999). Brittleness or simple index of brittleness (B) of glasses can be calculated from the method proposed by Lawn and Marshall (1979), and is given by the ratio of Vickers hardness (resistance to deformation, H_v) to fracture toughness (resistance to fracture, K_{IC})

$$B = \frac{H_v}{K_{IC}} \quad (2.26)$$

In order to choose the glasses for industrial and technological application detailed examination of mechanical as well as elastic properties is required. In this regard along with Young's modulus (E) (Makishima and Mackenzie 1973), the Poisson's ratio (σ) of the prepared glass system was evaluated by means of the equation (Makishima and Mackenzie 1975), which connects the Poisson's ratio to the determined packing density (V_i) of the glass samples, given by

$$\sigma = 0.5 - \frac{1}{7.5V_t} \quad (2.27)$$

Shear modulus (S) and bulk modulus (K) were evaluated by the equation given by,

$$S = \frac{E}{2(1+\sigma)} \quad (2.28)$$

$$K = 1.2V_t E \quad (2.29)$$

In the present investigation, the mechanical strength of the prepared glasses was studied in detail using Vickers micro-indentation studies. The Hardness (H_V) of the prepared glasses was measured using a Vickers micro-indenter (Clemex MMT X7) by applying 0.98 N with dwell time of 10 s. The procedure is repeated ten times for each glass specimen and the mean value is considered for further calculations. Fracture toughness for the samples is measured using the median-radial cracks generated by indentations made on glass samples at 4.9 N. The length of the generated crack was estimated by imaging the surface of the samples using optical microscope.

2.2.8 Error analysis

All scientific measurements, however carefully made, are always associated with inevitable uncertainties (Taylor 1997). Since, scientific studies involve measurement, it is crucial to assess these uncertainties and keep them as minimum as possible. Hence, error analysis is carried out to study and estimate these inevitable experimental uncertainties and to keep the errors as small as possible. In present experimental measurements, error in measured quantities was estimated by taking the standard deviation of the mean (SDOM) of all the measurements. Error in calculated quantities was obtained from error in related measured quantities using the quadrature sum of uncertainty rule of error propagation.

2.2.8.1 Standard deviation of the mean (SDOM)

If N measurements of a quantity made using same instrument and procedure are x_1, x_2, \dots, x_N , then the best estimate for the quantity x is obtained by taking average or mean \bar{x} of x_1, x_2, \dots, x_N . Here \bar{x} is calculated as

$$\bar{x} = \frac{x_1 + x_2 + \dots + x_N}{N} = \frac{\sum_i x_i}{N}$$

Uncertainty in x_{best} or \bar{x} is estimated by taking the standard deviation of the mean (SDOM) or standard error of the N measurements and is given by the equation

$$\sigma_{\bar{x}} = \frac{\sigma_x}{N}$$

where $\sigma_{\bar{x}}$ is standard deviation of the mean and σ_x is standard deviation, which measures average uncertainty of N measurement. Standard deviation (σ_x) is given by the relation

$$\sigma_x = \sqrt{\frac{1}{N-1} \sum_i d_i^2} = \sqrt{\frac{1}{N-1} (x_i - \bar{x})^2}$$

where difference $(x_i - \bar{x}) = d_i$ gives the deviation of i^{th} measurement x_i from mean value \bar{x} . If these deviations are very small then measurement carried out will be precise. Some deviations may be positive and some may be negative, so averaging the deviations may not give reliable uncertainty in the measurements. Thus, deviations are squared first to obtain a set of positive numbers and then square root of the average of set of positive numbers are obtained to get a quantity having same unit as the measurements. This root mean square (RMS) deviation of the measurements is known as standard deviation, σ_x , which is found to be useful in characterizing reliability of measurements.

Standard deviation of the mean ($\sigma_{\bar{x}}$) is preferred over standard deviation (σ_x) to obtain uncertainty in the \bar{x} . Because, as the number of measurements increases, $\sigma_{\bar{x}}$ will give more reliable uncertainty in the final result due to the presence of factor \sqrt{N} in the denominator. But, σ_x will not change appreciably with increase in number of measurements.

Final result (X) of N number of measurements is represented as

$$X = \bar{x} + \delta x = \bar{x} + \frac{\sigma_x}{\sqrt{N}}$$

2.2.8.2 Quadrature sum of uncertainty

In many cases quantity cannot be measured directly, instead value of the physical quantities of interest is calculated from the other measured quantities. When a quantity is obtained through calculations, uncertainty also propagates through calculations and final result contains propagated errors. When uncertainty in measured quantities are independent and random, uncertainty in final calculated quantity is obtained by adding uncertainty in quadrature as given below.

Considering that quantities m, \dots, r are measured with uncertainties m, \dots, r and these quantities were used to calculate x , which is given as

$$x = \frac{m \times \dots \times o}{q \times \dots \times r}$$

Suppose error in m, \dots, r are independent and random, then fractional uncertainty in x is obtained by summing the quadrature of fractional uncertainties of measured quantities

$$\frac{\delta x}{|x|} = \sqrt{\left(\frac{\delta m}{m}\right)^2 + \dots + \left(\frac{\delta o}{o}\right)^2 + \left(\frac{\delta q}{q}\right)^2 + \dots + \left(\frac{\delta r}{r}\right)^2}$$

Then δx is obtained by multiplying $|x|$ with quadrature of fractional uncertainties of measured quantities.

Considering that the uncertainty in experimental measurements carried out in the present investigation are independent and random, error in measured quantities such as density, measured Young's modulus, Vickers hardness and half crack length were evaluated by taking the standard deviation of the mean (SDOM) of their measurements. Error in calculated quantities like molar volume, packing density, bulk modulus, shear modulus, fracture toughness and brittleness was obtained from error in related measured quantities using the quadrature sum of uncertainty rule of error propagation.

Errors are not shown for theoretically calculated parameters. All the errors reported in this thesis are rounded to one significant figure.

Chapter 3

INVESTIGATION OF MIXED ALKALI EFFECT ON MECHANICAL, STRUCTURAL AND THERMAL PROPERTIES OF THREE-ALKALI BORATE GLASS SYSTEM

The results of investigation on mixed alkali effect (MAE) in mechanical, structural and thermal properties of alkali zinc borate glasses with nominal composition $5\text{Li}_2\text{O}-(25-x)\text{K}_2\text{O}-x\text{Na}_2\text{O}-60\text{B}_2\text{O}_3-10\text{ZnO}$ ($x= 0, 5, 10, 15, 20$ and 25 mol %) are presented in this chapter. The samples were prepared using standard melt quenching technique. Amorphous nature of the samples were confirmed using X-ray powder diffraction studies. Fourier transform infrared (FTIR) spectroscopy, differential scanning calorimetry (DSC) and Vickers indentation studies were performed to investigate the mixed alkali effect in the samples. From the DSC studies, it was observed that the thermal parameters viz., glass transition temperature (T_g), glass melting temperature (T_m), glass crystallization temperature (T_c), glass stability (S) and fragility (F) exhibited a non linear variation with respect to increase in compositional parameter (R_{Na}). This behavior clearly indicates the presence of strong MAE in the samples. FTIR studies confirmed the presence of both $[\text{BO}_3]$ and $[\text{BO}_4]$ units, indicating the present glass networks to be made up of these two units placed in different structural groups. The non linear variation of peak positions of B-O-B bending and stretching of $[\text{BO}_3]$ and $[\text{BO}_4]$ units of each glass sample explain the role of modifier alkali elements validating the existence of strong MAE. The microhardness and fracture toughness of the samples were measured using Vickers micro indentation technique and a non linear variation of both the properties which confirmed the presence of MAE in these glass samples was observed.

3.1 Results and Discussion

3.1.1 X-ray diffraction studies

X-ray diffraction (XRD) patterns of powdered samples obtained between diffraction angle (2θ) $10^\circ - 80^\circ$ are depicted in figure 3.1. Presence of a broad hump like

feature in the range of 20° - 40° seen in all XRD patterns and the absence of sharp peaks in the pattern confirm the amorphous nature of the synthesized samples.

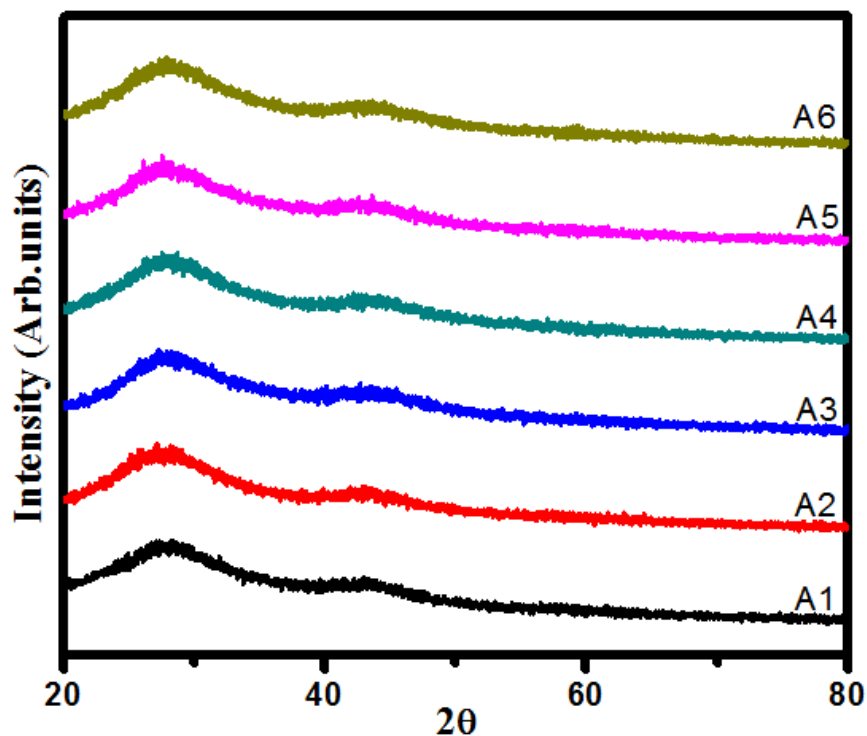


Figure 3.1: X-ray diffractogram of $5\text{Li}_2\text{O}-(25-x)\text{K}_2\text{O}-x\text{Na}_2\text{O}-60\text{B}_2\text{O}_3-10\text{ZnO}$ glass system.

3.1.2 Fourier Transform Infrared Spectroscopy

Infrared spectroscopy is one of the most powerful tools to study the structure of glass system (Kamitsos, 1990). Upon adding some additives to the borate unit, modifications in its structural groups can be observed. Hence the study of the infrared spectra of synthesized glasses is an important technique to get knowledge of chemical bonding in borate glass structure. Alkali elements are well known for their network modifying ability in glass system. The addition of alkali elements into borate glass matrix converts the planar BO_3 unit to most stable tetrahedral BO_4 units and leads to the formation of Non Bridging Oxygens (NBO), during the process of conversion. Alkali elements are having the ability to modify the B_2O_3 and give rise to different structural groups, which can be boroxyl ring, penta-borate, tri-borate, di-borate, meta-

borate ring, meta-borate chain, loose BO_4 tetrahedra, pyroborate, orthoborate, borate tetrahedral with two bridging oxygens (Kamitsos, 1990). Infrared spectra of present glass system recorded in the range of 400 to 4000 cm^{-1} is presented in figure 3.2.

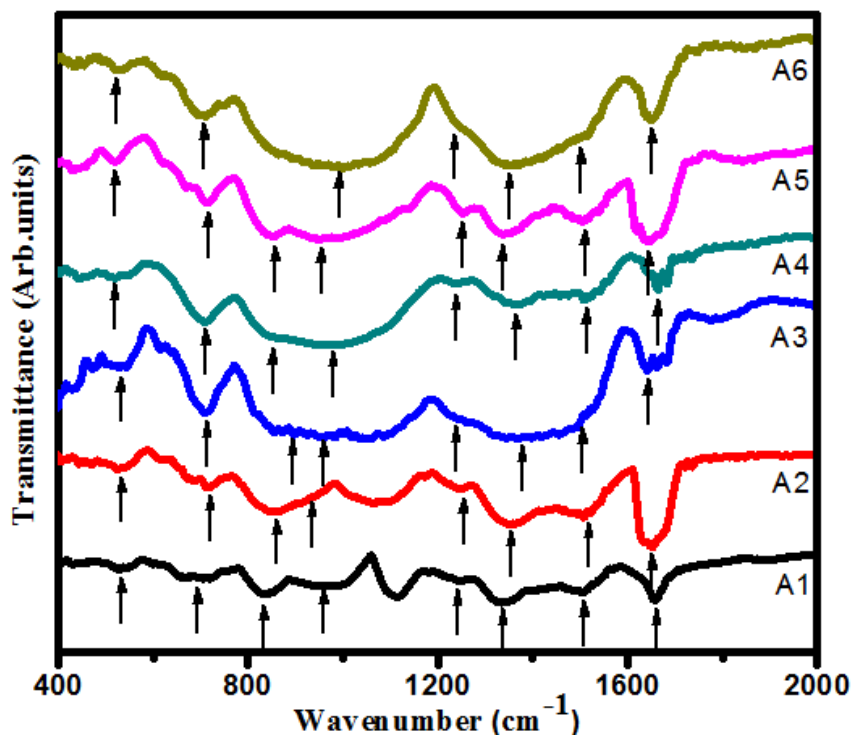


Figure 3.2: FTIR spectra of $5\text{Li}_2\text{O}-(25-x)\text{K}_2\text{O}-x\text{Na}_2\text{O}-60\text{B}_2\text{O}_3-10\text{ZnO}$ glass system.

The observed vibrational bands are compared with that of crystalline lithium-borate, sodium-borate, potassium-borate systems and vitreous borate structure reported by earlier investigators (Kamitsos, 1990, Ulagaraj Selvaraj, 1984, Gan Fuxi, 1982). In modified borate glasses, the major vibrational modes are active in mainly three regions viz., $600-800\text{cm}^{-1}$, $800-1200\text{cm}^{-1}$ and $1200-1600\text{cm}^{-1}$. The observed absorption region of $1200-1600\text{cm}^{-1}$ is attributed to the stretching vibrations of B-O bond in the trigonal BO_3 unit, $800-1200\text{cm}^{-1}$ is due to the tetrahedral BO_4 stretching vibrations and $600-800\text{cm}^{-1}$ is attributed to the bending vibrations of the B-O-B. The lower wave number regions are due to the specific cation vibrations and deformation modes. The band assignments of the present glass system are given in the table 3.1. Ulagaraj Selvaraj et al. (1984) have studied the single as well as mixed alkali borate glass systems and found that, in pure lithium diborate glasses, the absorption

peaks at 1360 cm^{-1} , 980 cm^{-1} and 703 cm^{-1} were quite broad but the absorption band which was prominent in these glasses at 760 cm^{-1} was absent in case of sodium and potassium diborate glasses. They observed the B-O stretching vibrations of three coordination boron at 1330 cm^{-1} and corresponding bending vibration at 730 cm^{-1} . Further, those authors observed a sensitive non linear variations in the peak positions of both B-O stretching and bending modes when peak positions and the corresponding molar concentration of alkali oxides were plotted.

Table 3.1: Band assignments for IR spectra of $5\text{Li}_2\text{O}-(25-x)\text{K}_2\text{O}-x\text{Na}_2\text{O}-60\text{B}_2\text{O}_3-10\text{ZnO}$ glass system

Compositional Parameter R_{Na}						Band Assignments
0	0.2	0.4	0.6	0.8	1	
430	472	426	443	432	445	O-B-O bond bending, Li-O, Na-O, K-O cation vibrations. (Sevaraj et al. 1984)
528	524	528	522	520	536	Vibrations of $[\text{BO}_4]$ tetrahedral. (Sevaraj et al. 1984)
705	715	707	711	715	709	Bending vibrations of B-O-B linkage. (ElBatal, 2012)
833	862	896	850	858	---	Stretching vibrations of NBOs of BO_4 groups from tri, tetra, and penta borate units. (Gaafar et al. 2013)
968	939	958	977	954	990	B-O stretching vibrations of BO_4 tetrahedra. (Naresh et al. 2012)
1249	1251	1244	1242	1251	1245	B-O stretching of $[\text{BO}_3]^{3-}$ unit in meta borate chain and ortho borates. (Saritha et al. 2008)
1334	1352	1369	1373	1336	1353	Stretching vibrations of the B-O bonds of $[\text{BO}_3]^{3-}$ unit involving mainly the linkage oxygen connecting different groups. (ElBatal, 2012)
1502	1508	1514	1506	1504	1515	Antisymmetric stretching vibrations with three(NBOs) of O-B-O groups. (Naresh et al. 2012)
1658	1652	1645	1660	1649	1647	O-H bending modes. (Samee et al. 2013)

The variation in those two alkali systems was not much pronounced. In the present study of three-alkali glass system absorption band due to bending vibrations of B-O-B at 707-715 cm^{-1} (ElBatal, 2012) and stretching vibrations at 1334-1369 cm^{-1} are observed. Peak positions of B-O-B bending and stretching of $[\text{BO}_3]$ units with the compositional parameter R_{Na} are plotted in figure 3.3, as suggested by Ulagaraj Selvaraj et al. (1984). A clear non linear variation is observed. Hence it can be concluded that MAE is present in three-alkali system. Less pronounced absorption peaks are found in the range 426-476 cm^{-1} which are assigned to the B-O-B bending and may be due to the specific Li-O, Na-O, K-O cation vibrations. The absorption peaks at 532-540 cm^{-1} is attributed to the borate deformation modes. Gaafar et al. (2013) have studied the three-alkali borate glass system and the observed absorption band at 846-859 cm^{-1} was assigned to the stretching vibrations of NBO's of $[\text{BO}_4]$ units.

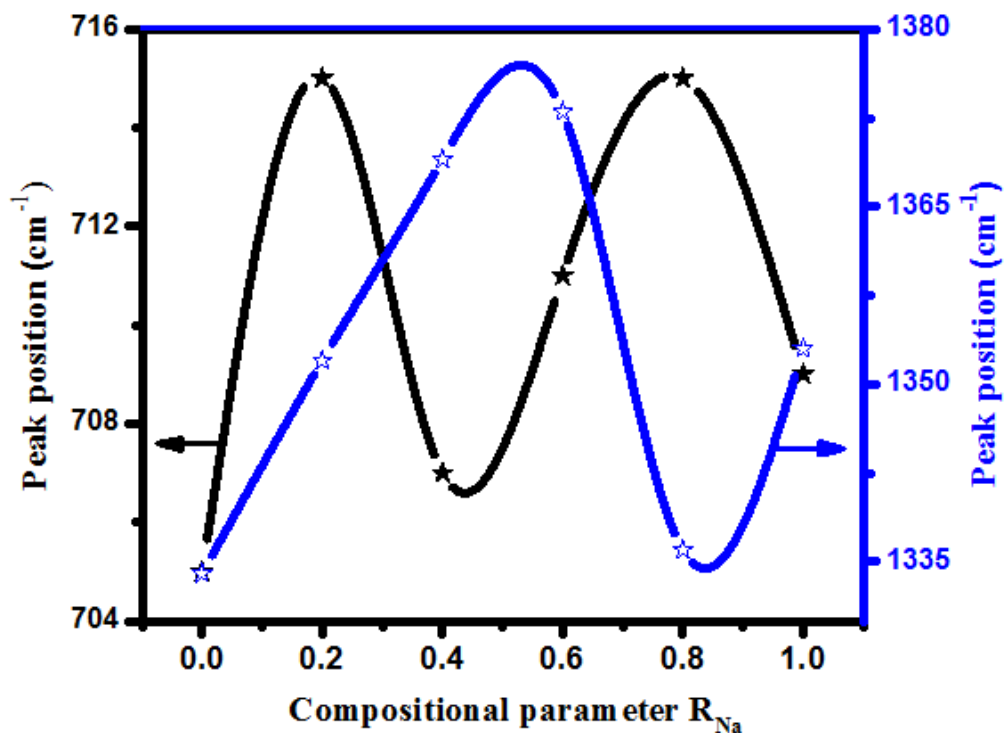


Figure 3.3: Peak positions variations of B-O-B bending (left Y-axis) and stretching (right Y-axis) as a function of compositional parameter R_{Na} .

Razvan et al. (2012) have studied the $x\text{CuO}(100-x) [55\text{B}_2\text{O}_3 \cdot 45\text{ZnO}]$ ($0 \leq x \leq 20$ mol%) glass system and found a band at 878-885 cm^{-1} and assigned it to the B-O

stretching vibrations mainly arising due to the tri, tetra and penta borate groups. In the present glass system absorption band of $833\text{-}896\text{ cm}^{-1}$ is assigned to the stretching vibrations of NBO's of BO_4 unit. These stretching vibrations are due to the tri, tetra and penta borate groups. Absorption peak near $940\text{-}990\text{ cm}^{-1}$ is attributed to the stretching vibrations of B-O bonds in BO_4 unit (Gaafar et al. (2013), Naresh et al. (2012), Gaafar et al. (2009)). Gaafar et al. (2009) and Motke et al. (2002), have studied the $(1-x)[29\text{Na}_2\text{O}-4\text{Al}_2\text{O}_3-67\text{B}_2\text{O}_3]-x\text{ZnO}$ ($0 \leq x \leq 35\text{ mol}\%$), $\text{PbO-ZnO-B}_2\text{O}_3$ glass systems respectively. They attributed the B-O stretching vibration of $[\text{BO}_3]^{3-}$ unit in ortho and meta borate chains to the absorption peak at 1240 cm^{-1} . The shoulders at 1234 cm^{-1} is due to B-O stretching vibrations of $[\text{BO}_3]^{3-}$ unit in meta borate chain and ortho borates (Kamitsos et al. 1990).

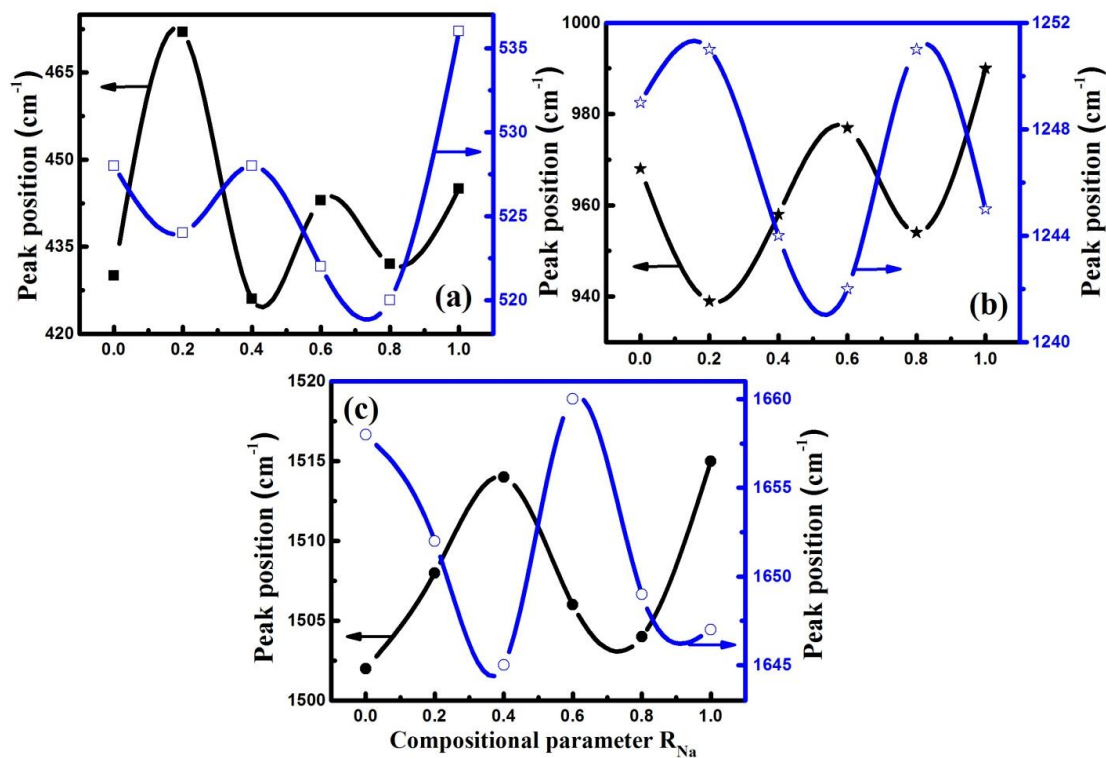


Figure 3.4: Peak position variations as a function of compositional parameter R_{Na} of (a) O-B-O bond bending and $[\text{BO}_4]$ tetrahedral vibration, (b) B-O stretching vibration of BO_4 tetrahedra and $[\text{BO}_3]^{3-}$ unit and (c) antisymmetric stretching vibrations of O-B-O group and OH bond bending modes, with compositional parameter R_{Na} .

In the present study, the vibration band at 1232-1251 cm^{-1} is assigned to the B-O stretching of trigonal $[\text{BO}_3]^{3-}$ unit in meta borate chain and orthoborates. The absorption band at 1504-1551 cm^{-1} is assigned to the asymmetric stretching vibrations of B-O-B, in trigonal BO_3 units (ElBatal et al. (2012), Naresh et al. (2012), Saritha et al. (2008)). Absorption band of 1637-1660 cm^{-1} is assigned to O-H bending modes, and may be attributed to the change of trigonal $[\text{BO}_3]$ unit to tetrahedral $[\text{BO}_4]$ unit. Figure 3.4 shows the peak position variation as a function of compositional parameter R_{Na} of (a) O-B-O bending and vibrations of $[\text{BO}_4]$ tetrahedral, (b) B-O stretching vibrations of BO_4 tetrahedra and B-O stretching of $[\text{BO}_3]^{3-}$ unit in meta borate chain and ortho borates and (c) Antisymmetric stretching vibrations with three (NBOs) of O-B-O groups and O-H bending modes, which shows the clear MAE in all bending and stretching vibrations. The pronounced non linear variation shows stronger MAE in this three-alkali system compared to the two alkali system reported by earlier investigators (Gaafar et al. (2013), Samee et al. (2013), Samee et al. (2011))

3.1.3 Density, Molar volume and atomic packing density

Density of the samples was measured using Archimedes method, since it plays an important role in finding out the ionic packing ratio. The molar volume of the samples was calculated using the formula $V_m = \frac{M}{\rho}$, where M is the molar mass and ρ is the density of the sample.

Table 3.2: Density (ρ), and molar volume (V_m) of $5\text{Li}_2\text{O}-(25-x)\text{K}_2\text{O}-x\text{Na}_2\text{O}-60\text{B}_2\text{O}_3-10\text{ZnO}$ glass system

Compositional Parameter R_{Na}	ρ (g/cm^3) ± 0.005	V_m (cm^3) ± 0.05
0	2.392	31.33
0.2	2.421	30.29
0.4	2.442	29.38
0.6	2.471	28.37
0.8	2.480	27.63
1	2.484	26.93

The results obtained from these measurements are tabulated in table 3.2 and depicted in figure 3.5.

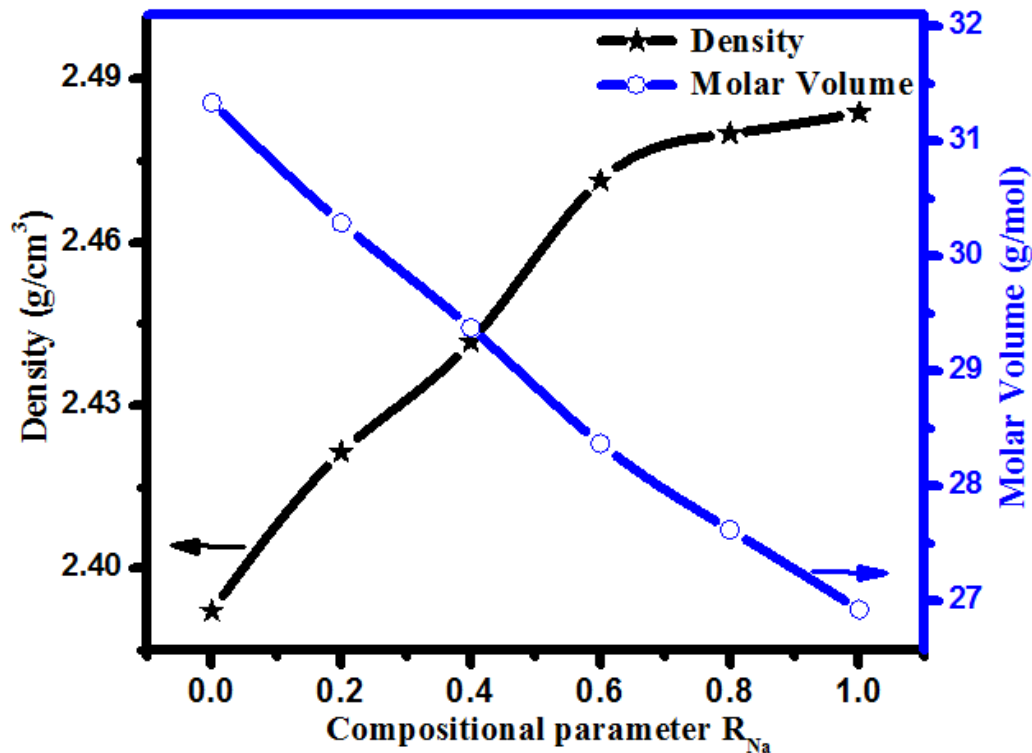


Figure 3.5: Variation of density and molar volume as a function of compositional parameter R_{Na} .

It is seen from the figure 3.5 that the density is increasing and the molar volume is decreasing with the compositional parameter R_{Na} [$R_{Na} = \frac{mol\% (Na_2O)}{mol\% (Na_2O + K_2O)}$]. This behaviour is attributed to the contraction of the glass matrix due to the replacement of the larger K^+ ions by the smaller Na^+ ions. Replacement of K^+ ions by Na^+ ions leads to the conversion of triangular BO_3 units to tetrahedral BO_4 units. Conversion of BO_3 units into BO_4 with increase in Na_2O is further confirmed from FTIR studies. Since the mol% of all other constituent ions is kept unchanged, it is assumed that only K_2O is replaced by Na_2O . Therefore, the conclusion of increase in density due to the replacement of K ions by Na ions is drawn. The linear behaviour of the molar volume indicates that the atomic packing depends on additivity. The change in density reveals that each oxide in glass would contribute to the overall density with a specific factor.

Similar variation of density and molar volume were reported in alkali glass systems which show MAE (Ulagaraj Selvaraj et al. 1984). However, density of the present glass system is less affected by the MAE, which shows only $\pm 10\%$ deviation from linearity depending on the composition of sodium (R_{Na}). On the other hand, molar volume does not show any deviations from linearity.

3.1.4 Thermal Analysis

DSC studies were performed on as-quenched amorphous glass samples and the thermal parameters like glass transition temperature (T_g), onset of glass crystallization temperature (T_{cx}), glass crystallization temperature (T_c), glass melting temperature (T_m) and glass transition width (ΔT_g) are determined. Figure 3.6 represents the variation of T_g and T_c over compositional parameter R_{Na} . The results obtained from the analysis of DSC thermograms are summarized in table 3.3. From the figure 3.6, non-linear variation has been observed in T_g and T_c which confirms the MAE in the present glass system. The deviation from linearity is huge in all the thermal parameters when compared to reported two alkali systems which also indicates the stronger MAE in three-alkali system. In alkali borate glasses, alkali oxides enter the glass network and modify the trigonal $[BO_3]$ unit to tetrahedral $[BO_4]$ unit. In the process they create NBO's in the glass network. Due to this, depolymerization of oxide network takes place. The thermodynamic stability (S) of the glass system is determined by taking the difference between glass crystallization temperature and glass transition temperature ($S = T_{cx} - T_g$). In glass physics, the thermodynamic stability tells about the strength of the glass against thermal shock (Srivastava et al. 2008). Thermodynamic fragility of any glass system can be calculated using the relation, (Souri, 2011)

$$F = \frac{0.151 - \chi}{0.151 + \chi}$$

where $\chi = \frac{\Delta T_g}{T_g}$, ΔT_g is glass transition width. Fragility in glass physics gives information about the speed with which the dynamics of material changes as the glass is cooled down to glass transition temperature (T_g).

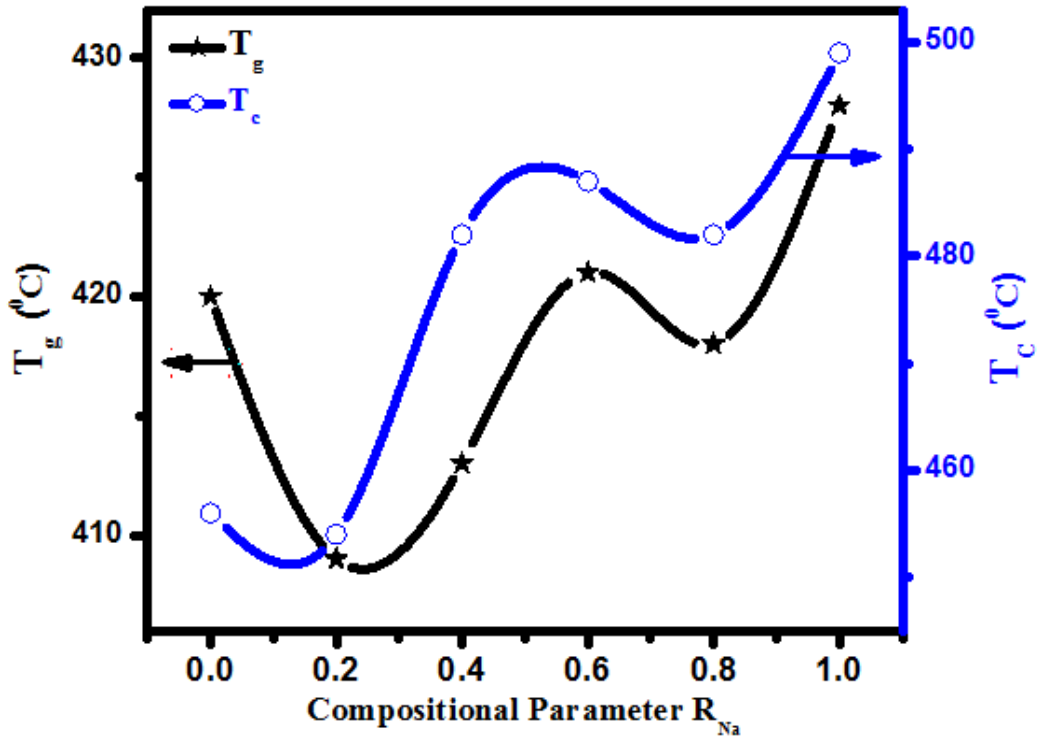


Figure 3.6: Variation of Glass transition temperature (T_g) and glass crystallization temperature (T_c) as a function of compositional parameter R_{Na} .

Table 3.3: Thermal parameters of $5Li_2O-(25-x)K_2O-xNa_2O-60B_2O_3-10ZnO$ glass system

Compositional Parameter R_{Na}	T_g °C	T_{cx} °C	T_m °C	$S = T_g - T_{cx}$	ΔT_g °C	Fragility
0	420	456	568	36	37	0.263
0.2	409	454	565	45	31	0.332
0.4	413	482	551	69	52	0.091
0.6	421	487	545	66	54	0.081
0.8	418	482	557	64	41	0.212
1	428	499	562	71	57	0.063

Fragility can be correlated with glass transition width ΔT_g , where relatively high fragility materials have narrow transition width. Figure 3.7 shows the large non linear variation both in fragility and transition width indicating strong MAE.

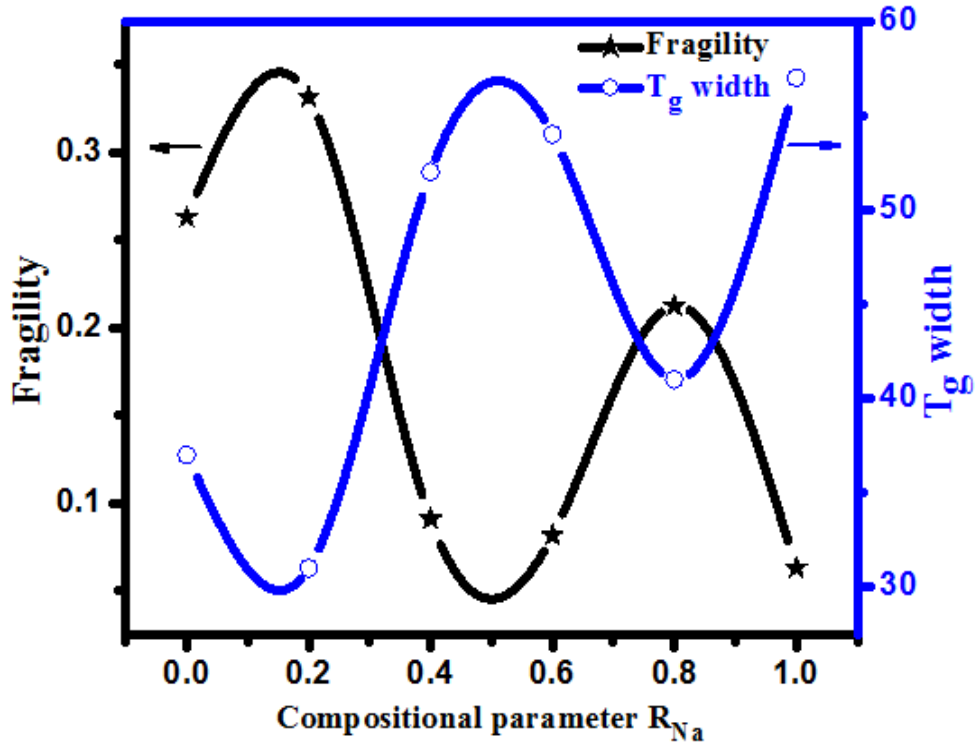


Figure 3.7: Variation of thermodynamic fragility and glass transition width as a function of compositional parameter R_{Na} .

3.1.5 Mechanical Properties

Figure 3.8 depicts the variation of Vickers hardness and crack length as a function of compositional parameter R_{Na} of the investigated samples. The Vickers hardness was calculated using the equation,

$$H_v = \frac{1.854P}{d^2}$$

where H_v is Vickers hardness in GPa, P is applied load (0.98N) and d is the half of the average length of the two diagonals of the indentation. It is observed that all the samples in the present investigation exhibit non linear variation of both Vickers hardness and

crack length with respect to increasing compositional parameter R_{Na} . This non linear variation indicates the presence of MAE in these samples which presumably happens due to the replacement of K_2O by Na_2O leading to the conversion of BO_3 unit to BO_4 units. On the other hand, the glass samples are prone to undergo both compression and shear, during the measurement of hardness due to the high stress developed during the indentation process.

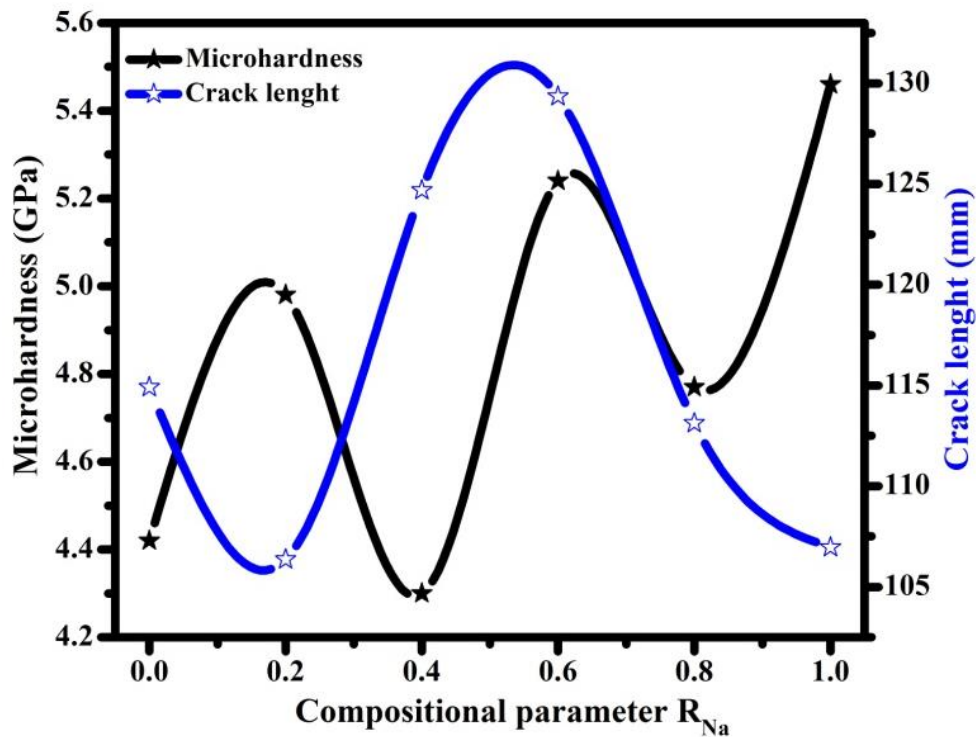


Figure 3.8: Variation of micro hardness and brittleness as a function of compositional parameter R_{Na} .

This in turn leads to various changes in samples viz., plastic deformation, plastic flow and densification. Rao and Shashikala (2014a), have attributed the variation of hardness of mixed alkali glasses to the variation in their plastic deformation, since the densification of the samples remains unaffected even for different alkali ion ratios. Figure 3.8 confirms the existence of prominent mixed alkali effect, as there exist a non linear variation of crack length, which is consistent with the microhardness properties studied.

The measured crack lengths were further utilized to determine the fracture toughness of the samples using the model proposed by Anstis et al. (1981), given by,

$$K_{IC} = 0.016 \left[\frac{E}{H_v} \right]^{1/2} \left[\frac{P}{C^{3/2}} \right]$$

where E , H_v , C and P are Young's modulus (GPa), Vickers hardness (GPa), half of the crack length (mm) and applied load (19.6N), respectively. Variation of crack length with respect to the compositional parameter R_{Na} is presented in figure 3.8. It confirms the existence of prominent mixed alkali effect, as there exist a non linear variation of crack length, which is consistent with the microhardness properties studied. Figure 3.9 shows the SEM micrographs of the indents made at 4.9 N load on glass sample A5.

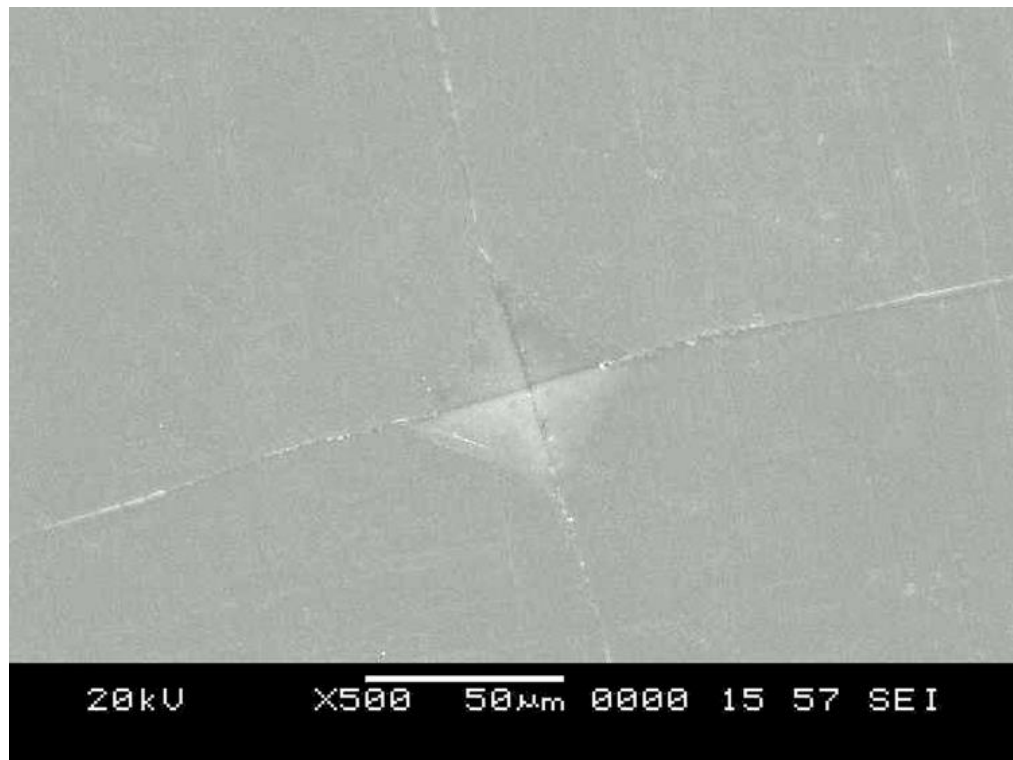


Figure 3.9: Scanning electron micrograph of Vickers impression with radial cracks of glass sample A5.

Straight cracks were generated from the four corners of the pyramidal Vickers indentation, which confirmed that fracture pattern for the glasses were penny-like

median-radial cracks. The crack lengths generated by Vickers indentations were also measured using an optical microscope. Figure 3.10 depicts the variation in fracture toughness with respect to compositional parameter R_{Na} . Further, the estimated values of Vickers hardness and fracture toughness are utilized to estimate the brittleness, B of the samples using a model proposed by Lawn and Marshall (1979), which is given by,

$$B = \frac{H_v}{K_{IC}}$$

where K_{IC} is the fracture toughness ($\text{MPa}\cdot\text{m}^{1/2}$). The non-linear variation of the properties viz., hardness, crack length, fracture toughness and brittleness with compositional parameter R_{Na} is a consequence of mixed alkali effect in the glass samples.

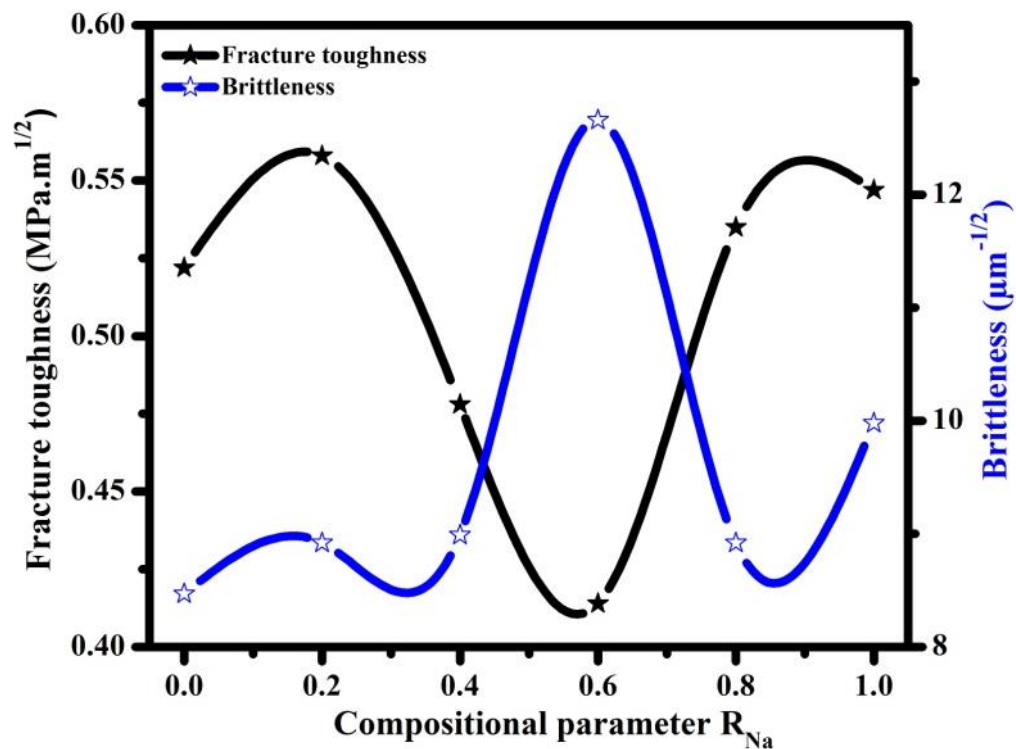


Figure 3.10: Variation of crack length and fracture toughness as a function of compositional parameter, R_{Na} .

3.2 SUMMARY

In summary, the mixed alkali effect in mechanical, structural and thermal properties of three-alkali borate $5\text{Li}_2\text{O}-(25-x)\text{K}_2\text{O}-x\text{Na}_2\text{O}-60\text{B}_2\text{O}_3-10\text{ZnO}$ glass system is presented. XRD studies confirmed the amorphous nature of the prepared samples. Peak positions of different vibration modes in FTIR of glass samples vary non linearly, which explains the role of modifier alkali elements and the existence of strong MAE. Density measurements show a slight positive deviation from linearity showing less MAE on the property. Infrared spectra show clear modifications in the structure which confirm the presence and conversions of $[\text{BO}_3]$ and $[\text{BO}_4]$ unit. Thermal parameters like glass transition, crystallization, melting temperature, fragility and glass stability exhibit non linear variation which validates the presence of MAE in the studied glass system. The non-linear variation of the mechanical properties viz., hardness, crack length, fracture toughness and brittleness is also a consequence of mixed alkali effect in the glass samples. From the observed non linearity in the mechanical, thermal and structural properties, it can be inferred that the MAE is strong in three-alkali ion added glass systems.

Chapter 4

EFFECT OF TMO ADDITION ON THE PROPERTIES OF 5Li₂O-25Na₂O-60B₂O₃-9.9ZnO-0.1TMO AND 5Li₂O-5K₂O-20Na₂O-60B₂O₃-9.9ZnO-0.1TMO GLASS SYSTEMS: A COMPARATIVE STUDY OF LN-TM AND LNK-TM ZINC BORATE GLASS SYSTEM.

In the present chapter, the results of comparative studies carried out on the effect of 0.1 mol% of TMO ions (TMO= Cr₂CO₃, MnO₂, Fe₂O₃, Co₃CO₄, and Ni₂CO₃) addition on the properties of LN-TM glass system with that of the LNK-TM glass system are presented. XRD results, for both LN-TM and LNK-TM series, confirmed the amorphous nature of the synthesized glasses. The IR vibrational modes were mainly active in three major regions, for both LN-TM and LNK-TMO series of glass samples corresponding to the B-O stretching vibrations of BO₃ and BO₄ units. It can be noticed from the FTIR spectra of examined glasses the existence crucial bands of vitreous B₂O₃ and a trivial shift from their original position. The results obtained by the FTIR spectra analysis were further supported by the Raman spectral analysis. The optical studies indicated that the TMO doped LN-TM and LNK-TM glass systems exhibit an extra characteristic absorption band corresponding to each TM ion in its specific valence or coordinate state. It was also observed that the TM ions favor the high valence or tetrahedral coordination states in borate host glass. The median-radial cracks produced due to Vickers indentation were studied for both LN-TM and LNK-TM glass systems. The TMO ions such as Fe, Mn and Ni doped glass systems were observed to exhibit higher Vickers hardness. Brittleness was found to be relatively higher in Cr₂O₃ incorporated glass sample. Further efforts have been made to analyze and correlate the physical and mechanical properties with the structure of the studied glass system.

4.1 Results and Discussion

4.1.1 X-ray diffraction studies

The XRD patterns of the all the prepared samples are presented in the figure 4.1 (a) & (b).

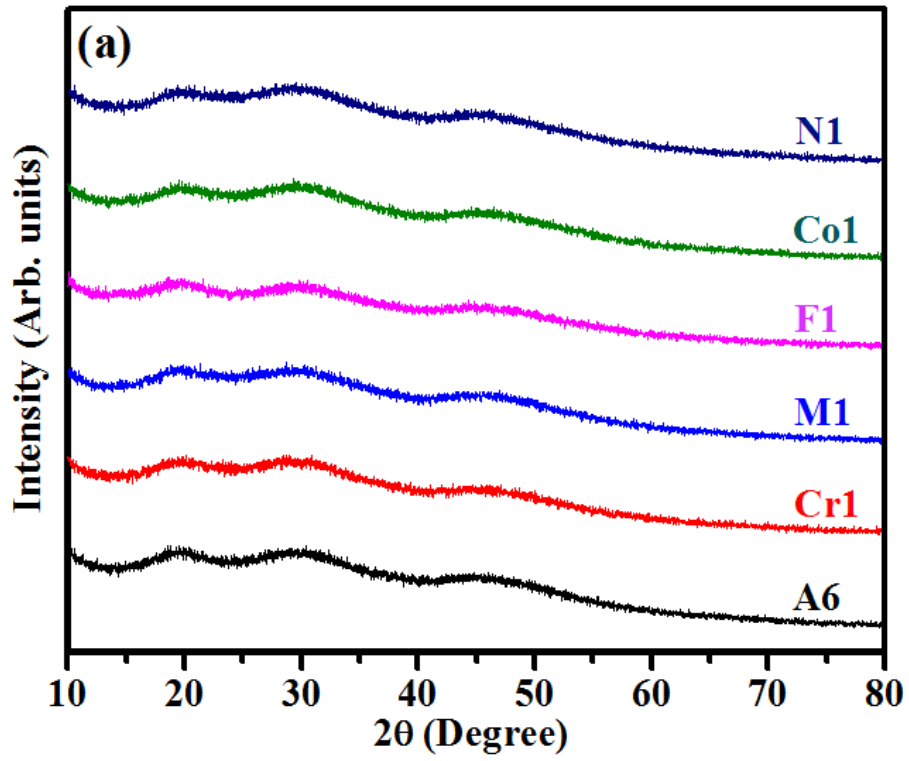


Figure 4.1 (a): X-ray Diffraction patterns of TMO doped LN-TM glass system.

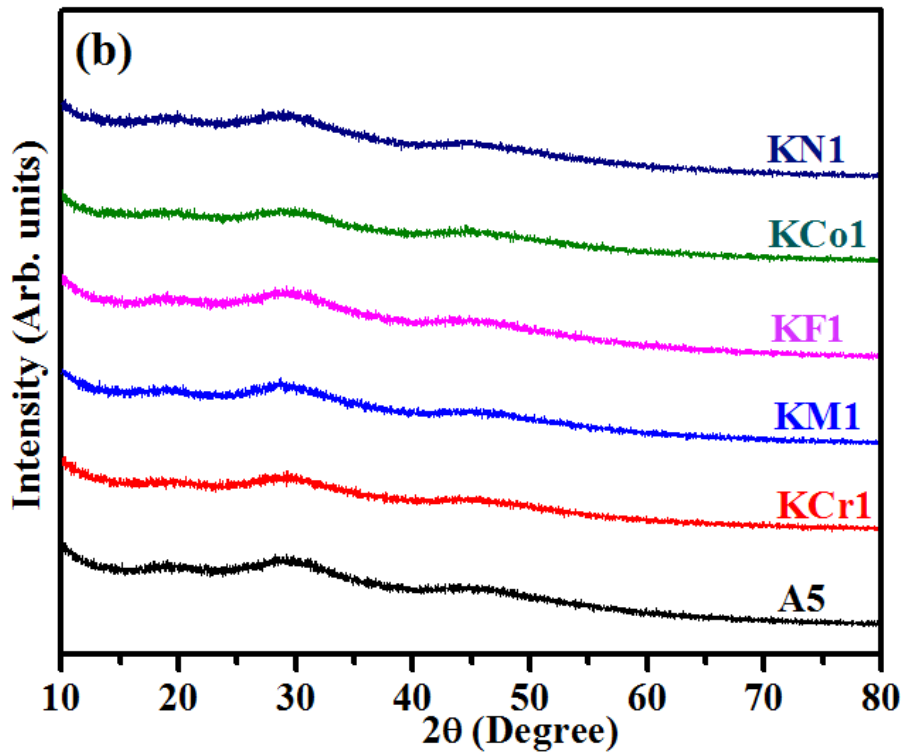


Figure 4.1 (b): X-ray Diffraction patterns of TMO doped LNK-TM glass system.

The measurements were done using powdered samples between diffraction angle 10° - 80° . It is noticed that all the samples show a broad hump like feature and there are no Bragg peaks observed for any of the samples. This result confirms that the prepared LN-TM and LNK-TM glass system are amorphous in nature and the incorporation of 1 mol% transition metal ions do not modify the amorphous nature of prepared glass samples.

4.1.2 Structural Studies

In this section the structural analysis through the FTIR and Raman spectroscopy techniques are presented. These complimentary techniques are considered as one of the most sensitive methods in order to find out the basic structural units present in the glass system as well as to determine the corresponding super structural units present. These studies are helpful to find out the concentration of NBOs per formula unit. In addition, they are also helpful in identifying the resident building blocks which are establishing the glass network and the anionic sites accommodating the modifier transition metal (TM) cations and superstructural units, viz., different types of rings, a combination of rings along with chains and chains alone.

4.1.2.1 Fourier Transform Infrared Spectroscopy studies

Figure 4.2(a) & (b) depicts the FTIR spectra of two alkali and three alkali glass systems. Each spectra consists of bands with particular intensity and centre corresponding to the structural group present in the glass samples. In order to extract all the possible information from any over lapped bands in the spectrum, deconvolution has been done on each spectrum using Gaussian function. The deconvoluted FTIR spectrum is represented in figure 4.3 (a) & (b). It is well known that, in the borate glass system there are majorly three active regions in the IR spectrum viz., $600\text{-}800\text{ cm}^{-1}$, $800\text{-}1200\text{ cm}^{-1}$ and $1200\text{-}1500\text{ cm}^{-1}$. The first region i.e., $600\text{-}800\text{ cm}^{-1}$ corresponds to the bending modes from different groups of borate units, the second region i.e., $800\text{-}1200\text{ cm}^{-1}$ belongs to stretching vibrations of B-O bonds which are connected with BO_4 units and the last region i.e., $1200\text{-}1500\text{ cm}^{-1}$ corresponds to the stretching vibrations of B-O bonds involved in BO_3 units.

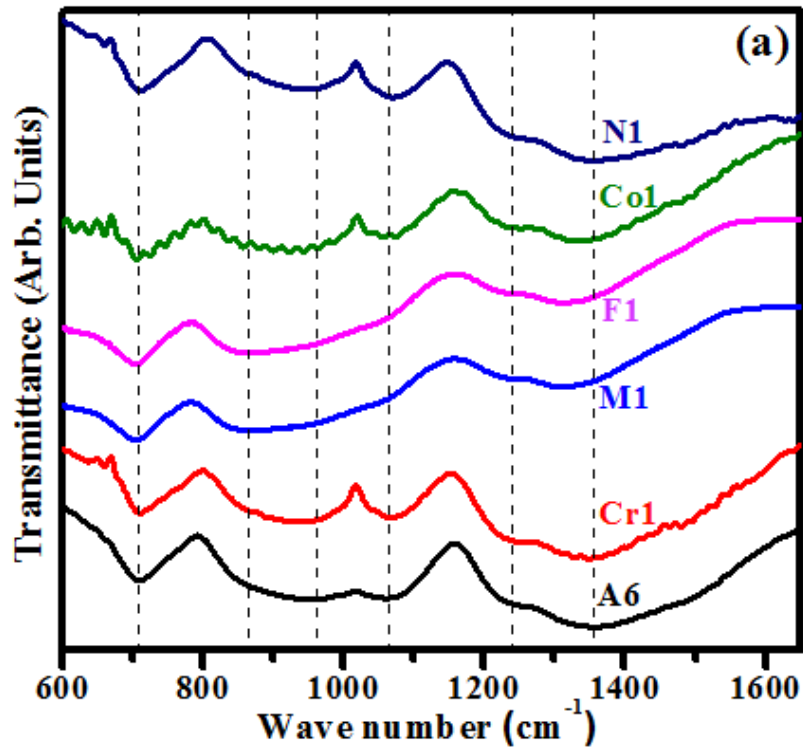


Figure 4.2 (a): FTIR spectra of TMO doped LN-TM glass system.

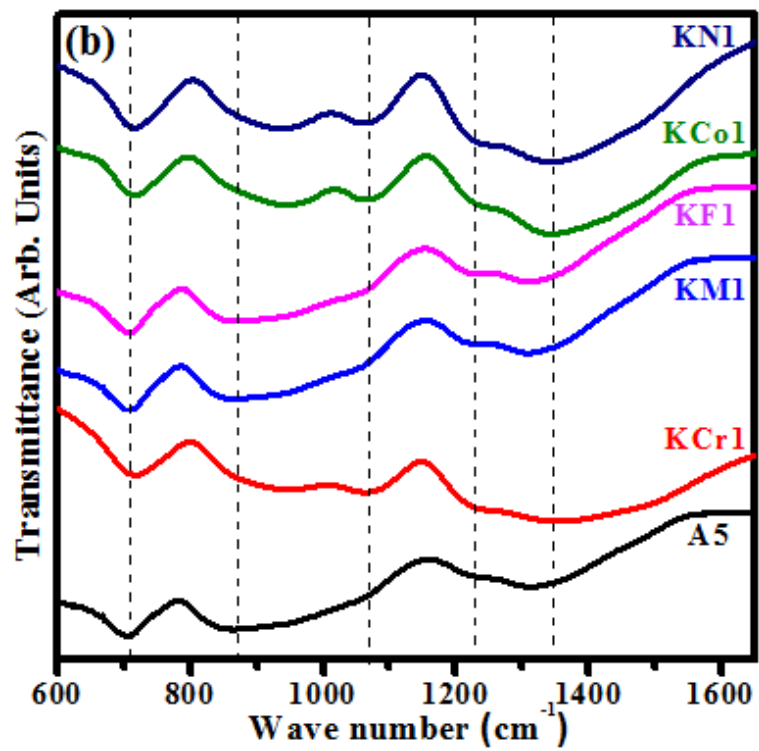


Figure 4.2 (b): FTIR spectra of TMO doped LNK-TM glass system.

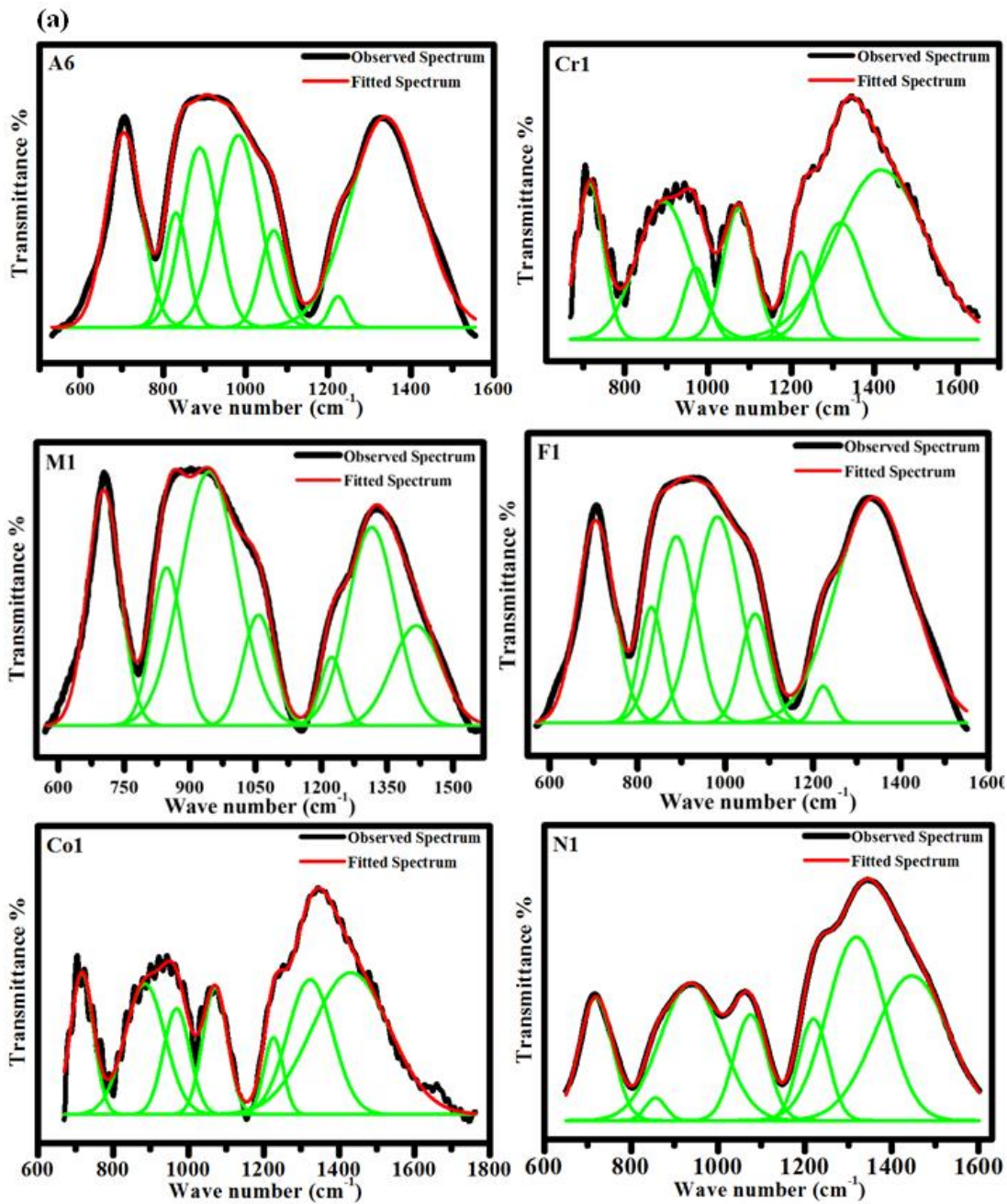


Figure 4.3 (a): Deconvoluted FTIR peaks of TM doped LN-TM glass system.

It can be noticed that the FTIR spectra of examined glasses includes the crucial bands of vitreous B₂O₃ with a trivial shift from their original position. Band assignments are presented in table 4.1. The two alkali glass sample i.e., A6 is exhibits a band at 711 cm⁻¹, which can be attributed to the bending vibration of B-O-B linkage

of the borate glass network (Subhashini et al. 2016, Kamitsos and Chryssikos 1991, Pascuta et al. 2010).

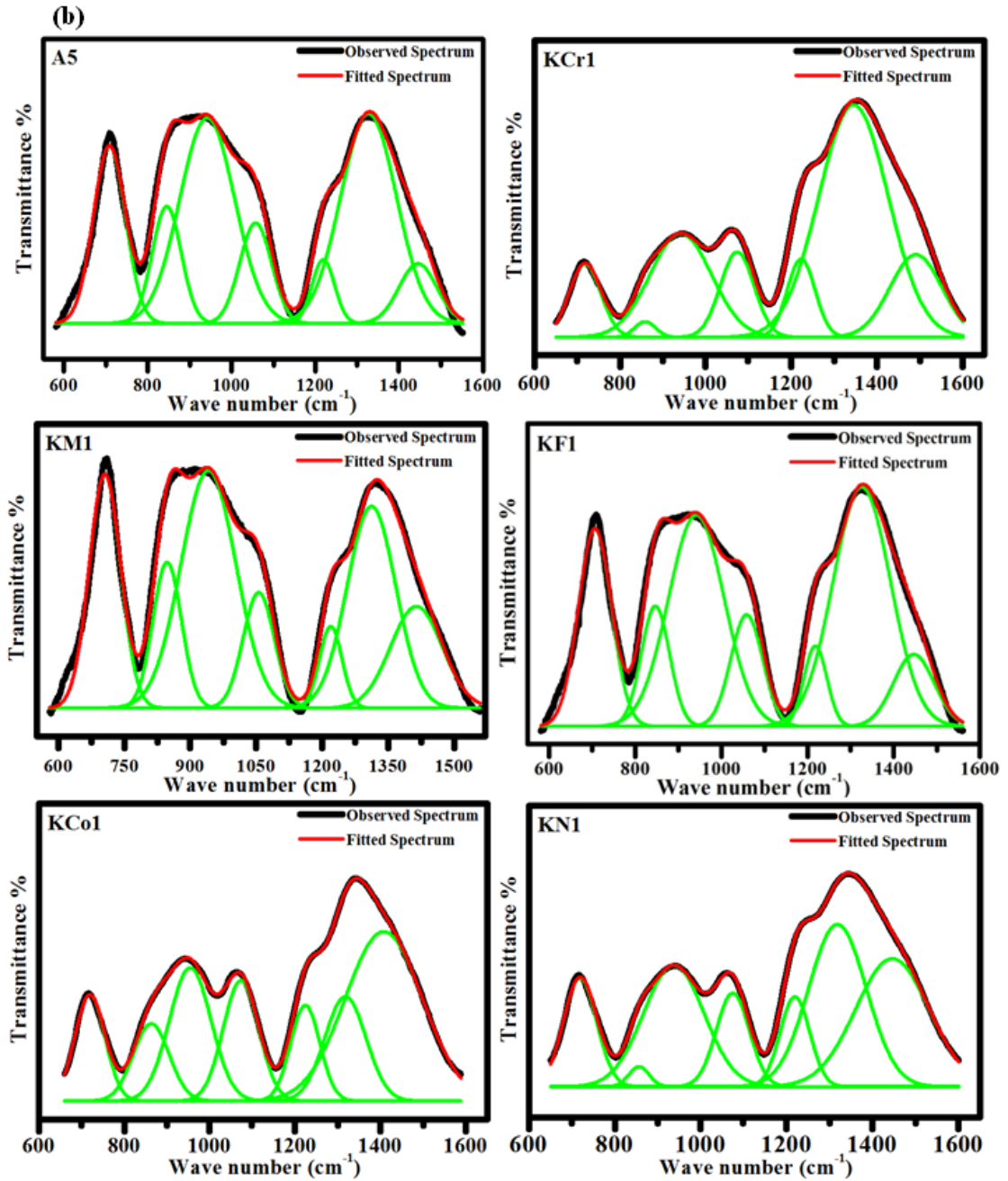


Figure 4.3 (b): Deconvoluted FTIR peaks of TM doped LNK-TM glass system.

Table 4.1. Assignment of absorption bands present in FTIR spectra of TMO doped LN-TM and LNK-TM glass system.

Band position (cm ⁻¹)	FTIR band assignments
705, 711	B-O-B bending vibrations. (Selvarajan et al. 1984)
865	Stretching vibrations of B-O bonds in BO ₄ . (Fayad et al. 2017)
950	Stretching vibrations of B-O bonds in BO ₄ from diborate groups. (Gaafar et al. 2013)
1060	B-O stretching vibrations of BO ₄ units in tri-, tetra-, and penta-borate groups. (Reddy et al. 2008)
1250	Symmetric stretching vibrations of B-O bonds in BO ₃ . (ElBatal 2012)
1313-1350	Stretching vibrations of B-O in BO ₃ units from different borate groups. (Naresh et al. 2012)

The addition of third alkali element i.e., K₂O to the A6 glass sample shifts band observed around 711 cm⁻¹ towards the lower wave number i.e., 705 cm⁻¹ this can be also attributed to the bending vibrations of B-O-B linkage. In two alkali glass system it can be observed that the band position of bending vibrations of B-O-B linkage is shifting towards the lower wave number for transition metal doped two alkali borate glass sample (A6) and on the other hand there is a shift in the same band position towards the higher wave number in case of transition metal doped three alkali glass sample (A5) this may be attributed to the change in field strength of the glass samples. This indicates the fact that even though there is no significant coordination change occurred but there is a slight modification in the structure of glass samples with the incorporation of transition metal ions in both LN-TM and LNK-TM glass systems. The comparative influence of the different alkali oxides present in the glass system may be ascribed to different ionic radii of alkali ions. In the present glass system both LN-TM and LNK-TM contains 5 mol% of Li₂O content, which easily enter the glass network and occupies the void spaces in the glass network without disturbing the glass structure. Another important aspect is the oxygen ions present in the vicinity of the sodium or potassium ion must be more polarized in vicinity to the lithium ion (Fayad et al. 2017). The band observed around 950 cm⁻¹ with a shoulder around 865 cm⁻¹ in both LN-TM

and LNK-TM glass system can be attributed to the stretching vibrations of B-O bonds of BO_4 units involved in diborate units. The shoulder around 865 cm^{-1} is present in only chromium, manganese and iron doped glasses in both two and three alkali glasses and absent in the cobalt and nickel doped glass samples this band can be attributed to the stretching vibrations of tri- tetra- and pent borate units apart from this, the band can be also attributed to the deformation modes of the network structure which gives the clear hint that the chromium, manganese and iron ions directly influence the structure of the glass system. Another prominent band around 1060 cm^{-1} is attributed to the B-O stretching vibrations of BO_4 units. The broad band around $1313\text{-}1350\text{ cm}^{-1}$ with a prominent shoulder around 1250 cm^{-1} can be attributed to the stretching vibrations of B-O bonds in BO_3 units involved in different borate groups mainly with pyro- and ortho- borates (Subhashini et al. 2016, Reddy et al. 2008).

4.1.2.2 Raman Spectroscopy studies

The recorded Raman spectra of transition metal doped two and three alkali glass systems were represented in figure 4.4 (a) & (b). In order to collect all the possible information from superposed bands of the spectrum deconvolution has been done using Gaussian function. The deconvoluted Raman spectrum is depicted in figure 4.5 (a) & (b). The band assignments are represented in the table 4.2. The band around 465 cm^{-1} in LN-TM and LNK-TM glass system can be attributed to the B-O-B bending vibrations from the isolated diborate groups (Meera and Ramakrishna 1993). The relatively sharp band present around $725\text{-}735\text{ cm}^{-1}$ observed in both the glass system may be due to the symmetric breathing vibrations ascribed to the six membered structure involved in the different kinds of ring type structures containing two units of four-fold boron atom viz., di-tri-borate or di-penta-borate (Meera and Ramakrishna 1993, Maniu et al. 1999). The band appeared around $958\text{-}955\text{ cm}^{-1}$ and $1100\text{-}1070\text{ cm}^{-1}$, in LN-TM glass system can be ascribed to the vibrations of diborate groups in the structure (Meera and Ramakrishna 1993). Similarly, the band appearing around 850 cm^{-1} and $950\text{-}1180\text{ cm}^{-1}$, in LNK-TM glass system are due to same reason as in LN-TM glass system.

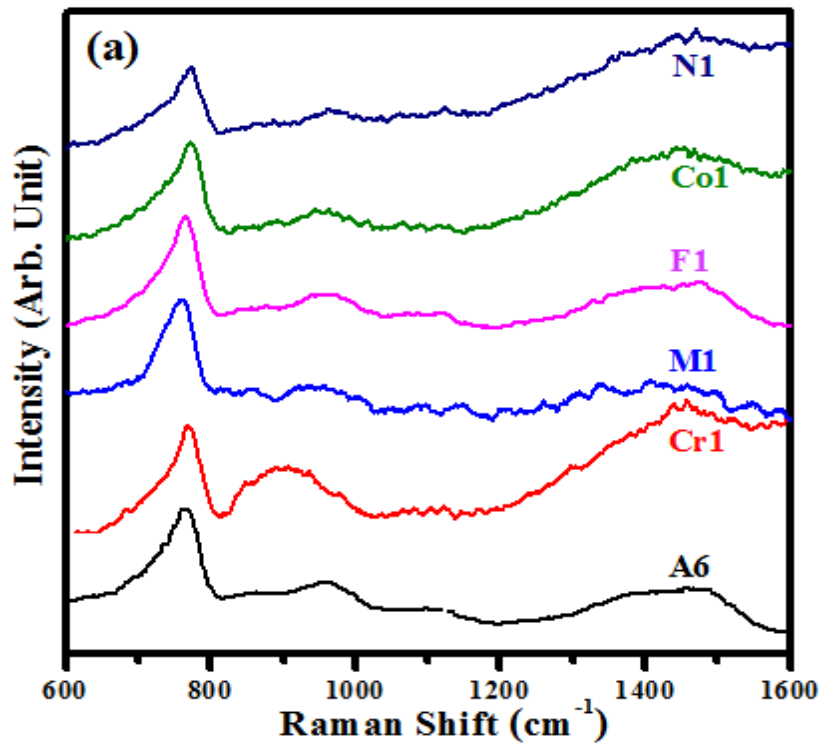


Figure 4.4 (a): Raman spectra of TMO doped LN-TM glass systems.

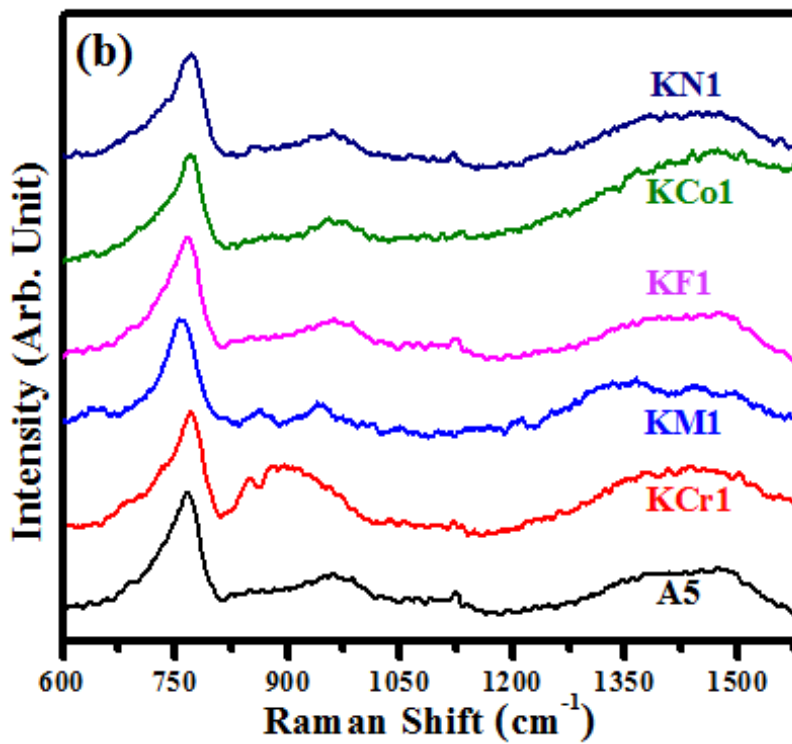


Figure 4.4 (b): Raman spectra of TMO doped LNK-TM glass systems.

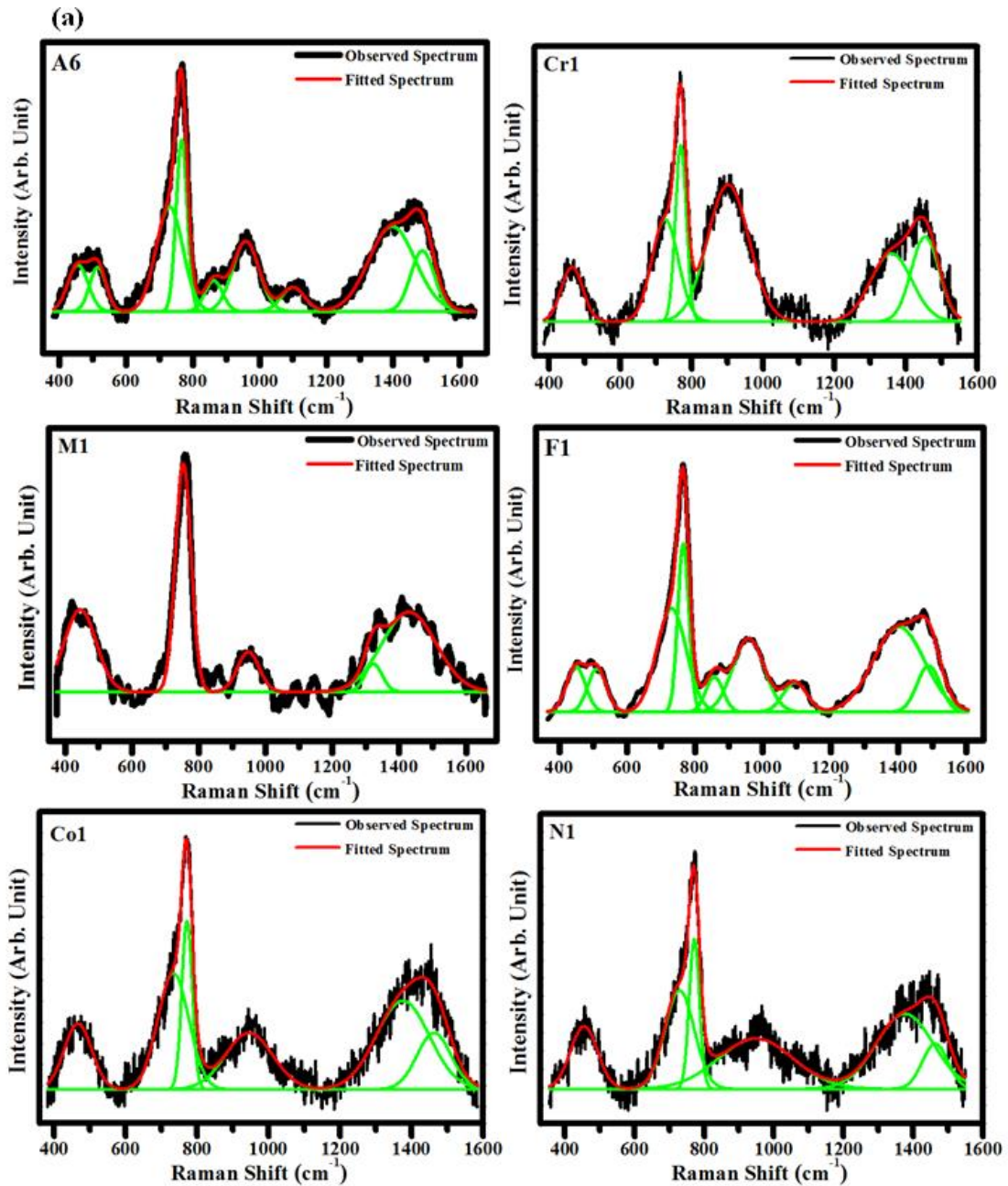


Figure 4.5 (a): Deconvoluted Raman spectra of TMO doped LN-TM glass system.

The bands around $1396\text{-}1364\text{ cm}^{-1}$ in LN-TM glass system and the band around 1350 cm^{-1} with the minor shoulder around $1120\text{-}1250\text{ cm}^{-1}$ in LNK-TM glass system can be attributed to the BO_2O^- triangles associated to BO units. Lastly the broad band in the region of $1489\text{-}1481\text{ cm}^{-1}$ and around $1477\text{-}1485\text{ cm}^{-1}$ respectively in LN-TM and LNK-TM glass system can be assigned to the BO_2O^- triangular structures connected to the borate units.

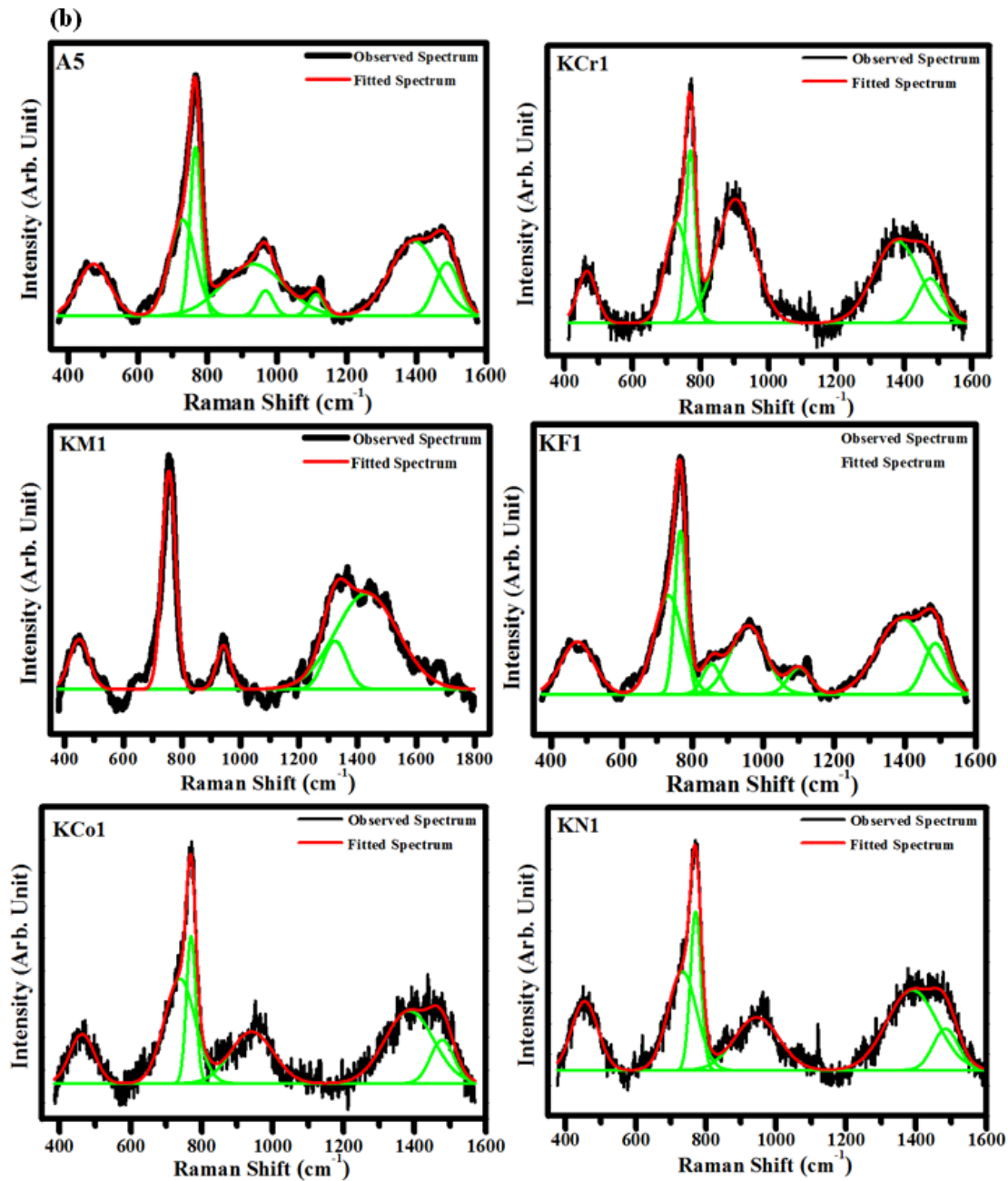


Figure 4.5 (b): Deconvoluted Raman spectra of TMO doped LNK-TM glass system.

In general, the borate glass systems possess various structural groups like $[\text{BO}_3]$, $[\text{BO}_4]$, tri-borate, di-borate, etc., which are observed in present investigation as well. It is expected, in general, that there are outnumbered diborate units present in stoichiometric diborate glass structures (Reddy et al. 2008), which can be further confirmed from the band assignments of FTIR and Raman spectra. The diborate units

are associated with two [BO₄] units along with two [BO₃] units in bridging position, which formulate a rigid symmetrical geometry in the glass network.

Table 4.2. Assignment of absorption bands present in Raman spectra of TMO doped LN-TM and LNK-TM glass system.

Band position (cm ⁻¹)	Raman band assignments
448-455	Isolated diborate groups. (Meera and Ramakrishna 1993)
508-519	Vibrations of TMO. (Meera and Ramakrishna 1993)
725-735	Symmetric breathing vibrations of six members ring with one or two BO ₄ units (ditri- or dipenta-borate). (Maniu et al. 1999)
765	B-O-B bending mode, and symmetric stretching vibrations of six members ring with two tetrahedral borate units (i.e., diborate). (Maniu et al. 1999)
955-958	TMO vibrations and vibrations of diborate groups in the structure. (Meera and Ramakrishna 1993)
1100-1180	Vibrations of diborate groups. (Meera and Ramakrishna 1993)
1364-1396	BO ₂ O ⁻ triangles linked to B-O units. (Meera and Ramakrishna 1993)
1481-1489	BO ₂ O ⁻ triangles linked to other triangular borate units. (Reddy et al. 2008)

4.1.3 Optical Studies

Optical properties of LN-TM and LNK-TM glass systems were studied using UV-Visible absorption spectroscopy studies. TMO doped LN-TM and LNK-TM glass systems exhibit extra characteristic absorption bands, as shown in figure 4.6 (a) & (b), due to each TM ion in its specific valence or coordinate state. The optical spectra show that the TM ions favor the high valence or tetrahedral coordination states in borate host glass. Infrared absorption bands of all the prepared glasses reveal the appearance of both triangular BO₃ units and tetrahedral BO₄ units within their characteristic vibrational modes. The TM ions cause minor effects in structural properties because of the low doping concentration (0.1 mol %). The LN-TM and LNK-TM glass system containing chromium ions exhibit a strong absorption band around 370, 610 and 650 nm corresponding to the $^4A_{2g}(F) \rightarrow ^4T_{1g}(P)$, $^4A_{2g}(F) \rightarrow ^4T_{2g}(P)$ and $^4A_{2g}(F) \rightarrow ^4T_{2g}(t)$

respectively.

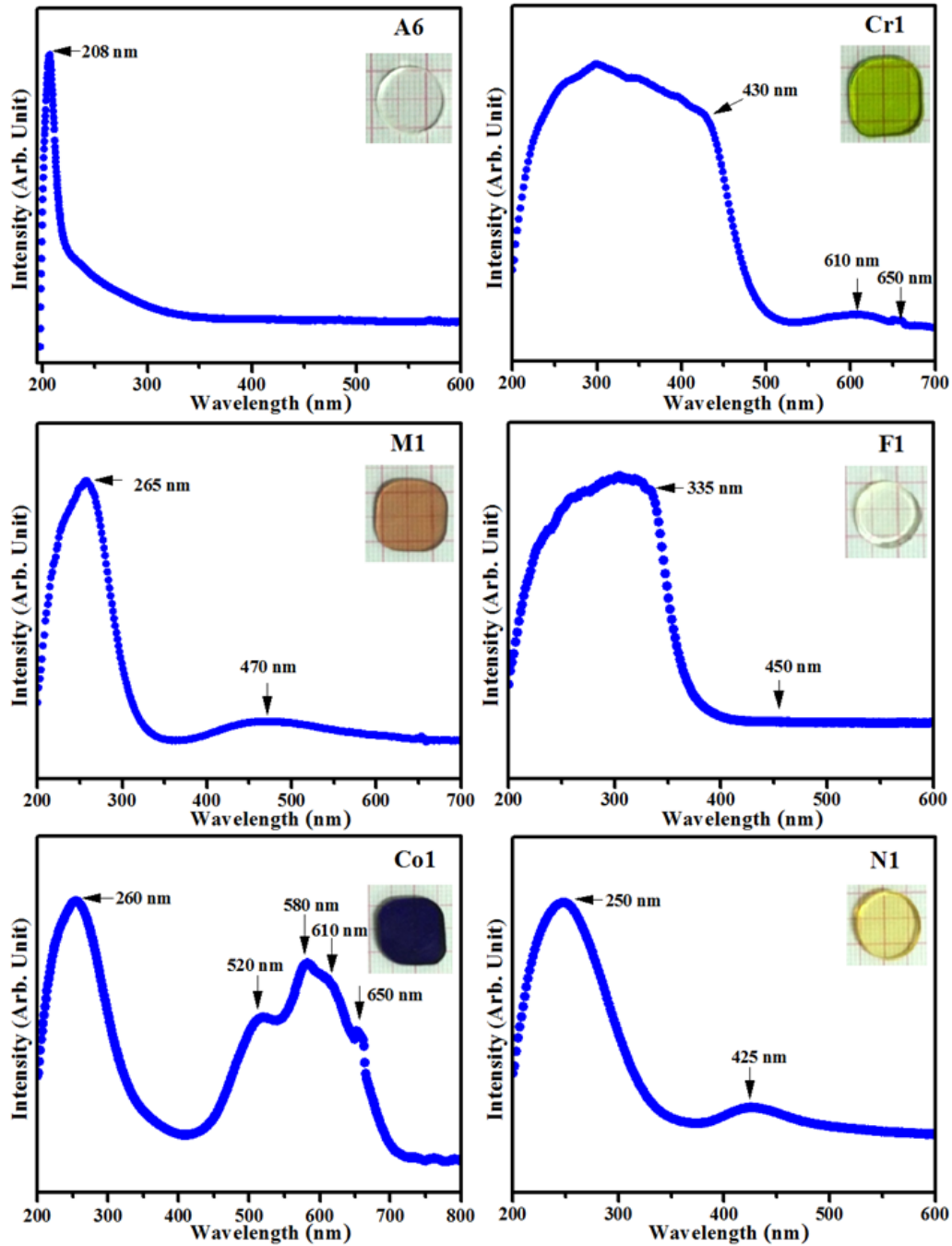


Figure 4.6 (a): UV-visible absorption spectra for the TMO doped LN-TM glass system.

The absorption band from 350 to 370 nm is attributed to the charge transformation. The chromium ions are present in both Cr^{3+} and Cr^{6+} states with octahedral environment. In case of Mn doped LN-TM and LNK-TM glass system, the

divalent manganese ions (Mn^{2+}) present in distorted octahedral symmetry.

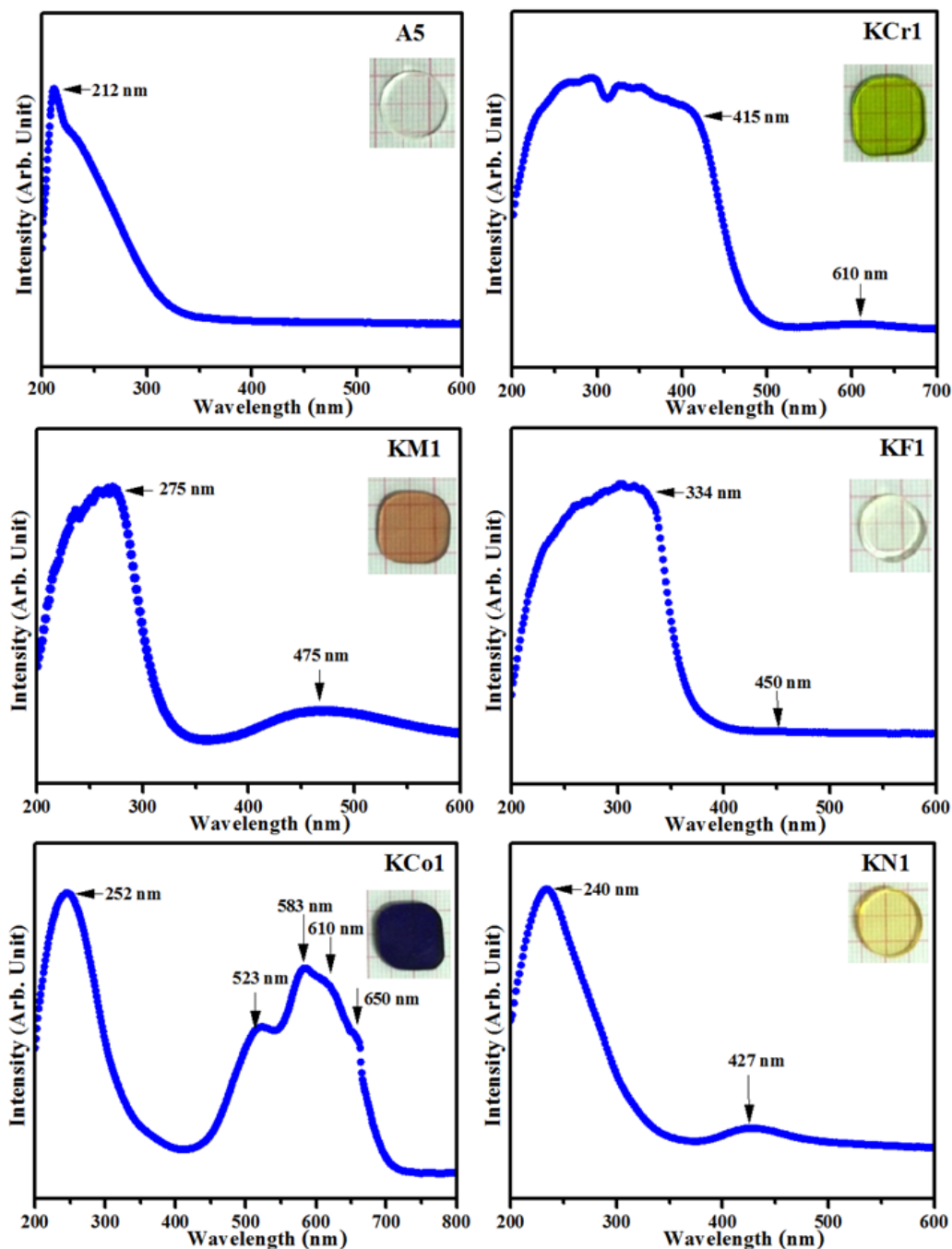


Figure 4.6 (b): UV-visible absorption spectra for the TMO doped LN-TM glass system.

This is confirmed by the absorption band observed at 475 nm owing to the ${}^6A_{1g}(S) \rightarrow {}^4T_{1g}(G)$ transition. In Fe_2O_3 doped LN-TM and LNK-TM glass system, a broad absorption band appeared around 450 nm revealing the presence of Fe^{3+} ions in

distorted octahedral state and the broad band around 450 nm is attributed to the ${}^6A_{1g}(S) \rightarrow {}^4T_{2g}(G)$ transition. The cobalt doped glass samples exhibit deep royal blue colour due to the presence of triple split in the visible region as shown in the figure 4.6 (a) & (b). In case of cobalt there exist both spin allowed and spin forbidden transitions. The three splits from 520 to 650 nm confirm the divalent state of cobalt ions in both tetrahedral and octahedral symmetry. The nickel doped LN-TM and LNK-TM glass samples exhibiting two major absorption bands around 425 nm and 770 nm are respectively attributed to the ${}^3A_{2g}(F) \rightarrow {}^3T_{1g}(P)$ and ${}^3A_{2g}(F) \rightarrow {}^3T_{2g}(F)$ transitions. These transitions reveal the presence of nickel ions in Ni^{2+} state in octahedral symmetry. The optical absorption spectra of different transition metal ions reveal that the addition of TM ions to the LN-TM and LNK-TM glass system greatly influences the optical properties despite of having low concentration (0.1 mol%) of TM ions. Their specific valence and coordination states exhibit absorption band at different wavelengths indicating the possibility of using these glass samples as optical filters. The Fe_2O_3 and MnO_2 were chosen to study the doping effect of them in the LN-TM and LNK-TM glass system with increasing concentration of them. This was done to carry out further studies to understand the influence of TM ions on various properties of studied glass systems.

The systematic learning of UV-visible spectra yields evidence about the structure of electronic bands and optical transitions of glass system. It is well known that glass obeys dipole selection rule hence direct or indirect transition occurs. The absorption coefficient (α) can be calculated using the equation (2.10). The magnitude of absorption coefficient (α) can be linked to the optical band gap energy E_g , using equation (2.10) with the equation (2.11) known as Davis and Mott relation (Fu et al. 2012). Since indirect allowed transition takes place in glasses, considering the value of n as 2, equation (2.11) can be simplified and written as equation (2.12). The optical band gap energy (E_g), can be determined by plotting $(\alpha h\nu)^{1/2}$ against photon energy which is named as Tauc plot and is depicted in figure 4.7 (a) & (b) for the present glass system. The determined values of E_g are tabulated in table 4.3.

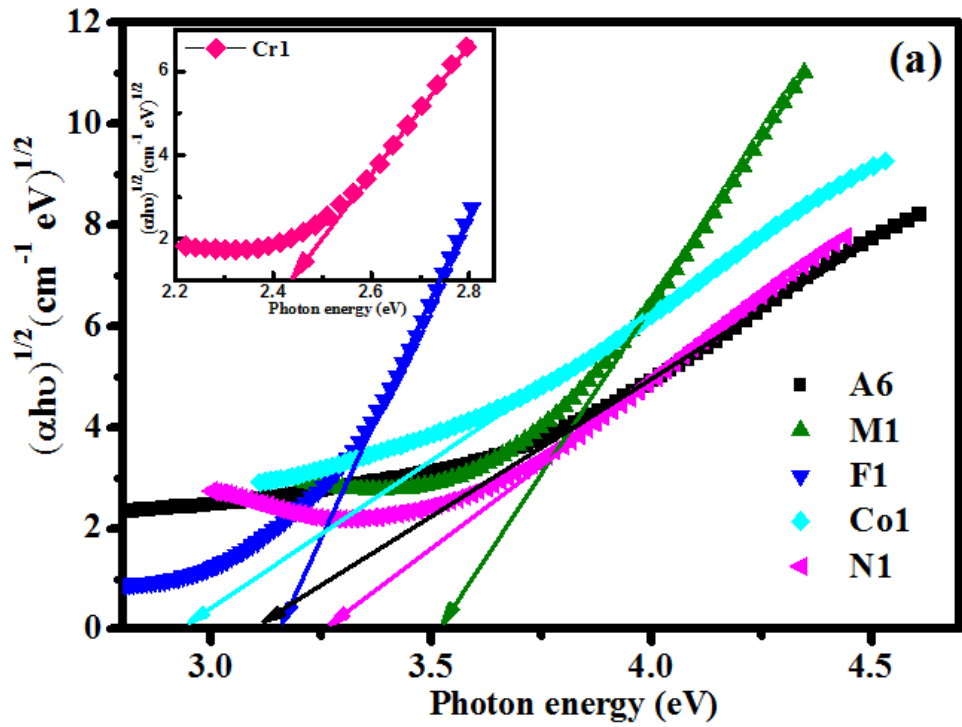


Figure 4.7 (a): Variation of $(\alpha h\nu)^{1/2}$ as a function of photon energy ($h\nu$) for the TMO doped LN-TM glass system.

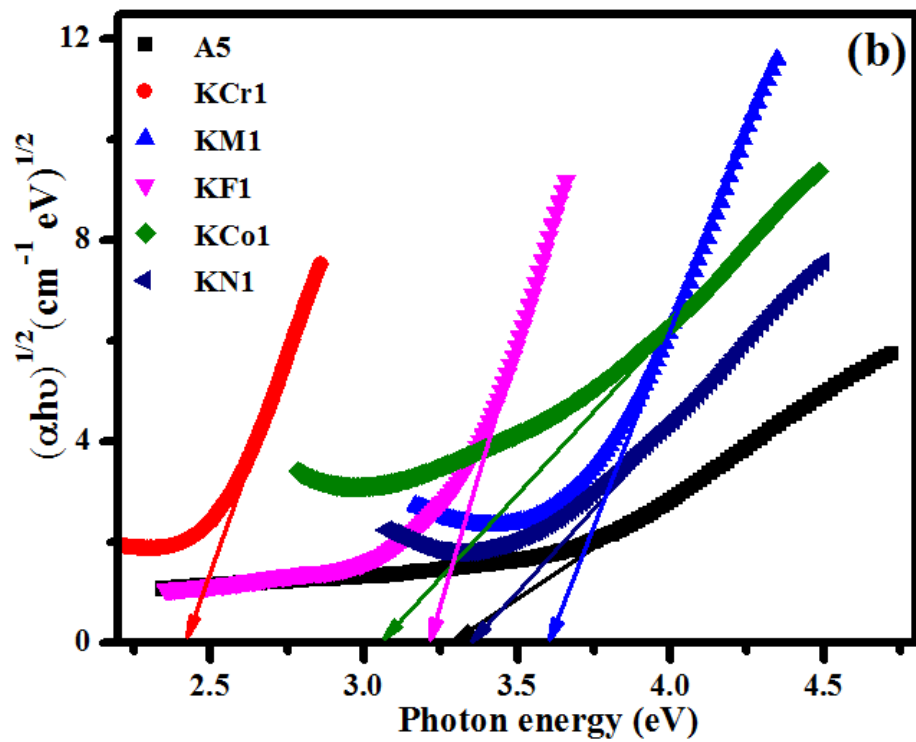


Figure 4.7 (b): Variation of $(\alpha h\nu)^{1/2}$ as a function of photon energy ($h\nu$) for the TMO doped LNK-TM glass system.

From the tabulated data it can be observed that E_g of A6 sample is 5.40 ± 0.1 eV upon the incorporation of third alkali metal (K_2O) it has reduced to 3.67 ± 0.1 eV. This reduction of E_g may be ascribed to the structural differences occurring due to the addition of relatively lower field strength K_2O ($0.12 \times 10^{-20} \text{ m}^{-2}$) to higher field strength Na_2O ($0.17 \times 10^{-20} \text{ m}^{-2}$). The average bond energy is another key factor which affects the E_g . The replacement of relatively higher bond energy Na_2O (8.4 KJ/mol) with relatively lower bond energy K_2O (12.2 KJ/mol) may cause the reduction in the average bond energy of the glass network, which lowers the energy of the conduction band edge and hence results in reduction of E_g . In the present study addition of 0.1 mol% transition metal oxide to A5 and A6 glass samples results in significant variation in the optical band gap energy (E_g). In LN-TM series Mn ion doped glass samples exhibit comparatively higher values of E_g whereas glasses Cr ion exhibits relatively lower E_g values as shown in the table 4.3.

Table 4.3. Optical band gap energy (E_g) and Urbach energy (E_u) of TMO doped LN-TM and LNK-TM glass systems.

Glass system	Glass code	E_g (eV, ± 0.1)	E_u (eV, ± 0.1)
LN-TM	A6	5.40	0.14
	Cr1	2.37	0.15
	M1	3.58	0.19
	F1	3.19	0.17
	Co1	2.96	0.27
	N1	3.25	0.21
LNK-TM	A5	3.67	0.16
	KCr1	2.42	0.17
	KM1	3.16	0.20
	KF1	3.22	0.18
	KCo1	3.07	0.28
	KN1	3.35	0.23

In LNK-TM series, Ni ion doped glass has the highest E_g with Cr ion doped glass having the lowest E_g . This can be attributed to the increasing concentration of non-bridging oxygen (NBO), which are created during the structural rearrangement occurring in the glass network upon addition of TMO content. The band tails are characterized by Urbach energy, E_U (Narayanan et al. 2015) which is given by the equation (2.13).

Taking natural log on both sides of the equation (2.13), it can be simplified and written as represented in equation (2.14). Figure 4.8 (a) & (b) represents the reciprocal of the slope of the linear region. The determined values of Urbach energy, E_U are summarized in table 4.3. It is noticed that the value of the E_U is observed to increase with the addition of TMO content. This can be attributed to the presence of defects occurring due to the modifications of the structure. It is witnessed that the absorption tail is broad owing to the indirect electronic transitions assisted by the presence of phonons. Consequently, Urbach energy values endorse the presence of electronic transitions assisted by the phonons in the current investigated glass samples.

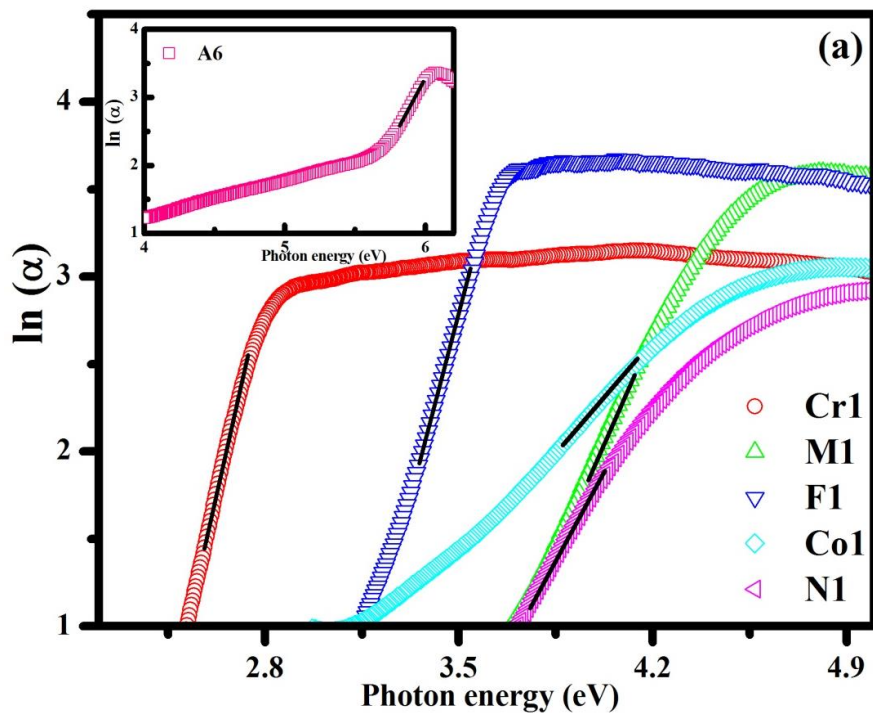


Figure 4.8 (a): Variation of $\ln(\alpha)$ as a function of photon energy ($h\nu$) for the TMO doped LN-TM glass system.

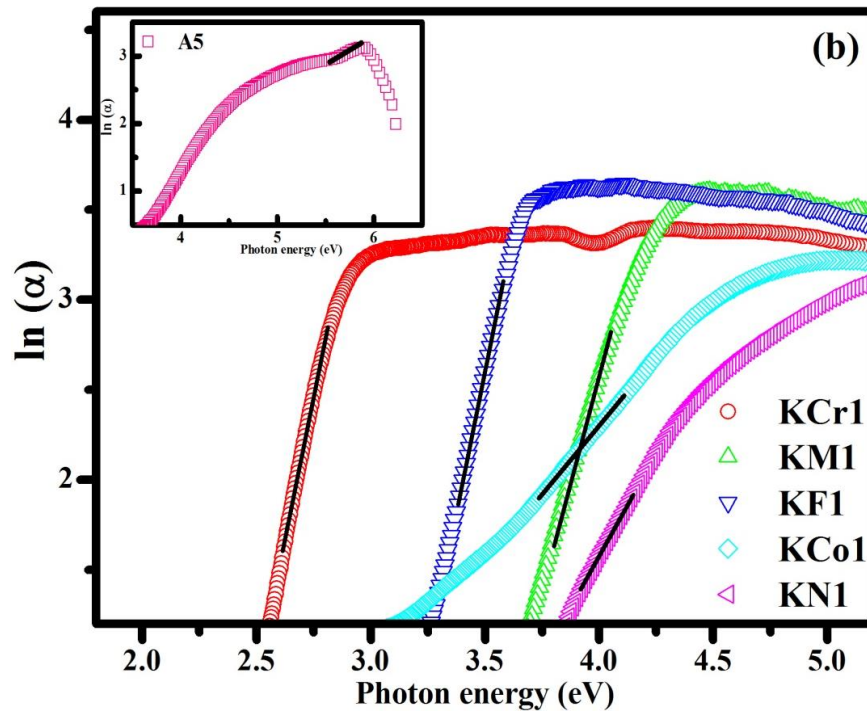


Figure 4.8 (b): Variation of $\ln(\alpha)$ as a function of photon energy ($h\nu$) for the TMO doped LNK-TM glass system.

4.1.4 Mechanical properties

Mechanical strength of glass material plays crucial role in choosing glass samples for practical applications. The mechanical strength and fracture toughness of the prepared glass samples were determined using Vickers micro-indentation technique. To rule out any kind of experimental errors, each sample was indented ten times and standard deviation was calculated. The measured values of Vickers micro-hardness were presented in table 4.4. The measured Vickers micro-hardness values were found to decrease from 4.992 to 4.760 GPa for A6 and A5 samples, respectively. This may be ascribed to the partial replacement of relatively lower radius and higher field strength Na^{2+} with higher radius and lower field strength K^{2+} . Partial substitution of potassium ions having higher radius increases the distance between modifier cations and anions in the glass network. This leads to the weakening of glass structure and decreases the Vickers micro-hardness. Further it can be noticed that, there is a slight decrease in the Vickers micro-hardness in the glass samples incorporated with TMO in both LN-TM and LNK-TM glass series. In both the series Fe_2O_3 doped samples exhibit

relatively higher hardness values and Cr₂O₃ exhibits lower hardness values. This may be ascribed to the relatively higher radius of the chromium ions which increases the distance between modifier cation and anion in the glass matrix. Mechanical strength of the prepared glass samples can be evaluated by studying the crack initiation and propagation patterns, which are the two major factors in determining the strength of the glasses. The fracture toughness, (K_{IC}) which is the measure of how easily a crack can propagate through the material with the applied load is determined using the relation (2.22) suggested by Anstis (1981). The determined fracture toughness (K_{IC}) values are represented in table 4.4. It is evident that K_{IC} of Cr₂O₃ incorporated glass sample is exhibiting relatively lower fracture toughness whereas Fe₂O₃ incorporated glass sample exhibiting relatively higher fracture toughness value in both LN-TM and LNK-TM glass samples.

Table 4.4. Vickers hardness (H_v), half crack length (C), fracture toughness (K_{IC}) and Brittleness (B) of TMO doped LN-TM and LNK-TM glass system.

Glass systems	Glass code	Measured Vickers hardness (GPa) \pm 0.004	Measured Half crack length (μm) \pm 1	Fracture toughness (MPa (m) ^{1/2}) \pm 0.003	Brittleness ($\mu\text{m}^{-1/2}$) \pm 0.02
LN-TM	A6	4.992	57.18	0.730	6.84
	Cr1	4.946	57.89	0.713	6.94
	M1	4.963	57.60	0.724	6.85
	F1	4.977	57.53	0.725	6.86
	Co1	4.957	57.73	0.717	6.91
	N1	4.968	57.33	0.721	6.89
LNK-TM	A5	4.760	59.05	0.705	6.75
	KCr1	4.643	60.57	0.687	6.75
	KM1	4.682	60.30	0.695	6.75
	KF1	4.687	60.12	0.696	6.77
	KCo1	4.665	60.40	0.691	6.75
	KN1	4.685	59.88	0.695	6.74

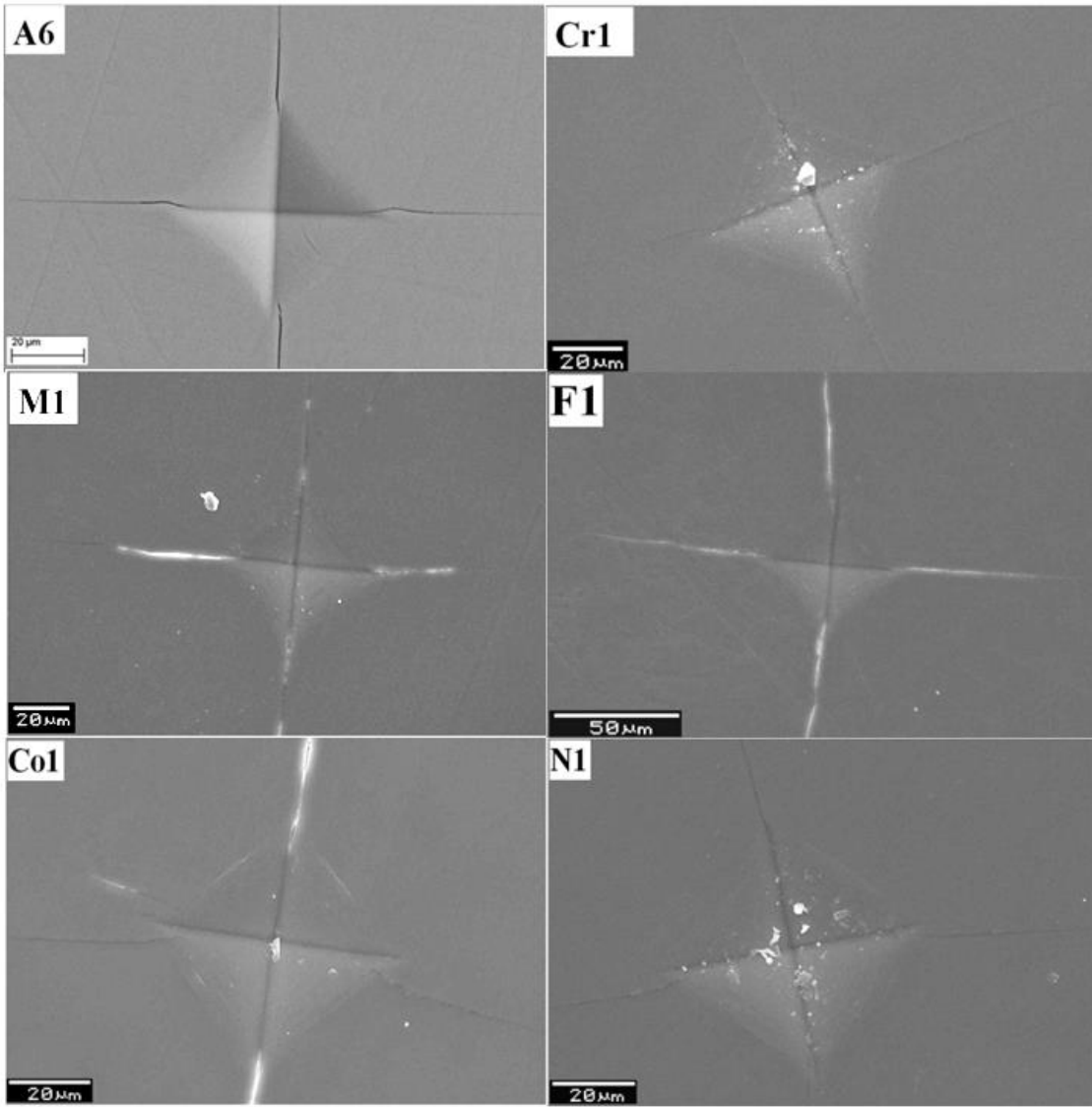


Figure 4.9 (a): SEM micrograph of Vickers indentation of TMO doped LN-TM glass system.

This can be attributed to the slight reduction of Vickers hardness and enhancement in half crack length. Another influencing factor of crack initiation and propagation is the index of brittleness, which is called as Brittleness (B). The brittleness of the prepared glasses was estimated by the equation (2.26) involving the measured Vickers hardness H_v and determined fracture toughness K_{IC} as proposed by Lawn and Marshall (1979). The evaluated brittleness values are presented in table 4.4.

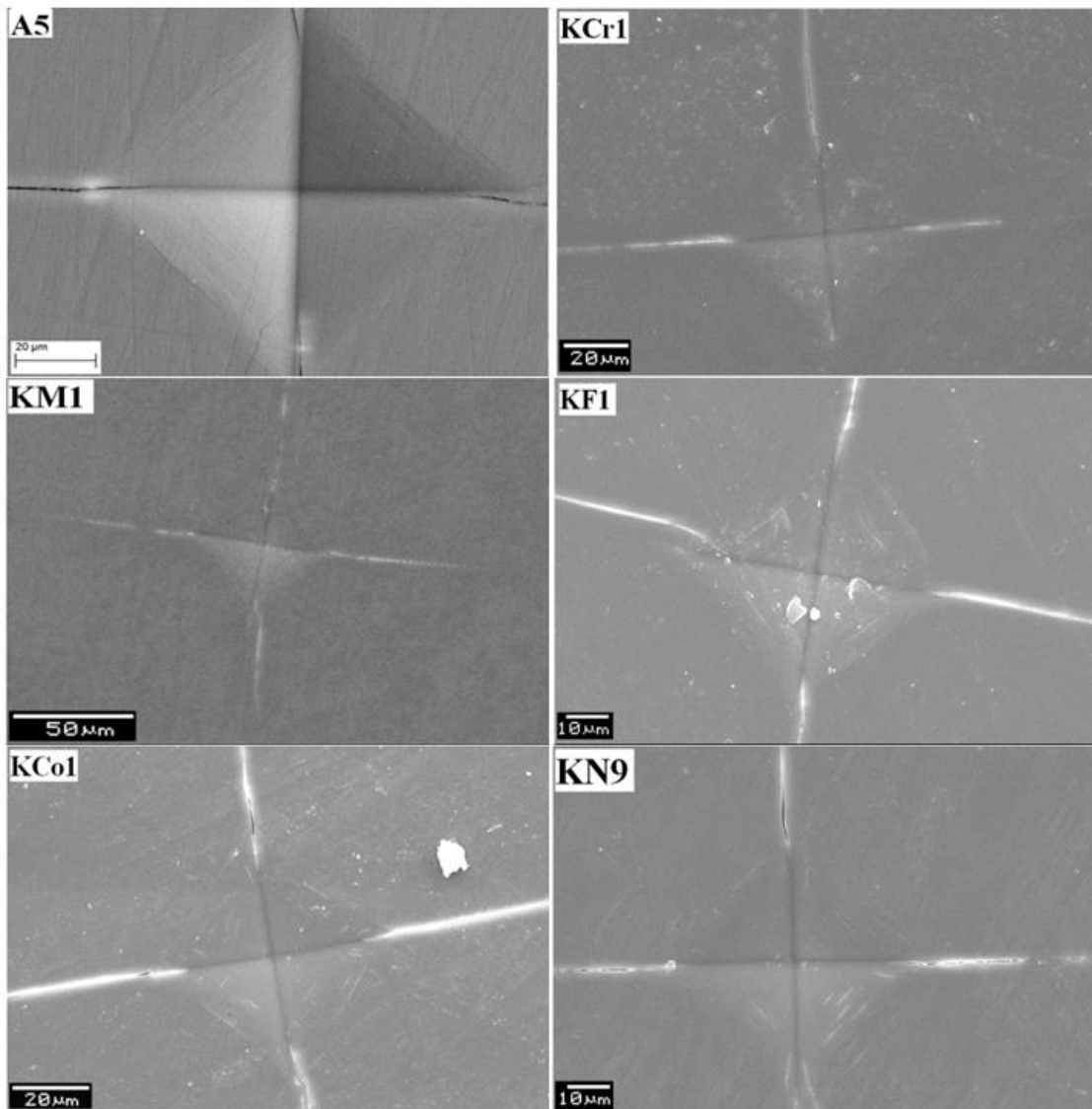


Figure 4.9 (b): SEM micrograph of Vickers indentation of TMO doped LNK-TM glass system.

In general, the plastic flow by means of deformation and densification before the crack initiation determine the brittleness of glass systems. Brittleness is found to be relatively higher in Cr_2O_3 incorporated glass sample. This increase in the brittleness is further confirmed by SEM micrographs represented in figure 4.9 (a) & (b). E is the Young's modulus (GPa) which is calculated using equation (2.23), H is the experimentally determined Vickers hardness (GPa), P is the load applied (4.9 N) and C is the measured half crack length (μm). Young's modulus of the poly component system is obtained by the theoretical model suggested by Makishima and Mackenzie (1973)

using the equation (2.23). The atomic packing fraction, V_t is calculated using the equation (2.24). The determined values of Young's modulus (E), shear modulus (S), bulk modulus (K) and atomic packing fraction, V_t are summarized in table 4.5.

Table 4.5. Young's modulus (E), bulk modulus (K), shear modulus (S), and atomic packing density (V_t) of TMO doped LN-TM and LNK-TM glass system.

Glass systems	Glass code	Young's modulus, E (GPa)	Bulk modulus, K (GPa)	Shear Modulus, S (GPa)	Atomic packing density, V_t
LN-TM	A6	80.95	59.14	31.82	0.609
	Cr1	79.33	56.76	31.30	0.596
	M1	80.96	59.14	31.83	0.609
	F1	81.05	59.26	31.86	0.609
	Co1	79.80	57.47	31.45	0.600
	N1	79.07	56.40	31.22	0.594
LNK-TM	A5	79.33	57.39	31.25	0.603
	KCr1	80.19	56.76	31.30	0.596
	KM1	79.51	57.58	31.30	0.604
	KF1	79.41	57.43	31.27	0.603
	KCo1	79.80	57.47	31.45	0.600
	KN1	79.07	56.40	31.22	0.594

5.2 Summary

In the present chapter, the results of comparative studies carried out on the effect of TM ions addition on the properties of LN-TM glass system with that of the LNK-TM glass system are discussed in detail. The XRD results, for both the series, confirmed the amorphous nature of the glass systems. It can be noticed from the FTIR spectra of examined glasses the presence of the crucial bands of vitreous B_2O_3 and a trivial shift from their original position. The two alkali glass sample i.e., A6 exhibits a band at 711 cm^{-1} , which can be attributed to the bending vibration of B-O-B linkage of the borate glass network. The optical spectra show that the TM ions favour the high valence

or tetrahedral coordination states in borate host glass. Infrared absorption bands of all the prepared glasses reveal the appearance of both triangular BO_3 units and tetrahedral BO_4 units within their characteristic vibrational modes. The LN-TM and LNK-TM glass system containing chromium ions exhibit a strong absorption band around 370, 610 and 650 nm corresponding to the ${}^4\text{A}_{2g}(\text{F}) \rightarrow {}^4\text{T}_{1g}(\text{P})$, ${}^4\text{A}_{2g}(\text{F}) \rightarrow {}^4\text{T}_{2g}(\text{P})$ and ${}^4\text{A}_{2g}(\text{F}) \rightarrow {}^4\text{T}_{2g}(\text{t})$ respectively. Their specific valence and coordination states exhibit absorption band at different wavelengths indicating the possibility of using these glass samples as optical filters. The mechanical strength and fracture toughness of the prepared glass samples were determined using Vickers micro-indentation technique. The measured Vickers micro-hardness values were found to decrease from 4.992 to 4.760 GPa for A6 and A5 samples, respectively. Further it can be noticed that, there is a slight decrease in the Vickers micro-hardness in the glass samples incorporated with TMO in both LN-TM and LNK-TM glass series. The inclusion of TMO ions has proved to be of great importance in tailoring the properties of the glass systems to make them promising candidates for technological applications. The Mn and Fe transition metal ion doped glasses were chosen for detailed investigation on the effect of their composition on various properties in LN and LNK glass systems. Based on the superior properties exhibited by the Mn and Fe transition metal ions doped LN-TM and LN-TMO glasses over others studied these two glasses in both glass system were chosen for further investigations.

Chapter 5

EFFECT OF Fe^{3+} ADDITION ON THE PROPERTIES OF $5Li_2O-25Na_2O-60B_2O_3-(10-x)ZnO-xFe_2O_3$ AND $5Li_2O-xK_2O-(25-x)Na_2O-60B_2O_3-(10-y)ZnO-yFe_2O_3$ GLASS SYSTEMS: A COMPARATIVE STUDY OF LN-Fe AND LNK-Fe ZINC BORATE GLASS SYSTEM.

In the present chapter, the results of comparative studies carried out on the effect of Fe^{3+} addition on the properties of LN-Fe glass system with that of the LNK-Fe glass system are presented. XRD results, for both LN-Fe and LNK-Fe series, confirmed the amorphous nature of the synthesized glasses. The IR and Raman spectral analysis revealed that the Fe_2O_3 acted as a network modifier for both LN-Fe and LNK-Fe series in the present investigation. The prepared samples exhibited good thermal stability, which got enhanced as Fe_2O_3 content was increased. The glass forming ability has been enhanced with the partial incorporation of third alkali ion and Fe^{3+} ion in the LNK-Fe system. The glass transition temperature was found to reduce, for both LN-Fe and LNK-Fe series, as Fe_2O_3 content increased. This is due to the opening of diborate units by Fe_2O_3 in order to compensate its own coordination requirements. The median-radial cracks produced due to Vickers indentation were studied and it was confirmed that the brittleness of the samples enhanced, for both LN-Fe and LNK-Fe series, as Fe_2O_3 content was increased. Optical band gap energy, E_g of the studied glass system was found to reduce with increasing Fe_2O_3 content. Addition of Fe_2O_3 to B_2O_3 glass opens up the diborate glass network and decreases the energy of E_g resulting in the shift of absorption edge towards the higher wavelength region. It was noticed, in both LN-Fe and LNK-Fe series of prepared glasses enhanced refractive index as Fe_2O_3 content increased owing to the replacement of relatively lower polarizability Zn^{2+} (0.283 \AA^{-3}) by Fe^{3+} (0.437 \AA^{-3}). The absorption band observed, in both the series, around 450 nm in UV-Visible absorption spectra was due to the d-d transition of ${}^6A_{1g}(S) \rightarrow {}^4T_{2g}(G)$ which indicates the presence of an iron ion in trivalent state (Fe^{3+}) with distorted octahedral symmetry. Further efforts have been made to analyze and correlate the physical and mechanical properties with the structure of the studied glass system.

5.1 Results and Discussion

5.1.1 X-ray diffraction studies

The XRD measurement data of powdered samples of both LN-Fe and LNK-Fe series recorded between diffraction angle 10° - 80° are presented in figure 5.1 (a) & (b). It can be observed that all the samples exhibit a broad hump like feature without pronounced Bragg peaks. This result confirms the prepared glass samples to be amorphous in nature.

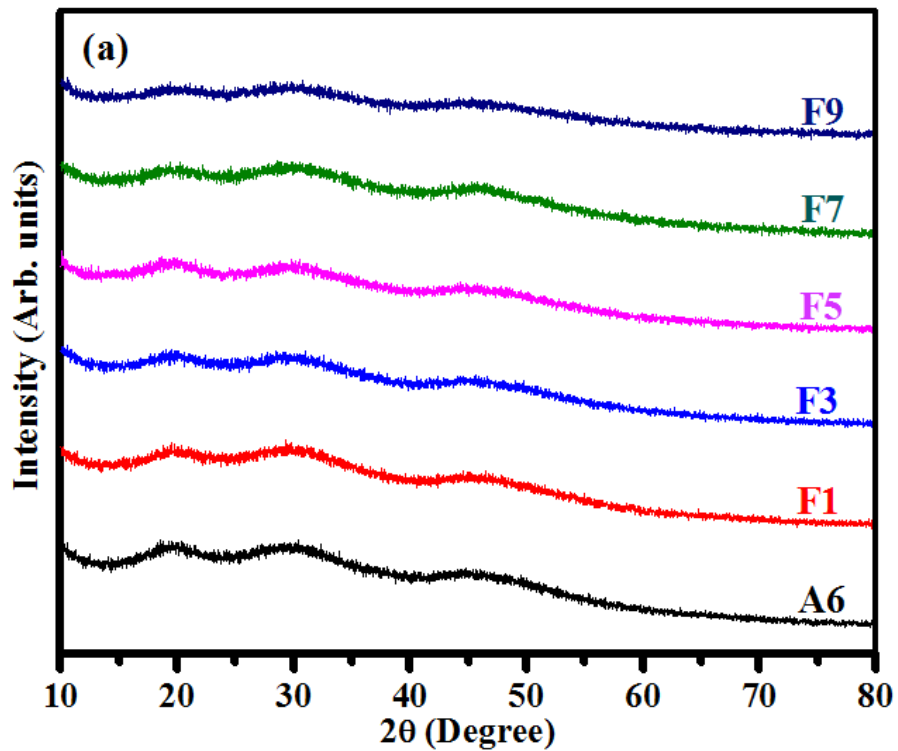


Figure 5.1 (a): X-ray Diffraction patterns of Fe_2O_3 doped LN-Fe glass system.

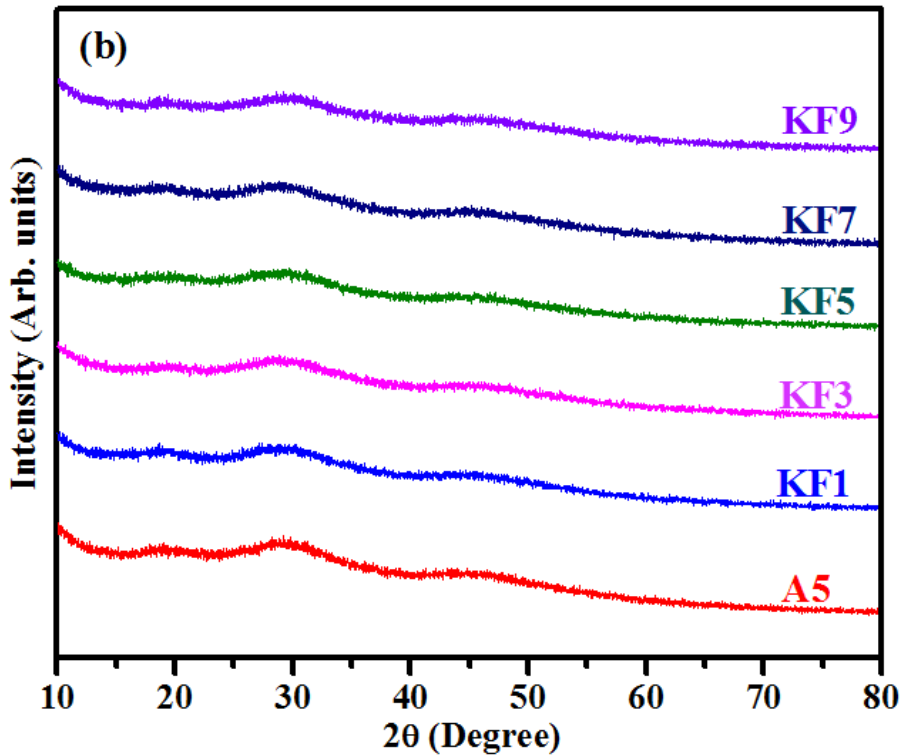


Figure 5.1 (b): X-ray Diffraction patterns of Fe₂O₃ doped LNK-Fe glass system.

5.1.2 Structural Studies

In the present section the FTIR and Raman spectroscopy data for the structural analysis of Fe³⁺ added glasses is discussed. These complementary techniques proved to be extremely important in differentiating the trigonal and tetrahedral borate units and to determine the concentration of NBOs per unit. In addition, they are also helpful in identifying the resident building blocks which are establishing the glass network and the anionic sites accommodating the modifier transition metal (TM) cations and superstructural units, viz., different types of rings, a combination of rings along with chains.

5.1.2.1 Fourier Transform Infrared Spectroscopy studies

Figure 5.2 (a) & (b) depicts the FTIR spectra of Fe₂O₃ doped LN-Fe and LNK-Fe glass systems. Each spectrum has its corresponding bands emerging due to the structural variations.

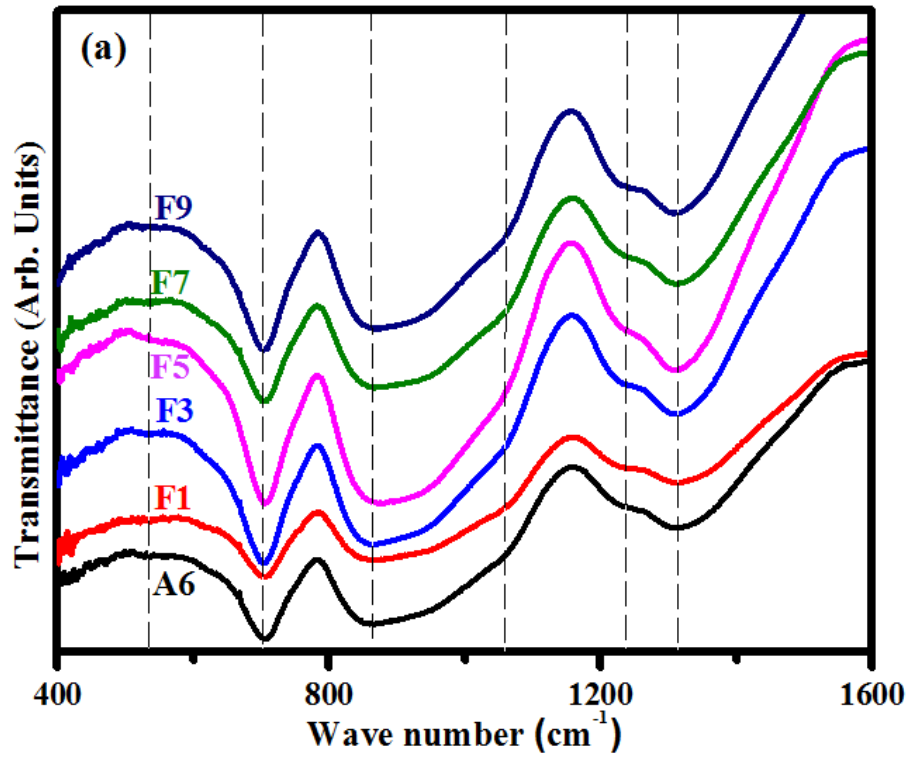


Figure 5.2 (a): FTIR spectra of Fe₂O₃ doped LN-Fe glass system.

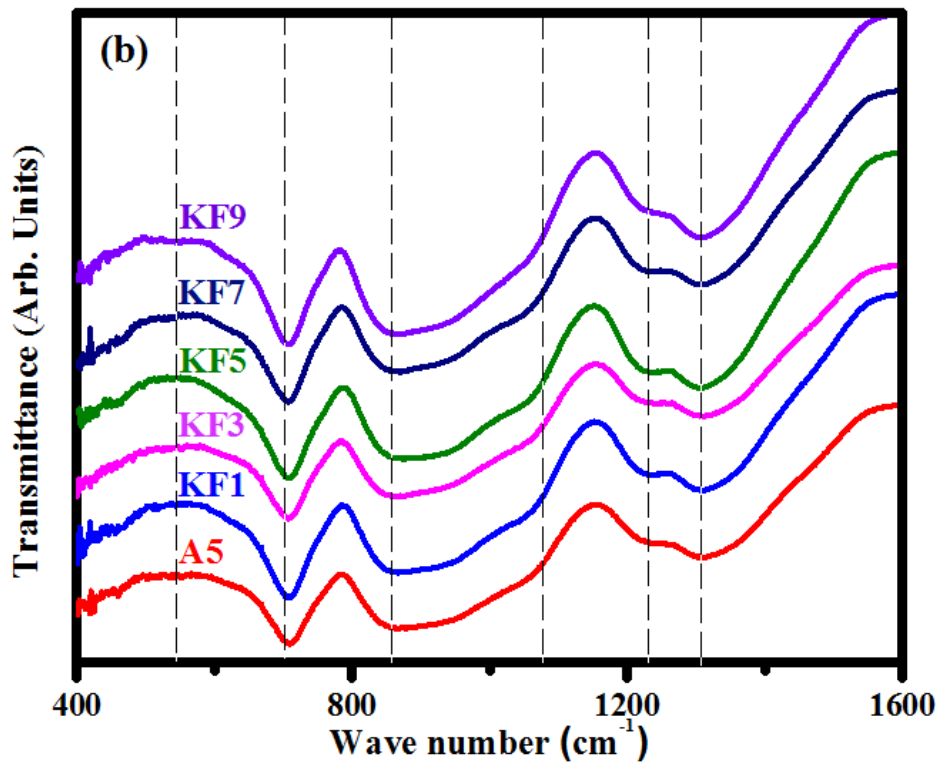


Figure 5.2 (b): FTIR spectra of Fe₂O₃ doped LNK-Fe glass system.

The resultant bands have specific area, intensity and centre corresponding to its structural group. In order to extract all the information regarding this, the broad peaks in the spectrum deconvoluted and the representative deconvoluted peaks are shown in figure 5.3 (a) & (b).

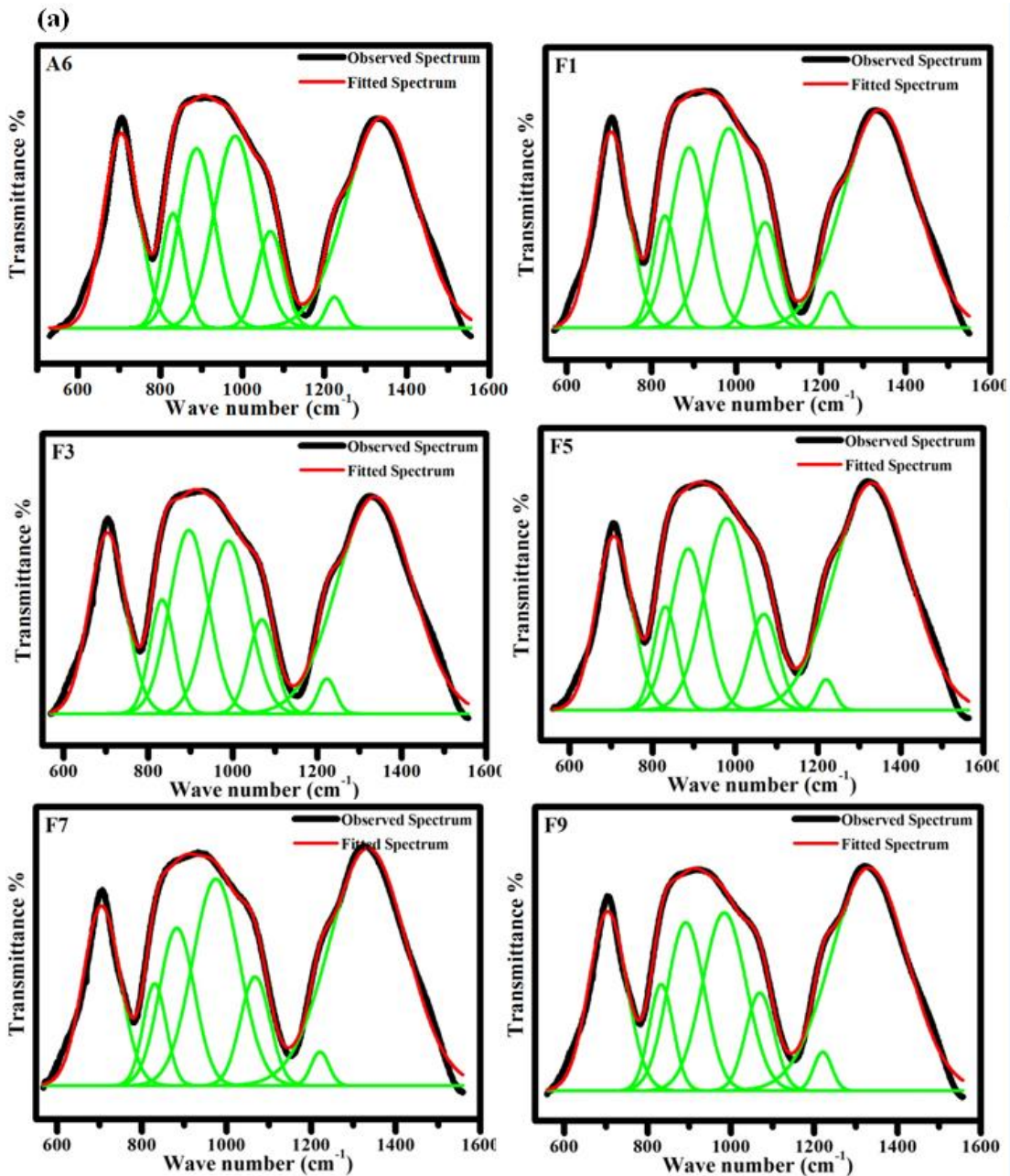


Figure 5.3 (a): Deconvoluted FTIR peaks of Fe₂O₃ doped LN-Fe glass system.

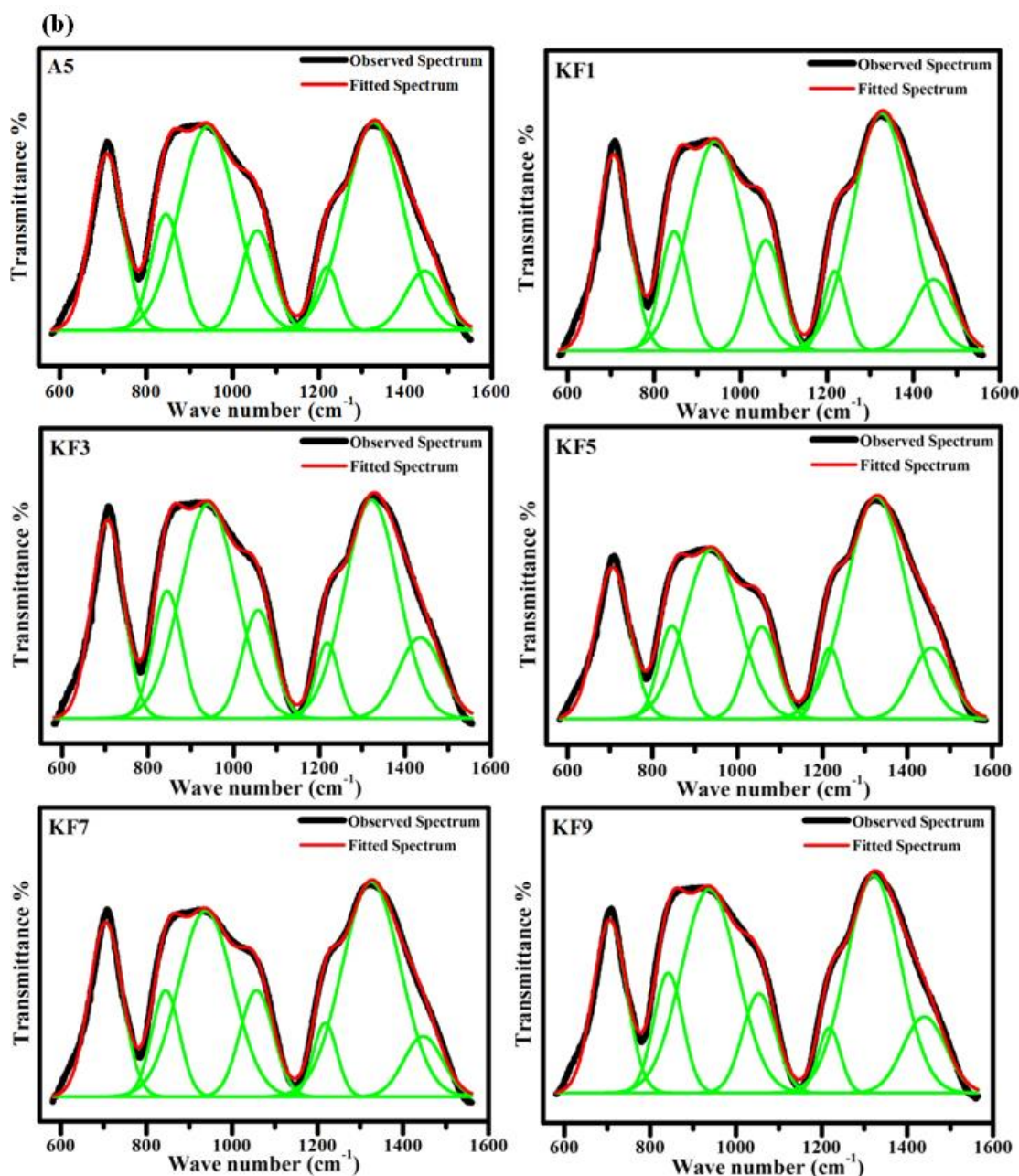


Figure 5.3 (b): Deconvoluted FTIR peaks of Fe_2O_3 doped LNK-Fe glass system.

The IR vibrational modes are mainly active in three major regions, for both LN-Fe and LNK-Fe series of glass samples, viz., 600 to 800 cm^{-1} which correspond to the bending modes from different types of borate units, 800-1200 cm^{-1} associated with the stretching vibrations of B-O bonds in BO_4 units, and 1200-1500 cm^{-1} corresponds to the B-O stretching vibrations of BO_3 units. It can be noticed from the FTIR spectra

of examined glasses the crucial bands of vitreous B₂O₃ and a trivial shift from their original position. Band assignments are presented in table 5.1.

Table 5.1. Assignment of absorption bands present in FTIR spectra of Fe₂O₃ doped LN-Fe and LNK-Fe glass system.

Band position (cm ⁻¹)	FTIR band assignments
705	B-O-B bending vibrations. (Pascuta et al. 2010)
830	Diborate linkage, B-O-B network vibrations. (Pascuta et al. 2009)
882-896	Stretching vibrations of B-O bonds in BO ₄ . (Pascuta et al. 2010)
975-989	Stretching vibrations of B-O bonds in BO ₄ from diborate groups. (Pascuta et al. 2010)
1068	B-O stretching vibrations of BO ₄ units in tri-, tetra-, and penta-borate groups. (Pascuta et al. 2010)
1220	Symmetric stretching vibrations of B-O bonds in BO ₃ . (Pascuta et al. 2009)
1330-1338	Stretching vibrations of B-O in BO ₃ units from different borate groups. (Reddy et al. 2008)

All the samples, of both the series, exhibit a band at 705 cm⁻¹, attributed to the bending vibration of B–O–B linkage in the borate network (Pascuta et al. 2010, Pascuta et al. 2009). The observed increase in the intensity of B-O-B bending may be ascribed to the breaking down of, the diborate units and a more relaxed glass structure. Hence there will not be any constraint for bending. The broad band appearing around 882-896 cm⁻¹ to 1068 cm⁻¹ is associated with the B-O bond stretching of tetrahedral [BO₄] units (Pascuta et al. 2010, Pascuta et al. 2009). The band from 975-989 cm⁻¹ in LN-Fe glass system (figure 5.2 (a)) and a band around 1058 cm⁻¹ with a small shoulder like anomaly observed around 947 cm⁻¹ (figure 5.2 (b)) in LNK-Fe glass system are ascribed to the stretching vibrations of B-O bonds in BO₄ units from diborate groups. These stretching vibrations may arise due to the tri, penta- and tetra- borate groups (Pascuta et al. 2010). The band around 1220 cm⁻¹ can be attributed to the symmetric stretching vibrations of B-O bonds in [BO₃] triangular units with NBO atoms. The band in the region 1330-1338 cm⁻¹ is ascribed to stretching vibrations of three fold borate unit linked with pyro-borate and ortho-borates (Subhashini et al. 2016).

5.1.2.2 Raman Spectroscopy studies

The Raman spectra were recorded for both LN-Fe and LNK-Fe samples and the results of the analysis are presented in this section. Figure 5.4 (a) & (b) depicts the Raman spectra of Fe₂O₃ doped LN-Fe and LNK-Fe glass systems. All the recorded spectra were deconvoluted using Gaussian function in order to recognize the existing vibration bands of the spectrum. Raman spectra proved to be more sensitive to the change in the concentration of Fe₂O₃ in the glass systems. Figure 5.5 (a) & (b) represent the deconvoluted Raman spectrum of both the series of samples. The band assignments are presented in table 5.2. The assigned bands and their evolution with the addition of Fe ion made using the Raman spectra are consistent with the FTIR analysis results. New structural groups are identified using the Raman data, for the studied glass systems.

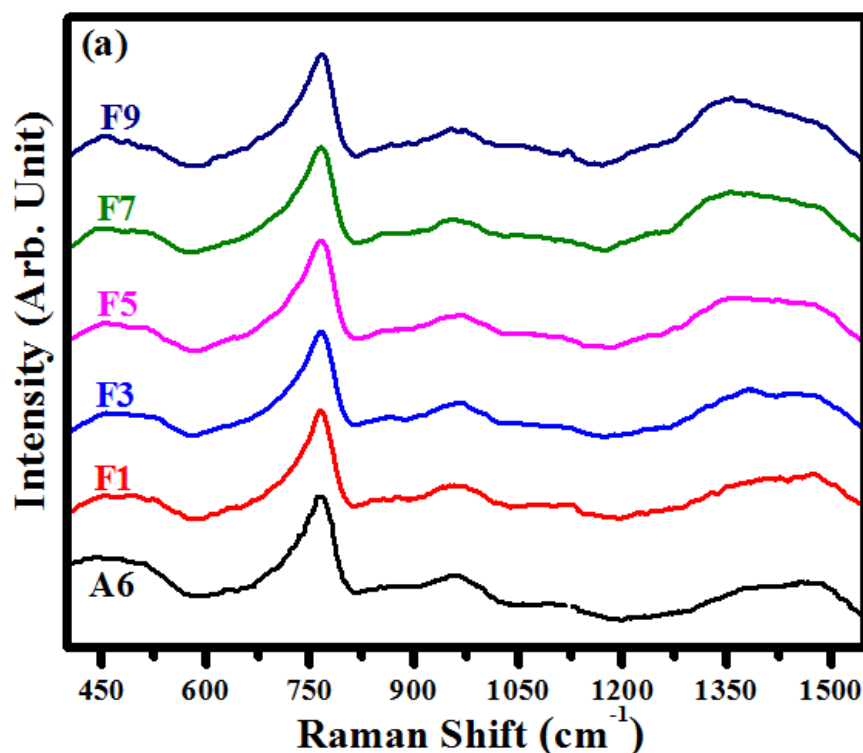


Figure 5.4 (a): Raman spectra of Fe₂O₃ doped LN-Fe glass systems.

The band around 448-455 cm⁻¹, observed in both LN-Fe and LNK-Fe glass systems, is ascribed to the B-O-B bending vibrations from the isolated diborate groups (Meera et al. 1993). The relatively sharp band around 722-730 cm⁻¹ in Fe₂O₃ doped

LN-Fe and at around 766 cm^{-1} in LNK-Fe glass system are may be due to the symmetric breathing vibrations ascribed to the six-membered structure involved in the different types of ring type structures two units of four-fold boron viz., di-tri-borate or di-penta-borate (Maniu et al. 1999). The band appearing around $958\text{-}955\text{ cm}^{-1}$ and $1100\text{-}1070\text{ cm}^{-1}$, in LNK-Fe series, are respectively ascribed to the vibrations of Fe-O and diborate groups in the structure (Meera et al. 1993). Similarly, the band appearing around 850 cm^{-1} and $950\text{-}1180\text{ cm}^{-1}$, in LNK-Fe series, are due to same reason an in LNK-Fe system. The bands around $1396\text{-}1364\text{ cm}^{-1}$ in LNK-Fe series and the band around 1350 cm^{-1} with the minor shoulder around $1120\text{-}1250\text{ cm}^{-1}$ in LNK-Fe series can be attributed to the BO_2O^- triangles associated to BO units.

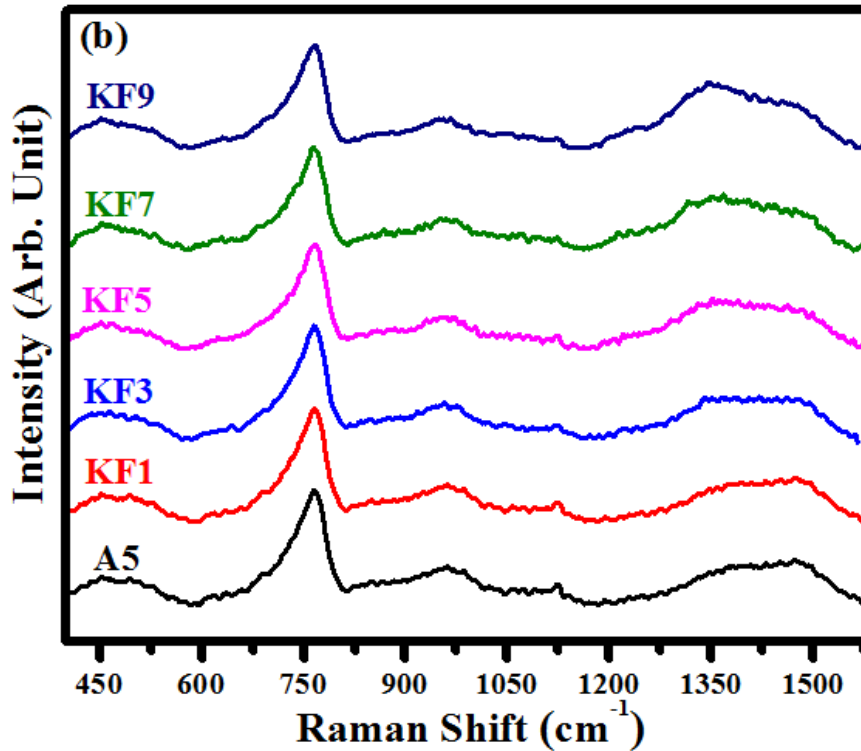


Figure 5.4 (b): Raman spectra of Fe_2O_3 doped LNK-Fe glass systems.

Lastly the broad band in the region of $1489\text{-}1481\text{ cm}^{-1}$ and around $1477\text{-}1485\text{ cm}^{-1}$ respectively in LN-Fe and LNK-Fe glass system are also assigned to the BO_2O^- triangular structures connected to the borate units. It can be noted that the increase in the intensities of these bands further confirms the overall increase in BO_3 units associated with NBOs (Meera et al. 1993).

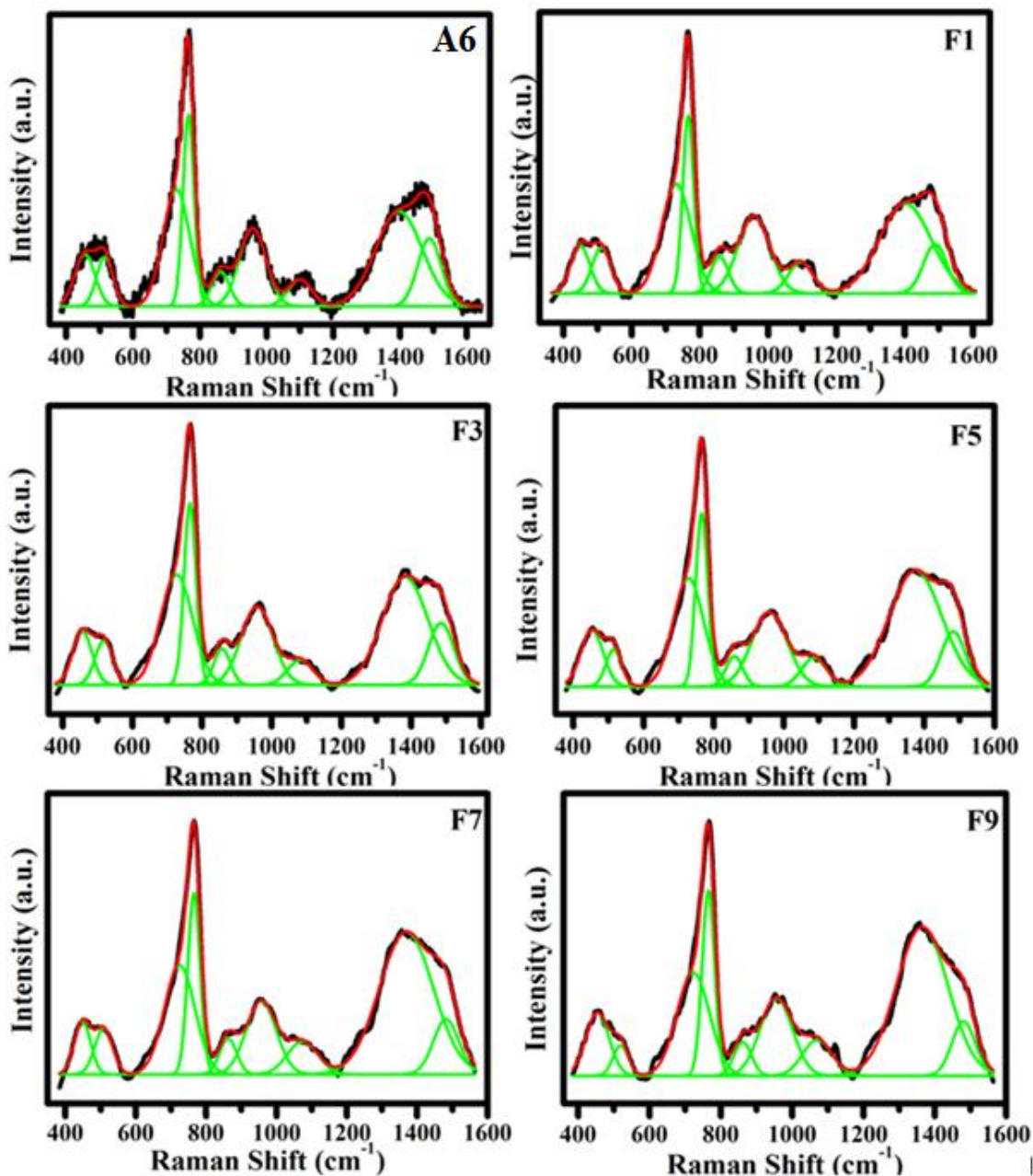


Figure 5.5 (a): Deconvoluted Raman spectra of Fe₂O₃ doped LN-Fe glass system.

In general, the borate glass systems possess various structural groups like [BO₃], [BO₄], tri-borate, di-borate, etc., which are observed in present investigation as well. It is expected, in general, that there are outnumbered diborate units present in stoichiometric diborate glass structures (Gowda et al. 2007), which can be further confirmed from the band assignments of FTIR and Raman spectra.

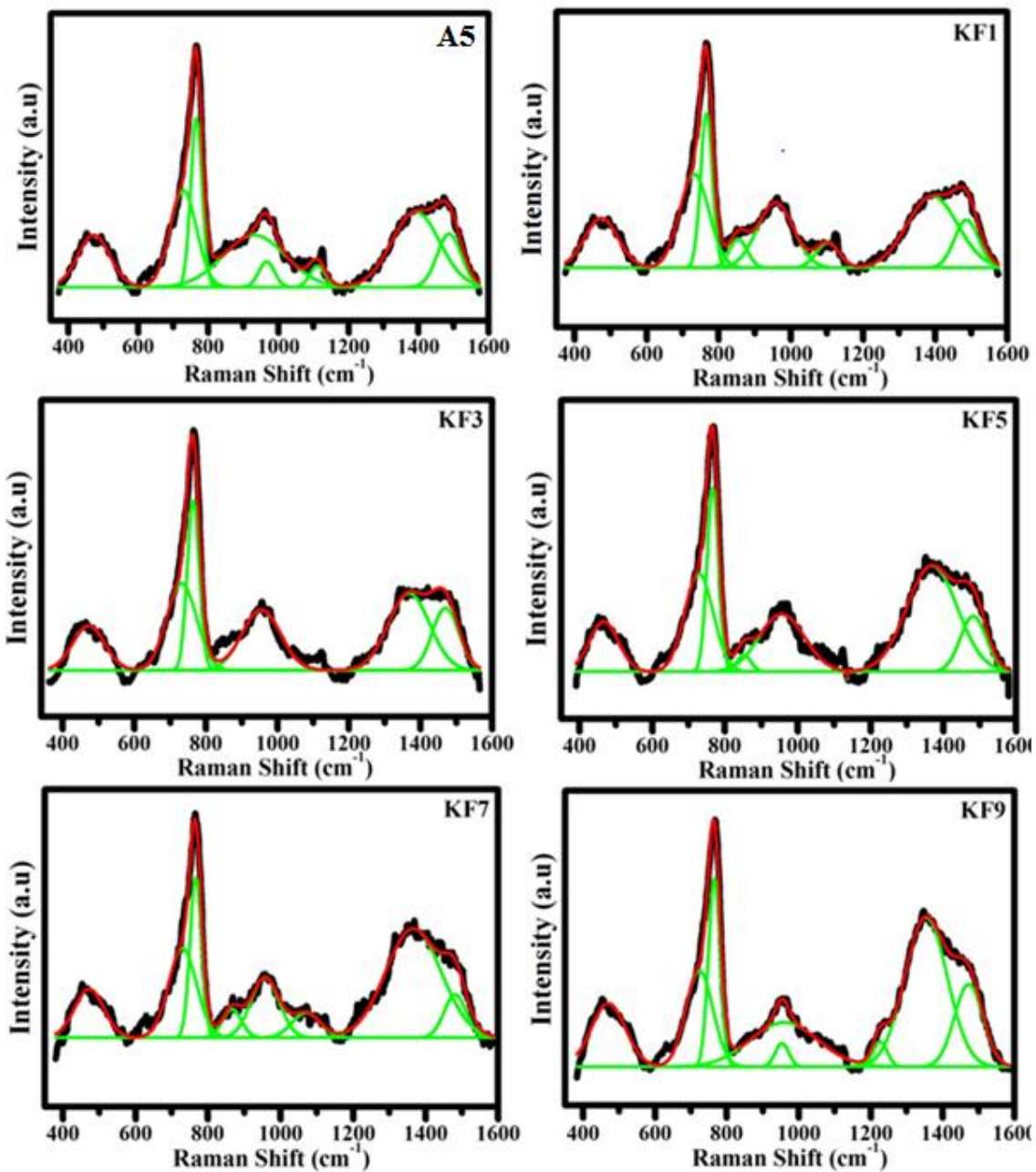


Figure 5.5 (b): Deconvoluted Raman spectra of Fe_2O_3 doped LNK-Fe glass system.

The diborate unit is associated with two $[\text{BO}_4]$ units along with two $[\text{BO}_3]$ units in bridging position, which formulate a rigid symmetrical geometry in the glass network. This tightly bound diborate unit is not associated with the NBOs, and retains a charge of -2 which remains delocalized throughout the unit. Partial incorporation of Fe_2O_3 content into this glass matrix, breaks the rigidly bound di-borate units and

expands the glass network. The diborate structure becomes more relaxed when enlarged due to breaking up of the bridges and the ring.

Table 5.2. Assignment of absorption bands present in Raman spectra of Fe₂O₃ doped LN-Fe and LNK-Fe glass system.

Band position (cm⁻¹)	Raman band assignments
448-455	Isolated diborate groups. (Meera et al. 1983)
508-519	Vibrations of Fe-O. (Meera et al. 1983)
722-730	Symmetric breathing vibrations of six members ring with one or two BO ₄ units (diti- or dipenta-borate). (Maniu et al. 1999)
765	B-O-B bending mode, and symmetric stretching vibrations of six members ring with two tetrahedral borate units (i.e., diborate). (Meeta et al. 1993)
955-958	Fe-O vibrations and vibrations of diborate groups in the structure. (Gowda et al. 2007)
1070-1100	Diborate groups. (Meeta et al. 1993)
1364-1396	BO ₂ O ⁻ triangles linked to B-O units. (Meeta et al. 1993)
1481-1489	BO ₂ O ⁻ triangles linked to other triangular borate units. (Meeta et al. 1993)

This can be clearly seen from Raman data, where there is a shift of band towards lower frequency from 1100 to 1070 cm⁻¹ in LN-Fe and from 1180 to 1080 cm⁻¹ in LNK-Fe glass system which is assigned to diborate units. The splitting of the diborate structure extends added connectivity to the diborate units and enhances the requirement of oxygen coordination, which leads to the competition for charge compensation among the modifier atoms. The competition for oxygen coordination in the glass network tends to further breakdown the diborate units. When diborate unit opens up it may become monocyclic and chain [B₄O₇]⁻² unit, which has larger flexibility associated with the diborate unit and can supply supplementary NBO coordination to iron atoms with a trivial change in the volume. Hence the incorporated Fe₂O₃ may promote the breaking of the diborate unit, beneficial to fulfil its own coordination necessities. Indeed, iron prefers six coordination position in borate glasses (Cochain et al. 2012). Hence the

addition of Fe₂O₃ to the glass network breaks down the diborate and causes a structural rearrangement in the glass network by occupying the octahedral position, which is further confirmed from UV-Visible spectroscopy studies.

5.1.3 Density (ρ), Molar volume (V_m) and atomic packing density (OPD)

Density (ρ) is considered to be an important tool to understand the modifications in the structure of glasses due to their high sensitivity to the properties viz., compactness, softening, cross link density, modifications of geometrical configuration, coordination numbers, and dimension of interstitial spaces of the glass (Saddeek et al. 2009). It is also crucial in exploring information about the short-range structure of oxide glasses. In this section, the results of density measurement for all the prepared samples are tabulated in table 5.3.

Table 5.3. The density (ρ), molar volume (V_m) and oxygen packing density (OPD) of Fe₂O₃ doped LN-Fe and LNK-Fe glass system.

Glass system	Glass code	ρ (g/cm ³) \pm 0.005	V_m (cm ³) \pm 0.05	OPD
LN-Fe	A6	2.473	27.05	81.33
	F1	2.476	27.05	81.41
	F3	2.478	27.10	81.41
	F5	2.482	27.11	81.51
	F7	2.485	27.14	81.56
	F9	2.486	27.19	81.57
LNK-Fe	A5	2.450	27.97	78.66
	KF1	2.452	27.98	78.71
	KF3	2.454	28.01	78.76
	KF5	2.458	28.03	78.84
	KF7	2.462	28.06	78.92
	KF9	2.467	28.06	79.04

The measured density is found to be slightly increasing with the increase in Fe₂O₃ content. This may be due to the addition of higher molecular mass Fe₂O₃ (159.69 g/mol) in the place of comparatively lower molecular mass ZnO (81.408 g/mol). The molar volume (V_m) can be determined using the measured density i.e, $V_m = \frac{\rho}{M}$, where M is the total molecular weight. The determined values of V_m are presented in table 5.3. The V_m for both the series of samples is observed to increase slightly with increase in Fe³⁺ content. This may be ascribed to the replacement of relatively lower field strength cation Zn²⁺ (0.53) by higher field strength Fe³⁺ (0.76) ions which promotes the formation of NBOs. Oxygen packing density (OPD), the number of oxygen atoms per formula unit, of the samples was calculated using the equation (2.3) and the estimated values are given in table 5.3. OPD is defined as the number of oxygen atoms present per formula unit. It is noted that there is a slight increase in the OPD with an increase in Fe₂O₃ content. This clearly indicates the presence of tight packing of the oxide network. In other words, the increase in OPD reveals the efficient packing of oxygen atoms, which is further substantiated by thermal studies.

5.1.4 Thermal studies

Thermal parameters like T_g (onset of glass transition region), T_x (onset crystallization temperature), T_c (glass crystallization temperature) and T_m (glass melting temperature) are determined using DSC thermographs which are obtained by plotting heat flow versus temperature plots as depicted in figure 5.6 (a) & (b). The determined thermal parameters values are summarized in table 5.4. It can be noted, from figure 5.6 (a) & (b), that for a given uniform heating rate, there exists a single glass transition endothermic peak (T_g) and a single exothermic crystallization peak (T_c) and the commencement of T_c considered as onset glass crystallization temperature (T_x). The endothermic peak at the end of thermograph represents the glass melting temperature (T_m). It can be seen that there is a sudden decrease in glass transition temperature T_g , from sample A6 to A5. Basically, T_g can be used to indicate the rigidity of the glass network. In general, T_g of an oxide glass depends mainly on bond strength, compactness of glass structure and cross-link density (Ray 1974).

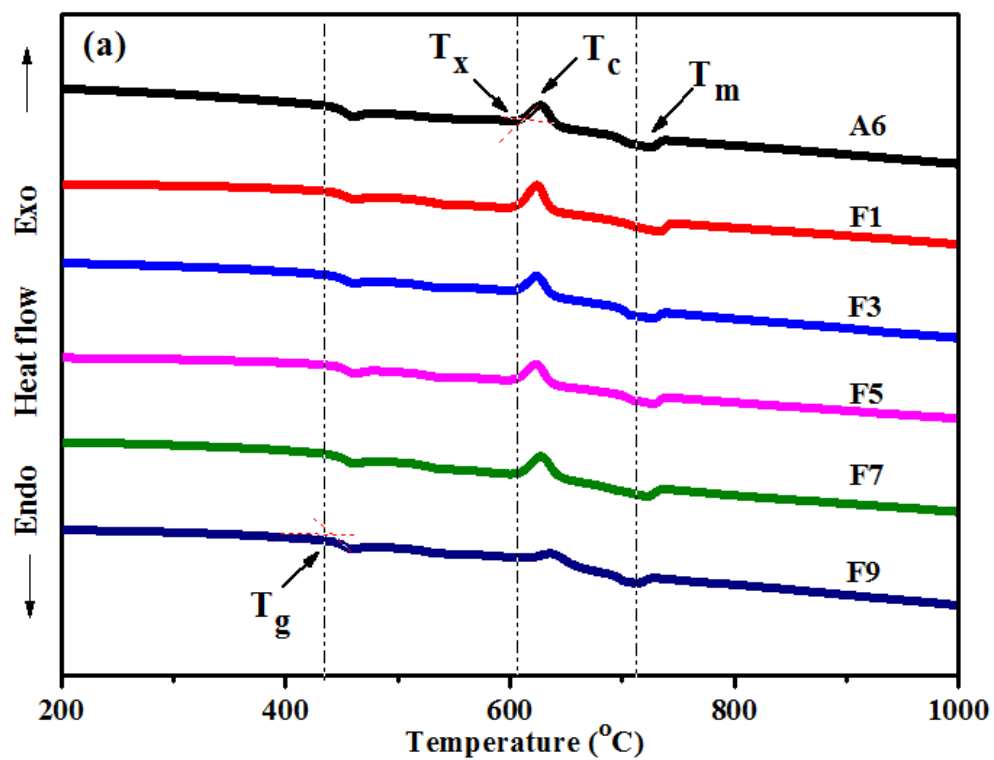


Figure 5.6 (a): DSC thermographs of Fe₂O₃ doped LN-Fe glass system.

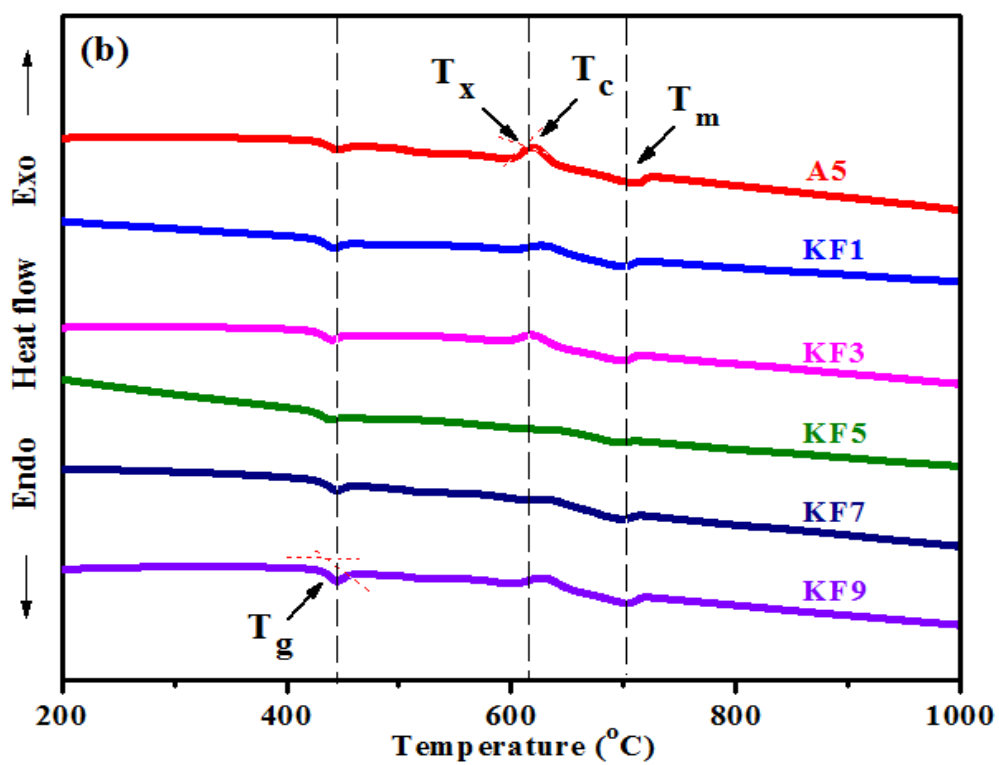


Figure 5.6 (b): DSC thermographs of Fe₂O₃ doped LNK-Fe glass system.

In the present case, the introduction of third alkali metal (K₂O) to the A6 sample of LN-Fe glass system decreased the T_g from 446 °C to 427 °C. This may be attributed to the replacement of relatively higher single bond strength and lower ionic radii Na₂O (20 Kcal/mol and 0.78 Å respectively) by lower single bond strength and higher ionic radii K₂O (13 Kcal/mol and 1.33 Å respectively). The single bond strength and ionic size of the network modifiers directly influence the glass transition temperature, since glass transition mainly includes the alteration of bonds between modifier cation and anions present in the network. Hence, comparatively heavier K₂O acts more effectively in the reduction of glass transition temperature than the lighter Na₂O. The reduction of T_g can also be ascribed to the fact that the relatively higher field strength Na₂O ($0.17 \times 10^{-20} \text{ m}^{-2}$) is replaced by relatively lower field strength K₂O ($0.12 \times 10^{-20} \text{ m}^{-2}$) which indeed weakens the glass network.

Table 5.4. Glass transition temperature (T_g), onset crystallization temperature (T_x), crystallization temperature (T_c), melting temperature (T_m), glass forming ability (T_{rg}), glass stability (ΔT) and Hurby's parameter (H_R) of Fe₂O₃ doped LN-Fe and LNK-Fe glass system.

Glass system	Glass code	T_g (°C)	T_x (°C)	T_c (°C)	T_m (°C)	T_{rg} (°C)	ΔT	H_R	K_I (°C)	K_2	K_W	K_{LL}
LN-Fe	A6	446	601	620	736	0.606	155	1.15	290	0.817	0.211	0.508
	F1	445	603	623	733	0.607	158	1.22	288	0.823	0.216	0.512
	F3	444	605	623	728	0.610	161	1.31	284	0.831	0.221	0.516
	F5	443	606	624	725	0.611	163	1.37	282	0.836	0.225	0.519
	F7	443	609	627	722	0.614	166	1.47	279	0.843	0.230	0.523
	F9	442	616	635	712	0.621	174	1.81	270	0.865	0.244	0.534
LNK-Fe	A5	427	597	620	711	0.601	170	1.49	284	0.840	0.239	0.525
	KF1	426	600	621	709	0.601	174	1.60	283	0.846	0.245	0.529
	KF3	425	603	625	706	0.602	178	1.73	281	0.854	0.252	0.533
	KF5	424	606	626	703	0.603	182	1.88	279	0.862	0.259	0.538
	KF7	424	608	628	700	0.606	184	2.00	276	0.869	0.263	0.541
	KF9	423	610	629	698	0.606	187	2.13	275	0.874	0.268	0.544

From the table 5.4, it can be clearly observed that after addition of Fe₂O₃ content there is a slight decrease in T_g . This can be ascribed to the fact that the added Fe₂O₃

content may prompt breaking up of the diborate units to fulfil its own coordination requirements and mixed bonding may occur during glass formation resulting in the decrease of the glass transition temperature. Glass stability criterion estimated by considering the temperature difference between the onset glass crystallization and transition temperature, ($\Delta T = T_x - T_g$) was also evaluated for both the series of samples. The glass stability can be described as the ability of glass to bypass crystallization upon heating. It is one of the important aspects of the preparation of large scale glasses for practical applications (Zheng et al. 2012). The estimated values of ΔT are given in table 5.4. It can be seen, from table 5.4, that ΔT is found to increase from 155 °C to 158 °C as Fe₂O₃ content increased from 0 mol% to 0.9 mol% in LN-Fe glass samples. Addition of K₂O to the A6 sample of LN-Fe glass system exhibits a sudden increase in the thermal stability from 155 °C to 170 °C and later increase upto 187 °C upon increasing the Fe₂O₃ content. Hence with the incorporation of third alkali metal to the LN-Fe system, it is possible to tune the stability of glasses and network rigidity. On the other hand, with this knowledge of LNK-Fe glass system, one can make the selection of better glass composition for different practical applications. It is advantageous to have a glass host with greater ΔT value. Glasses with $\Delta T > 100$ °C are very much stable during fibre drawing and also stable against devitrification (Mehta et al. 2006). It is observed, from table 5.4, that the examined glass samples have higher thermal stability which satisfies the condition of conventional fibre drawing ability. The increase in ΔT with the addition of third alkali metal ion (K₂O) and with increase in Fe₂O₃ content in both LN-Fe and LNK-Fe glass systems result in a substantial enhancement in thermal stability against crystallization. The glass transition temperature is found to decrease with increasing Fe₂O₃ content in both LN-Fe and LNK-Fe glass systems. This may be due to the fact that the Fe₂O₃ tends to break up the diborate units in order to satisfy its own coordination necessities. During the formation of the glass, mixed bonding Fe-O-B is possible which may lead to a consequent decrease in T_g . The glass forming ability (GFA) is another important aspect in glass science. It is a measure of how easily melt is vitrified by a given composition or can be defined in terms of resistance to the crystallization of melt during cooling. For a glass forming system, according to Kauzmann assumption (Kauzmann 1948), the value range of T_{rg} must lie in between

1/2 and 2/3, where $T_{rg} = \frac{T_g}{T_m}$ (Clavaguera-Mora 1995). From the values of T_{rg} presented in table 5.4, it is evident that the glass systems in the present study are in the recommended range. Hurby proposed a parameter named as Hurby's parameter (H_R) which can be used to find the glass forming ability of oxide glasses given by the equation (2.5). The larger values of Hurby's parameter for glasses exhibit their greater stability against crystallization on supplying heat. H_R is predominantly associated with nucleation and growth aspect of the phase transformation. The estimated H_R values are represented in table 5.4 and it is evident that the observed increasing trend in the quantity $T_x - T_g$ hinders the nucleation process. On the other hand, there is a decreasing trend in $T_m - T_x$ indicating that the growth process of the nucleated crystals is retarded. It is a well-known fact that any glass with Hurby's parameter lesser than 0.1 is comparatively difficult to form since it requires faster cooling, on the other hand glasses with Hurby's parameter greater than 0.5 need comparatively lesser effort to form glass with normal quenching (Abdel-Rahim, 2008). It is witnessed that both H_R and $T_x - T_g$ enhanced with the addition of K_2O and Fe_2O_3 content. This indicates that there is a significant improvement in thermal stability against crystallization together with the enhancement in the GFA owing to the addition of third alkali cation and Fe_2O_3 in the studied glass systems.

In the present studies, the other thermal parameters proposed for oxide glasses have been evaluated using the equations (2.6), (2.7), (2.8) and (2.9). All the estimated values using the above mentioned relations are tabulated in table 5.4. The evaluated values lie in the recommended range for glass applications. This enhanced thermal property of the investigated glass system is suitable for the optoelectronic applications.

5.1.5 Optical studies

With a view to understanding the electronic band structure and optical transitions, UV-visible spectra of samples of both LN-Fe and LNK-Fe glass systems were recorded. Figure 5.7 (a) & (b) represents the absorption spectra of both the series. The optical absorption spectra (figure 5.7 (a) & (b)) reveals, that the absorption edges are not sharply defined, which is a characteristic feature of amorphous materials.

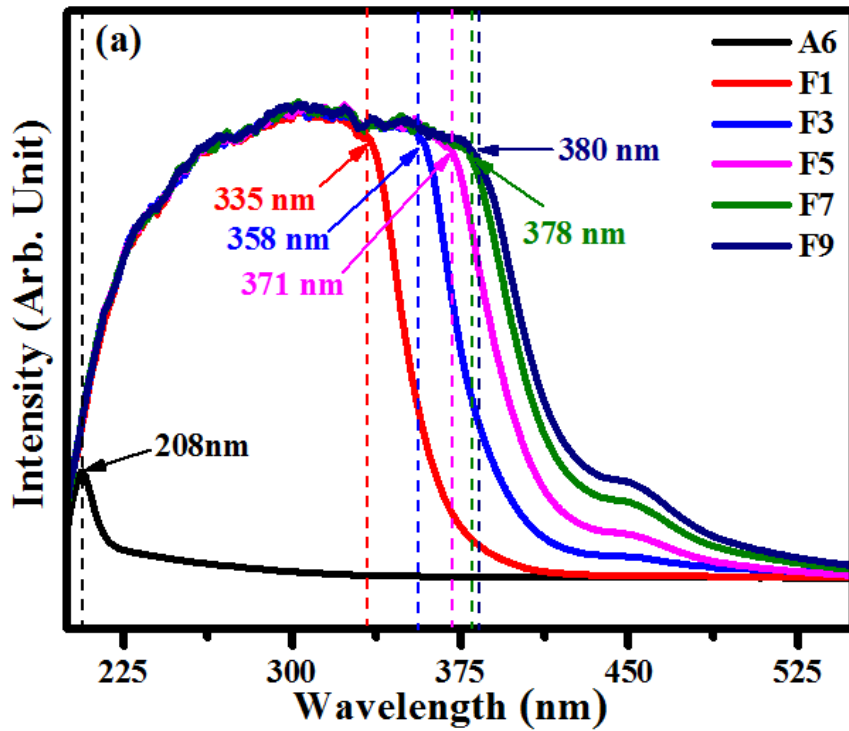


Figure 5.7 (a): UV-visible absorption spectra for the Fe₂O₃ doped LN-Fe glass system.

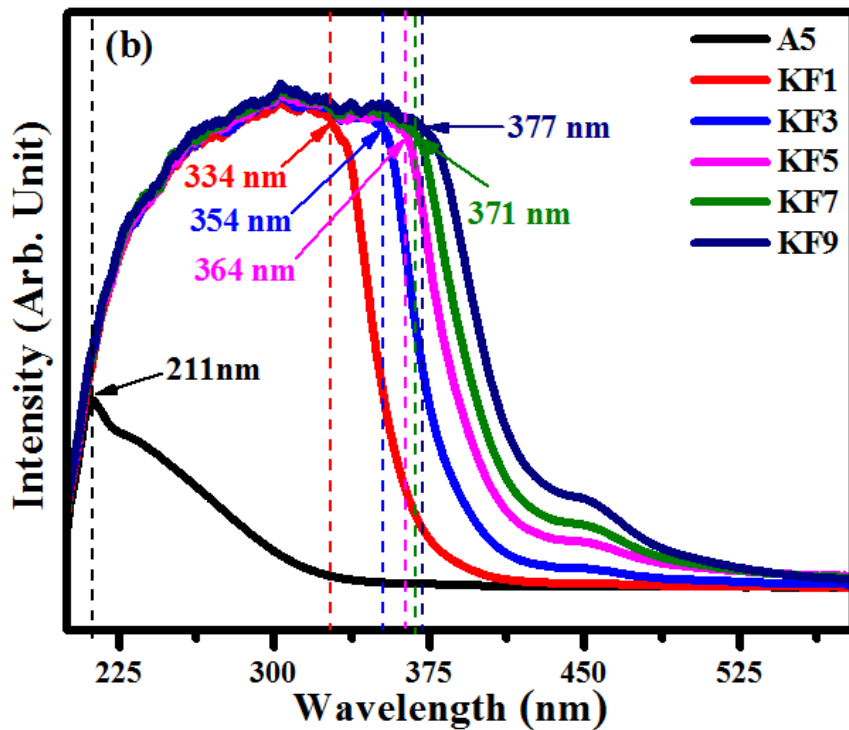


Figure 5.7 (b): UV-visible absorption spectra for the Fe₂O₃ doped LNK-Fe glass system.

The wavelengths corresponding to the absorption edge of LN-Fe glass system with 0, 0.1, 0.3, 0.5, 0.7 and 0.9 mol% of Fe₂O₃ are 208nm, 335nm, 358nm, 371nm, 379nm and 380nm respectively. Similarly, the wavelengths corresponding to the absorption edge for Fe₂O₃ doped LNK-Fe glass system for mol% of 0, 0.1, 0.3, 0.5, 0.7 and 0.9 are 212nm, 334nm, 354nm, 364nm, 371nm and 377nm respectively. It is evident, from figure 5.7 (a) & (b), that there is a drastic increase in the cut off wavelength with the incorporation of Fe₂O₃ content in both the series of glass samples. It is evident from the values that there is a redshift in the absorption edge from 208nm to 335nm in LN-Fe and from 334 nm to 377 nm in LNK-Fe systems. This shift in absorption edge is a result of the introduction of a modifier which causes the transition of a valence electron of an oxygen ion to vacant excited state (Chethana et al. 2018). The shift in the absorption edge also signifies that the Fe₂O₃ acts as an oxidizing agent as well as the network modifier. The shift in UV absorption edge is also partly attributed to the presence of impurities particularly the transition metal ions. It can be (figure 5.7 (a) & (b)) observed that there exists an additional band at 450 nm in both the series of samples with non-zero Fe₂O₃ concentration. The intensity of the band is found to increase gradually with increase in Fe₂O₃ content. This band is ascribed to the change of configuration from (t_{2g})³(e_g)² to (t_{2g})⁴(e_g)¹ at 450 nm and is attributed to the d-d transition of ⁶A_{1g}(S) → ⁴T_{2g}(G). The observed band position is consistent with the report published elsewhere (Naresh et al. 2012).

The optical energy gap (E_g) has been determined using the Tauc plot depicted in figure 5.8 (a) & (b). The power law proposed by Davis and Mott (Fu et al. 2012) has been utilized to correlate the E_g with that of the magnitude of absorption coefficient (α) at absorption edge. The absorption coefficient (α) as a function of photon energy ($h\nu$) for direct and indirect optical transitions is given by the equation (2.11). Considering $n=1/2$ and taking square root on both sides, equation (2.11) can be rewritten as, equation (2.12) E_g for all the glass samples has been evaluated by finding the x-intercept of the straight line graph obtained using equation (2.12). The band gap energy of the prepared samples is summarized in table 5.5.

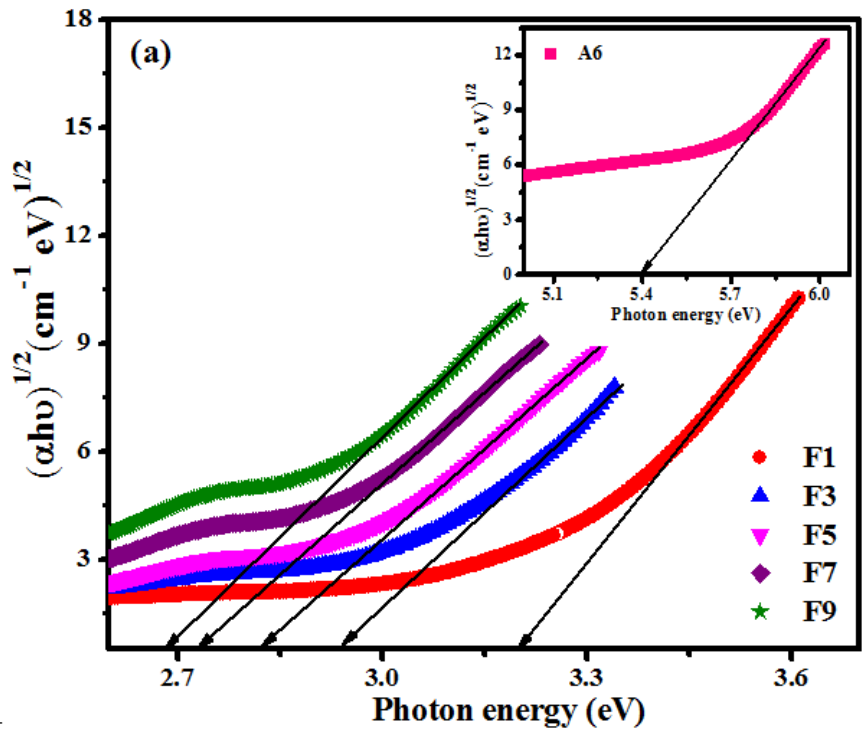


Figure 5.8 (a): Variation of $(\alpha h\nu)^{1/2}$ as a function of photon energy ($h\nu$) for the Fe_2O_3 doped LN-Fe glass system.

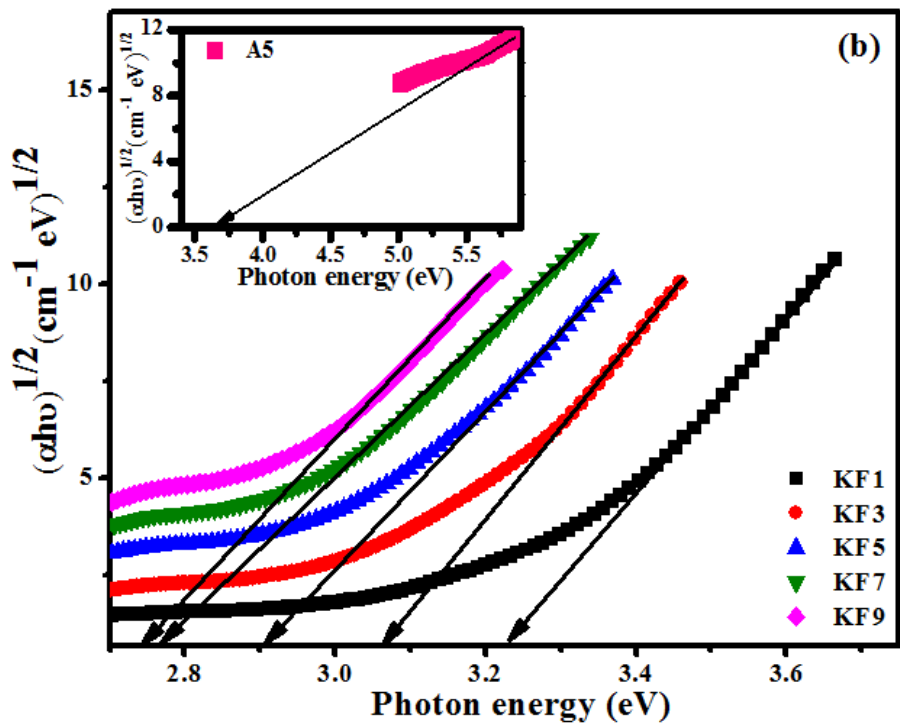


Figure 5.8 (b): Variation of $(\alpha h\nu)^{1/2}$ as a function of photon energy ($h\nu$) for the Fe_2O_3 doped LNK-Fe glass system.

In the present investigation, here is a sudden decrease in the optical band gap energy, E_g from 5.40 ± 0.1 eV to 3.67 ± 0.1 eV upon the incorporation of third alkali metal (K_2O) to the A6 sample of LN-Fe glass system. This reduction of E_g may be ascribed to the structural differences occurring due to the addition of relatively lower field strength K_2O ($0.12 \times 10^{-20} \text{ m}^{-2}$) by higher field strength Na_2O ($0.17 \times 10^{-20} \text{ m}^{-2}$). The average bond energy is the another key factor which affects the optical band gap energy, E_g . The replacement of relatively higher bond energy Na_2O (8.4 KJ/mol) with relatively lower bond energy K_2O (12.2 KJ/mol) may cause the reduction in the average bond energy of the glass network, which effects in lowering the energy of the conduction band edge and hence results in reduction of E_g . In addition to this, it is observed (table 5.5) that the E_g value is decreasing with the increasing Fe_2O_3 content in both LN-Fe and LNK-Fe glass systems. This can be attributed to the increase in the concentration of non-bridging oxygen (NBO), which are created during the structural rearrangement occurring in the glass network upon addition of Fe_2O_3 content. The addition of Fe_2O_3 opens up the tightly bound diborate unit as a result of which the number of NBOs increases. NBOs bind the excited electrons less tightly compared to bridging oxygens. The relatively higher magnitude negative charge possessed by the NBOs supports the excitation of electrons to the conduction band of respective cations, which leads to further decrease in optical band gap energy with increase in Fe_2O_3 content.

The amorphous nature of glassy materials is associated with the increased number of localized electron states extending into the band gap and results in the formation of an exponential band tail generally known as Urbach tail. These band tails are characterized by a band tail parameter known as Urbach energy, E_U (Narayanan et al. 2015) given by the equation (2.13). Taking natural log on either sides of the equation (2.13), it can be written as equation (2.14). Figure 5.9 (a) & (b) represents the reciprocal of the slope of the linear region. The values of the E_U are represented in table 5.5. It is observed that the value of the E_U is decreased in the beginning but observed to increase later as Fe_2O_3 content increases in both the series of glass systems. The increase in E_U may be ascribed to the presence of defects and possible modifications in the structure. A broad absorption tail is observed owing to the indirect electronic transitions assisted

by the presence of phonons. Consequently, Urbach energy values endorse the presence of electronic transitions assisted by the phonons in the current investigated glass samples. Refractive index, n is measured using Abbe refractometer and the values are tabulated in table 5.5. It can be observed that the partial substitution of third alkali ion i.e., K^+ to the A6 sample of LN-Fe system increases the refractive index, n . This increase in the refractive index can be attributed to the partial replacement of lower polarizable ion Na^+ (0.175 \AA^3) by higher polarizable cation K^+ (0.821 \AA^3). Further, it can be witnessed that there is a gradual increase in the refractive index with the increase in Fe_2O_3 content in both the series of glass samples. This experimental observation can be ascribed to the partial substitution of Fe^{3+} which has relatively higher polarizability (0.437 \AA^3) than that of Zn^{2+} (0.283 \AA^3). It reveals that, in addition to density and compactness of the glass system, the refractive index is also influenced by the cation polarizability which again confirms the network modifier role of Fe_2O_3 .

Table 5.5. Optical band gap energy (E_g), Urbach energy (E_u), refractive index (n), molar refractivity (R_m), refractive index based oxide ion polarizability ($\alpha_{O^{2-}}^{(n)}$), band gap energy based electronic polarizability ($\alpha_{O^{2-}}^{(E)}$), optical basicity (Λ) and metallization criteria (M) of Fe_2O_3 doped LN-Fe and LNK-Fe glass system.

Glass code	E_g (eV, ± 0.1)	E_u (eV, ± 0.1)	n (± 0.001)	R_m	α_m (\AA^3)	$\alpha_{O^{2-}}^{(n)}$ (\AA^3)	$\alpha_{O^{2-}}^E$ (\AA^3)	Λ	M
A6	5.40	0.27	1.537	8.448	5.154	1.490	2.311	0.549	0.688
F1	3.19	0.17	1.555	8.675	6.444	1.529	2.895	0.578	0.679
F3	2.94	0.20	1.575	8.955	6.623	1.577	2.970	0.611	0.670
F5	2.78	0.20	1.632	9.666	6.744	1.702	3.020	0.689	0.644
F7	2.70	0.21	1.688	10.352	6.811	1.821	3.044	0.753	0.619
F9	2.65	0.23	1.697	10.469	6.856	1.839	3.059	0.762	0.615
A5	3.67	0.11	1.540	8.769	3.480	1.533	2.835	0.581	0.687
KF1	3.22	0.18	1.542	8.798	3.491	1.537	2.970	0.583	0.686
KF3	3.05	0.19	1.545	8.858	3.515	1.545	3.022	0.589	0.684
KF5	2.87	0.21	1.550	8.923	3.541	1.554	3.078	0.595	0.682
KF7	2.74	0.22	1.554	8.995	3.570	1.564	3.119	0.602	0.679
KF9	2.70	0.22	1.559	9.054	3.593	1.571	3.127	0.607	0.677

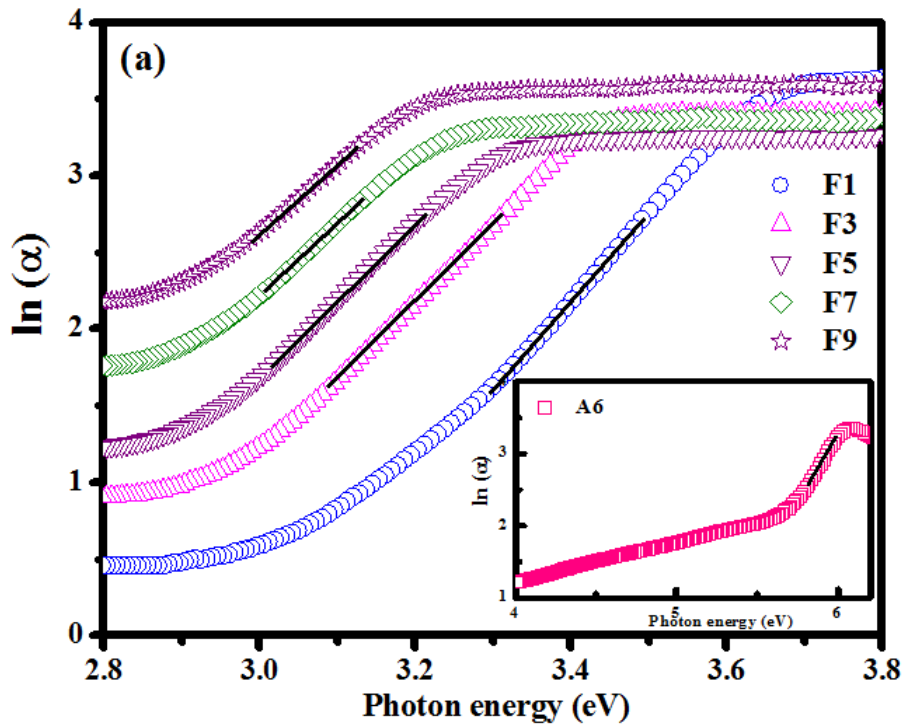


Figure 5.9 (a): Variation of $\ln(\alpha)$ as a function of photon energy ($h\nu$) for the Fe_2O_3 doped LN-Fe glass system.

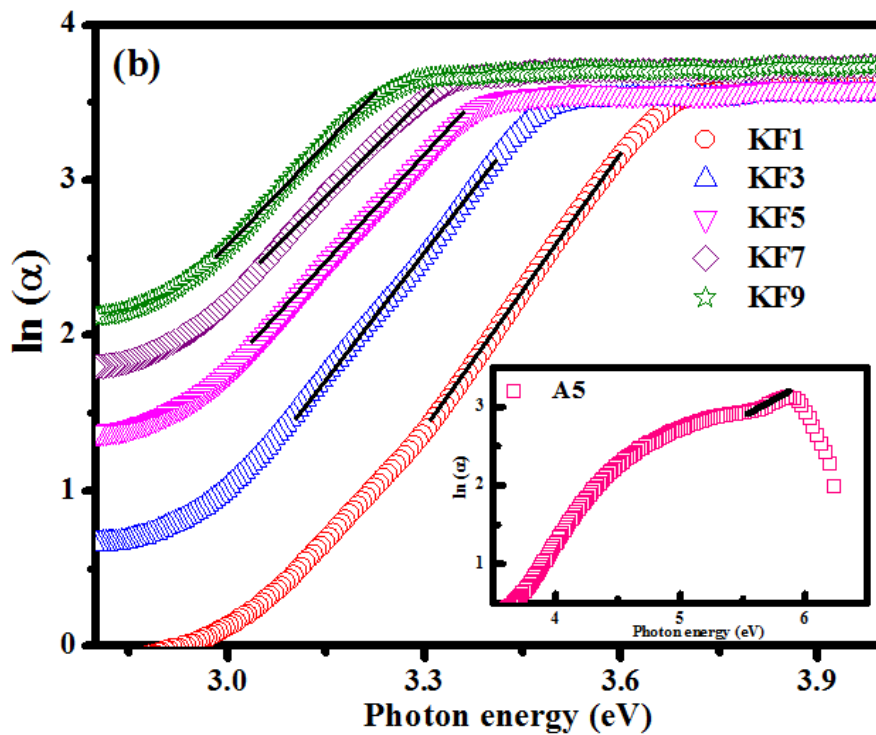


Figure 5.9 (b): Variation of $\ln(\alpha)$ as a function of photon energy ($h\nu$) for the Fe_2O_3 doped LNK-Fe glass system.

5.1.5.1 Electronic polarizability

The cationic and anionic polarizability is consistent when they are combined with the corresponding stoichiometric batch composition (Dimitrov et al. 1996). Consequently, the estimation of oxide ion polarizability for glasses is decisive as it plays a vital role in optoelectronic materials. For crystals, liquids, and glasses the molar refraction (R_m) based on n and V_m is determined using the equation (2.15) known as Lorentz-Lorenz equation. The obtained values of R_m for both the series of glass systems are summarized in table 5.5. The molar polarizability, α_m can be determined using the equation (2.16). The values of α_m for the studied LN-Fe and LNK-Fe glass systems are presented in table 5.5 and found to be in the range of 5.154 Å³ to 6.856 Å³ and 3.480 Å³ to 3.593 Å³ for Fe₂O₃ doped LN-Fe and LNK-Fe glass system respectively.

The oxide ion polarizability based on refractive index and optical band gap energy for both the series of glass systems has been determined using the equations (2.17) & (2.18). The determined values of electron oxide polarizability for both the series of samples are presented in table 5.5. It is noticed that the oxide ion polarizability is increasing monotonically as Fe₂O₃ content increases. In the present investigation, the ratio of total alkali content to boron is maintained constant, and Na₂O is partially replaced with K₂O, similarly, ZnO is replaced with Fe₂O₃ content. It can be noted that the polarizability of K⁺ (0.821 Å³) ion and Fe³⁺ (0.437 Å³) ion are relatively much higher than that of the Na⁺ (0.175 Å³) and Zn²⁺ (0.283 Å³) ions. This can be the reason for the observed increase in determined oxide ion polarizability. On the other hand, the increase in the number of NBOs with an increase in Fe₂O₃ content may also contribute to the increase in overall polarizability of the investigated glass system. Since the Fe³⁺ ion has affinity towards electrons, it tends to take away electrons by creating mixed bonding with the surrounding anions through appropriate reaction. It is noticed that the ionic radius (r_i) reduces with increasing Fe₂O₃ content. As a consequence, the oxide ion polarizability will be altered owing to the diminishing number of overlying orbitals (Dimitrov et al. 1996), which is consistent with Fazan's rule (Dimitrov and Komatsu 2010).

5.1.5.2 Optical basicity

Owing to the chemical reaction among constituent oxides in the glass systems, oxygen ions, O^{2-} always possess a tendency to transfer its negative charge to the cations. This ability of oxide ions to donate electrons to the surrounding cations is termed as optical basicity. The optical basicity of the both the series of glass systems is calculated using the equation (2.19) proposed by Duffy (1996). The evaluated values are tabulated in table 5.5. In the perspective of network modification, it can be noted that, the acidity is reduced due to the acid-base reaction between the glass forming oxide and the modifier oxide ions. This knowledge can be utilized to find out the ionic or (and) covalent nature of the glass samples. Basically, ionicity is a measure of basicity. It is seen that the optical basicity increases from 0.549 to 0.581 with the partial incorporation of K_2O content to the glass matrix. This may be ascribed to the partial replacement of relatively lower optical basicity Na_2O (1.10) with higher optical basicity K_2O (1.31). It is also observed that the increase in Fe_2O_3 content monotonically increases the optical basicity of both LN-Fe and LNK-Fe glass samples. This increase may be ascribed to the partial replacement of ZnO having lower optical basicity of 0.9 compared to that of Fe_2O_3 having higher optical basicity of 1.04. This increase indicates that the glass systems are becoming chemically more basic with the increasing Fe_2O_3 content. The basicity provides the magnitude of negative charge carried by the oxygen ions (Dimitrov and Komatsu 2010).

5.1.5.3 Metallization criterion

The quantity $\frac{R_m}{V_m}$ provides the polarizability density of the glass systems. According to Hertzfeld metallization theory (Duffy 1996), if a material is densified to have the ratio $\frac{R_m}{V_m} = 1$ then the quantity $n^2 - 1$ will become equal to $n^2 + 2$, which can materialize only when $n = \infty$. According to this discussion, the electrons in the valance state which are quasi-elastically connected to the atoms are now liberated by means of polarization in the condensed state and this process is referred to as ‘polarization catastrophe’ (Reddy et. al. (2008)) The solid materials having the ratio $\frac{R_m}{V_m} > 1$ behave

as metallic conductors whereas the materials having the ratio $\frac{R_m}{V_m} < 1$ behave as insulators. Dimitrov et. al. (1996) have evaluated the metallization criterion, M for the glass modifier oxides with borate and silicate glasses having greater M , which lie in the range of 0.5-0.7. It is established that the materials with least value of metallization criterion usually exhibit narrow E_g . The M of the current glass systems was calculated and summarized in table 5.5. It is observed to decrease with increasing Fe_2O_3 content in both LN-Fe and LNK-Fe glass system. Consequently, gap between the valence band and conduction band is reduced. It is consistent with the E_g values for both the glass systems.

5.1.6 Mechanical properties

Mechanical properties of the prepared glass samples play a crucial role in order to use them for practical applications. In this regard, to understand the mechanical strength of the prepared glass samples, the Vickers micro-hardness measurements were performed and the results are summarized in table 5.6. Error in the hardness measurement is determined by calculating the standard deviation of the average of hardness values. It observed, from table 5.6, that the Vickers micro-hardness value has decreased from 4.992 GPa to 4.760 GPa with the partial incorporation of K_2O content to the glass matrix of A6 system. This may be due to the partial replacement of relatively lower radius and higher field strength Na_2O with higher radius and lower field strength K_2O . Partial substitution of potassium ions having higher radius increases the distance between modifier cations and anions in the glass network, which leads to the weakening of glass structure and decreases the Vickers micro-hardness. Further, it is seen that the Vickers micro-hardness of both LN-Fe and LNK-Fe system of glasses is slightly decreasing with the partial incorporation of Fe_2O_3 content. This may be due to the breaking up of tightly bound diborate structure and a slight increase in NBOs. Crack initiation and crack propagation are the two factors which determine the strength of the glasses. The propagation of the crack, determined using fracture toughness (K_{IC}), is a measure of how easily a crack is able to disseminate in a given material. In the current investigation, fracture toughness of the prepared glass sample is determined by an equation (2.22) proposed by Anstis et al. (1981).

Table 5.6. Vickers hardness (H_v), half crack length (C), fracture toughness (K_{IC}) and Brittleness (B) of Fe_2O_3 doped LN-Fe and LNK-Fe glass system.

Glass System	Glass code	Measured Vickers hardness (GPa) \pm 0.004	Measured Half crack length (μm) \pm 1	Fracture toughness (MPa (m) ^{1/2}) \pm 0.003	Brittleness ($\mu\text{m}^{-1/2}$) \pm 0.02
LN-Fe	A6	4.992	57.18	0.730	6.84
	F1	4.977	57.48	0.722	6.98
	F3	4.955	58.35	0.706	7.14
	F5	4.927	59.00	0.695	7.25
	F7	4.891	59.90	0.680	7.42
	F9	4.862	61.08	0.663	7.72
LNK-Fe	A5	4.760	59.05	0.705	6.75
	KF1	4.687	60.12	0.692	6.77
	KF3	4.667	61.18	0.676	6.90
	KF5	4.655	62.43	0.657	7.08
	KF7	4.640	63.02	0.650	7.14
	KF9	4.594	63.80	0.642	7.16

Young's modulus of the poly component system is obtained by the theoretical model suggested by Makishima and Mackenzie (1973) using the equation (2.23). The atomic packing fraction, V_t is calculated using the equation (2.24). The determined fracture toughness (K_{IC}) values are summarized in table 5.6. It is evident that K_{IC} is decreasing gradually. This can be attributed to the slight reduction of Vickers hardness and increase in half crack length. The crack length in both the series of glass systems is observed to increase with increasing Fe_2O_3 content. This signifies that the ease of crack propagation through the glasses is enhanced with increasing Fe_2O_3 content. The effortless propagation of cracks in the glasses is always facilitated by the weakest bonds present in the samples. In the samples under present investigation, the formation of more bonds linking NBOs and modifying cations facilitate the easy propagation of cracks due to the very low strength of these bonds.

Brittleness is another property that controls the crack initiation (Sehgal et al. 1999). The brittleness (B) is evaluated using the equation (2.26) suggested by Lawn and Marshall (1979) and the evaluated brittleness values are presented in table 5.6. In general, the plastic flow modes of deformation and densification before the crack initiation determine the brittleness of glass systems. The brittleness is found to increase with the increasing Fe_2O_3 content in both the series of samples.

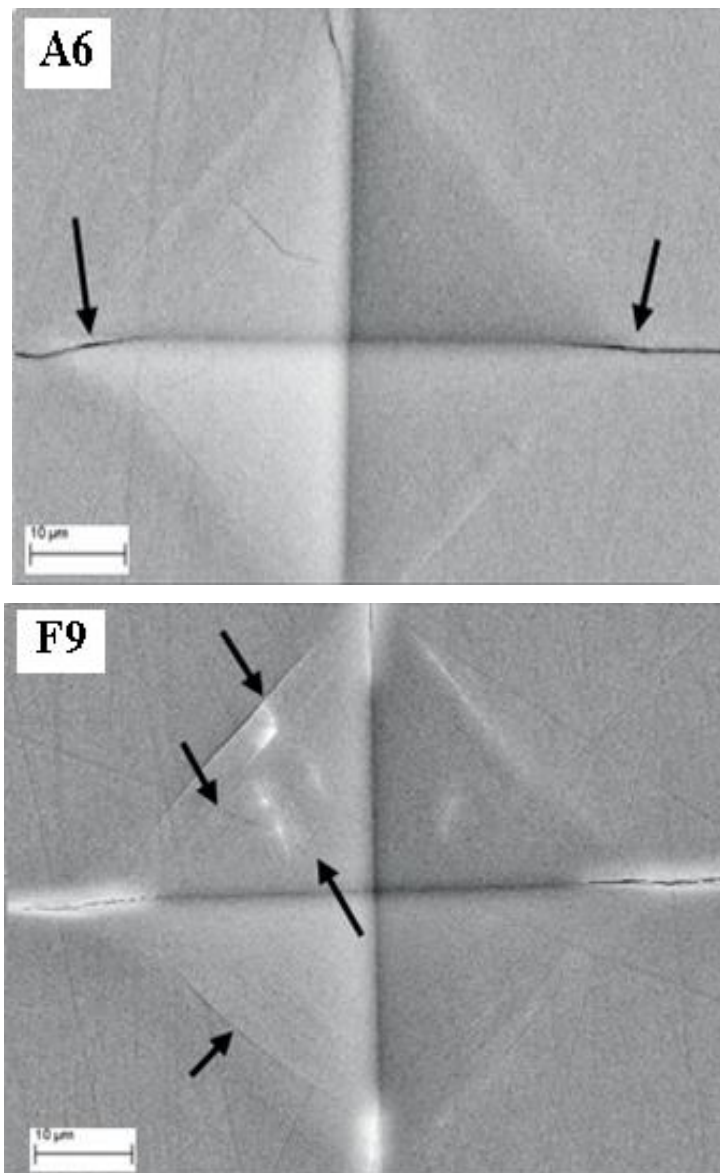


Figure 5.10 (a): SEM micrograph of Vickers indentation of A6 and F9 glass samples of LN-Fe glass system.

This enhancement is further confirmed by the SEM morphology obtained on the indentation pattern showing the formation of cracks and chipping as represented in figure 5.10 (a) and (b) for LN-Fe and LNK-Fe glass systems, respectively. One can clearly witness, from the figure 5.10 (a) and (b), the median-radial cracks (or palmqvist cracks), which are formed due to the Vickers indentation.

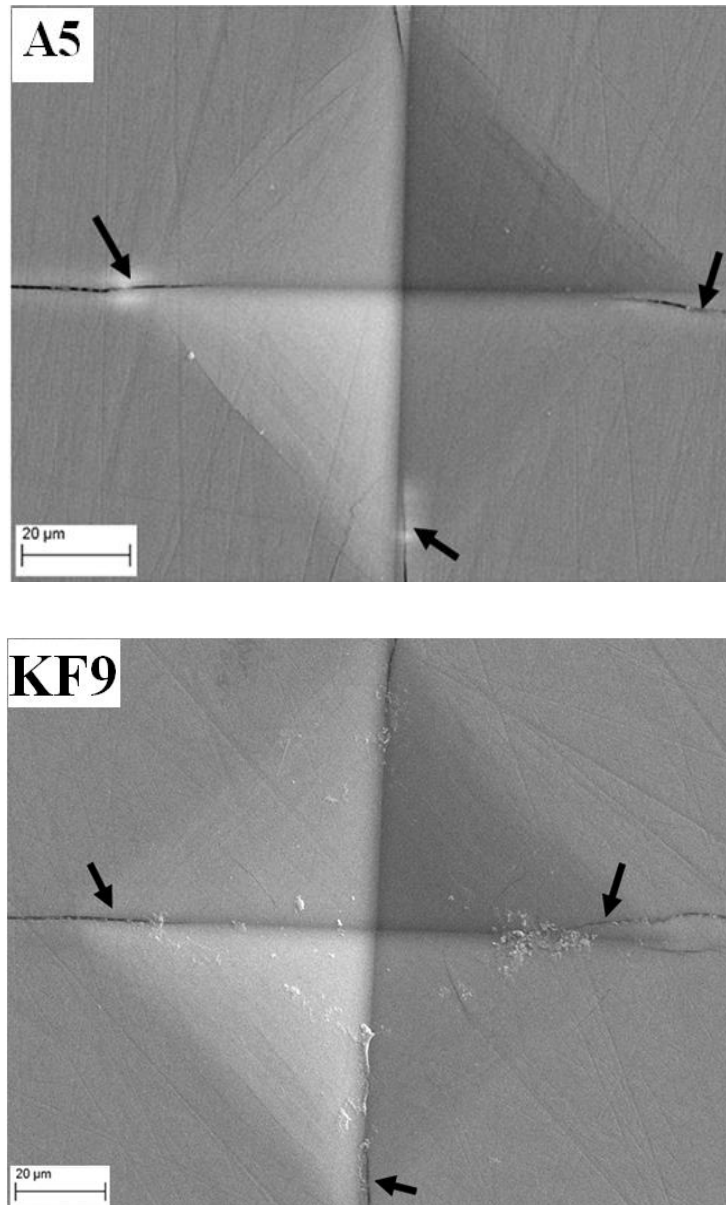


Figure 5.10 (b): SEM micrograph of Vickers indentation of A5 and KF9 glass samples of LNK-Fe glass system.

The cracks formed on the examined glass samples mainly originate from the four corners of the Vickers indentation which is highlighted with black arrows. These cracks are often originating from the flaws and extend if the stress applied crosses the specific individual threshold. In the studies, median-radial cracks were generated when the applied indentation load equal was increased to 4.9 N. This load was maintained constant for all the studied glass samples. The white reflections shown in F9 of figure 5.10 (a) indicate the apparent surface chipping and shear cracks (which is absent in A6). This reveals the higher brittleness of F9 glass sample in comparison with A6. Both surface chipping and shear cracks have increased with increase in Fe₂O₃ content. Hence there must be an increase in elastic properties of the LN-Fe glass system with an increase in Fe₂O₃. Detailed study of mechanical investigation using Vickers indentation technique and study of elastic properties of the glass samples are essential for the choice of suitable glasses for industrial and technological applications. Therefore, along with Young's modulus (E), the Poisson's ratio (σ) of the prepared glass system was also evaluated by means of the equation (2.27). The Shear modulus (S) and bulk modulus (K) were evaluated by the equations (2.28) & (2.29). The determined values of Young's (E), shear modulus (S) and bulk modulus (K) are summarized in table 5.7. It is seen from table 5.7, that the calculated values of Young's modulus, shear modulus and bulk modulus are increasing with increase in Fe₂O₃ content. The partial substitution of K₂O by Na₂O and partial replacement of ZnO by Fe₂O₃ in the investigated glass samples result in an increase of over all elastic moduli. This may be due to the higher dissociation energy and packing factor of incorporated modifiers. The replacement of ZnO by Fe₂O₃ in both LN-Fe and LNK-Fe glass systems result in an increase of elastic moduli. This may be due to the higher dissociation energy, G_i (18.76 Kcal/cm³) and packing factor, V_i (21.6 cm³/mol) of Fe₂O₃ compared to that of ZnO ($G_i = 11.93$ Kcal/cm³, $V_i = 21.6$ cm³/mol). Poisson's ratio of all the studied samples is least affected due to the trivial variation of packing density. The estimated poisson's ratio for both LN-Fe and LNK-Fe series by means of equation (2.27) is 0.27 which is in good agreement with earlier investigations and lie in the reported range for borate glasses (Makishima and Mackenzie, 1973).

Table 5.7. Young's modulus (E), bulk modulus (K), shear modulus (S), and atomic packing density (V_t) of Fe_2O_3 doped LN-Fe and LNK-Fe glass system.

Glass System	Glass code	Young's modulus, E (GPa)	Bulk modulus, K (GPa)	Shear Modulus, S (GPa)	Atomic packing density, V_t
LN-Fe	A6	80.95	59.14	31.82	0.609
	F1	81.05	59.26	31.86	0.609
	F3	81.11	59.31	31.88	0.609
	F5	81.27	59.48	31.94	0.610
	F7	81.38	59.60	31.98	0.610
	F9	81.45	59.64	32.00	0.610
LNK-Fe	A5	79.33	57.35	31.25	0.602
	KF1	79.41	57.43	31.27	0.603
	KF3	79.51	57.54	31.31	0.603
	KF5	79.65	57.69	31.36	0.604
	KF7	79.78	57.83	31.41	0.604
	KF9	79.96	58.03	31.47	0.605

5.2 SUMMARY

In the present chapter, the results of comparative studies carried out on the effect of Fe^{3+} addition on the properties of LN-Fe glass system with that of the LNK-Fe glass system are discussed in detail. The XRD results, for both the series, confirmed the amorphous nature of the glass systems. The IR and Raman spectral analysis revealed that the Fe_2O_3 acts as a network modifier for both the series in the present investigation. It is observed that the prepared samples exhibit good thermal stability, which gets enhanced as Fe_2O_3 content increases. The glass forming ability has been enhanced with the partial incorporation of third alkali ion and Fe^{3+} ion in the LNK-Fe system. The glass transition temperature is found to reduce, for both the series, as Fe_2O_3 content increases. This is due to the opening of diborate units by Fe_2O_3 in order to compensate its own coordination requirements. The median-radial cracks produced due to Vickers

indentation were studied and it was confirmed that the brittleness of the samples enhances, for both the series, as Fe₂O₃ content increases. Optical band gap energy, E_g of the studied glass system found to reduce with increasing Fe₂O₃ content. Addition of Fe₂O₃ to B₂O₃ glass opens up the diborate glass network and decreases the energy of E_g resulting in the shift of absorption edge towards the higher wavelength region. It was noticed, in both the series of prepared glasses, that the refractive index increased as Fe₂O₃ content was enhanced owing to the replacement of relatively lower polarizability Zn²⁺ (0.283 Å⁻³) by Fe³⁺ (0.437 Å⁻³). The band observed, in both the series, around 450 nm in UV absorption spectra is due to the d-d transition of ${}^6A_{1g}(S) \rightarrow {}^4T_{2g}(G)$ which indicates the presence of an iron ion in trivalent state (Fe³⁺) with distorted octahedral symmetry. Further efforts have been made to analyze and correlate the physical and mechanical properties with the structure of the studied glass system. It seen that the Vickers micro-hardness value has decreased from 4.992 GPa to 4.760 GPa with the partial incorporation of K₂O content to the glass matrix of A6 system. This may be due to the partial replacement of relatively lower radius and higher field strength Na₂O with higher radius and lower field strength K₂O. Further, it is seen that the Vickers micro-hardness of both LN-Fe and LNK-Fe system of glasses is slightly decreasing with the partial incorporation of Fe₂O₃ content. This may be due to the breaking up of tightly bound diborate structure and a slight increase in NBOs. Crack initiation and crack propagation are the two factors which determine the strength of the glasses. It is evident that K_{IC} is decreasing gradually. This can be attributed to the slight reduction of Vickers hardness and increase in half crack length. The crack length in both the series of glass systems is observed to enhance with increasing Fe₂O₃ content. This signifies that the ease of crack propagation through the glasses is enhancing with increasing Fe₂O₃ content. Hence, it can be concluded that the inclusion of third alkali element into the matrix of LN-Fe system influences different properties of the studied glass system to a greater extent. It is also observed that the doping of ZnO by Fe₂O₃ modifies the basic structure of the glass matrix both in LN-Fe and LNK-Fe glass systems. The inclusion of Fe₂O₃ has proved to be of great importance in tailoring the properties of the glass systems to make them promising candidates for technological applications.

Chapter 6

EFFECT OF Mn²⁺ ADDITION ON THE PROPERTIES OF 5Li₂O-25Na₂O-60B₂O₃-(10-x) ZnO-xMnO₂ AND 5Li₂O-xK₂O-(25-x)Na₂O-60B₂O₃-(10-y)ZnO-yMnO₂ GLASS SYSTEMS: A COMPARATIVE STUDY OF LN-Mn AND LNK-Mn GLASS SYSTEM.

In the present chapter, the results of comparative studies carried out on the effect of MnO₂ addition on the properties of LN-Mn glass system with that of the LNK-Mn glass system are presented. XRD results, for both the series, confirmed the amorphous nature of the synthesized glasses. Fourier Transform Infrared (FTIR) and Raman spectroscopy techniques were used in order to explore the structural rearrangement occurred due to the partial substitution of modifier cations. The prepared glass samples exhibited good thermal stability, which got enhanced with the incorporation of MnO₂ content in both LN-Mn and LNK-Mn glass systems. UV-visible spectroscopy was performed for all the samples in order to understand the electronic band structure and optical transitions in them. A broad band is observed at about 475 nm in both LN-Mn and LNK-Mn glass system with the incorporation of MnO₂ content. This is due to the ⁶A_{1g}(S) → ⁴T_{1g}(G) transition representing the divalent state of Mn in octahedral symmetry. It is observed that the partial incorporation of MnO₂ content exhibit drastic redshift, from 208 to 258 nm and 212 to 275 nm, in the absorption edge of LN-Mn and LNK-Mn glass systems respectively. Mechanical strength and fracture toughness of the prepared glass samples were determined using Vickers micro-indentation technique. The prepared glass samples exhibit superior mechanical properties with the incorporation of MnO₂ content.

6.1 Results and Discussion

6.1.1 X-ray diffraction studies

The XRD measurement data of powdered samples obtained between diffraction angle 10°-80° are presented in figure 6.1 (a) & (b).

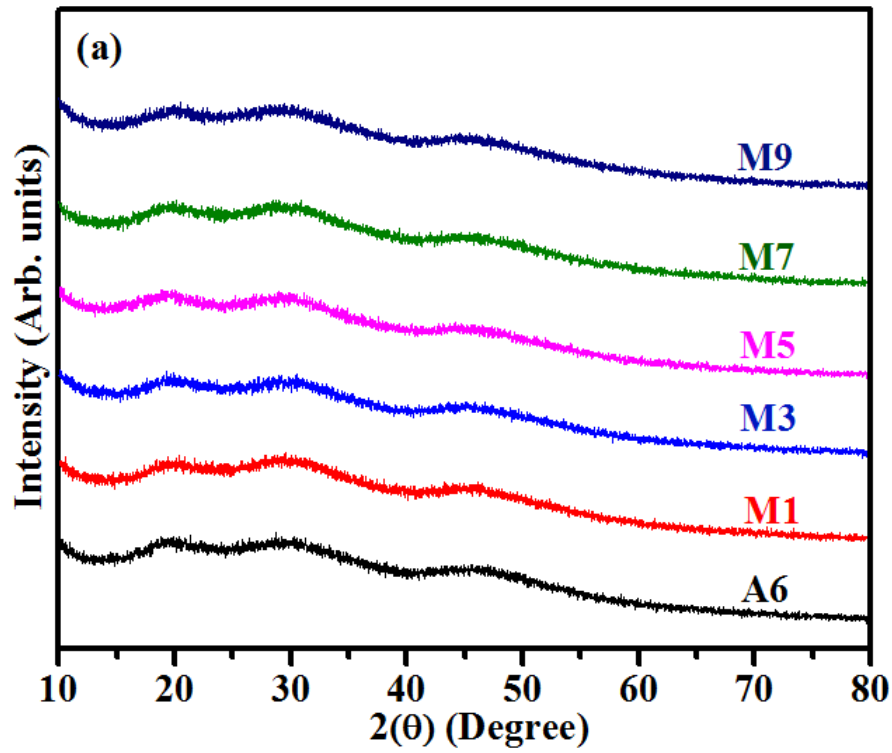


Figure 6.1 (a): X-ray Diffraction patterns for the MnO₂ doped LN-Mn glass system.

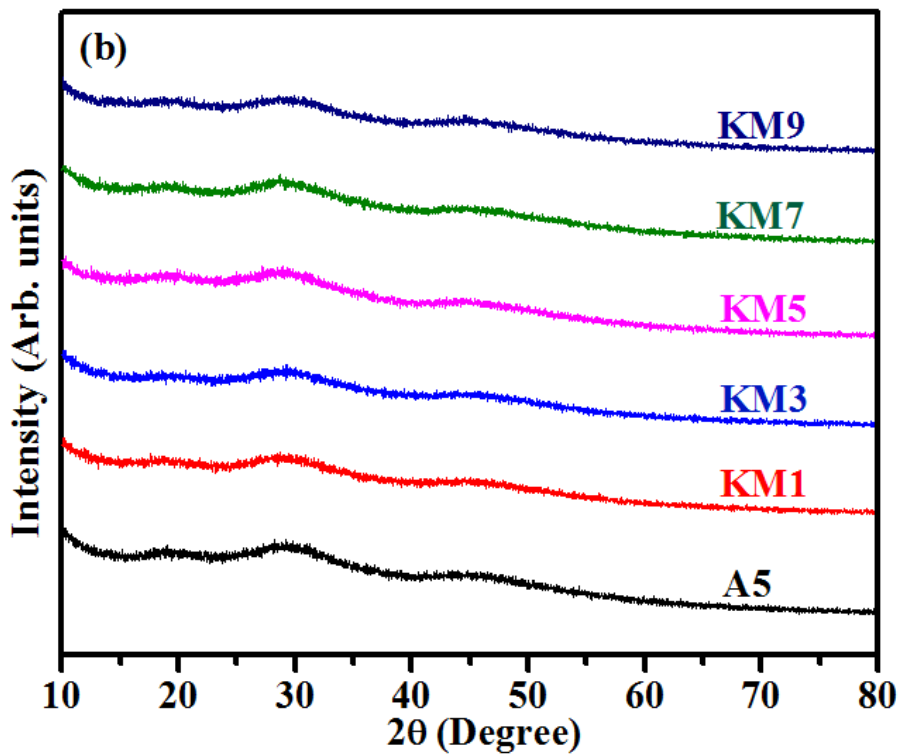


Figure 6.1 (b): X-ray Diffraction patterns for the MnO₂ doped LNK-Mn glass system.

It can be observed that all the samples exhibit a broad hump like feature without pronounced Bragg peaks. This result confirms the prepared glass samples are amorphous in nature.

6.1.2 Structural Studies

Detailed understanding of structural features of the investigated glass system is important, since most of the glass properties depends on the structural arrangements of the glass network. Fourier Transform Infrared (FTIR) and Raman spectroscopy techniques were used in order to explore the structural rearrangement occurred due to the partial substitution of modifier cations. These two techniques are highly sensitive to determine the basic structural units and super structural units viz., triangular BO_3 units, tetrahedral BO_4 units, boroxol rings, and diborate units etc.,

6.1.2.1 Fourier Transform Infrared Spectroscopy studies

FTIR spectrum of the studied glass system are presented in figure 6.2 (a) & (b). Each spectra consists of specific area, intensity and band centre corresponding to the structural groups present in the glass samples. In order to gather all these information, entire spectrum was deconvoluted using Gaussian function, the representative deconvoluted spectrums are given in figure 6.3 (a) & (b). It can be noticed from figure 6.3 (a) & (b) that, there are majorly three active regions present in FTIR spectrum viz., around $400\text{-}650\text{ cm}^{-1}$ with relatively lower intensity corresponds to the bending vibrations of B-O-B bonds as well as deformation of borate rings, $600\text{-}800\text{ cm}^{-1}$ is associated with the bending vibrations occurred due to the different types of borate units and one more major band around $1200\text{-}1500\text{ cm}^{-1}$ which is predominantly corresponding to the B-O stretching vibrations of BO_3 units (Lewandowski et al. 2017). The band assignments of the studied glass systems spectrum were briefly summarized in table 6.1. The investigated LN-Mn and LNK-Mn glass systems exhibit a band around 705 cm^{-1} which can be attributed to the bending vibrations of B-O-B linkage in the borate glass matrix. The FTIR spectra of examined glasses includes the crucial bands of vitreous B_2O_3 and observed a trivial shift from their original position.

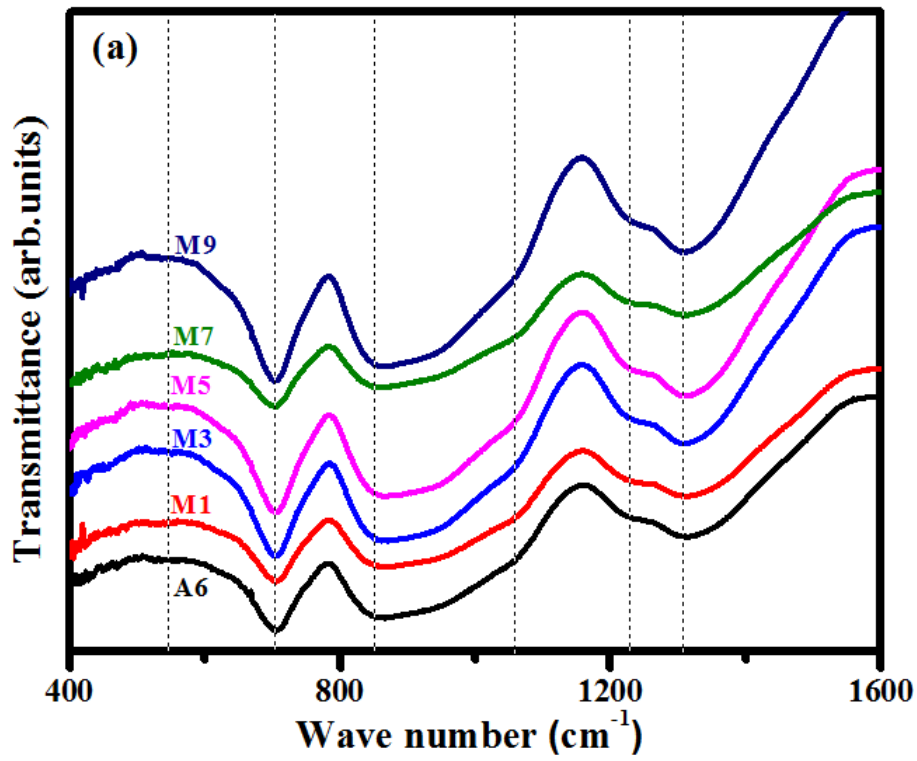


Figure 6.2 (a): FTIR spectra of MnO₂ doped LN-Mn glass system.

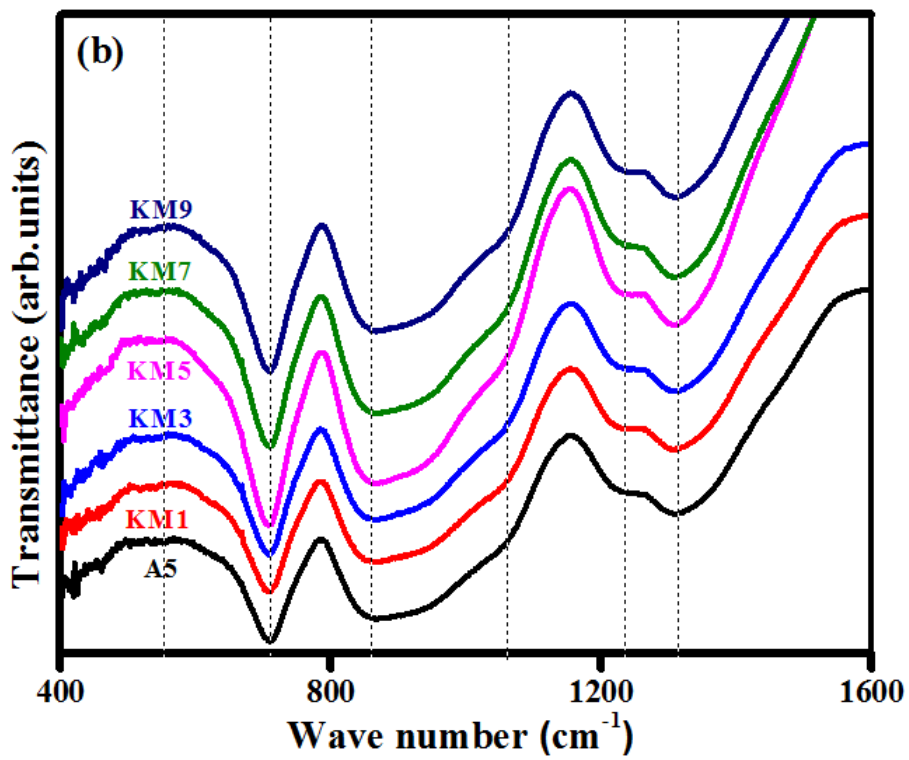


Figure 6.2 (b): FTIR spectra of MnO₂ doped LNK-Mn glass system.

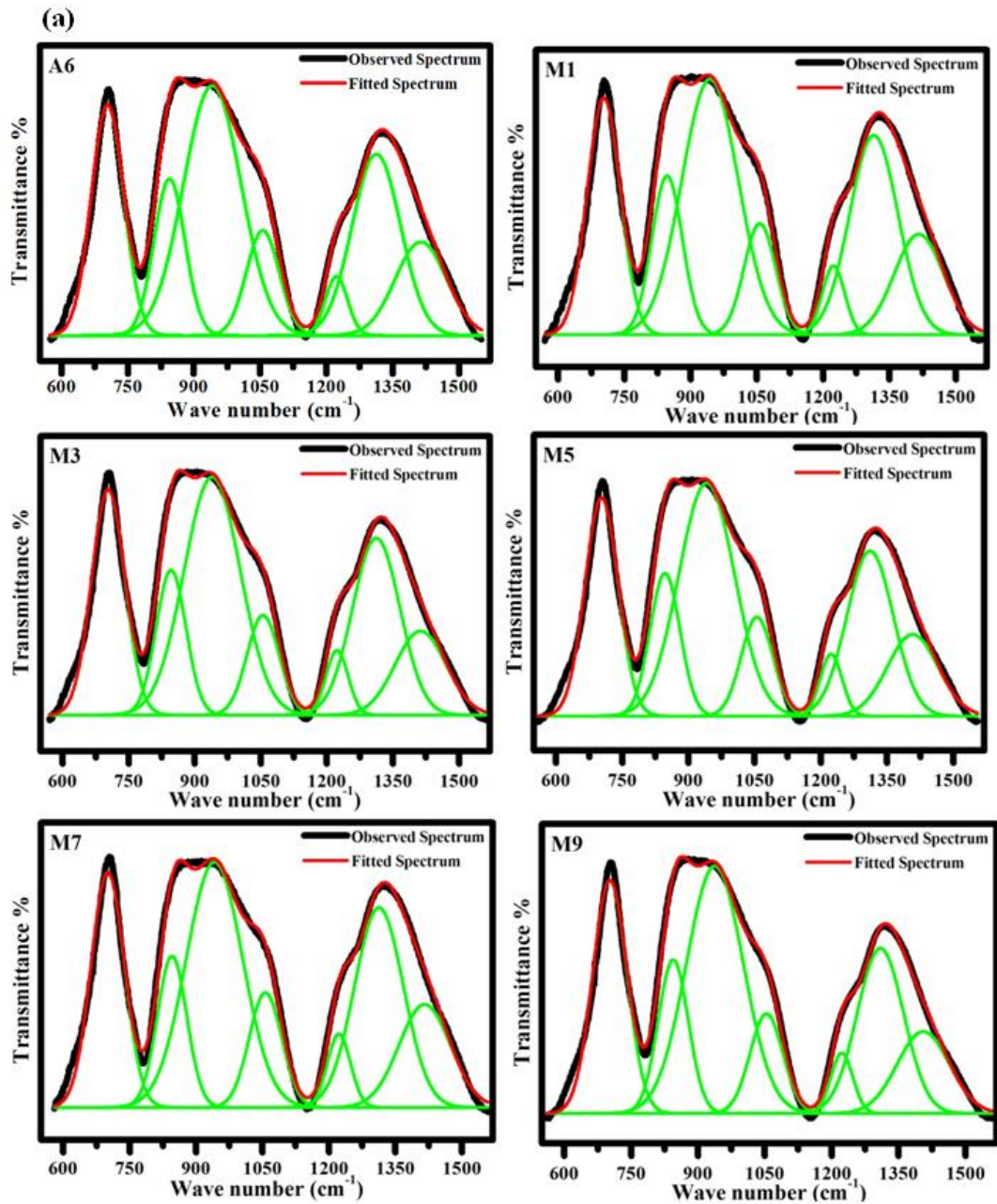


Figure 6.3 (a): Deconvoluted FTIR spectra of MnO₂ doped LN-Mn glass systems.

All the samples exhibit a band around 703-705 cm⁻¹, attributed to the bending vibration of B–O–B linkage in the borate network (Hammad et al. 2018, Colak et al. 2016). The increase in the intensity of B-O-B bending may be ascribed to the breaking down of the diborate units and a more relaxed glass structure. Hence there will not be any constraints for bending.

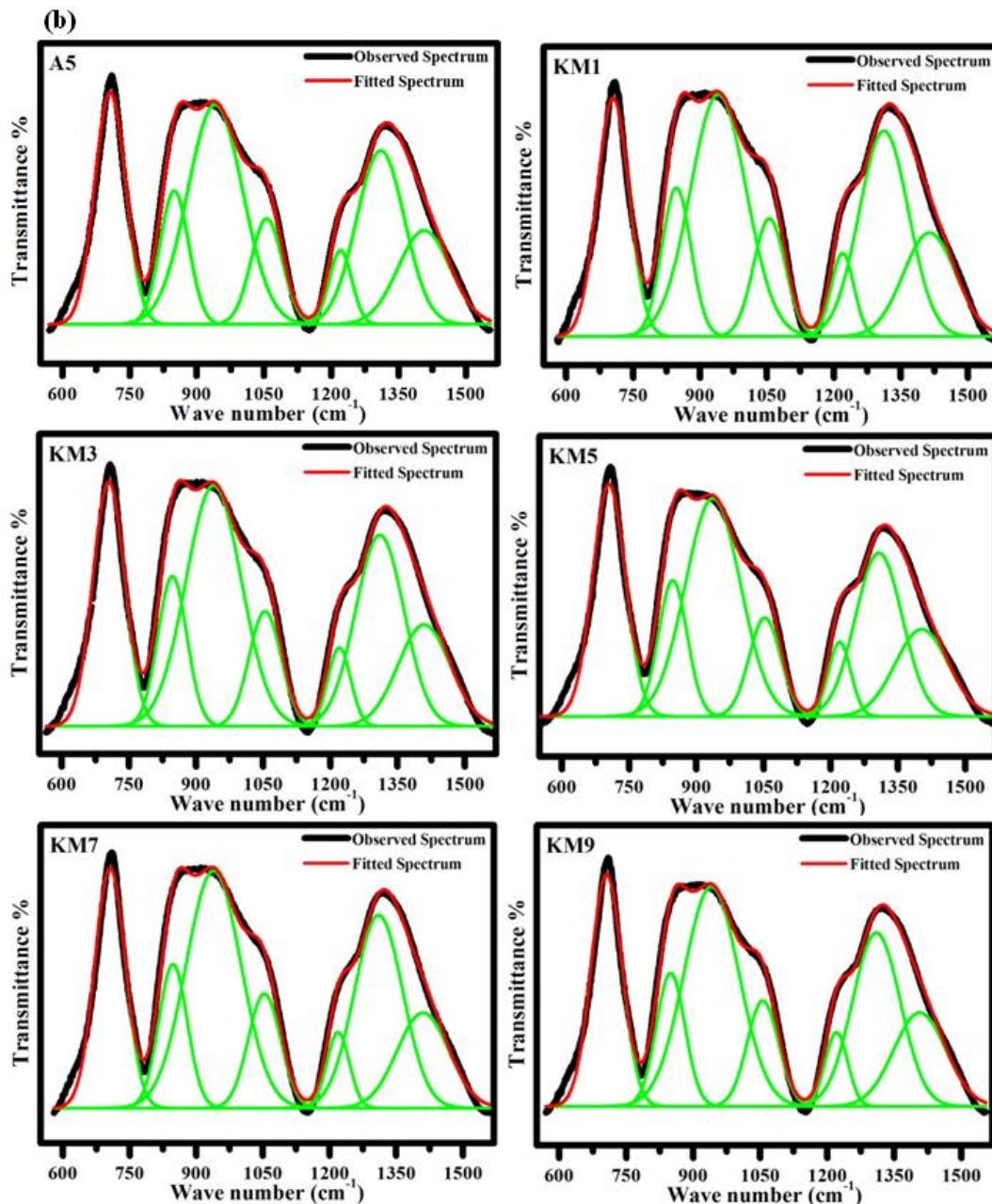


Figure 6.3 (b): Deconvoluted FTIR spectra of MnO₂ doped LNK-Mn glass systems.

The broad band around 845-849 cm⁻¹ may be due to the B-O bond stretching modes of tetrahedral BO₄ units (Hammad et al. 2018, Colak et al. 2016, Colak 2017). The broad band around 1052-1056 cm⁻¹ with shoulder around 937-942 cm⁻¹ can be due to the diborate groups and stretching vibrations of BO₄ groups, tri-, and tetra borates respectively (Wen et al. 2016 and Moustafa et al. 2013).

Table 6.1. Assignment of absorption bands present in FTIR spectra of MnO₂ doped LN-Mn and LNK-Mn glass systems.

Band position (cm ⁻¹)	FTIR band assignments
703-705	B-O-B bending vibrations. (Hammad et al. 2018)
845-849	Stretching modes of [BO ₄] tetrahedral borons. (Colak et al. 2017)
882-896	Stretching vibrations of B-O bonds in BO ₄ . (Colak et al. 2016)
937-942	Diborate group stretching vibrations. (Wen et al. 2016)
1052-1056	B-O stretching vibrations of BO ₄ units in di-, tri-, tetra-, and penta-borate groups. (Mustafa et al. 2013)
1219-1223	Symmetric stretching vibrations of B-O bonds in [BO ₃] triangular units involving NBO atoms. (Satyanarayana et al. 2013)
1307-1338 1403-1418	Stretching vibrations of B-O in BO ₃ units from meta-, pyro-, ortho- and groups containing large number of NBOs. (Satyanarayana et al. 2013)

The band observed around 1307-1314 cm⁻¹ with a prominent shoulder around 1219-1223 cm⁻¹ can be due to the symmetric stretching vibrations of B-O bonds in [BO₃] triangular units involving NBO atoms and the wide band may be ascribed to the stretching vibrations of three fold borate unit linked with pyro-borate and ortho-borates (Satyanarayana et al. 2013).

6.1.2.2 Raman Spectroscopy studies

The Raman spectra were recorded for all the investigated samples to understand the structural variations thoroughly since it is a sensitive tool to gather all kind of minute vibrations occur in the glass system. The recorded Raman spectra are presented in figure 6.4 (a) & (b). The collected spectrums were deconvoluted using Gaussian function in order to get all the superimposed spectrum details. Figure 6.5 (a) & (b) represents the deconvoluted Raman spectra of both the MnO₂ doped LN-Mn and LNK-Mn glass system. Some of the new bands are identified in Raman spectrum which were absent in FTIR spectrum.

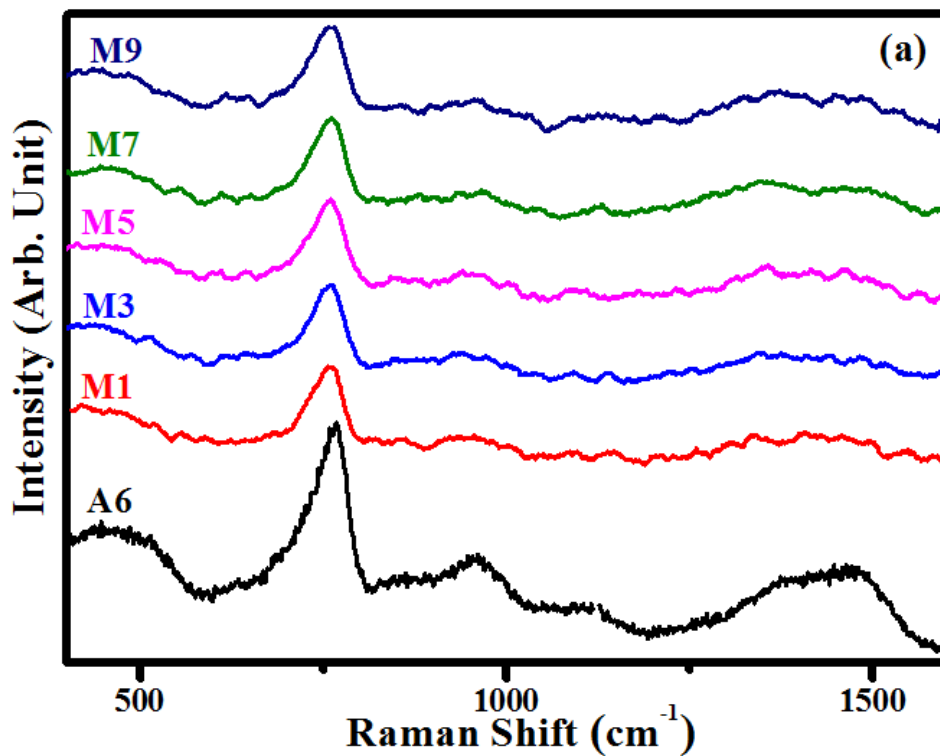


Figure 6.4 (a): Raman spectra of MnO₂ doped LN-Mn glass systems.

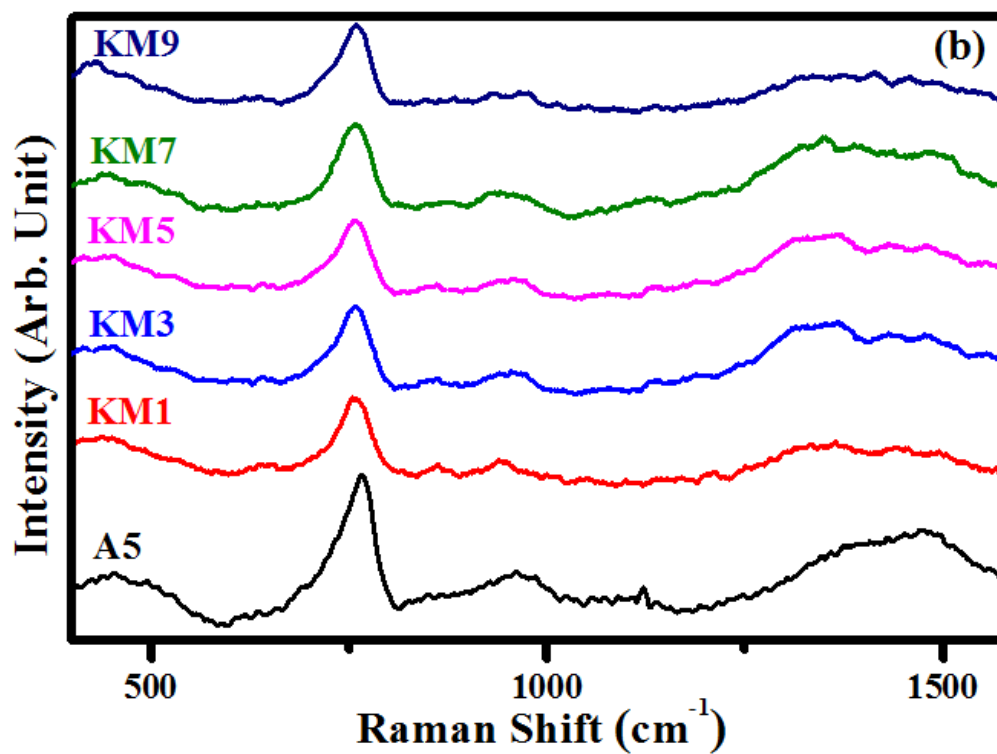


Figure 6.4 (b): Raman spectra of MnO₂ doped LNK-Mn glass systems.

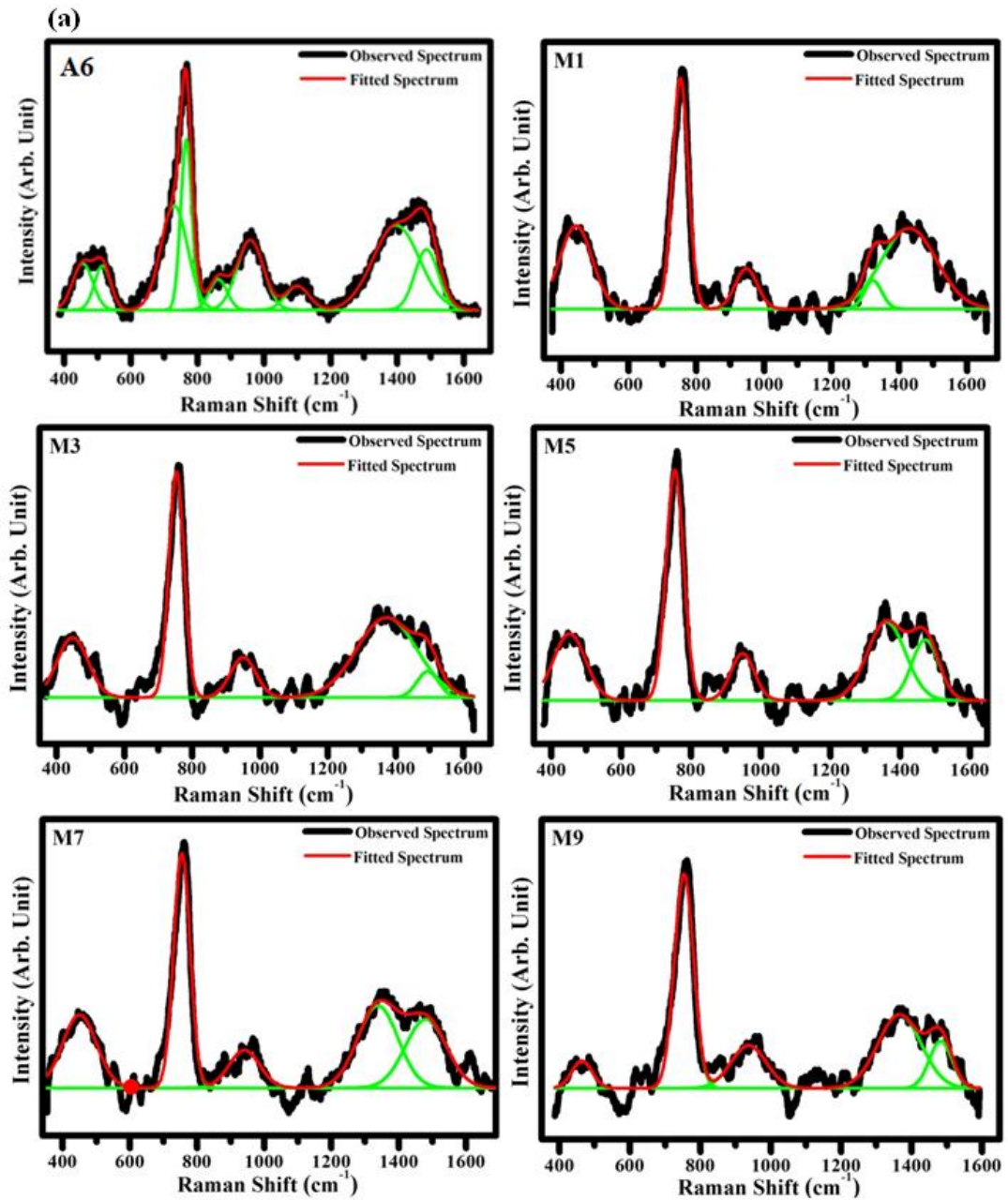


Figure 6.5 (a): Deconvoluted Raman spectra of MnO₂ doped LN-Mn glass system.

The broad band around 439-473 cm⁻¹ which has centre about 450 cm⁻¹ may be ascribed to the bending vibrations of B-O-B bonds involved in the isolated diborate groups (Hammad et al. 2018 and Saddeek et al. 2009). It can be seen, from the figure 6.5 (a) & (b), that there exists a prominent and comparatively sharp band at around 755 cm⁻¹. This is due to the symmetric breathing vibrations ascribed to the six-membered structure involved with the different types of ring type structures enclosing with two

[BO₄] units namely, di-, tri-, di-penta- borates (Saddeek et al. 2009 and Zheng et al. 2012).

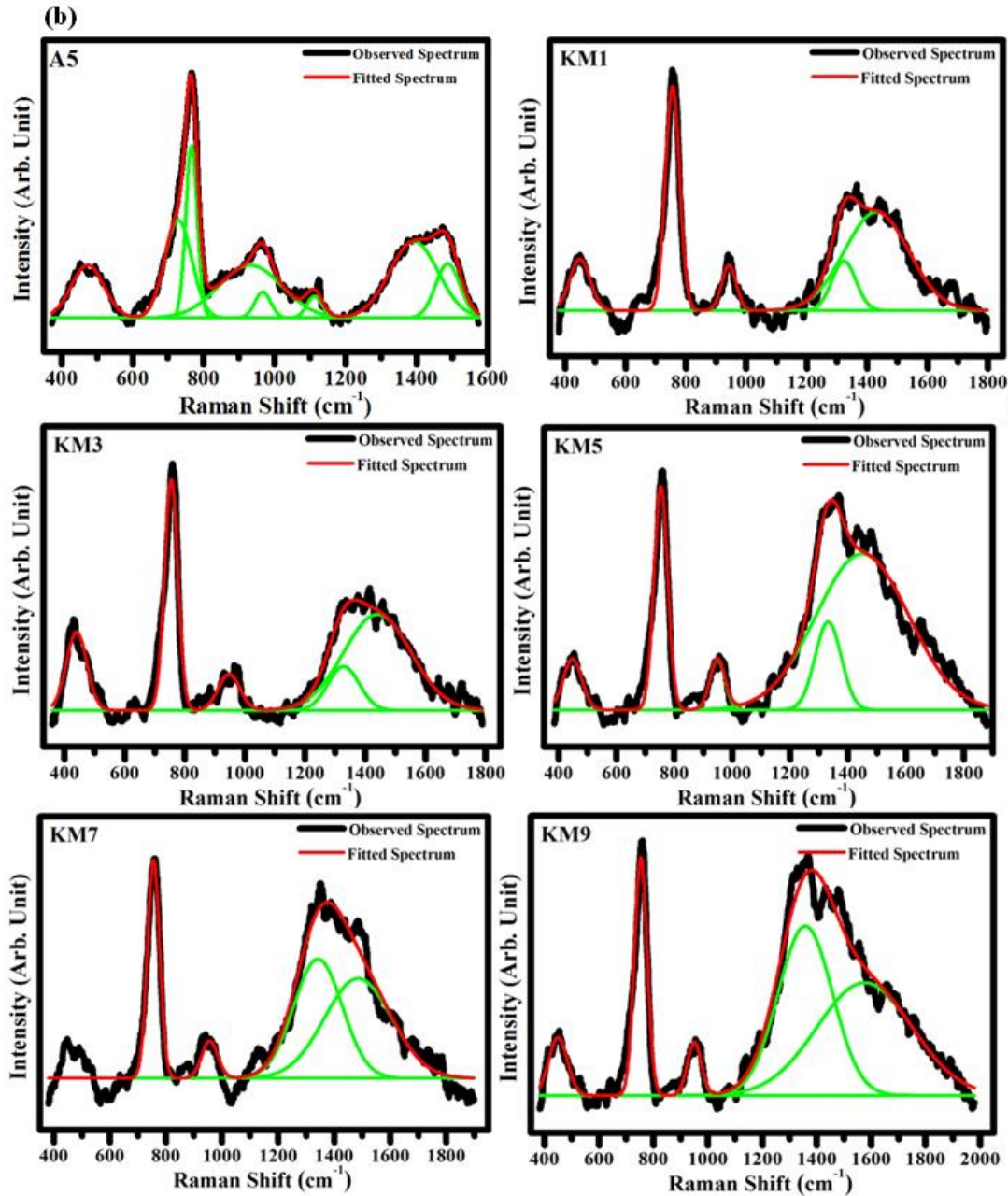


Figure 6.5 (b): Deconvoluted Raman spectra of MnO₂ doped LNK-Mn glass systems.

The band appeared around 950-1180 cm⁻¹ can be ascribed to the vibrations of Mn-O and diborate groups in the studied glass structure (Hammad et al. 2018 and Zheng et al. 2012). The band at high frequency range centred around 1450 cm⁻¹ found to be

shifting toward the comparatively lower frequency about 1350 cm^{-1} . The decrease in the intensity of higher frequency band, as the content of MnO_2 increased, indicates the destruction of interconnected network resulting in small, highly charged groups with NBOs (Zheng et al. 2012). The broad and major band around $1477\text{-}1485\text{ cm}^{-1}$ can be assigned to the BO_2O^- triangular structures connected to the borate units. From the observations and analysis made based on deconvolution spectral data, one can witness the enhancement in the intensities of the band connected with the $[\text{BO}_3]$ units, which are associated with the NBOs (Zheng et al. 2012). The band assignments of all the studied glass samples are summarized in table 6.2. All the band assignments of Raman spectra and their evolution with the addition of Mn ion are validating the results of FTIR analysis.

Table 6.2. Assignment of absorption bands present in Raman spectra of MnO_2 doped LN-Mn and LNK-Mn glass systems.

Band position (cm^{-1})	Raman band assignments
439-473	Bending vibrations of B-O-B bonds involved in isolated diborate groups. (Saddeek et al. 2009, Hammad et al. 2018)
955-958	Mn-O vibrations and vibrations of diborate groups in the structure. (Hammad et al. 2018, Zheng et al. 2012)
1070-1100	Stretching vibrations of diborate groups. (Zheng et al. 2012)
1350	BO_2O^- triangles linked to B-O units. (Zheng et al. 2012)
1477-1485	BO_2O^- triangles linked to other triangular borate units connected to NBOs. (Zheng et al. 2012)

In general, when the stoichiometric ratio of alkali to borate content maintained as 1:2, the glass structure is more likely consist of the rigidly bound di-borate units (Meera and Ramakrishna 1993). In addition to this, borate glasses possess different kinds of structural units like $[\text{BO}_3]$, $[\text{BO}_4]$, tri-borate, di-borate, etc., which are further substantiated from the band assignments of FTIR and Raman spectra. The diborate units are associated with two units of $[\text{BO}_4]$ and $[\text{BO}_3]$ each in the bridging position, which formulates a rigid symmetrical geometry in the glass network. This tightly bound diborate unit is not associated with the NBOs, meanwhile retains a charge of -2 which

remains delocalized throughout the unit. Partial incorporation of MnO₂ content into this glass matrix, breaks the rigidly bound di-borate units and expands the glass network. In this process of expansion, firstly breaking up of the bridge will take place and then that of the ring, hence the diborate structure turn out to be less rigid. This can be witnessed from the deconvoluted Raman spectra, where there is a shift of band (1170 to 1100 cm⁻¹) towards lower frequency which is assigned to diborate units. The breaking up of the diborate structure promotes more connectivity to the structure which further increases the requirement of oxygen coordination in the glass matrix. Hence there exists a competition for charge compensation among the modifier cations. This competition in the glass network promotes further breakdown of the diborate units for charge compensation. When diborate unit breakdowns further, it attains monocyclic and chain structure and holds greater flexibility and shares NBO to iron ions. Hence substitution of MnO₂ content to the diborate glass system causes breaking down of diborate unit in order to fulfil its own coordination requirements since it prefers to be in six coordination position specially in borate glass system (Lu et al. 2003). This observation is further substantiated by the UV-visible absorption studies.

6.1.3 Density (ρ), Molar volume (V_m) and atomic packing density (OPD)

The density of the prepared glass samples in the current investigation was measured in order to understand the modifications in the structure of glasses. The results are tabulated in table 6.3. Density is considered to be an important tool to understand the modifications in the structure of glasses due to their high sensitivity to the properties viz., compactness, softening, cross link density, modifications of geometrical configuration, coordination numbers, and dimension of interstitial spaces of the glass (Saddeek et al. 2009). It is also crucial in exploring information about the short-range structure of oxide glasses. The density of the samples is observed to slightly decrease with increasing MnO₂ content in both LN-Mn and LNK-Mn glass systems. This may be attributed to the replacement of higher molecular mass ZnO (81.408 g/mol) by relatively lower molecular mass MnO₂ (70.937 g/mol). The determined V_m (using equation (2.2)) for all the samples is given in table 6.3 and is observed to show opposite trend compared to density. The oxygen packing density (OPD) can be defined as the

number of oxygen atoms per formula unit and can be determined using the equation (2.3) and the evaluated values are given in table 6.3.

Table 6.3. Density (ρ) and molar volume (V_m) and oxygen packing density (OPD) of LN-Mn and LNK-Mn glass system.

Glass System	Glass code	ρ (g/cm ³) ± 0.005	V_m (cm ³) ± 0.05	OPD
Ln-Mn	A6	2.473	27.052	81.32
	M1	2.472	27.059	81.30
	M3	2.471	27.061	81.30
	M5	2.470	27.064	81.28
	M7	2.469	27.066	81.28
	M9	2.468	27.069	81.27
LNK-Mn	A5	2.450	27.964	78.81
	KM1	2.449	27.971	78.77
	KM3	2.446	27.997	78.71
	KM5	2.443	28.022	78.66
	KM7	2.441	28.037	78.62
	KM9	2.439	28.051	78.59

It is observed that there is a slight decrease in the OPD with an increase in MnO₂ content in both LN-Mn and LNK-Mn glass systems. This clearly shows the presence of loose packing of the oxide network.

6.1.4 Thermal studies

Thermal parameters like T_g (onset of glass transition region), T_x (onset crystallization temperature), T_c (glass crystallization temperature) and T_m (glass melting temperature) are determined using DSC thermographs which are obtained by plotting heat flow versus temperature plots as depicted in figure 6.6 (a) & (b). The determined thermal parameter values are summarized in table 6.4. It is evident, from table 6.4, that there is a substantial decrease in T_g from 446 °C to 427 °C when third alkali ion is introduced to the A6 glass sample of LN-Mn glass system.

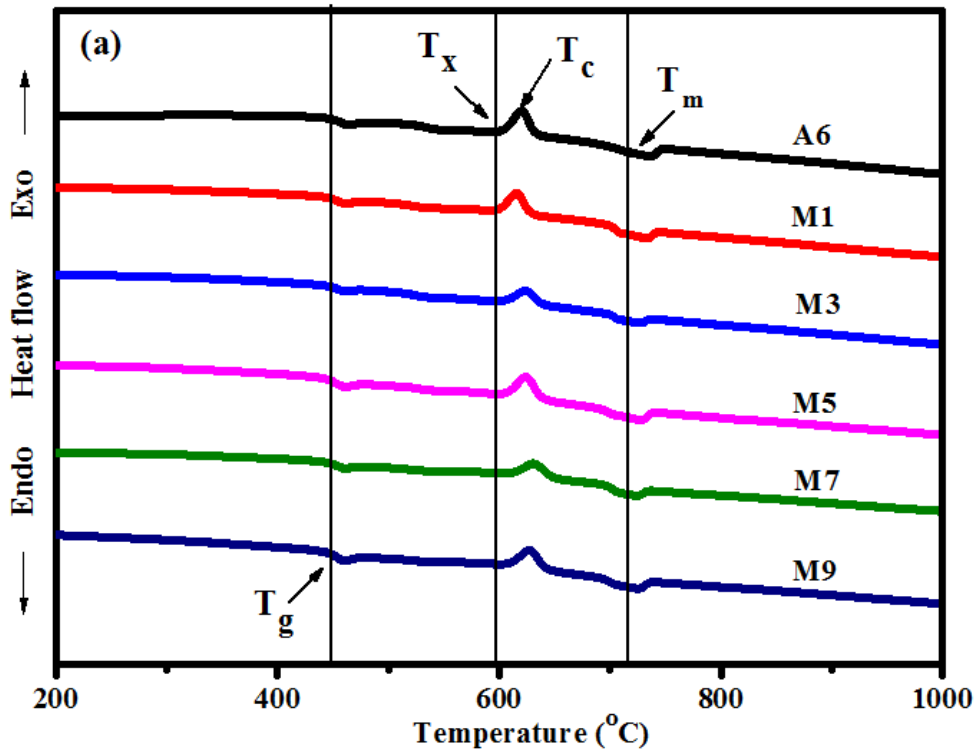


Figure 6.6 (a): DSC thermographs of MnO₂ doped LN-Mn glass system.

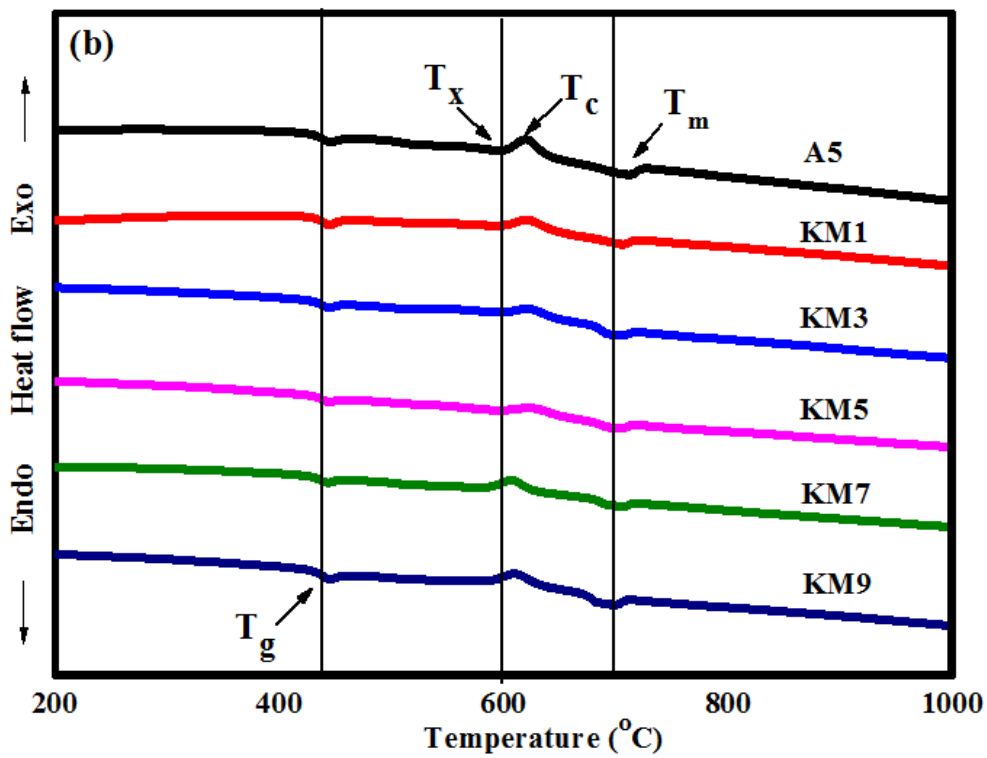


Figure 6.6 (b): DSC thermographs of MnO₂ doped LNK-Mn glass system.

In other words, the addition of third alkali (i.e., K₂O) ion reduces the rigidity of the glass sample. In case of oxide glasses, glass transition temperature depends on certain crucial factors like strength between bonds, compactness in glass network and cross-link density. The reduction of T_g , in Mn free LN-Mn and LNK-Mn glass system, may be attributed to the replacement of relatively higher single bond strength and lower ionic radii Na₂O (20 Kcal/mol and 0.78 Å respectively) by lower single bond strength and higher ionic radii K₂O (13 Kcal/mol and 1.33 Å respectively). It is also important to note that, the glass transition mainly involves the transformation from solid to liquid state by breaking up of the weakest chemical bonds. Therefore, consideration of single bond strength and ionic size of the incorporated modifier ions plays a vital role in deciding the T_g . Therefore, partial incorporation of heavier network modifiers K₂O is more effective in reducing T_g than lighter Na₂O. The reduction of T_g can also be ascribed to the replacement of relatively higher field strength Na₂O ($0.17 \times 10^{-20} \text{ m}^{-2}$) by relatively lower field strength K₂O ($0.12 \times 10^{-20} \text{ m}^{-2}$) which indeed weakens the glass network. It can be clearly observed, from the table 6.4, that the addition of MnO₂ content slightly decreases the T_g in both LN-Mn and LNK-Mn glass systems.

The thermal stability of glass (ability of glass to bypass crystallization upon heating) is considered as one of the most significant aspects in the production of large scale glass for the practical applications (Zheng et al. 2012). In this regard the determination of thermal stability for the prepared glass system is a crucial factor. Glass stability criterion (or thermal stability) can be determined by considering the temperature differences between T_g and T_x , i.e., $\Delta T = T_x - T_g$. The evaluated thermal stability values are summarized in table 6.4. The thermal stability values are lying in the range of 155 °C to 187 °C. Usually, the glasses having ΔT values greater than 100 °C with low temperature intervals ($T_m - T_x$) are good host materials for optical fiber fabrication. These glasses yields a crystal-free fiber, since the fiber drawing technology mainly involves reheating and in the process of fabrication any kind of crystallization leads to scattering loss which eventually lowers the efficiency of the fiber. It can be seen from table 6.4 that, the studied glass systems possess considerably higher thermal stability (ΔT) values which fulfils the condition of conventional fibre drawing ability.

The increase in ΔT indicates that the addition of third alkali metal (K_2O) content significantly improves the thermal stability against crystallization.

Table 6.4. Glass transition temperature (T_g), onset crystallization temperature (T_{cx}), crystallization temperature (T_c), melting temperature (T_m), glass stability (ΔT), varies glass forming ability and thermal stability parameters (K_1 , K_2 , K_3 , K_w , K_{LL} and K_{gl}) and Hruby's parameter (H_R) of LN-Mn and LNK-Mn glass system.

Glass system	Glass code	T_g (°C)	T_x (°C)	T_c (°C)	T_m (°C)	ΔT (°C)	K_1 (°C)	K_2 (°C)	K_w	K_{LL}	H_R
LN-Mn	A6	446	601	620	736	155	290	0.817	0.211	0.508	1.15
	M1	446	602	620	733	156	287	0.821	0.213	0.511	1.19
	M3	445	604	623	729	159	284	0.829	0.218	0.514	1.27
	M5	444	607	625	727	163	283	0.835	0.224	0.518	1.36
	M7	443	610	627	725	167	282	0.841	0.230	0.522	1.45
	M9	441	611	630	723	170	282	0.845	0.235	0.525	1.52
LNK-Mn	A5	427	597	620	711	170	284	0.840	0.239	0.525	1.49
	KM1	426	601	621	707	175	281	0.850	0.248	0.531	1.65
	KM3	425	603	623	705	178	280	0.855	0.252	0.535	1.75
	KM5	425	604	625	703	179	278	0.859	0.255	0.537	1.81
	KM7	424	607	626	699	183	275	0.868	0.262	0.555	1.99
	KM9	422	609	627	669	187	247	0.910	0.280	0.573	2.12

It can be seen, from table 6.4, that unlike the T_g , there is no considerable difference seen in the glass stability with partial incorporation of third alkali (K_2O) ion. On the other hand, incorporation of MnO_2 content enhanced the glass stability drastically in both LN-Mn and LNK-Mn glass systems. It can be observed that glass stability criterion has increased from 155 °C to 170 °C (refer table 6.4) in LN-Mn glass system and increased from 170 °C to 187 °C in LNK-Mn glass system. This clearly indicates that the glass stability is more affected by MnO_2 content in LNK-Mn glass system compared to that of the LN-Mn glass system. Therefore, partial replacement of third alkali (K_2O) metal in the LN-Mn glass system can be utilized to tune the stability and network rigidity of the studied glass systems.

Further, the glass forming ability (GFA) factor is to be considered in the production of large scale glasses. GFA is a measure of resistance possessed by a melt against becoming crystalline in the process of cooling. Hurby's parameter is determined using the equation 2.5 and the values are summarized in table 6.4. Gradual increase in the quantity T_x-T_g , seen from the table 6.4, implies that the nucleation process is delayed, and decrease in the quantity T_m-T_x indicates that the growth process of nucleated crystal is retarded. The H_R values were varied from 1.15 to 1.52 and 1.49 to 2.12 in LN-Mn and LNK-Mn glass systems respectively with partial incorporation and increase in the MnO_2 content. Comparatively, glass forming ability of LNK-Mn glass system affected more than that of the LN-Mn glass system by the addition of MnO_2 content. This observation indicates the substantial improvement of thermal stability against crystallization together with enhancement in GFA owing to the incorporation of the third alkali (K_2O) metal and MnO_2 in the present glass network.

Since thermal stability and glass forming ability play a crucial role in preparing large scale glasses for practical applications and academic studies, the other thermal parameters which are proposed for the oxide glass system (Lu et al. 2003, Nascimento et al. 2005 and Saffarini et al. 2000) are also evaluated using the equations (2.6), (2.7), (2.8) and (2.9). The estimated thermal stability and GFA values from the above mentioned relations are tabulated in table 6.4. The evaluated values lie in the recommended range and exhibit greater thermal stability. This knowledge of thermal stability and GFA of the investigated glass system will be helpful in tuning and altering the composition of the glasses for glass applications.

6.1.5 Optical studies

It is essential to study the optical absorption spectra to understand the electronic band structure and optical transitions of glass samples. In this regard UV-visible spectra of glass samples have been recorded in the range of 200 to 1100 nm. Figure 6.7 (a) & (b) represents the absorption spectra of studied glass samples. It can be clearly seen, from figure 6.7 (a) & (b), that there are no sharp absorption edges present in the studied glass systems and is a typical characteristic of amorphous materials. The glass samples without MnO_2 exhibits the cut off wavelength at 208 nm for A6 glass sample and 212

nm for A5 glass sample. Partial incorporation of MnO₂ content resulting in drastic redshift in the absorption edge of LN-Mn and LNK-Mn glass system from 208 to 258 nm and 212 to 275 nm respectively. It can be clearly seen, from the figure 6.7 (a) & (b), that even though a small amount (0.1 mol %) of MnO₂ content brings considerable shift in the absorption edge in LN-Mn and LNK-Mn glass systems respectively, further increase in the MnO₂ content increases the redshift of absorption edge up to 303 nm in the case of LN-Mn glass system and 312 nm in the case of LNK-Mn glass system. This shift in absorption edge in both the glass systems can be ascribed to the transition of a valence electron of an oxygen ion to vacant excited state (Chethana et al. 2012). It also indicates the oxidizing and modifier role of MnO₂ content in the investigated glass systems. It can also be noticed, from figure 6.7 (a) & (b), that there exists a broad band around 475 nm in both the studied glass system with incorporation of MnO₂ content. Further, there observed a prominent increase in intensity of the band with increase in MnO₂ content. This may be attributed to the ${}^6A_{1g}(S) \rightarrow {}^4T_{1g}(G)$ transition, representing their divalent (Mn²⁺) state in octahedral symmetry (Taha et al. 2018). The increase in the intensity of the band with increase in MnO₂ content may be ascribed to the presence of Mn²⁺ ions in octahedral symmetry which results in relatively large average distance between Mn²⁺ ions. Intensity of the absorption band in LNK-Mn glass system is relatively higher than that of LN-Mn glass system. This indicates the suitability of prepared glass system in various technological applications like optical filters and tunable solid state lasers (Taha et al. 2018). Systematic study of UV-visible spectra provides the information about structure of electronic bands and optical transitions of glass systems. In general, various types of transitions exist in absorption edge. In case of glasses since it obeys dipole selection rule, possibility of transitions may be direct or indirect. The absorption coefficient (α) can be calculated using the equation (2.10). The magnitude of absorption coefficient (α) can be linked to the optical band gap energy E_g , using equation (2.10) with the equation (2.11) known as Davis and Mott relation (Fu et al. 2012).

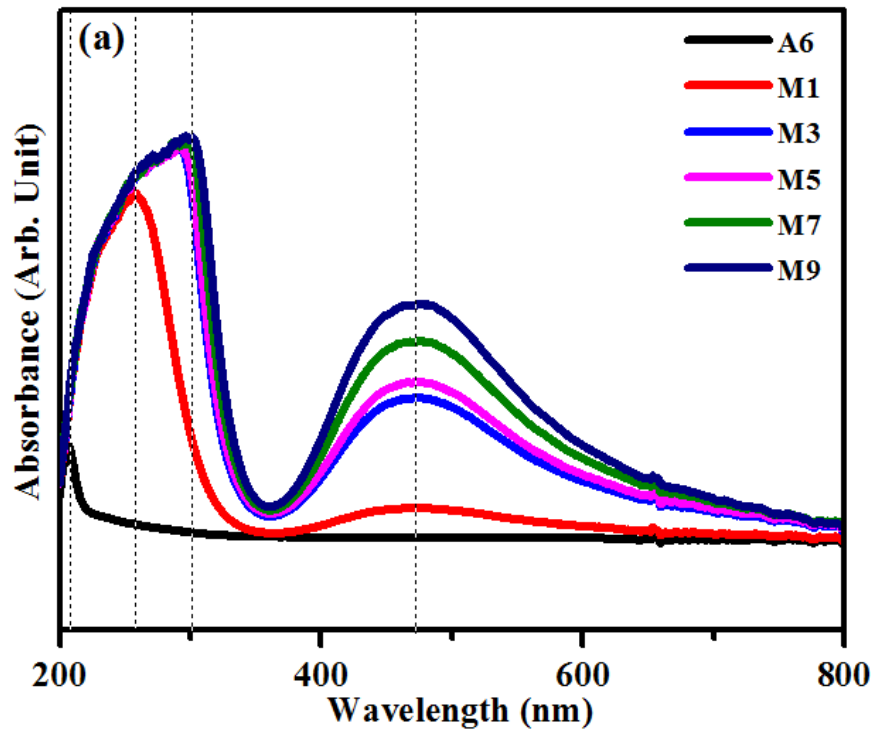


Figure 6.7 (a): UV-visible absorption spectra for the MnO₂ doped LN-Mn glass system.

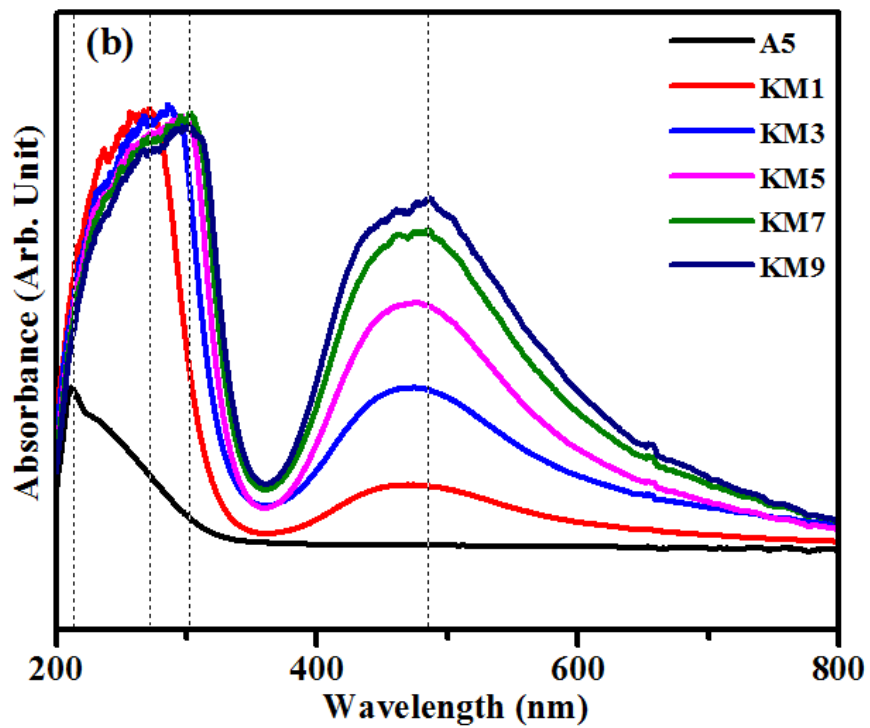


Figure 6.7 (b): UV-visible absorption spectra for the MnO₂ doped LNK-Mn glass system.

Since indirect allowed transition takes place in glasses, considering the value of n as 2, equation (2.11) can be simplified and written as equation (2.12). The optical band gap energy (E_g), can be determined by plotting $(\alpha h\nu)^{1/2}$ against photon energy which is named as Tauc plot and is depicted in figure 6.8 (a) & (b) for the present glass system. The determined values of E_g are tabulated in table 6.5. In the present investigation, there is a sudden decrease in E_g from 5.40 ± 0.1 eV to 3.67 ± 0.1 eV upon the incorporation of third alkali metal (K_2O) to the A6 glass sample of LN-Mn glass system. This reduction of E_g may be ascribed to the structural differences occurring due to the addition of relatively lower field strength K_2O ($0.12 \times 10^{-20} \text{ m}^{-2}$) to higher field strength Na_2O ($0.17 \times 10^{-20} \text{ m}^{-2}$). The average bond energy is another key factor which affects the E_g . The replacement of relatively higher bond energy Na_2O (8.4 KJ/mol) with relatively lower bond energy K_2O (12.2 KJ/mol) may cause the reduction in the average bond energy of the glass network, which lowers the energy of the conduction band edge and hence results in reduction of E_g . In addition to this, the addition of more MnO_2 content to the glass samples further results in reduction of E_g from 3.58 ± 0.1 eV to 3.51 ± 0.1 eV and 3.61 ± 0.1 eV to 3.38 ± 0.1 eV in LN-Mn and LNK-Mn zinc borate glass systems, respectively. This can be attributed to the increasing concentration of non-bridging oxygen (NBO), which are created during the structural rearrangement occurring in the glass network upon addition of MnO_2 content. The addition of MnO_2 opens up the tightly bound diborate units as a result of which the number of NBOs increases. NBOs bind the excited electrons less tightly compared to bridging oxygens. The relatively higher negative charge possessed by the NBOs supports the excitation of electrons to the conduction band of respective cations, which leads to further decrease in E_g with increase in MnO_2 content.

The band tails are characterized by Urbach energy, E_U (Narayanan et al. 2015) which is given by the equation (2.13). Taking natural log on both sides of the equation (2.13), it can be simplified and written as represented in equation (2.14). Figure 6.9 (a) & (b) represents the reciprocal of the slope of the linear region. The determined values of Urbach energy, E_U are summarized in table 6.5. It is noticed that the value of the E_U is observed to increase with the increase in MnO_2 content.

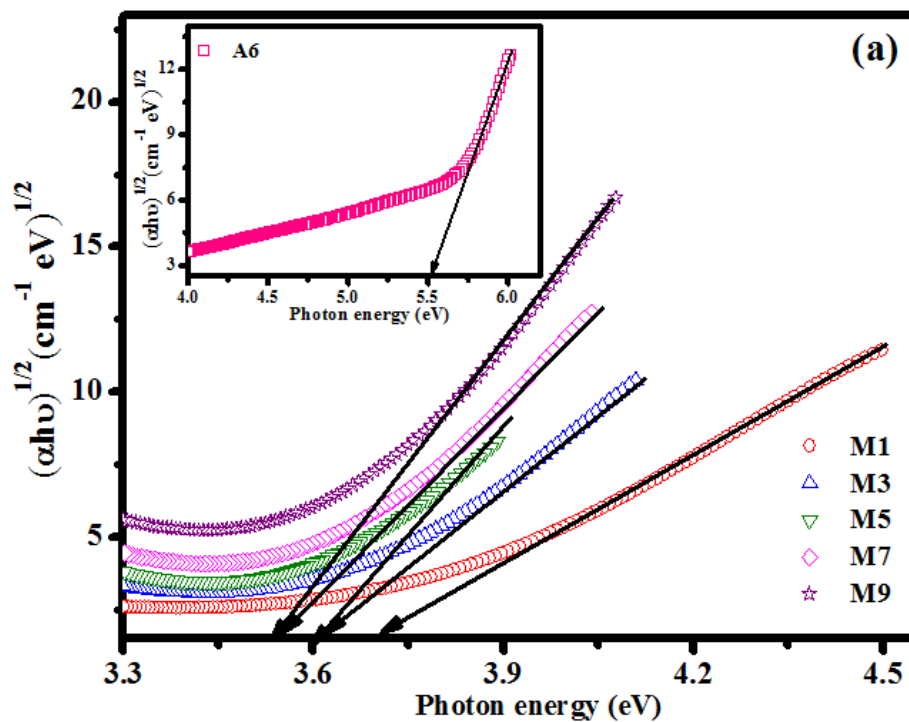


Figure 6.8 (a): Variation of $(\alpha h\nu)^{1/2}$ as a function of photon energy ($h\nu$) for the MnO_2 doped LN-Mn glass system.

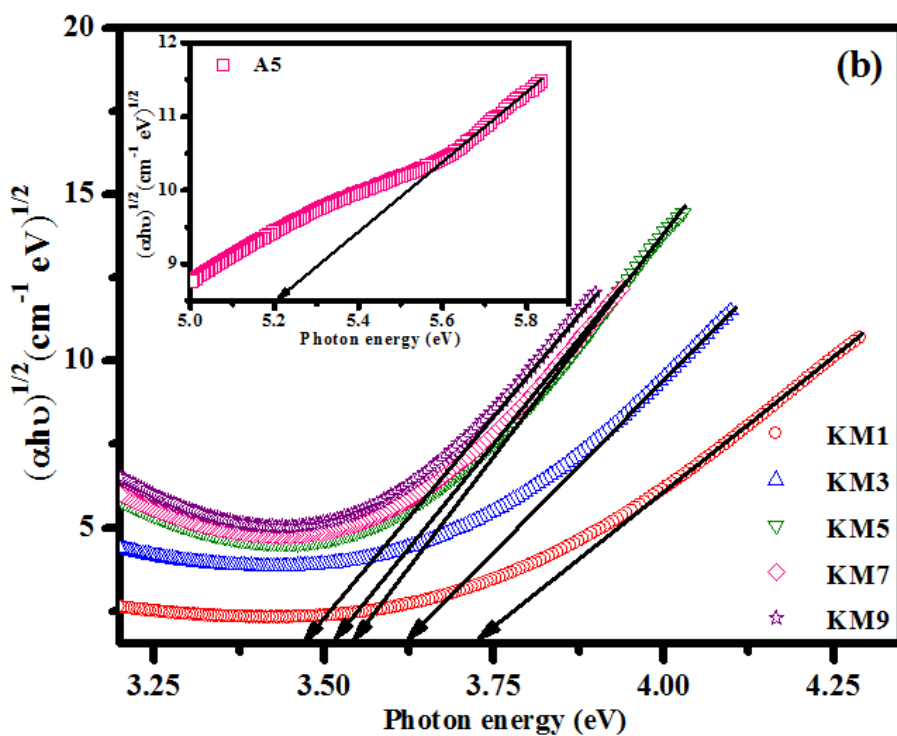


Figure 6.8 (b): Variation of $(\alpha h\nu)^{1/2}$ as a function of photon energy ($h\nu$) for the MnO_2 doped LNK-Mn glass system.

Table 6.5. Optical band gap energy (E_g) and Urbach energy (E_u) of LN-Mn and LNK-Mn glass systems.

Glass code	E_g (eV, ±0.1)	E_u (eV, ±0.1)	n (±0.001)	R_m	α_m (Å ³)	$\alpha_{O^{2-}}^{(n)}$ (Å ³)	$\alpha_{O^{2-}}^E$ (Å ³)	Λ	M
A6	5.40	0.14	1.537	8.448	3.353	1.490	2.311	0.549	0.688
M1	3.58	0.19	1.675	10.161	4.032	1.799	2.451	0.742	0.624
M3	3.53	0.21	1.681	10.232	4.061	1.811	2.463	0.748	0.622
M5	3.51	0.22	1.684	10.269	4.075	1.818	2.467	0.751	0.621
M7	3.47	0.22	1.685	10.287	4.082	1.821	2.476	0.753	0.620
M9	3.40	0.23	1.694	10.387	4.122	1.839	2.494	0.762	0.616
A5	3.67	0.16	1.540	8.751	3.473	1.530	2.341	0.581	0.686
KM1	3.61	0.20	1.670	10.433	4.140	1.833	2.358	0.759	0.626
KM3	3.52	0.21	1.680	10.556	4.189	1.855	2.384	0.770	0.622
KM5	3.47	0.21	1.683	10.609	4.210	1.865	2.398	0.774	0.621
KM7	3.41	0.23	1.690	10.698	4.245	1.880	2.415	0.782	0.618
KM9	3.38	0.25	1.693	10.729	4.258	1.886	2.423	0.784	0.617

This increasing trend in Urbach energy can be attributed to the presence of defects occurred due to the modifications of the structure. It is witnessed that the absorption tail is broad owing to the indirect electronic transitions assisted by the presence of phonons. Consequently, Urbach energy values endorse the presence of electronic transitions assisted by the phonons in the current investigated glass samples. The refractive index, n of all the prepared samples were measured using Abbe refractometer and the measured values are represented in table 6.5. It can be noticed that the partial incorporation of K₂O by reducing Na₂O slightly increases the refractive index, n . This increase may be due to the replacement of Na⁺ (0.175 Å³) ion having relatively lower polarizability compared to that of the K⁺ (0.821 Å³) ion. Further, the increase in the MnO₂ content enhances the refractive index of both LN-Mn and LNK-Mn glass systems. This experimental observation can be ascribed to the partial substitution of Mn²⁺ ion which has relatively higher polarizability (0.544 Å³) than that of Zn²⁺ (0.283 Å³).

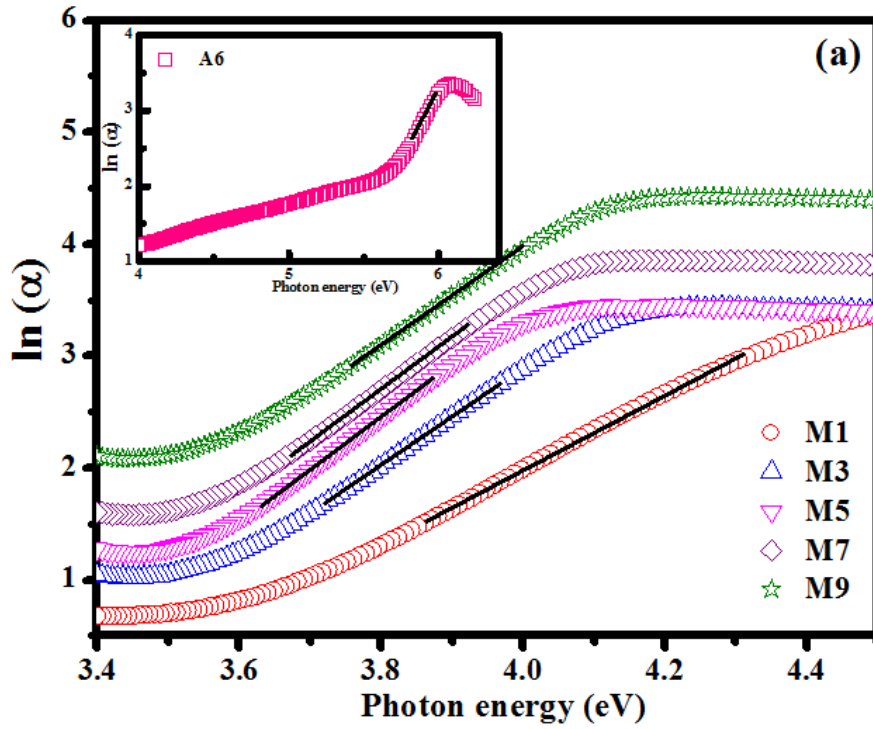


Figure 6.9 (a): Variation of $\ln(\alpha)$ as a function of photon energy ($h\nu$) for the MnO_2 doped LN-Mn glass system.

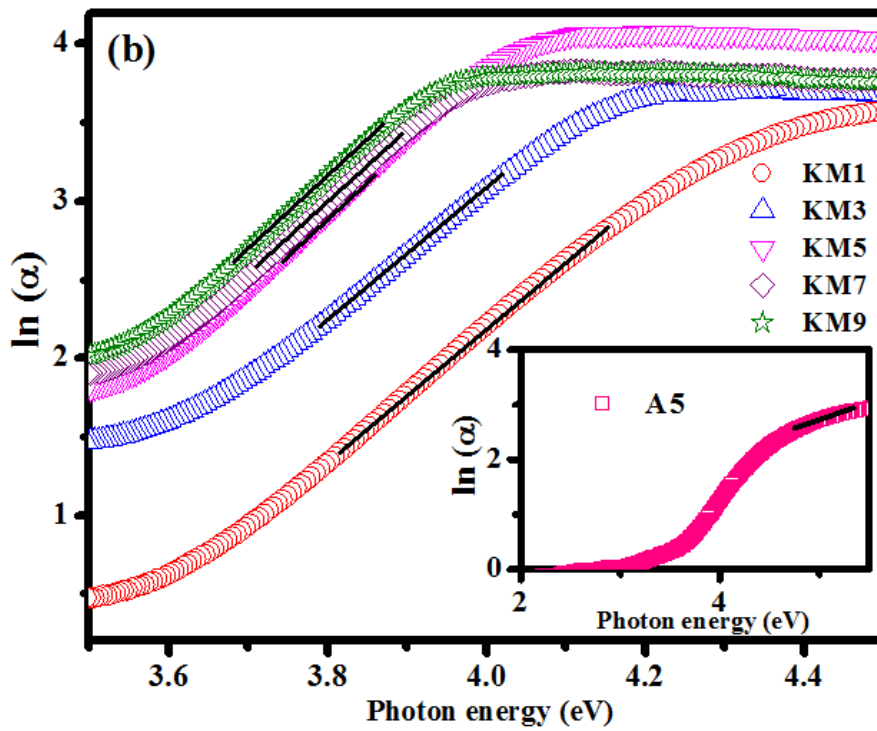


Figure 6.9 (b): Variation of $\ln(\alpha)$ as a function of photon energy ($h\nu$) for the MnO_2 doped LNK-Mn glass system.

It reveals that, in addition to density and compactness of the glass system, the refractive index also is influenced by the cation polarizability. This once again confirms the network modifier role of MnO₂.

6.1.5.1 Electronic polarizability

Molar refraction (R_m) and the molar polarizability (α_m) are determined, using the equation (2.15) and (2.16) respectively, for both the series of glass systems. The determined values are summarized in table 6.5. The values of α_m found to be in the range of 3.352 Å³ to 4.122 Å³ and 3.473 Å³ to 4.258 Å³ for MnO₂ doped LN-Mn and LNK-Mn system respectively.

The oxide ion polarizability based on refractive index and optical band gap energy of both the series of glass systems has been determined using the equations (2.17) & (2.18) and presented in table 6.5. It is noticed that the oxide ion polarizability is increasing monotonically as MnO₂ content increases. This can be attributed to the partial replacement of Na₂O with K₂O, and similarly the partial replacement of ZnO with MnO₂ as the polarizability of K⁺ (0.821 Å³) ion and Mn²⁺ (0.544 Å³) ion are relatively much higher than that of the Na⁺ (0.175 Å³) and Zn²⁺ (0.283 Å³) ions. In addition, the increase in the number of NBOs with an increase in MnO₂ content may also contribute to the increase in overall polarizability of the investigated glass system. It is noticed that the ionic radius (r_i) reduces with increasing MnO₂ content. As a consequence, the oxide ion polarizability will be altered owing to the diminishing number of overlying orbitals (Dimitrov et al. 1996), which is consistent with Fazan's rule (Dimitrov and Komatsu, 2010).

6.1.5.2 Optical basicity

The optical basicity of the both the series of glass systems is calculated using the equation (2.19) and the values are tabulated in table 6.5. It is seen that the optical basicity increases from 0.549 to 0.581 with the partial incorporation of K₂O content to the glass matrix. This may be ascribed to the partial replacement of relatively lower optical basicity Na₂O (1.10) with higher optical basicity K₂O (1.31). It is also observed

that the increase in MnO₂ content monotonically increases the optical basicity of both LN-Mn and LNK-Mn glass samples. This increase may be ascribed to the partial replacement of ZnO having lower optical basicity of 0.9 compared to that of MnO₂ having relatively higher optical basicity of 0.96. This increase indicates that the glass systems are becoming chemically more basic with the increasing MnO₂ content (Dimitrov and Komatsu, 2010).

6.1.5.3 Metallization criterion

The metallization criterion, (M) for the current glass systems were calculated and summarized in table 6.5. It is observed to decrease with increasing MnO₂ content in both LN-Mn and LNK-Mn glass system. Consequently, gap between the valence band and conduction band is reduced. It is consistent with the E_g values for both the glass systems.

6.1.6 Mechanical properties

Mechanical strength of glass material play crucial role in choosing glass samples for practical applications. The mechanical strength and fracture toughness of the prepared glass samples were determined using Vickers micro-indentation technique. To rule out any kind of experimental errors, each sample was indented ten times and standard deviation was calculated. The measured values of Vickers micro-hardness were presented in table 6.6. The measured Vickers micro-hardness values were found to decrease from 4.92 to 4.760 GPa for A6 and A5 samples, respectively. This may be ascribed to the partial replacement of relatively lower radius and higher field strength Na₂O with higher radius and lower field strength K₂O. Partial substitution of potassium ions having higher radius increases the distance between modifier cations and anions in the glass network. This leads to the weakening of glass structure and decreases the Vickers micro-hardness. Further it can be noticed that, Vickers micro-hardness with the partial incorporation of MnO₂ content is slightly decreasing from 4.992 to 4.792 GPa and 4.760 to 4.589 GPa for LN-Mn and LNK-Mn glass systems respectively. This can be ascribed to the breaking down of tightly bound diborate units and increase in NBOs in the glass network with increase in MnO₂ content. Mechanical

strength of the prepared glass samples can be evaluated by studying the crack initiation and propagation patterns, which are the two major factors in determining the strength of the glasses.

Table 6.6. Vickers hardness (H_v), half crack length (C), fracture toughness (K_{IC}) and Brittleness (B) of MnO₂ doped LN-Mn and LNK-Mn glass system. .

Glass systems	Glass code	Measured Vickers hardness (GPa) \pm 0.004	Measured Half crack length (μm) \pm 1	Fracture toughness (MPa (m) ^{1/2}) \pm 0.003	Brittleness ($\mu\text{m}^{-1/2}$) \pm 0.02
LN-Mn	A6	4.992	57.18	0.730	6.84
	M1	4.963	57.60	0.724	6.92
	M3	4.921	57.48	0.724	6.93
	M5	4.873	57.70	0.721	6.94
	M7	4.839	58.03	0.717	6.95
	M9	4.792	58.33	0.713	6.96
LNK-Mn	A5	4.760	59.05	0.705	6.75
	KM1	4.682	60.30	0.695	6.75
	KM3	4.654	60.31	0.688	6.84
	KM5	4.632	61.01	0.680	6.87
	KM7	4.617	61.51	0.674	6.89
	KM9	4.589	62.22	0.666	6.90

The fracture toughness, (K_{IC}) which is the measure of how easily a crack can be able to propagate through the material with the applied load is determined using the equation (2.22) suggested by Anstis (1981). E is the Young's modulus (GPa) which is calculated using equation (2.23), H is the experimentally determined Vickers hardness (GPa), P is the load applied (4.9 N) and C is the measured half crack length (μm). Young's modulus of the poly component system is obtained by the theoretical model suggested by Makishima and Mackenzie (1973) using the equation (2.23). The atomic packing fraction, V_i is calculated using the equation (2.24). The determined fracture

toughness (K_{IC}) values are represented in table 6.6. It is evident that K_{IC} is decreasing gradually. This can be attributed to the slight reduction of Vickers hardness and enhancement in half crack length. In the present investigation crack length is found to be increasing gradually with the increase in modifier content. This may be ascribed to the fact that the bonds between modifier cation and NBO are considerably weaker compared to the strength of bonds between boron and bridging oxygen (BO) or boron and NBO atom. In the present investigation, incorporation of MnO_2 content lead to breaking of the tightly bound diborate units and resulting in the formation of mixed bonding. This facilitates the easy propagation of cracks through the weaker bonds.

Another influencing factor of crack initiation and propagation is the index of brittleness, which is called as Brittleness (B). The brittleness of the prepared glasses was estimated by the equation (2.26) involving the measured Vickers hardness H_v and determined fracture toughness K_{IC} as proposed by Lawn and Marshall (1979). The evaluated brittleness values are presented in table 6.6. In general, the plastic flow by means of deformation and densification before the crack origination determine the brittleness of glass systems. Brittleness is found to be increase with the increasing MnO_2 content. This enhancement in the brittleness is further confirmed by SEM micrographs represented in figure 6.10. SEM micrographs revealed the pattern of cracking and chipping associated with the surface of examined glass samples upon indentation with particular load. It can be seen, from figure 6.10 that the studied glass samples show crack propagation patterns which originate from the four corners (identified as median-radial cracks) of the Vickers indentation. These cracks are often initiated from the flaws and extend if the stress applied crosses the specific individual threshold. In the present investigation, these cracks were generated and propagated by applying load equal to 4.9 N. This load was maintained constant for all the studied glass samples. With increase in the MnO_2 content, chipping and shear cracks start emerging which is evident from sample KF5 represented in figure 6.10. Hence there must be an increase in elastic properties of the LKNBZ glass system with an increase in MnO_2 .

In order to choose the glasses for industrial and technological application detailed examination of mechanical as well as elastic properties is required. In this

regard along with Young's modulus (E), the Poisson's ratio (σ) of the prepared glass system was evaluated by means of the equations (2.23) & (2.27), respectively.

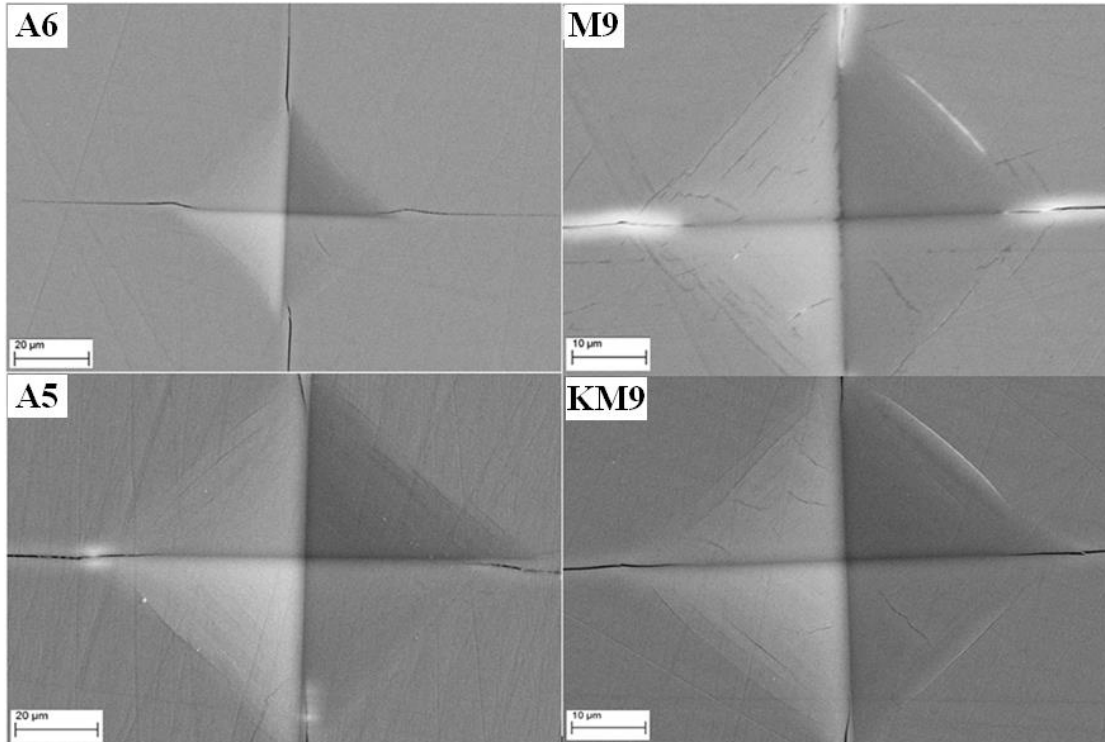


Figure 6.10: Representative SEM micrograph of Vickers indentation of A6 & M9 samples of LN-Mn and A5 & KM9 samples of LNK-Mn glass systems.

The shear modulus (S) and bulk modulus (K) were evaluated by the equations (2.28) & (2.29). The values of the elastic moduli's obtained are tabulated in table 6.7. It is seen from table 6.7 that the values of Young's modulus, shear modulus and bulk modulus are increasing with the increase in modifier content. The partial substitution of K_2O by Na_2O and partial replacement of ZnO by MnO_2 in the investigated glass samples result in an increase of over all elastic moduli. This may be ascribed to greater dissociation energy and packing factor of incorporated modifiers. Poisson's ratio of the studied samples is least affected due to the trivial variation of packing. The estimated Poisson ratio in the present investigation for all the samples by means of equation (2.27) is 0.27. The obtained Poisson ratio value is in good agreement with earlier investigations and lies in the reported range for borate glasses (Rouxel 2007).

Table 6.7. Young's modulus (E), bulk modulus (K), shear modulus (S), and atomic packing density (V_t) of MnO₂ doped LN-Mn and LNK-Mn glass system.

Glass code	Young's modulus, E (GPa)	Bulk modulus, K (GPa)	Shear Modulus, S (GPa)	Atomic packing density, V_t
A6	80.95	59.14	31.82	0.609
M1	80.96	59.14	31.83	0.609
M3	81.10	59.30	31.88	0.609
M5	81.21	59.42	31.92	0.610
M7	81.33	59.55	31.96	0.610
M9	81.44	59.67	32.00	0.611
A5	79.33	57.35	31.25	0.602
KM1	79.51	57.58	31.30	0.604
KM3	79.56	57.62	31.33	0.604
KM5	79.63	57.68	31.35	0.605
KM7	79.71	57.75	31.38	0.605
KM9	79.80	57.84	31.42	0.605

6.2 SUMMARY

In the present chapter, the results of comparative studies carried out on the effect of MnO₂ addition on the properties of LN-Mn glass system with that of the LNK-Mn glass system are discussed in detail. XRD results, for both the series, confirmed the amorphous nature of the glass systems. Fourier Transform Infrared (FTIR) and Raman spectroscopy techniques were used in order to explore the structural rearrangement occurred due to the partial substitution of modifier cations. It is noticed that the prepared glass samples exhibit good thermal stability with the incorporation of MnO₂ content. Incorporation of MnO₂ content drastically enhanced the glass stability in both LN-Mn and LNK-Mn glass systems. These glass systems therefore are good host materials for optical fiber fabrication which yields a crystal-free fiber. It is clearly seen that the glass stability is more affected by MnO₂ content in LNK-Mn glass system compared to that

of the LN-Mn glass system. UV-visible spectroscopy is performed for all the samples in order to understand the electronic band structure and optical transitions in them. A broad band is observed at about 475 nm in both the studied glass system with incorporation of MnO₂ content owing to the ${}^6A_{1g}(S) \rightarrow {}^4T_{1g}(G)$ transition representing the divalent state of Mn in octahedral symmetry. It is observed that the partial incorporation of MnO₂ content exhibit drastic redshift in the absorption edge of LN-Mn and LNK-Mn glass system from 208 to 258 nm and 212 to 275 nm respectively. Mechanical strength and fracture toughness of the prepared glass samples were determined using Vickers micro-indentation technique. It was noticed that the prepared glass samples exhibit superior mechanical properties with the incorporation of MnO₂ content. SEM micrographs revealed the pattern of cracking and chipping associated with the surface of examined glass samples upon indentation with particular load.

Chapter 7

SUMMARY AND CONCLUSIONS

This chapter summarizes the important findings of the present research work along with conclusions. In addition to that the scope for the future work is also included in the present chapter.

7.1 SUMMARY AND CONCLUSIONS

From result and discussions of chapters 3, 4, 5 and 6, it can be summarized that:

Chapter 3: Peak positions of different vibration modes in FTIR of glass samples vary non linearly, which explains the role of modifier alkali elements and the existence of strong mixed alkali effect (MAE). Infrared spectra show clear modifications in the structure which confirm the presence and conversions of $[BO_3]$ and $[BO_4]$ unit. Thermal parameters like glass transition, crystallization, melting temperature, fragility and glass stability exhibit non linear variation which validates the presence of MAE in the studied glass system. The non-linear variation of the properties viz., hardness, crack length, fracture toughness and brittleness is also a consequence of mixed alkali effect in the glass samples. From the observed non linearity in the mechanical, thermal and structural properties, it can be inferred that the MAE is strong in three-alkali ion added glass systems.

Chapter 4: The results of comparative studies carried out on the effect of TM ions addition on the properties of LN-TM glass system with that of the LNK-TM glass system are discussed in detail. The inclusion of TMO ions has proved to be of great importance in tailoring the properties of the glass systems to make them promising candidates for technological applications. The Mn and Fe transition metal ions are chosen for detailed investigation on the effect of their addition on various properties in LN and LNK glass systems. Mn and Fe have been chosen based on the superior properties exhibited by the Mn and Fe transition metal ions doped LN-TM and LN-TMO glass systems over other ions studied under the present investigation.

Chapter 5: It is observed that the prepared samples exhibit good thermal stability, which gets enhanced as Fe₂O₃ content increases. The glass forming ability has been enhanced with the partial incorporation of third alkali ion and Fe³⁺ ion in the LNK-Fe system. Addition of Fe₂O₃ to B₂O₃ glass opens up the diborate glass network and decreases the energy of E_g resulting in the shift of absorption edge towards the higher wavelength region. The band observed, in both the series, around 450 nm in UV absorption spectra is due to the d-d transition of ${}^6A_{1g}(S) \rightarrow {}^4T_{2g}(G)$ which indicates the presence of an iron ion in trivalent state (Fe³⁺) with distorted octahedral symmetry. The inclusion of Fe₂O₃ has proved to be of great importance in tailoring the properties of the glass systems to make them promising candidates for technological applications.

Chapter 6: It is noticed that the prepared glass samples exhibit good thermal stability with the incorporation of MnO₂ content. Incorporation of MnO₂ content drastically enhanced the glass stability in both LN-Mn and LNK-Mn glass systems. These glass systems therefore are good host materials for optical fiber fabrication which yield a crystal defect free fiber. It is observed that the partial incorporation of MnO₂ content exhibits drastic redshift in the absorption edge of LN-Mn and LNK-Mn glass system from 208 to 258 nm and 212 to 275 nm respectively. It was noticed that the prepared glass samples exhibited superior mechanical strength with the incorporation of MnO₂ content.

The following conclusions were drawn from the present work.

- The addition of third type alkali ion to the two alkali glass system has considerably enhanced the MAE. The same is evidently observed in the mechanical, thermal and structural properties studied for the system of glasses.
- The addition of 1 mol% of transition metal oxides to both LN and LNK glass systems have considerable effect on the shift in absorption edge making them suitable candidates for optical filters.
- Addition of Fe₂O₃ and MnO₂ is observed to decrease the optical band gap energy of the synthesized glass systems making them more semiconducting.
- Addition of Fe₂O₃ and MnO₂ increases both thermal stability and mechanical properties of the synthesized glass systems.

7.2 SCOPE FOR FUTURE WORK

Designing glasses with unique functional properties is a topic of active research in view of providing solution to long standing problems in modern glass science and technology. Applications like photonics switching and information processing depend critically on the development of improved glass materials. This can be achieved by preparing glass materials with various dopants available such as rare earth ions, transition metal ions, chalcogenides, halides etc., as glasses possess inimitable capability to contain various dopants. Glasses are the best hosts for embedding active elements for the development of special properties like colour, high nonlinear susceptibility, emission of fluorescent light, etc. It is known that the chemical composition of glassy materials controls most of the properties of them. Doping of alkali ions into borate glass introduces interesting structural variations by creating BO_3 and BO_4 structural units and forming Non Bridging Oxygens (NBOs). These structural variations, pertaining to the mixed alkali effect (MAE), greatly controls the physical parameters of borate glasses. MAE enables the researchers to produce glasses according to industrial needs. In the present work, relatively less quantity of transition metal (less than 1mol%) ions are added which can considerably modify the optical properties of glasses with improved thermal and mechanical properties. These kind of glasses can be used as optical filters and in electro optical devices etc.

In view of this, a detailed investigation of various TMO added borate glass systems can be explored to study the structural, optical, thermal and mechanical properties. This will be beneficial for the synthesis of new materials with better properties for many technological applications. Further, investigations can be performed on the properties of the combination of various transition metal oxide nanoparticles and rare earth ions embedded glass matrix for laser and optical filter applications.

Bibliography

- Abdel-Rahim, M. A., El-Korashy, A., Hafiz, M. M., & Mahmoud, A. Z. (2008). "Kinetic study of non-isothermal crystallization of BixSe100-x chalcogenide glasses". *Physica B*, 403 (18), 2956-2962.
- Adam, J.L. (2001). "Non-oxide glasses and their application in optics". *J. Non-Cryst. Solids*, 287, 401-404.
- Ahmed, A. A., & Abbas, A. F. (1986). "Mixed-alkali effect in alkali borate glasses". *J. of Non-Cryst. Solids*, 80 (1): 371-378.
- Anstis, G. R., Chantikul, P., Lawn, B. R., and Marshall, D. B. (1981). "A critical evaluation of indentation techniques for measuring fracture toughness: I, direct crack measurements". *J. Am. Chem. Soc.*, 64 (9): 533–538.
- Arbuzov, V., Fedorov, Y., Kramarev, S., and Shashkin, A. (2013) "How process factors affect the limiting characteristics of neodymium phosphate glasses for large disk- and rod-shaped active elements". *J. Opt. Technol.* 80, 321-324.
- Azlan, M. N., Halimah, M. K., Shafinas, S. Z., and Daud, W. M. (2015). "Electronic polarizability of zinc borotellurite glass system containing erbium nanoparticles". *Mater. Express.*, 5 (3): 211-218.
- Bhogi, A., and Kistaiah, P. (2018). "Alkaline earth lithium borate glasses doped with Fe (III) ions—an EPR and optical absorption study". *Materials Today: Proceedings*, 5 (13), 26199-26206.
- Biscoe, J., and Warren, B. E. (1938). "X-ray diffraction study of soda-boric oxide glass". *J. Am. Ceram. Soc.*, 21 (8): 287–293.
- Bogomolova, L. D., and Glassova, M. P. (1980). "The impurity effects in vanadate semiconducting glasses". *J. of Non-Cryst. Solids*, 37, 423-426.
- Bray, P. J., and J. G. O'keefe. (1963) "Nuclear magnetic resonance investigations of the structure of alkali borate glasses." *Phys. Chem. Glasses* 4 (2): 37-46.
- Brown, R. J., and Kucernak, A. R. (2001). "The electrochemistry of platinum phthalocyanine microcrystals: III. Electrochemical behaviour in aqueous electrolytes". *Electrochimica acta*, 46 (16): 2573-2582.
- Bunde, A., Ingram, M. D., Maass, P., and Ngai, K. L. (1991). "Diffusion with memory: a model for mixed alkali effects in vitreous ionic conductors". *J. Phys. A: Math. Gen.*, 24 (15): L881.
- Chandrashekaraiyah, G., Reddy, N. S., Sujatha, B., Viswanatha, R., and Reddy, C. N. (2018). "Role of Er³⁺ and Bi³⁺ ions on thermal and optical properties of Li₂B₄O₇ glasses: Structural correlation". *J. Non-Cryst. Solids*, 498, 252-261.

Chethana, B. K., Reddy, C. N., and Rao, K. J. (2012). "Thermo-physical and structural studies of sodium zinc borovanadate glasses in the region of high concentration of modifier oxides". *Mater. Res. Bull.*, 47 (7): 1810-1820.

Clavaguera-Mora, M. T. (1995). "Glassy materials: thermodynamic and kinetic quantities". *J. Alloys Compd.*, 220 (1-2), 197-205.

Cochain, B., Neuville, D. R., Henderson, G. S., McCammon, C. A., Pinet, O., and Richet, P. (2012). "Effects of the Iron Content and Redox State on the Structure of Sodium Borosilicate Glasses: A Raman, Mössbauer and Boron K-Edge XANES Spectroscopy Study". *J. Am. Ceram. Soc.*, 95 (3): 962-971.

Colak, S. C. (2017). "Role of titanium ions on the optical and thermal properties of zinc borate glass doped with TiO₂", *Phys. Chem. Glass - Euro. J. Glass Sci. and Technol. B*, 58 (2): 41-48.

Colak, S. C., Akyuz, I., and Atay, F. (2016). "On the dual role of ZnO in zinc-borate glasses". *J. Non-Cryst. Solids*, 432, 406-412.

Day, D. E. (1976). "Mixed alkali glasses- their properties and uses". *J. of Non-Cryst. Solids*, 21 (3): 343-372.

Dimitrov, V. and Sakka, S. (1996). "Electronic oxide polarizability and optical basicity of simple oxides. I". *J. Appl. Phys.*, 79 (3):1736–1740.

Dimitrov, V., and Komatsu, T. (2010). "An interpretation of optical properties of oxides and oxide glasses in terms of the electronic ion polarizability and average single bond strength". *J. Univ. Chem. Technol. Metall*, 45 (3): 219-250.

Ding, L., Yang, Y., Jiang, X., Zhu, C., and Chen, G. (2008). "Photoluminescence of undoped and B-doped ZnO in silicate glasses". *J. of Non-Cryst. Solids*, 354(12), 1382-1385.

Donald, I. W., Metcalfe, B. L., Fong, S. K., and Gerrard, L. A. (2006). "The influence of Fe₂O₃ and B₂O₃ additions on the thermal properties, crystallization kinetics and durability of a sodium aluminum phosphate glass". *J. Non-Cryst. Solids*, 352 (28): 2993–3001.

Doremus, R. H. (1973). *Glass science*. John Wiley & Sons, Newyork.

Doweidar, H., El-Damrawi, G. M., Moustafa, Y. M., and Ramadan, R. M. (2005). "Density of mixed alkali borate glasses: A structural analysis". *Physica B* 362 (1), 123-132.

Duffy, J. A. (1996). "Optical basicity: A practical acid-base theory for oxides and oxyanions". *J. Chem. Edu.*, 73 (12): 1138.

Ehrt, D. (2000). "Structure, Properties and Applications of Borate Glasses." *GLASS TECHNOLOGY-PART A*, 41 (6): 182–85.

- ElBatal, H. A., Abdelghany, A. M., and Ali, I. S. (2012). "Optical and FTIR studies of CuO-doped lead borate glasses and effect of gamma irradiation". *J. Non-Cryst. Solids*, 358 (4): 820-825.
- Fayad, A. M., El-Kashef, I. M., & Moustaffa, F. A. (2017). "Infrared Absorption of Some Alkali Borate and Alkali Silicate Glasses Containing Nickel & Iron Oxides". *Silicon*, 9 (4): 555-561.
- Flower, G. L., Reddy, M. S., Baskaran, G. S., and Veeraiah, N. (2007). "The structural influence of chromium ions in lead gallium phosphate glasses by means of spectroscopic studies". *Opt. material.*, 30 (3): 357-363.
- Førland, T., and J. Krogh-Moe. (1958). "The structure of the high-temperature modification of sodium lithium sulfate". *Acta Crystallographica* 11 (3): 224-225.
- Fu, Shaobo., Baojiu, C. H. E. N., Xiangping, L. I., Zhang, J., Yue, T. I. A. N., Jiashi, S. U. N., and Zhongli, W. U. (2012). "Effect of RO (R= Ca, Sr, Ba, Zn or Pb) component on spectroscopic properties of Eu³⁺ in RO-B₂O₃ glasses". *J. Rare Earths*, 30 (10): 979-984.
- Gaafar, M. S., El-Aal, N. A., Gerges, O. W., and El-Amir, G. (2009). "Elastic properties and structural studies on some zinc-borate glasses derived from ultrasonic, FT-IR and X-ray techniques". *J. Alloys Comp.*, 475(1): 535-542.
- Gaafar, M. S., Marzouk, S. Y., Zayed, H. A., Soliman, L. I., and El-Deen, A. S. (2013). "Structural studies and mechanical properties of some borate glasses doped with different alkali and cobalt oxides". *Current App. Phys.*, 13 (1): 152-158.
- Galeener, F.L., and Geissberger, A.E., (1982). "Raman studies of B₂O₃ glass structure: 10B→11B isotopic substitution". *J. Phys. Colloques* 43 (C9) 343-346.
- Gan, F., Huang, G., and Chen, S. (1982). "Vibrational spectra of multicomponent inorganic glasses". *J. Non-Cryst. Solids*, 52 (1-3): 203-210.
- Gowda, V. V., Reddy, C. N., Radha, K. C., Anavekar, R. V., Etourneau, J., and Rao, K. J. (2007). "Structural investigations of sodium diborate glasses containing PbO, Bi₂O₃ and TeO₂: Elastic property measurements and spectroscopic studies". *J. Non-Cryst. Solids*, 353 (11-12): 1150-1163.
- Griscom, D. L. (1978). *Borate glass structure*. Springer, Boston, MA.
- Hammad, A. H., Elsaghier, H. M., Abbas, W., Zidan, N. A., and Marzouk, S. Y. (2018). "Investigation of some structural and optical properties of lithium sodium fluoroborate glasses containing cuprous oxide". *Measurement*, 116, 170-177.
- Harada, T., In, H., Takebe, H., and Morinaga, K. (2004). "Effect of B₂O₃ addition on the thermal stability of barium phosphate glasses for optical fiber devices". *J. Am. Chem. Soc.*, 87 (3): 408-411.
- Hench, L. L. (2006). "The story of bioglass". *J Mater Sci Mater Med* 17, 967-978.

- Isard, J. O. (1969). "The mixed alkali effect in glass". *J. of Non-Cryst. Solids*, 1 (3): 235-261.
- Kamitsos, E. I., and Chryssikos, G. D. (1991). "Borate glass structure by Raman and infrared spectroscopies". *J. Mol. Struct.*, 247, 1-16.
- Kamitsos, E. I., Patsis, A. P., Karakassides, M. A., and Chryssikos, G. D. (1990). "Infrared reflectance spectra of lithium borate glasses". *J. Non-Cryst. Solids* 126 (1-2): 52-67.
- Kauzmann, W. (1948). "The nature of the glassy state and the behaviour of liquids at low temperatures". *Chem. Rev.*, 43 (2), 219-256.
- Krogh-Moe, J. (1960). "The crystal structure of cesium triborate, $Cs_2O \cdot 3B_2O_3$ ". *Acta Crystallographica* 13 (11): 889-892.
- Krogh-Moe, J. (1962). "Structural interpretation of melting point depression in the sodium borate system". *Phys. Chem. Glasses*, 3 (4): 101-110.
- Krogh-Moe, J. (1965). "The crystal structure of silver tetraborate $Ag_2O \cdot 4B_2O_3$ ". *Acta Crystallographica*, 18 (1): 77-81.
- Kumari, G. K., Begum, S. M., Krishna, C. R., Sathish, D. V., Murthy, P. N., Rao, P. S., and Ravikumar, R. V. S. S. N. (2012). "Physical and optical properties of Co^{2+} , Ni^{2+} doped $20ZnO + xLi_2O + (30-x) K_2O + 50B_2O_3$ ($5 \leq x \leq 25$) glasses: Observation of mixed alkali effect". *Mater. Res. Bull.*, 47 (9): 2646-2654.
- Kurkjian, C. (2000). "Mechanical properties of phosphate glasses". *J. Non-Cryst. Solids*, 263, 207–212.
- Lawn, B.R. and Marshall, D.B. (1979). "Hardness, Toughness and Brittleness: an indentation analysis." *J. Am. Ceram. Soc.*, 62 (7-8): 347-350.
- Le Bourhis, E. (2008). *Glass: mechanics and technology*. John Wiley & Sons, Weinheim.
- Lewandowski, T., Łapiński, M., Walas, M., Przeźniak-Welenc, M., and Wicikowski, L. (2017). "Role of MnO in manganese–borate binary glass systems: a study on structure and thermal properties". *Bull. Mater. Sci.*, 40 (5): 933-938.
- Li, H. F., and Zheng, Y. F. (2016). "Recent advances in bulk metallic glasses for biomedical applications". *Acta biomaterialia*, 36, 1-20.
- Liu, H. S., Chin, T. S., and Yung, S. W. (1997). "FTIR and XPS studies of low-melting $PbO-ZnO-P_2O_5$ glasses". *Materials Chem. Phys.*, 50 (1): 1-10.
- Lu, Z. P., and Liu, C. T. (2003). "Glass formation criterion for various glass-forming systems". *Phys. Rev. Lett.*, 91 (11): 115505.
- Maass, P. (1999). "Towards a theory for the mixed alkali effect in glasses". *J. of Non-Cryst. Solids* 255 (1): 35-46.

- Makishima, A. and Mackenzie, J. D. (1973). "Direct calculation of Young's modulus of glass". *J. Non-Cryst. Solids*, 12 (1): 35–45.
- Makishima, A. and Mackenzie, J. D. (1975). "Calculation of bulk modulus, shear modulus and Poisson's ratio of glass". *J. Non-Cryst. Solids*, 17(2):147–157.
- Mallur, S. B., Czarnecki, T., Adhikari, A., and Babu, P. K. (2015). "Compositional dependence of optical band gap and refractive index in lead and bismuth borate glasses". *Mater. Res. Bull.*, 68, 27-34.
- Maniu, D., Ardelean, I., Iliescu, T., Cînta, S., Nagel, V., and Kiefer, W. (1999). Raman spectroscopic investigations on oxide glass system $(1-x)[3\text{B}_2\text{O}_3 \cdot \text{K}_2\text{O}] \cdot x\text{TiO}_2$ ". *J. mol. Struct.*, 480, 657-659.
- Marshall, D. B. (1983). "Controlled flaws in ceramics: a comparison of Knoop and Vickers indentation". *J. Am. Chem. Soc.*, 66 (2): 127–131.
- Marshall, J. (1990). *Glass source book*. Chartwell House.
- Martin, S.W. (1991). "Ionic Conduction in Phosphate Glasses". *Eur. J. Solid State Inorg. Chem.* 74 (8): 1767-1784.
- Meera, B. N., and Ramakrishna, J. (1993). "Raman Spectral Studies of Borate Glasses". *J. Non-Cryst. Solids*, 159 (1-2): 1–21.
- Mehta, N., Tiwari, R. S., and Kumar, A. (2006). "Glass forming ability and thermal stability of some Se–Sb glassy alloys". *Mater. Res. Bull.*, 41 (9): 1664-1672.
- Meyer, K. (1997). "Characterization of the structure of binary zinc ultraphosphate glasses by infrared and Raman spectroscopy". *J. Non-Cryst. Solids*, 209 (3): 227–239.
- Mohajerani, A., and Zwanziger, J. W. (2012). "Mixed alkali effect on Vickers hardness and cracking". *J. of Non-Cryst. Solids*, 358 (12): 1474-1479.
- Motke, S. G., Yawale, S. P., and Yawale, S. S. (2002). "Infrared spectra of zinc doped lead borate glasses". *Bull. Mater. Sci.*, 25 (1): 75-78.
- Moustafa, F. A., Fayad, A. M., Ezz-Eldin, F. M., and El-Kashif, I. (2013). "Effect of gamma radiation on ultraviolet, visible and infrared studies of NiO, Cr₂O₃ and Fe₂O₃-doped alkali borate glasses". *J. of Non-Cryst. Solids*, 376, 18-25.
- Naga Raju, G., Veeraiyah, N., Nagarjuna, G., and Satyanarayana, P. V. V. (2006). "The structural role of chromium ions on the improvement of insulating character of ZnO-ZnF₂-B₂O₃ glass system by means of dielectric, spectroscopic and magnetic properties". *Physica B* 373, 297-305.
- Narayanan, M.K. and Shashikala, H.D. (2015). "Thermal and optical properties of BaO–CaF₂–P₂O₅ glasses". *J. Non-Cryst. Solids*, 422, 6–11.

- Naresh, V., and Buddhudu, S. (2012). "Studies on Optical, Dielectric and Magnetic Properties of Mn^{2+} , Fe^{3+} & Co^{2+} Ions Doped LFBCd Glasses". *Ferroelectrics*, 437 (1): 110-125.
- Nascimento eng, Q., Mauro, J. C., Smedskjaer, M. M., Youngman, R. E., Potuzak, M., and Yue, Y. (2012). "Glass-forming ability of soda lime borate liquids". *J. Non-Cryst. Solids*, 358 (3), 658-665.
- Nascimento, M. L., Souza, L. A., Ferreira, E. B., and Zanotto, E. D. (2005). "Can glass stability parameters infer glass forming ability?". *J. Non-Cryst. Solids*, 351 (40): 3296-3308.
- Nazabal, V., Fargin, E., Le Flem, G., Briois, V., Cartier Dit Moulin, C., Buffeteau, T., and Desbat, B. (2001). "Structural modification on silica glass surface induced by thermal poling for second harmonic generation". *J. Sync. Rad.*, 8 (2): 788-790.
- Nazabal, V., Poulain, M., Olivier, M., Pirasteh, P., Camy, P., Doualan, J.L., Guy, S., Djouama, T., Boutarfaia, A. and Adam, J.L. (2012). "Fluoride and oxyfluoride glasses for optical applications". *J. Fluorine Chem.*, 134, 18-23.
- Nazabal, V., Poulain, M., Olivier, M., Pirasteh, P., Camy, P., Doualan, J.L., Guy, S., Djouama, T., Boutarfaia, A. and Adam, J.L. (2012). "Fluoride and oxyfluoride glasses for optical applications." *J. Fluorine Chem.*, 134, 18-23.
- Pascuta, P., Bosca, M., Pop, L., Rada, S., Culea, E., and Borodi, G. (2009). "Preparation and structural characterization of some Fe_2O_3 - B_2O_3 -ZnO glasses and glass ceramics", *J. Phys.: Conf. Series*, 182 (1): 3-7.
- Pascuta, Petru, Rares Lungu, and Ioan Ardelean. (2010). "FTIR and Raman Spectroscopic Investigation of Some Strontium-Borate Glasses Doped with Iron Ions." *J. Mater. Sci.: Mater Electronics* 21 (6): 548-553.
- Pavić, L., Graca, M. P. F., Skoko, Ž., Moguš-Milanković, A., and Valente, M. A. (2014). "Magnetic Properties of Iron Phosphate Glass and Glass-Ceramics". *J. Am. Ceram. Soc.*, 97(8): 2517-2524.
- Rao, G. V. and Shashikala, H. D. (2014a). "Optical and mechanical properties of calcium phosphate glasses". *Glass Phys. Chem.*, 40 (3): 303-309.
- Rao, K. J. (2002). *Structural chemistry of glasses*. Elsevier Science Ltd., UK.
- Ray, N. H. (1974). "Composition-property relationships in inorganic oxide glasses". *J. Non-Cryst. Solids*, 15 (3), 423-434.
- Razvan, S., Culea, E., and Pascuta, P. (2012). "The effect of copper ions addition on structural and optical properties of zinc borate glasses". *J. Non-Cryst. Solids*, 358 (4): 839-846.

- Reddy, C. N., Gowda, V. V., and Chakradhar, R. S. (2008). "Elastic properties and structural studies on lead–boro–vanadate glasses". *J. Non-Cryst. Solids*, 354 (1): 32-40.
- Rouxel, T. (2007). "Elastic Properties and Short-to Medium-Range Order in Glasses". *J. Am. Ceram. Soc.*, 90 (10): 3019–3039.
- Saddeek, Y. B., Gaafar, M. S., Abd El-Aal, N. S., and Abd El-Latif, L. (2009). "Structural analysis of some alkali diborate glasses". *Acta Phys. Pol. A* 116 (2), 211.
- Saffarini, G. (2000). "Differential Scanning Calorimetry and X-Ray Photoelectron Spectroscopy Studies on $\text{Se}_{100-x}\text{In}_x$ System". *physica status solidi (a)*, 179 (1), 109-115.
- Samee, M. A., Awasthi, A. M., Shripathi, T., Bale, S., Srinivasu, C., and Rahman, S. (2011). "Physical and optical studies in mixed alkali borate glasses with three types of alkali ions". *J. Alloys Compd.*, 509 (6): 3183-3189.
- Samee, M. A., Edukondalu, A., Ahmmad, S. K., Taqiullah, S. M., and Rahman, S. (2013). "Mixed-alkali effect in $\text{Li}_2\text{O}-\text{Na}_2\text{O}-\text{K}_2\text{O}-\text{B}_2\text{O}_3$ glasses: Infrared and optical absorption studies". *J. electronic mater.*, 42 (8): 2516-2524.
- Sanghera, J. S., Pureza, P. C., and Aggarwal, I. (1999). U.S. Patent No. 5,953,478. Washington, DC: U.S. Patent and Trademark Office.
- Saritha, D., Markandeya, Y., Salagram, M., Vithal, M., Singh, A. K., and Bhikshamaiah, G. (2008). "Effect of Bi_2O_3 on physical, optical and structural studies of $\text{ZnO}-\text{Bi}_2\text{O}_3-\text{B}_2\text{O}_3$ glasses". *J. Non-Cryst. Solids*, 354 (52-54): 5573-5579.
- Sastry, S. S. and Rao, B. R. V. (2014). "Spectroscopic studies of copper doped alkaline earth lead zinc phosphate glasses". *Physica B*, 434,159–164.
- Satyanarayana, T., Valente, M. A., Nagarjuna, G., and Veeraiah, N. (2013). "Spectroscopic features of manganese doped tellurite borate glass ceramics". *J. Phys. Chem. Solids*, 74 (2): 229-235.
- Sdiri, N., Elhouichet, H., Elakermi, E., Dhifallah, A., and Ferid, H.J. (2015). "Structural investigation of amorphous $\text{Na}_2\text{O}-\text{P}_2\text{O}_5-\text{B}_2\text{O}_3$ correlated with its ionic conductivity". *J. Non-Cryst. Solids* 409, 34–42.
- Sehgal, J. and Ito, S. (1999). "Brittleness of glass." *J. Non-Cryst.Solids.*, 253 (1-3), 126-132.
- Sehgal, J. and Ito, S. (1999). "Brittleness of glass". *J. Non-Cryst. Solids*, 253(1):126– 132.
- Sehgal, J., Nakao, Y., Takahashi, H., and Ito, S. (1995). "Brittleness of glasses by indentation". *J. Mater. Sci. Lett.*, 14 (3): 167–169.

- Selvaraj, U., and Rao, K. J. (1984). "Infrared spectroscopic study of mixed-alkali effect in borate glasses". *Spectrochimica Acta Part A: Molecular Spectroscopy*, 40 (11-12): 1081-1085.
- Shah, K., Goswami, M., Aswal, D., Shrikande, V., Gupta, S., and Kothiyal, G. (2006). "Effect of Na₂O/K₂O substitution on thermophysical properties of PbO based phosphate glasses". *J. Therm. Analysis and Cal.*, 89 (1): 153-157.
- Shelby, J. E. (2000). "Properties of alkali-alkaline earth metaphosphate glasses". *J. Non-Cryst. Solids*, 263, 271-276.
- Shelby, J. E. (2005). *Introduction to glass science and technology*. Royal Society of Chemistry, Cambridge, UK.
- Silver, A. H., and Bray, P. J. (1958). "Nuclear Magnetic Resonance Absorption in Glass. I. Nuclear Quadrupole Effects in Boron Oxide Soda-Boric Oxide, and Borosilicate Glasses". *J. Chem. Phys.*, 29 (5): 984-990.
- Souri, D. (2011). "DSC and elastic moduli studies on tellurite-vanadate glasses containing antimony oxide". *Euro. Phys. J. B*, 84 (1): 47-51.
- Srivastava, S., Zulfequar, M., Agrahari, S. K., and Kumar, A. (2008). "Kinetics of crystallization in glassy Se₇₀Te₃₀- xZnx using DSC technique". *Physica B*, 403 (19-20): 3429-3433.
- Subhashini, H. D., Shashikala, and N. K. Udayashankar. (2016). "Investigation of Mixed Alkali Effect on Mechanical, Structural and Thermal Properties of Three-Alkali Borate Glass System". *J. Alloys Compd.* 658, 996-1002.
- Taha, T. A., & Abouhaswa, A. S. (2018). "Preparation and optical properties of borate glass doped with MnO₂". *J. Mater. Sci.: Mater. Electronics*, 29 (10): 8100-8106.
- Taylor, J. R. (1997). *An Introduction to Error Analysis: The Study of Uncertainties in Physical Measurements*. University Science Books, California.
- Uchida, K., Kaneko, S., Omi, S., Hata, C. L., Tanji, H. L., Asahara, Y., Ikushima, A. J., Tokizaki, T., and Nakamura, A. (1994). "Optical nonlinearities of a high concentration of small metal particles dispersed in glass: copper and silver particles". *J. Opt. Soc. Am. B*, 11(7):1236-1243.
- Van Ass, H. M. J. M., and Stevels, J. M. (1974). "Internal friction of mixed alkali metaphosphate glasses:(I). Results". *J. of Non-Cryst. Solids*, 15 (2): 215-238.
- Van Ass, H. M. J. M., and Stevels, J. M. (1974). "Internal friction of mixed alkali metaphosphate glasses:(II). Discussion". *J. of Non-Cryst. Solids*, 16 (1): 27-45.
- Varshneya, A. K. (1994). *Fundamentals of inorganic glasses*, Acad. Press, New York.

- Velli, L. L., Varsamis, C. P. E., Kamitsos, E. I., Moncke, D., and Ehrhart, D. (2005). "Structural investigation of metaphosphate glasses". *Phys. Chem. Glasses*, 46 (2): 178–181.
- Venkata Krishnaiah, K., Rajeswari, R., Upendra Kumar, K., Surendra Babu, S., Martín, I. R., and Jayasankar, C. K. (2014). "Spectroscopy and radiation trapping of Yb³⁺ ions in lead phosphate glasses". *J. Quant. Spect. Rad. Trans.* 140, 37–47.
- Warren, B. E., Krutter, H., and Morningstar, O. (1936). "Fourier analysis of x-ray patterns of vitreous SiO₂ and B₂O₃", *J. Am. Ceram. Soc.*, 19 (1): 202–206.
- Wen, H., Tanner, P. A., and Cheng, B. M. (2016). "Optical properties of 3dN transition metal ion-doped lead borate glasses". *Mater. Res. Bull.*, 83, 400-407.
- Wright, A. C. (2015). "My Borate Life: An Enigmatic Journey". *Int. J. Appl. Glas. Sci.*, 6 (1): 45–63.
- Wu, J. M., and Huang, H. L. (1999). "Microwave properties of zinc, barium and lead borosilicate glasses". *J. of Non-Cryst. Solids*, 260 (1): 116-124.
- Yamane, M. and Asahara, Y. (2000). *Glasses for photonics*. Cambridge University Press, UK.
- Zachariasen, W. H. (1932). "The atomic arrangement in glass". *J. Am. Chem. Soc.*, 54 (10): 3841–3851.
- Zhao, X., Wang, X., Lin, H., and Wang, Z. (2007). "Correlation among electronic polarizability, optical basicity and interaction parameter of Bi₂O₃–B₂O₃ glasses". *Physica B*, 390 (2): 293-300.

LIST OF PUBLICATIONS

MANUSCRIPTS IN PEER-REVIEWED JOURNALS

- Subhashini., Shashikala, H. D. and Udayashankar, N.K. (2016). "Investigation of mixed alkali effect on mechanical, structural and thermal properties of three-alkali borate glass system", *J. Alloys Compd.*, 658, 996-1002.
- Subhashini., Shashikala, H. D. and Udayashankar, N.K. (2019). "Influence of Fe³⁺ ions on optical, structural, thermal and mechanical properties of Li₂O–Na₂O–K₂O–ZnO–B₂O₃ based glass system", *Ceram. Int.* 46 (4) 5213-5222.

MANUSCRIPTS IN CONFERENCE PROCEEDINGS JOURNALS

- Subhashini, Soumalya Bhattacharya, Shashikala, H.D. and Udayashankar, N.K. (2014). "Synthesis and studies on microhardness of alkali zinc borate glasses", *AIP Conference Proc.*, 1591, 749-750.

PAPERS PRESENTED IN INTERNATIONAL CONFERENCES

- Subhashini, Soumalya Bhattacharya, Shashikala, H.D. and Udayashankar, N.K., "Synthesis and studies on microhardness of alkali zinc borate glasses", 58th DAE–Solid state physics symposium, Thapar University, Patiala, Punjab, December 17–21, 2013.
- Subhashini, Shashikala, H. D. and Udayashankar, N. K., "Effect of Temperature on Certain Physical and Mechanical Properties of Alkali Zinc Borate Glasses", International Union of Materials Research Society (IUMRS), The International Concerence in Asia, IISc, Bangalore, India, December, 2013.

CURRICULUM VITAE



SUBHASHINI

Permanent Address :

W/O Manjunatha S O
220-A, Near Police Station,
Sirigere, Chitradurga Dist,
Karnataka, India - 577541

Mobile: (+91) - 8095299668
E-mail: subhashini.p.p@gmail.com

Academic Qualifications :

Master of Science **CGPA : 8.03**
Manipal University

Bachelor of Science **Score : 70%**
Kuvempu University

Research Publications :

Articles in International Journals : 2
Articles in conference proceedings : 1
Papers presented in conferences : 2